The Boundary Element Method for Sound Field Calculations

by

Peter Møller Juhl
The Acoustics Laboratory
Technical University of Denmark

PREFACE

This thesis is submitted in partial fulfilment of the requirements for the Danish Ph.D. degree. The work has been carried out under guidance of associate professor Finn Jacobsen at the Acoustics Laboratory, Technical University of Denmark, from February 1, 1991, to August 16, 1993.

First of all I would like to thank Finn Jacobsen for his encouragement and for many valuable discussions during the course of this study.

I would also like to thank

- Knud Rasmussen and Erling Sandermann Olsen for providing experimental data and for valuable discussions during the work presented in chapter 7.
- Karsten Bo Rasmussen for his interest in my work and for good co-operation during our joint work presented in chapter 8.

Finally, I would like to thank Søren Laugesen for very careful proofreading of the manuscript, and everybody at the Acoustics Laboratory for providing a pleasant atmosphere.

Lyngby, August 1993

Peter Møller Juhl

SUMMARY

This thesis is concerned with the numerical solution of the steady state wave equation - Helmholtz equation - exterior to one or several bodies positioned in free space. The current work may without complications be applied to interior problems and problems concerning other fluids in which Helmholtz equation is valid.

The approximate numerical solution to an acoustic radiation or scattering problem is obtained by bringing Helmholtz equation to its integral form: Helmholtz integral equation. Helmholtz integral equation is then solved numerically by means of the Boundary Element Method (BEM). The boundary element method is suitable for the approximate numerical solution of exterior acoustic problems due to two features: i) the radiation condition is automatically satisfied, and ii) only the boundary of the domain in interest needs to be discretized.

During the course of this study computer programs have been developed for calculating the sound field exterior to bodies of axisymmetric or general three-dimensional shape, positioned in free space.

Since this is the first study of the boundary element method in acoustics carried out at the Acoustics Laboratory, the emphasis has been on general aspects of the method rather than on details.

The author hopes that this thesis may serve as a basis for further investigations of the boundary element method.

RESUMÉ

Denne rapport omhandler den numeriske løsning af bølgeligningen for tidsharmoniske bølger - Helmholtz ligning - i luft omkring et eller flere legemer. Dette arbejde kan direkte overføres til beregninger af lydfeltet i hulrum og i andre medier hvor Helmholtz ligning gælder.

Den approximative numeriske løsning til et spredningseller udstrålingsproblem findes ved at bringe Helmholtz ligning til dens integralform: Helmholtz integralligning. Helmholtz integralligning løses numerisk ved hjælp af boundary element metoden. Boundary element metoden er særligt velegnet til den numeriske løsning af akustiske feltproblemer af to grunde:

1) Udstrålingsbetingelsen er automatisk opfyldt, og
2) kun grænserne af løsningsområdet behøver at modelleres numerisk.

I løbet af dette studium er udviklet programmer til beregning af lydfeltet omkring både rotationssymmetriske og generelle tre-dimensionale legemer i frit rum.

Eftersom nærværende rapport repræsenterer det første arbejde med boundary element metoden på Laboratoriet for Akustik er en generel gennemgang af metoden prioriteret højere end en detaljeret undersøgelse af nogle af de særlige aspekter der er knyttet til boundary element metoden.

Forfatteren håber at denne rapport kan tjene som basis for videre undersøgelser af boundary element metoden.

TABLE OF CONTENTS

1. INTRODUCTION

During the last few decades the development of digital computers has caused numerical calculations to be a discipline of increasing importance. Nowadays computers have changed from being a relatively expensive tool available to a very limited group of scientists to being a tool on almost every desk in the offices of scientists, consulting engineers ect. Thus the interest for numerical calculations is now as great as ever.

In some scientific areas, such as structural mechanics and stress analysis, a very powerful numerical method - the Finite Element Method (FEM) - appeared as an alternative to the finite difference method, which was the first widespread numerical method able to solve differential equations by dividing the domain of interest into elements. One of the main advantages of the finite element method over the finite difference method is its ability to handle elements of different sizes.

The finite element method was developed almost at the same time as powerful computers appeared, and this fact combined with the universal usability of the finite element method meant an enormous success for the finite element method. Thus the finite element method was for many years practically the only numerical method used in structural mechanics, and still today the finite element method is the dominating numerical method in that area. From this starting point the use of the finite element method then became more widespread and was also applied to acoustics. However, the finite element method has never become as successful in acoustics as it has in mechanics. This is probably due to two facts:

a) A large class of acoustical problems involves domains of infinite extent. As the finite element method requires a discretization of the entire domain into elements, any infinite domain must be handled by approximating the infinite domain with a finite one. Thus certain conditions must be imposed far away from the part of the domain of interest.

b) For a large class of interior problems, such as room acoustics, the frequency range for which numerical calculations would be desirable extend to so high frequencies, that a very large number of elements must be used if a usable solution is to be obtained. Still with the explosive development of modern computers, where the speed and storage capacity are approximately doubled every second year, the size of the domain in these problems imposes a severe upper limit on the frequency range in which calculations can be carried out for the next several years.

Hence, in acoustics the finite element method has mainly been used for calculations in relatively small enclosures or in enclosures for which the dimension of the problem could be reduced due to e.g. symmetry.

Due to the problem of the finite element method with respect to domains of infinite extent, integral equation methods received interest from scientists working in areas such as elasticity and potential theory. The main advantage of these integral equation methods compared to the finite element and the finite difference methods is the representation of the field in the entire domain by means of the field on the boundary of the domain only. The dimension of the problem is thereby reduced by one, and the problem with domains of infinite extend simply vanishes! The study of integral equation methods spread relative quickly to scientists in acoustics, and numerical formulations based on integral equations for constant frequency sound fields were reported during the sixties in Banaugh 1963 [5], Chen & Schwikert 1963 [17], Chertock 1964 [20], Copley 1967 [27], and Schenck 1967 [78]. A very recommendable historical survey of boundary integral equation methods has recently been given by R.P.Shaw [92]. During the years several integral equation methods which operates by dividing the boundary of the domain into elements was proposed, and they may therefore all be referred to as Boundary Element Methods (BEM) [43,47,57,66, 91,94,104]. However, one of these numerical methods based on the surface Helmholtz integral equation has turnes out to be a particular powerful and yet general method, and in the later

years this method has almost become synonymous to the boundary element method. This last method is the subject of the present study.

In the early years, the numerical implementation of Helmholtz integral equation was most often carried out by assuming that the acoustic variables were constant on each element. A milestone in the development of boundary element methods was therefore the introduction of more advanced interpolation functions to represent both the variation of the acoustic variables and the geometry over the elements. These advanced interpolation functions were adopted from the finite element method by Seybert and his co-workers [18-19,80-90,93,106-110].

Apart from alleviating the problem with domains of infinite extend, the reduction of the three-dimensional partial differential equation to a two-dimensional integral equation has another important advantage, which is related to the generation of the mesh. At the present stage automatic three-dimensional mesh generators exist for special geometries only, and generating a mesh is often required to be an interactive process. Much effort has been put into visualizing such a three-dimensional mesh in order to allow the user to check the mesh. It is clear that a two-dimensional mesh, which suffies for boundary element calculations, is much easier to handle. Another advantage is the much less effort required to regenerate a two-dimensional mesh compared to the regeneration of a three-dimensional mesh, when a slight change of the geometry has been made, as often is the case when using numerical calculations for design. Hence, it is expected that the boundary element method will become a valuable tool even for problems where the finite element method is faster with respect to computer time, becaurse of the less required pre-processing time needed to generate and alter the mesh.

The present thesis presents the first work on the boundary element method carried out at The Acoustics Laboratory besides the authors M.Sc. thesis. The author has therefore attempted to write a text which hopefully may serve as a part of the basis for further investigation of the method. On one hand generality

and clarity has been stressed in the text, but on the other hand some details are given which may help the reader in implementing the formulations. Hence, at certain stages the level of detail is beyond the requirements of the average reader.

The thesis consists of four parts:

I) Theory, chapter 2 and 3

II) Numerical aspects, chapter 4,5, and 6

III) Applications, chapters 7 and 8

IV) Discussion and Conclusions, chapters 9 and 10

Chapter 2 concerns the basic theory, which is the development of Helmholtz integral equation and its physical interpretation. Chapter 3 contains a development of an axisymmetric integral equation formulation. Chapter 4 addresses the numerical treatment of the axisymmetric and the three-dimensional formulation from an integral equation into a set of linear equations. In this chapter test cases are also provided, and the topic of convergence is introduced. Chapter 5 addresses the non-uniqueness problem, which - albeit not being a numerical problem - becomes severe *due* to the numerical treatment. In chapter 6 some methods of solving a set of linear equations are outlined. Chapter 7 concerns the application of the axisymmetric formulation to calculations on standard microphones, and chapter 8 shows an application of the boundary element method to spectral stereo theory. Chapter 9 contains a discussion with some suggestions for further work, and chapter 10 collects the conclusion of each chapter to a general conclusion.

2. BASIC THEORY

In a homogeneous, inviscid, compressible fluid the propagation of sound waves is governed by the wave equation:

$$\nabla^2 p_{ins} = \frac{1}{c^2}\frac{\partial^2 p_{ins}}{\partial t^2} \ , \tag{2.1}$$

where p_{ins} is the instant variation of pressure from the equilibrium pressure often termed the sound pressure, the acoustic pressure or just the pressure when the context is clear. The speed of sound c is given by $c^2=(\gamma P_0/\rho_0)$, where P_0 is the static fluid pressure, ρ_0 the static density and γ is the ratio of specific heats. Equation (2.1) may be derived assuming that the linear terms of the continuity equation and the momentum equation are much larger than the non-linear terms. For waves propagating in air, which is the main subject of the present study, this assumption is valid for a large class of problems. However, the results presented here are valid in any fluid for which equation (2.1) is valid. For a derivation of equation (2.1) the reader could refer to e.g. Pierce [69] or Morse & Ingard [65].

For the mathematical treatment of equation (2.1) it is convenient to assume time-harmonic waves, so that $p_{ins}(x,y,z,t)=\mathrm{Re}\{p(x,y,z)e^{i\omega t}\}$, where i is the imaginary unit and ω is the circular frequency $\omega=2\pi f$, where f is the frequency. The complex sound pressure $p(x,y,z)$ is often shortened to p for convenience. Problems with non-harmonic time dependence may be analyzed by means of Fourier transformation. Introducing time-harmonic waves allows equation (2.1) to be reduced to the Helmholtz equation:

$$\nabla^2 p + k^2 p = 0 \ , \tag{2.2}$$

where the time factor $e^{i\omega t}$ is omitted. The wavenumber k is defined as $k=\omega/c$. If the particle velocity v (a complex vector) is desired, it can be found from

$$\boldsymbol{v} = \frac{i}{\omega \rho_0} \nabla p \ , \tag{2.3}$$

where bold lettering denotes vectors. Thus the velocity potential is not used in this text.

2.1 GREEN'S FUNCTION

For the following development the concept of the acoustic monopole or point source is essential. The point source is a mathematical abstraction, which can not be realized physically. However, it proves to be a convenient tool for the mathematical describtion of quite a large class of acoustic phenomena, e.g. far-field radiation from a source with dimensions much smaller than a wavelenght. The point source may be considered as the limiting case of a radially oscillating (pulsating) sphere, where the radius of the sphere tends to zero in such a manner that the source strength remains constant. The Green's function may be shown (see Pierce [69]) to be the solution to the following inhomogeneous equation:

$$(\nabla^2 + k^2) G_k(r, r_0) = -4\pi\delta(r - r_0) \ , \tag{2.4}$$

where there is a point source with unit source strength located at $r_0 = (x_0, y_0, z_0)$. The Green's function depends on the specified boundary conditions, which are assumed to be passive. The free-space Green's function $G(R)$ is the solution to equation (2.4) for unbounded medium:

$$G(R) = \frac{e^{-ikR}}{R} \ , \tag{2.5}$$

where $R = |r - r_0|$ is the distance between the point source and the observation point. Note that some authors do not use the factor 4π on the right side of equation (2.4) - this results in a factor $1/(4\pi)$ on the right side of equation (2.5).

2.2 SOMMERFELD'S RADIATION CONDITION

For one or several sources that are within a finite region

centered at the origin of a spherical coordinate system, the Sommerfeld's radiation condition holds. In spherical coordinates this condition states

$$\lim_{r\to\infty}\left[r\left(\frac{\partial p_{ins}}{\partial r}+\frac{1}{c}\frac{\partial p_{ins}}{\partial t}\right)\right]=0\ , \tag{2.6}$$

and for time-harmonic waves

$$\lim_{r\to\infty}\left[r\left(\frac{\partial p}{\partial r}+ikp\right)\right]=0\ . \tag{2.7}$$

The derivation of Sommerfeld's radiation condition is outlined in Pierce [69]. By using equation (2.5) in equation (2.7) it is simple to show that the free-space Green's function satisfies Sommerfeld's radiation condition. If one considers the fact that far away from the sources any radiated wave locally resembles a plane wave and thus $\boldsymbol{v}\approx np/(\rho_0 c)$, Sommerfeld's radiation condition may be stated:

$$\lim_{r\to\infty}[r(p-\rho_0 c v_r)]=0\ , \tag{2.8}$$

where v_r is the radial particle velocity. Equation (2.8) allows $\rho_0 c$ to be identified as the apparent impedance $z_0=p/v$ associated with a sphere when the radius of the sphere tends to infinity. This quantity is also often denoted the specific acoustic impedance or the characteristic impedance. Hence energy may dissapear at infinity - and this appears to be an important condition for uniqueness of acoustic boundary value problems (see e.g. Pierce [69]).

2.3 A MATHEMATICAL DEVELOPMENT OF HELMHOLTZ INTEGRAL EQUATION

The following development (see Pierce [69]) takes its starting point in the vector identity:

$$G(\nabla^2+k^2)p-p(\nabla^2+k^2)G=\nabla\cdot(G\nabla p-p\nabla G)\ , \tag{2.9}$$

which easily may be shown to be true by writing out the term on the right side. Integrating (2.9) over the volume V consisting of all points outside a surface S that are within a large

sphere of radius A results in

$$-\int_V p(\nabla^2+k^2)G \, dV = \int_V \nabla\cdot(G\nabla p - p\nabla G) \, dV \, , \qquad (2.10)$$

as $(\nabla^2+k^2)p=0$ within V. See figure 2-1 for definition of geometry but note that the sphere A is not shown in the figure.

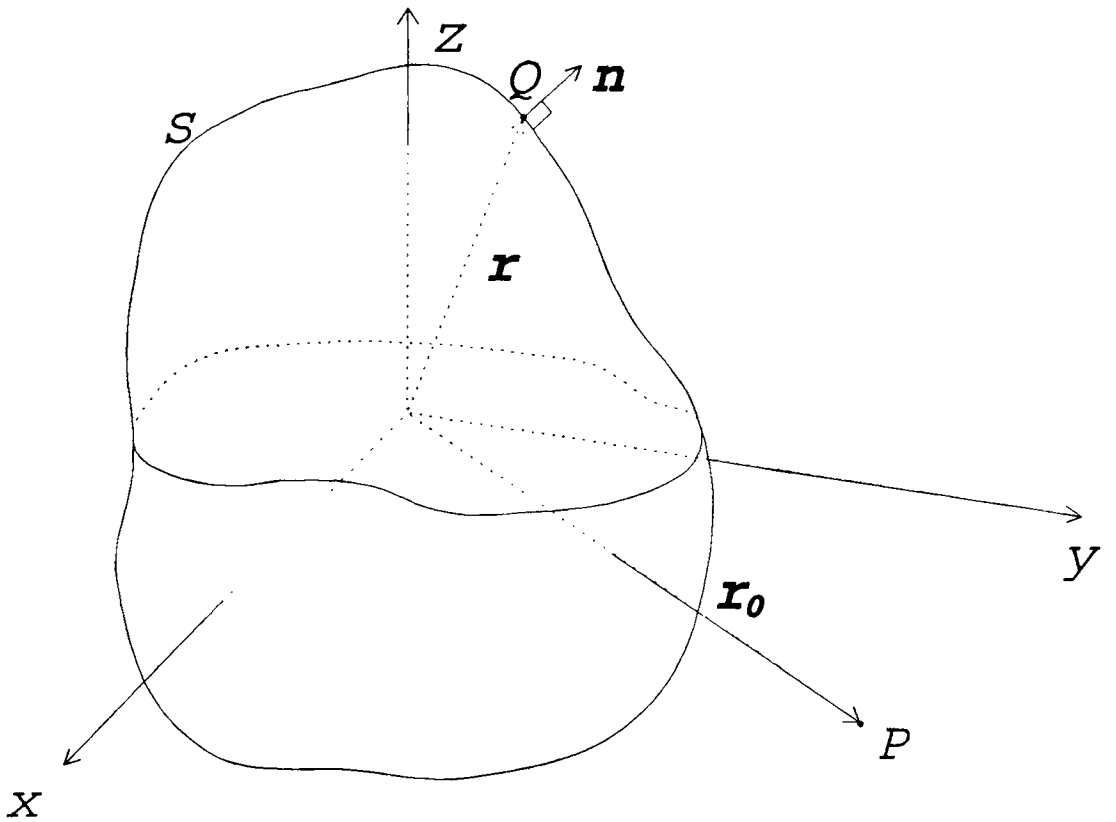

Figure 2-1. Sketch of the closed surface S, with indications of r, r_0, Q, P and n.

The integral on the right side of equation (2.10) may be transformed into a surface integral over S and over the outer sphere using Gauss' theorem:

$$-\int_V p(\nabla^2+k^2)G \, dV = -\int_S (G\nabla p - p\nabla G)\cdot n \, dS + I_A \, , \qquad (2.11)$$

where $\boldsymbol{n}$ is the unit vector perpendicular to S pointing into V, and

$$I_A = A^2 \int_0^{2\pi} \int_0^{\pi} \left(G \frac{\partial p}{\partial A} - p \frac{\partial G}{\partial A} \right) \sin\theta \, d\theta \, d\phi \ . \qquad (2.12)$$

Note that I_A is the only term in equation (2.11) which depends on A and hence I_A must be a constant. Now, let G be a Green's function $G_k(\boldsymbol{r}|\boldsymbol{r}_0)$. If G and p both satisfy Sommerfeld's radiation condition and goes towards zero at least as fast as $1/A$ for $A \to \infty$, it may be shown by using equation (2.7) in equation (2.12) that I_A vanishes as A goes to infinity, and hence $I_A=0$ for all A. Using equations (2.3) and (2.4) in equation (2.11) allows equation (2.11) to be rewritten as

$$4\pi \int_V p(\boldsymbol{r}) \, \delta(\boldsymbol{r}-\boldsymbol{r}_0) \, dV = \int_S p(\boldsymbol{r}) \frac{\partial G}{\partial n} + ikz_0 v(\boldsymbol{r}) G \, dS \ , \qquad (2.13)$$

where v is the particle velocity perpendicular to the surface S - also termed the normal velocity. Clearly the left side of equation (2.13) is zero for $\boldsymbol{r}_0$ within S and $4\pi p(\boldsymbol{r}_0)$ for $\boldsymbol{r}_0$ outside S. For $\boldsymbol{r}_0$ on the surface the left hand side equals $C(\boldsymbol{r}_0)p(\boldsymbol{r}_0)$ where $C(\boldsymbol{r}_0)$ is the solid angle measured from V [22]. This may be understood intuitively by approximating the delta function with a small sphere V_ϵ of radius ϵ centered at $\boldsymbol{r}_0$ so that

$$\Delta(\boldsymbol{r}-\boldsymbol{r}_0) = \begin{cases} \dfrac{1}{4/3\pi\epsilon^3} \ , & |\boldsymbol{r}-\boldsymbol{r}_0| \le \epsilon \\ 0 \ , & |\boldsymbol{r}-\boldsymbol{r}_0| > \epsilon \ . \end{cases} \qquad (2.14)$$

In the limit of small ϵ, p is constant within this small sphere, and hence it follows that the left side of equation (2.13) may be approximated as follows:

$$\begin{aligned} & p(\boldsymbol{r}_0) \int_V \Delta(\boldsymbol{r}-\boldsymbol{r}_0) \, dV \\ &= p(\boldsymbol{r}_0) \, 3/(4\pi\epsilon^3) \int_{V \cap V_\epsilon} 1 \, dV \\ &= p(\boldsymbol{r}_0) \psi \ , \end{aligned} \qquad (2.15)$$

where ψ is the solid angle measured from V. Alternatively it may be shown [81] that for $\boldsymbol{r}_0$ on the surface S

$$C(\boldsymbol{r}_0) = 4\pi + \int_S \frac{\partial}{\partial n}\left(\frac{1}{R}\right) dS \ , \qquad (2.16)$$

which is generally valid for any body having edges or corners. If the points P and Q are associated with $\boldsymbol{r}_0$ and $\boldsymbol{r}$ respectively, equation (2.13) may be rewritten as

$$C(P)p(P) = \int_S p(Q)\frac{\partial G(P,Q)}{\partial n} + ikz_0 v(Q)G(P,Q)\, dS \ . \qquad (2.17)$$

Hence equation (2.17) etablishes a relationship between the pressure $p(P)$ outside a vibrating body, and the pressure $p(Q)$ and the normal velocity $v(Q)$ on the body. Note that the pressure $p(Q)$ and the normal velocity $v(Q)$ on the body are related - only one of the two, or the ratio between them, may be specified independently on any part of the surface. Hence, if either the pressure or the normal velocity or the ratio between the two are known all over a closed body containing all sources, the pressure outside the body is uniquely given, and may be determined using equation (2.17). Note that the surface S may be any closed surface, and must not necessarily coincide with the surface of e.g. a radiating body.

Scattering problems may be handled by the traditional division of the total sound field into an incoming wave and a scattered wave [69]:

$$p = p^I + p^{sc} \ , \qquad (2.18)$$

where p^I is the complex amplitude of the incoming wave in absence of the body. The scattered wave p^{sc} satisfies Helmholtz equation and Sommerfeld's radiation condition. If an incoming wave is specified the scattering problem may be solved as an equivalent radiation problem where the boundary condition is fulfilled (e.g. v=0 for a rigid body). Hence equation (2.17) may be modified for scattering problems:

$$C(P)p(P) = \int_S p(Q)\frac{\partial G(P,Q)}{\partial n} + ikz_0 v(Q)G(P,Q)\, dS + 4\pi p^I(P) \ , \qquad (2.19)$$

where the incoming field is multiplied by 4π in order to match the factor 4π on the left side of equation (2.17) when P is

outside S.

Thus the tree-dimensional problem of acoustic radiation is reduced to a two-dimensional integral equation. Since Sommerfeld's radiation condition has been worked into equation (2.19) the solution to equation (2.19) will automatically satisfy the boundary condition at infinity. This gives numerical models based on equation (2.19) a major advantage over finite element and finite difference methods for calculating radiation or scattering problems.

Note that equations (2.17) and (2.19) allow some of the boundary conditions to be worked into the Green's function. If radiation or scattering from a body over a rigid plane is considered the half-space Green's function may be used to model the plane [87]. In this case only the surface of the radiating body rather than the entire surface of the body and the plane needs to be specified as the integration surface S, which is an important simplification for the numerical treatment. Hence, in some cases it is possible to take advantage of a 'trade-off' between the integration surface S and the Green's function. Vice versa equation (2.19) may be used to obtain Green's functions numerically for a complicated geometry by specifying the incoming field p^I as a point source and modelling the entire surface.

For interior problems a similar integral equation can be derived (see e.g. Baker and Copson [4]):

$$C^0(P)p(P) = \int_S p(Q)\frac{\partial G(P,Q)}{\partial \nu} + ikz_0 v_\nu G(P,Q)\, dS\,, \qquad (2.20)$$

where ν is the inward normal unit vector to S. For P on the surface S the term $C^0(P)$ equals the solid angle measured from inside the body, and may alternatively be calculated by [81]

$$C^0(P) = \int_S \frac{\partial}{\partial \nu}\left(\frac{1}{R}\right) dS\,. \qquad (2.21)$$

For P inside the surface S, $C^0(P)$ equals 4π, and for P outside the surface S, $C^0(P)$ vanishes.

2.4 A PHYSICAL INTERPRETATION OF HELMHOLTZ INTEGRAL EQUATION

In order to obtain a physical interpretation of Helmholtz integral equation one may turn to Huygens' principle, see Baker & Copson [4]. The standard 'text-book' version of Huygens' principle is to predict the wave front at some time $t_0+\Delta t$ as the envelope of secondary waves generated by secondary point sources placed at the wave front at $t=t_0$, see figure 2-2.

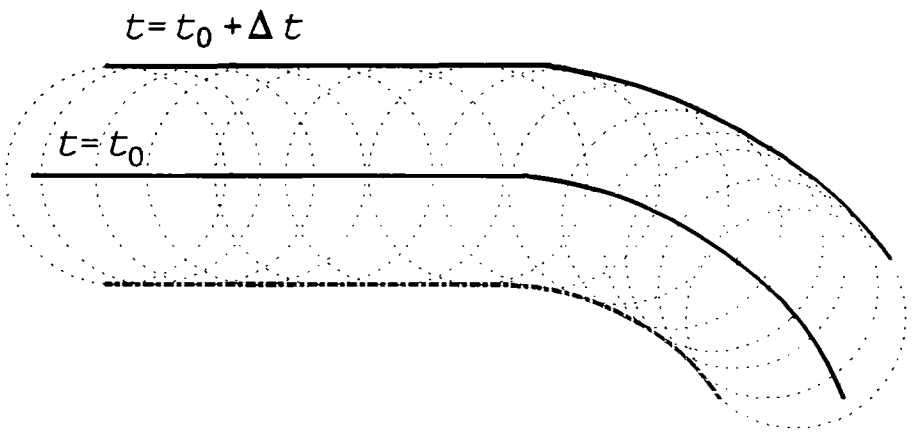

Figure 2-2. A simple construction following Huygens' principle. The bold dashed curve represents the undesired interior field.

The secondary sources each produce a spherical wave centred at the wave front at $t=t_0$ - their radii correspond to the speed of sound c multiplied by the elapsed time Δt. For this construction to be valid, the spacing between the secondary sources should be infinitesimally small, whereas the radii of the spheres (corresponding to Δt) may have a finite value. Hence, the resulting sound field outside a closed surface S is constructed by means of a distribution of monopoles over the surface. The corresponding numerical method of constructing the resultant sound field has been known as the simple source formulation.

In 1818 Fresnel made an important extention of Huygens' principle, see Baker & Copson [4]. For constant frequency

(monochromatic) fields, the resulting sound field should be constructed by interference of the field produced by sources placed on the surface S at some time $t=t_0$. Furthermore, since Fresnel considered a system of expanding waves, the field produced inside the surface shold be zero. As sketched in figure 2-2 the simple approach using only spherical waves does not ensure a null-field effect inside S, since positive interference also occurs at the bold dashed line in figure 2-2. Hence, an additional set of sources is needed in order to obtain the desired null-field inside S. Fresnel believed (although he never completed this programme) that this effect could be achived only by introducing a set of dipole sources on the surface. By introducing the set of dipoles on S the undesired field inside S can be cancelled without destoying the field outside S due to the direction dependance of the dipoles. The sound field outside S would then be generated by a combination of monopole and dipole sources. Clearly the strengths of the monopoles are not equal to the strengths found by the simple source formulation. Note that a formulation making use of dipole sources only - often denoted the double layer potential method - does not provide the desired null-effect inside S either.

Thus it is loosely justified that a formulation that satisfies Huygens' principle should contain a combination of monopole and dipole sources as does Helmholtz integral equation.

For a more rigorous development of these monopole and dipole terms, the following proof may be given, see Baker & Copson [4]. Consider a number of sources all lying inside a closed surface S as sketched in figure 2-1. Let Q be a typical point on S, P a point outside S and n the outward unit normal to S at Q. The distance between P and Q is r_1. With the time factor $e^{i\omega t}$ omitted, the pressure at Q is p_Q. The particle velocity along n is given by equation (2.3):

$$v(Q)=\frac{i}{\omega\rho_0}\frac{\partial p(Q)}{\partial n} \quad . \tag{2.22}$$

Thus air flows across the element dS at Q at the rate $v dS$. Due

to the pressure there is a force of magnitude $p_Q dS$ at Q as well. Now suppose that all the sources and all of the air inside S are destroyed. In order to reconstruct the effect outside S as specified by the 'late' sources, new sources must be introduced with the following properties:

a) Air should be created at dS at the rate $v dS$

b) A force $p_Q dS$ perpendicular to dS should act on the air in contact with dS.

The source strength $v dS$ at Q gives rise to a pressure p_1 at P of the magnitude [69]:

$$p_1 = i\omega\rho_0 \frac{1}{4\pi} \frac{e^{ikr_1}}{r_1} v_Q \, dS = ikz_0 \frac{e^{ikr_1}}{4\pi r_1} v_Q \, dS \, . \qquad (2.23)$$

According to Lamb [58, p.502] the force of magnitude $p_Q dS$ gives rise to a dipole of strength $p_Q dS/(4\pi)$, and hence the pressure p_2 at P due to the force is

$$p_2 = \frac{p_Q}{4\pi} \frac{\partial G(r_1)}{\partial n} dS \, . \qquad (2.24)$$

Thus the total pressure at P is the sum of p_1 and p_2 integrated over S:

$$p(P) = \int_S \frac{p_Q}{4\pi} \frac{\partial G(r)}{\partial n} + ikz_0 \frac{v_Q}{4\pi} G(r) \, dS \, , \qquad (2.25)$$

which is seen to be in agreement with equation (2.17).

2.5 CONCLUDING REMARKS

In chapter two the Helmholtz integral equation has been obtained by a mathematical development. The integral equation makes use of Green's function and automatically satisfies Sommerfeld's radiation condition. The integral equation was then justified from a more physical point of view using Huygen's principle. It may also be noted that the Helmholtz integral equation can be obtained from a purely numerical basis as a weighted residual statement of Helmholtz equation as shown in Brebbia [9].

The development of chapter two is summarised for convenience, and specialized to the case of exterior problems in free-

space.

For time-harmonic waves and with the time factor $e^{i\omega t}$ omitted, the Helmholtz integral formula can be expressed in terms of the complex pressure p and the complex surface velocity normal to the body v:

$$C(P)p(P) = \int_S \left(p(Q) \frac{\partial G(R)}{\partial n} + ikz_0 v(Q) G(R) \right) dS + 4\pi p^I(P) . \tag{2.26}$$

This formula is valid in an infinite homogeneous medium (e.g. air) outside a closed body B with a surface S. In the medium p satisfies $(\nabla^2+k^2)p=0$. Q is a point on the surface S, and P is a point either inside, on the surface of, or outside the body B. The quantity $R=|P-Q|$ is the distance between P and Q, and $G(R)=e^{-ikR}/R$ is the free-space Green's function; $k=\omega/c$ is the wavenumber, where ω is the circular frequency and c is the speed of sound; i is the imaginary unit and z_0 is the characteristic impedance of the medium; n is the unit vector perpendicular to the surface S at the point Q oriented away from the body. The quantity $C(P)$ has the value 0 for P inside B and 4π for P outside B. In the case of P on the surface S, $C(P)$ is the solid angle measured from the medium, and equals 2π for a smooth surface. In a scattering problem p^I is the complex pressure of the incident wave - in a radiation problem p^I vanishes.

3. AN AXISYMMETRIC INTEGRAL FORMULATION FOR NON-AXISYMMETRIC BOUNDARY CONDITIONS

In this chapter a formulation of the Helmholtz integral equation specialized to the case of an axisymmetric body in free space is developed. The main motivation for this work is the fact that the boundary element method as well as other element methods is quite computationally intensive with respect to time and storage. Hence, it is important to make use of any property that may reduce the time or storage needed to solve a problem within the desired accuracy.

3.1 PRELIMINARY CONSIDERATIONS

If the body is axisymmetric a reduction of both time and storage may be achieved. In this case the surface integral of the Helmholtz integral equation may be reduced to a combination of a line integral and an integral over the angle of revolution; only the former integral needs to be discretized, and thus the dimension of the problem is reduced to one. In order to allow for non-axisymmetric boundary conditions the sound field is expanded in a cosine series over the angle of revolution.

One of the complications in applying the boundary element method to a given problem is the evaluation of the integral in equation (2.26) when P is on the surface S. In this case the Green's function and its normal derivative becomes singular as Q approaches P. Although the singularities are integrable, they may give rise to numerical problems as will be demonstated in paragraph 4.3.4. This problem has been solved both for the general three-dimensional case [75,81], and for the case of an axisymmetric body with axisymmetric boundary conditions [82]. In the latter case the problem was efficiently handled by isolating the singularities and integrating them analytically using elliptic integrals.

Another paper [2] has been concerned with radiation from an axisymmetric body with a non-axisymmetric movement of the

surface using a cosine expansion around the axis of symmetry of the body. However, no use of elliptic integrals was made here and the integration over the angle of revolution had to be handled in a computationally inefficient manner.

Inspired by references [2] and [82] the author has developed an axisymmetric integral formulation for non-axisymmetric boundary conditions using a cosine expansion. The formulation is valid for both radiation and scattering problems. In order to optimize the formulation from a numerical point of view, the singularities of Green's function and its derivative are isolated in the integral of revolution, and the integrations are performed analytically using sums of elliptic integrals. Note that the cosine expansion is as general as a full Fourier expansion, since the total field can be expressed as superpositions of cosine expanded fields, where the expansion is rotated $\pi/(4m)$ with respect to the first expansion [2]. Here m refers to the m'th term in the cosine expansion as defined in equation (3.2). The result of this rotation corresponds to the sine term in a Fourier expansion. For scattering problems where the incident wave is plane or due to a point source, the coordinate system can always be chosen so that only a cosine expansion is needed; more general scattering problems (e.g. scattering problems where the incident wave is created by a dipole or several monopoles) must be treated by using the more general method mentioned above. The expansion is only useful for P on S, for P outside the body B, see Figure 3-1, the integral is non-singular and the integration is straightforward.

3.2 DEVELOPMENT OF AXISYMMETRIC INTEGRAL FORMULATION

For an axisymmetric body, as sketched in Figure 3-1 equation (2.26) becomes

$$C(P)p(P) = \int_L \int_0^{2\pi} \left(p(Q) \frac{\partial G(R)}{\partial n} + ikz_0 v(Q) G(R) \right) d\theta(Q) \rho(Q) dL(Q) + 4\pi p^I(P), \tag{3.1}$$

where a cylindrical coordinate system (ρ, θ, z) is used. The

expression for the $C(P)$ constants (equation (2.16)) may be reduced to

$$C(P) = 4\pi + \int_L \int_0^{2\pi} \frac{\partial}{\partial n}\left(\frac{1}{R}\right) d\theta(Q)\, \rho(Q)\, dL(Q) \ . \qquad (3.2)$$

In the fully symmetric case, (where the boundary conditions are axisymmetric as well, $p(Q)$ and $v(Q)$ are constants with respect to θ. Thus they can be set outside the integration with respect to θ, and thereby the discretization around the θ-axis can be omitted so that the dimension of the problem is reduced to one, as mentioned above.

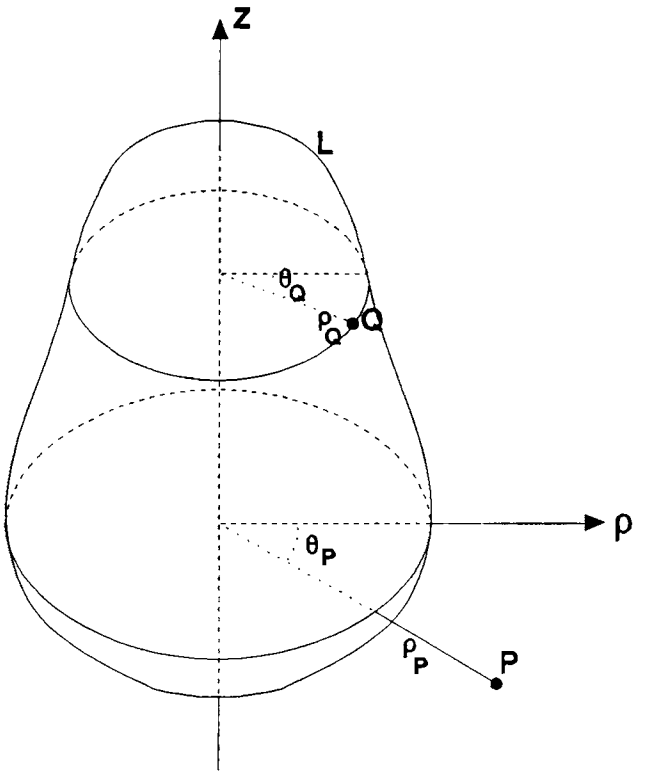

Figure 3-1. An axisymmetric body B i a cylindrical coordinate system (ρ,θ,z). The generator L is indicated as well as Q and P.

3.2.1 COSINE EXPANSION

Now suppose that $p(Q)$ and $v(Q)$ can be expanded in cosine series:

$$p(Q) = \sum_{m=0}^{\infty} p_m \cos m\theta_Q \ ,$$
$$v(Q) = \sum_{m=0}^{\infty} v_m \cos m\theta_Q \ . \tag{3.3}$$

Note that in the fully symmetric case all terms except $m=0$ vanish. Letting P be a point on the generator in the ρ-z plane ($\theta_P=0$), and shortly writing θ for θ_Q and making use of the orthogonality of the cosine terms yield the following equation for a given value of m:

$$\begin{aligned} C(P)p_m(P) = &\int_L p_m(Q) \left[\int_0^{2\pi} \cos m\theta \frac{\partial}{\partial n}\left(\frac{e^{-ikR}}{R}\right) d\theta\right] \rho_Q \, dL_Q \\ &+ ikz_0 \int_L v_m(Q) \left[\int_0^{2\pi} \cos m\theta \frac{e^{-ikR}}{R} d\theta\right] \rho_Q \, dL_Q \\ &+ 4\pi p_m^I(P) \ . \end{aligned} \tag{3.4}$$

For a scattering problem where the incident wave is created by a monopole, the coordinate system should be oriented so that the monopole is placed in the first or fourth quadrant of the ρ-z plane. For a plane wave the orientation should be so that the above condition holds when the plane wave is modeled by a very distant monopole. The equations for the expansion of the incident wave is then

$$p_m^I(P) = \left\{ \begin{array}{ll} \frac{1}{2\pi}\int_0^{2\pi} p^I(P) \, d\theta & , m=0 \\ \frac{1}{\pi}\int_0^{2\pi} \cos m\theta \, p^I(P) \, d\theta & , m=1,2,.. \end{array} \right\} . \tag{3.5}$$

Because of the symmetry the integrals can be simplified to

$$p_m^I(P) = \left\{ \begin{array}{ll} \frac{1}{\pi}\int_0^{\pi} p^I(P) \, d\theta & , m=0 \\ \frac{2}{\pi}\int_0^{\pi} \cos m\theta \, p^I(P) \, d\theta & , m=1,2,.. \end{array} \right\} . \tag{3.6}$$

For the cosine expansion of e.g. a prescribed normal velocity a

quite analogous formula is valid.

In the special case where the incident wave is a plane wave (dimensionless for convenience) with $\arg(p^I)=0$ in the origin of the coordinate system and travelling along the negative ρ-axis (i.e. $p^I = e^{ik\rho} = \cos(k\rho) + i\,\sin(k\rho)$), the integrals in equation (3.6) can be solved analytically, noting the θ dependence of $\rho=\rho_P$, where ρ_P is the ρ-coordinate of P. The integral in equation (3.6) then becomes

$$\int_0^{\pi} \cos m\theta \,(\cos k(\rho_P \cos\theta) + i \sin k(\rho_P \cos\theta))\, d\theta \ , \qquad (3.7)$$

which equals [40, p.402]:

$$\pi \cos\frac{m\pi}{2} J_m(k\rho_P) \ + \ i\pi \sin\frac{m\pi}{2} J_m(k\rho_P) \ , \qquad (3.8)$$

and therefore the incident plane wave can be written as

$$p^I(P) = J_0(k\rho_P) \ + \ 2\sum_{m=1}^{\infty} i^m J_m(k\rho_P) \ , \qquad (3.9)$$

in agreement with a solution given by Morse and Ingard [65, p.401]. In general cases equation (3.6) has to be integrated numerically.

3.2.2 EXPRESSION USING ELLIPTIC INTEGRALS

The integrals of revolution in equation (3.4) can be solved partly analytically using elliptic integrals. For this purpose it is convenient to introduce the quantities

$$F^A(P,Q,m) = \int_0^{2\pi} \cos m\theta \, \frac{e^{-ikR}}{R} \, d\theta \qquad (3.10)$$

and

$$F^B(P,Q,m) = \int_0^{2\pi} \cos m\theta \, \frac{\partial}{\partial n}\left[\frac{e^{-ikR}}{R}\right] d\theta \ . \qquad (3.11)$$

The distance $R=R(P,Q)$ may be written as

$$R = R(P,Q) = \sqrt{\rho_Q^2 + \rho_P^2 + (z_Q - z_P)^2 - 2\rho_Q\rho_P\cos\theta} \quad , \tag{3.12}$$

from which it can be seen that the integrals in equations (3.10) and (3.11) are symmetric with respect to θ and equals twice the integrals over only half a period. This is significant for the computational efficiency. In order to isolate the singularity in equation (3.10), equation (3.10) may be rewritten as

$$\begin{aligned} F^A = F^A(P,Q,m) &= F_1^A(P,Q,m) + F_2^A(P,Q,m) \\ &= F_1^A + F_2^A \\ &= 2\int_0^\pi \cos m\theta \left[\frac{e^{-ikR}-1}{R}\right] d\theta \\ &\quad + 2\int_0^\pi \cos m\theta \, \frac{1}{R}\, d\theta \ . \end{aligned} \tag{3.13}$$

Since F_1^A is non-singular, the attention is drawn to F_2^A. Defining

$$R^2 = (\rho_Q + \rho_P)^2 + (z_Q - z_P)^2 \tag{3.14}$$

gives

$$R = \sqrt{R^2 - 2\rho_Q\rho_P(1+\cos\theta)} \quad , \tag{3.15}$$

and substituting this into equation (3.10) yields

$$\begin{aligned} K_2^A &= 2\int_0^\pi \frac{\cos m\theta \, d\theta}{\sqrt{R^2 - 2\rho_P\rho_Q(1+\cos\theta)}} \\ &= \frac{2}{R}\int_0^\pi \frac{\cos m\theta \, d\theta}{\sqrt{1 - \frac{2\rho_P\rho_Q}{R^2}(1+\cos\theta)}} \\ &= \frac{2}{R}\int_0^\pi \frac{\cos m\theta \, d\theta}{\sqrt{1 - \frac{\bar{K}^2}{2}(1+\cos\theta)}} \ , \end{aligned} \tag{3.16}$$

where $\bar{K}^2 = 4\rho_Q\rho_P/R^2$. Substituting

$$\psi = \frac{\pi}{2} - \frac{\theta}{2} \; ; \; \frac{d\theta}{d\psi} = -2 \qquad (3.17a,\ 3.17b)$$

into equation (3.16) then yields

$$\begin{aligned} F_2^A &= \frac{2}{R}\int_{\frac{\pi}{2}}^{0} \frac{\cos m(\pi - 2\psi)\ (-2)\ d\psi}{\sqrt{1-\bar{K}^2\sin^2\psi}} \\ &= (-1)^m\ \frac{4}{R}\int_0^{\frac{\pi}{2}} \frac{\cos 2m\psi\ d\psi}{\sqrt{1-\bar{K}^2\sin^2\psi}} \qquad (3.18) \\ &= (-1)^m\ \frac{4}{R} X_m\ . \end{aligned}$$

Since [95]

$$\begin{aligned} \cos 2m\psi = \frac{1}{2}\Bigg\{ &(2\cos\psi)^{2m} - \frac{2m}{1}(2\cos\psi)^{2m-2} \\ &+ \frac{2m}{2}\binom{2m-3}{1}(2\cos\psi)^{2m-4} - \frac{2m}{3}\binom{2m-4}{2}(2\cos\psi)^{2m-6} \\ &+ \frac{2m}{4}\binom{2m-5}{3}(2\cos\psi)^{2m-8} - \ldots \Bigg\}\ , \end{aligned} \qquad (3.19)$$

X_m in equation (3.18) can be written as linear combinations of integrals of the type

$$I_n = \int_0^{\frac{\pi}{2}} \frac{\cos^n\psi\ d\psi}{\sqrt{1-\bar{K}^2\sin^2\psi}}\ ,\ n = 0,2,4,6,\ldots \quad . \qquad (3.20)$$

Integrals of this type can be looked up in tables [40, pp.158-162]. For the first two terms

$$I_0 = K(\bar{K}) \qquad (3.21)$$

and

$$I_2 = \frac{1}{\bar{K}^2}E(\bar{K}) - \frac{\bar{K}'^2}{\bar{K}^2}K(\bar{K}) \qquad (3.22)$$

is found. Here $\bar{K}' = \sqrt{1-\bar{K}^2}$. K and E are the complete elliptic integrals of the first and the second kind defined as

$$K(\bar{k}) \equiv \int_0^{\frac{\pi}{2}} \frac{d\psi}{\sqrt{1-\bar{k}^2\sin^2\psi}} , \tag{3.23}$$

$$E(\bar{k}) \equiv \int_0^{\frac{\pi}{2}} \sqrt{1-\bar{k}^2\sin^2\psi}\, d\psi . \tag{3.24}$$

Elliptic integrals are well known [15], and fast algorithms for calculation exist [1, pp.598-599]. Having evaluated the two integrals and thus equations (3.21) and (3.22), the recursive formula to calculate I_n may finally be used:

$$I_n = \frac{n-2}{n-1}\frac{2\bar{k}^2-1}{\bar{k}^2} I_{n-2} + \frac{n-3}{n-1}\frac{\bar{k}'^2}{\bar{k}^2} I_{n-4} \; ; \; n = 4,6,.. \tag{3.25}$$

As $\bar{k}$ in equations (3.22) and (3.25) is the denominator of a fraction, special formulations have to be specified for the case of $\bar{k}=0$. It is obvious from equation (3.23) that $I_0=\pi/2$ for $\bar{k}=0$, and by partial integration of equation (3.20) with $\bar{k}=0$

$$I_n = \frac{n-1}{n} I_{n-2} \; ; \; \bar{k} = 0 \tag{3.26}$$

is obtained. The integral in equation (3.10) is now completely described.

A similar approach may be used to solve the integral in equation (3.11):

$$\begin{aligned} F^B = F^B(P,Q,m) &= F_1^B(P,Q,m) + F_2^B(P,Q,m) \\ &= F_1^B + F_2^B \\ &= 2\int_0^{\pi} \cos m\theta \, \frac{\partial}{\partial n}\left[\frac{e^{-ikR}-1}{R}\right] d\theta \\ &\quad + 2\int_0^{\pi} \cos m\theta \, \frac{\partial}{\partial n}\frac{1}{R}\, d\theta . \end{aligned} \tag{3.27}$$

By writing

$$F_1^B = 2\int_0^\pi \cos m\theta \frac{\partial R}{\partial n}\frac{\partial}{\partial R}\left(\frac{e^{-ikR}-1}{R}\right) d\theta$$
$$= 2\int_0^\pi \cos m\theta \frac{\partial R}{\partial n}\frac{1-e^{-ikR}(1+ikR)}{R^2} d\theta \qquad (3.28)$$

it can be shown that the integrand in F_1^B is non-singular. Consider now F_2^B. Since the body is axisymmetric, the normal derivatives have no component in the θ-direction. Putting the differentiation outside the integration it is seen that the resulting integral equals F_2^A so that F_2^B becomes

$$F_2^B = \frac{\partial}{\partial n}\left((-1)^m \frac{4}{R} X_m\right) . \qquad (3.29)$$

In evaluating this expression the normal derivative of X_m is needed, and since X_m may be written as a linear combination of the integrals defined in equation (3.20) the derivatives

$$\frac{\partial I_n}{\partial n} = \frac{\partial \bar{K}}{\partial n}\frac{\partial}{\partial \bar{K}} I_n \qquad (3.30)$$

must be computed. Using [15]

$$\frac{\partial}{\partial \bar{K}} K(\bar{K}) = \frac{\partial}{\partial \bar{K}} I_0 = \frac{E(\bar{K}) - \bar{K}'^2 K(\bar{K})}{\bar{K}\,\bar{K}'^2} \qquad (3.31)$$

and

$$\frac{\partial}{\partial \bar{K}} E(\bar{K}) = \frac{E(\bar{K}) - K(\bar{K})}{\bar{K}} , \qquad (3.32)$$

the result

$$\frac{\partial}{\partial \bar{K}} I_2 = \frac{(2-\bar{K}^2) K(\bar{K}) - 2E(\bar{K})}{\bar{K}^3} \qquad (3.33)$$

is obtained. As the derivatives of equation (3.21) and equation (3.22) are now known, the differentiation of equation (3.25) can be performed:

$$\frac{\partial I_n}{\partial \bar{K}} = \frac{n-2}{n-1}\left[\frac{2}{\bar{K}^3} I_{n-2} + \frac{2\bar{K}^2-1}{\bar{K}^2}\frac{\partial I_{n-2}}{\partial \bar{K}}\right] + \frac{n-3}{n-1}\left[\frac{1-\bar{K}^2}{\bar{K}^2}\frac{\partial I_{n-4}}{\partial \bar{K}} - \frac{2}{\bar{K}^3} I_{n-4}\right] ; \quad n = 4,6,.. \tag{3.34}$$

Once again special care has to be taken when $\bar{k}=0$. By differentiation of equation (3.20) with respect to $\bar{k}$, and then setting $\bar{k}=0$ one obtains

$$\frac{\partial}{\partial \bar{K}} I_n = 0 \quad ; \bar{K} = 0 \; . \tag{3.35}$$

The integrals around the axis of symmetry are now completely described, and equation (3.4) may be rewritten using the quantities F^A and F^B:

$$C(P)p_m(P) = \int_L [\, p_m(Q)F^B(P,Q,m) + ikz_0 v_m(Q)F^A(P,Q,m)\,]\rho_Q \, dL_Q + 4\pi p_m^I(P) \; , \tag{3.36}$$

where

$$C(P) = 4\pi + \int_L F_2^B(P,Q,0)\,\rho(Q)\, dL_Q \; . \tag{3.37}$$

In a radiation or a scattering problem the total pressure on the body B may be found as a sum of cosine expanded pressures obtained by solving equation (3.36):

$$p(P,\theta) = \sum_{m=0}^{\infty} p_m(P)\cos\theta \; . \tag{3.38}$$

In practice only a finite number of p_m-terms are needed to ensure an accurate prediction of the pressure p on the body. Having both the pressure p and the normal velocity v on the body, the pressure outside the body is most conveniently obtained by quadrature of equation (3.1), since equation (3.1) for P outside B is non-singular.

3.3 CONCLUDING REMARKS

In this chapter an axisymmetric integral equation that allows for non-axisymmetric boundary conditions has been formulated. The formulation is a simplification of the general three-dimensional Helmholtz integral equation to bodies with axisymmetric shape. By making use of a cosine expansion, the unknown variable, which is usually the pressure, at any point on or outside the radiating or scattering body can be determined by the value on the generator for each term of the expansion. One of the advantages of this formulation is that only the generator of the body needs to be discretized resulting in shorter calculation time and less required storage for a given accuracy. Another advantage which significantly reduces the calculation time is associated with the analytical evaluation of the singularities in Green's function and its derivative.

4. NUMERICAL IMPLEMENTATION

Helmholtz integral equation (2.26) may be solved analytically only for a small number of bodies with simple shapes. In order to solve problems where the body has a more complex shape, numerical methods must be used. The purpose of this chapter is to give a rough survey of how the integral equation may be solved numerically. Then a brief account of some numerical concepts will be given in order to justify the reasons for the more sophisticated numerical methods commonly used.

4.1 A ROUGH NUMERICAL SOLUTION OF HELMHOLTZ INTEGRAL EQUATION

For convenience the problem of scattering by a rigid body is initially considered. In this case the normal velocity on the surface of the body v is zero, and hence equation (2.26) reduces to:

$$C(P)\,p(P) = \int_S p(Q)\,\frac{\partial G(R)}{\partial n}\,dS + 4\pi p^I(P)\ . \qquad (4.1)$$

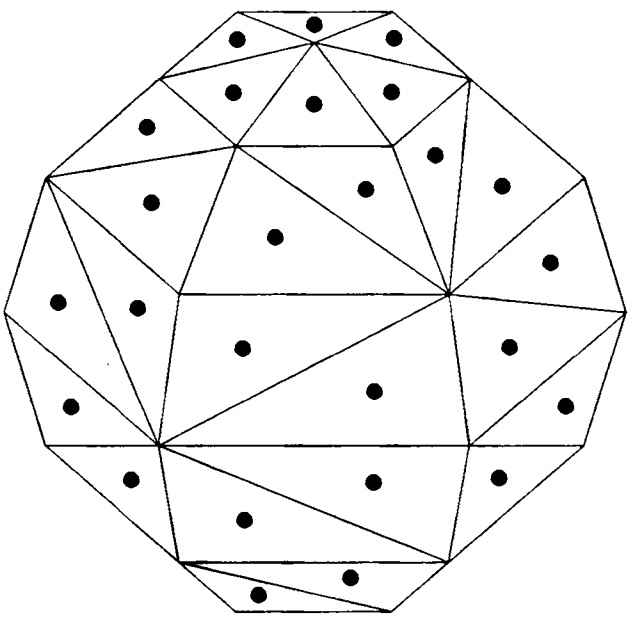

Figure 4-1. A body divided into triangular planar elements. The nodes in the centre of each element are shown as bold dots.

Now suppose that the body is divided in N triangular planar elements as sketched in Figure 4-1. Equation (4.1) may then be approximated by the following equation:

$$C(P)p(P) \approx \sum_{j=1}^{N} \int_{S_j} p(Q) \frac{\partial G(R)}{\partial n} \, dS_j + 4\pi p^I(P) \ , \qquad (4.2)$$

where the approximation is due to the representation of a general curved body by planar elements. Clearly the error due to this approximation tends to zero as the number of elements tends to infinity. In order to be able to evaluate the integrals of equation (4.2) the pressure is assumed to be constant within each element. Equation (4.2) may then be approximated by

$$\begin{aligned} C(P)p(P) &\approx \sum_{j=1}^{N} \left[p_j \int_{S_j} \frac{\partial G(R)}{\partial n} dS \right] + 4\pi p^I(P) \\ &= p_1 h_{P1} + p_2 h_{P2} + \cdots + p_N h_{PN} + 4\pi p^I(P) \ , \end{aligned} \qquad (4.3)$$

where the pressures p_j are constants representing the value of the sound pressure at the centre of each planar element - these values are termed the nodal values. The coefficients h_{Pj} of each p_j are integrals of the normal derivative of the Green's function over the j'th element, and hence these coefficients depend on the position of P and on the element in question. The assumption of constant pressure over each element causes the pressure to be discontinuous from one element to another on the surface of the scattering body, although the pressure will always be at least continuous when scattering from a closed rigid body is considered. However, the error due to the assumption of constant pressure over each element also tends to zero as the number of elements tends to infinity.

In order to obtain N equations to match the N unknown pressures of equation (4.3) two strategies may be chosen:

a) The interior formulation (see e.g. Copley [27]), where N calculation points are placed at different locations inside the body as sketched for the two-dimensional case in Figure 4-2 a). For each calculation point P_i equation (4.3) now states:

$$0 = p_1 h_{i1} + p_2 h_{i2} + \ldots + p_N h_{iN} + 4\pi p^I(P_i) \ , \qquad (4.4)$$

since $C(P_i)=0$ for P_i inside the body. Using N calculation points yields N equations and the problem may then be stated in matrix form:

$$\boldsymbol{H}\boldsymbol{p} = -4\pi \boldsymbol{p}^I \ , \qquad (4.5)$$

where capital bold symbols denote matrices and lower case bold symbols denote vectors. The p vector of equation (4.5) contains the unknown nodal pressures and the $\boldsymbol{p}^I$ vector on the right-hand side of the equation contains the nodal pressure of the incoming wave in absence of the body. The element h_{ij} of matrix H is the integral of the normal derivative of Green's function over the j'th element with respect to the i'th calculation point.

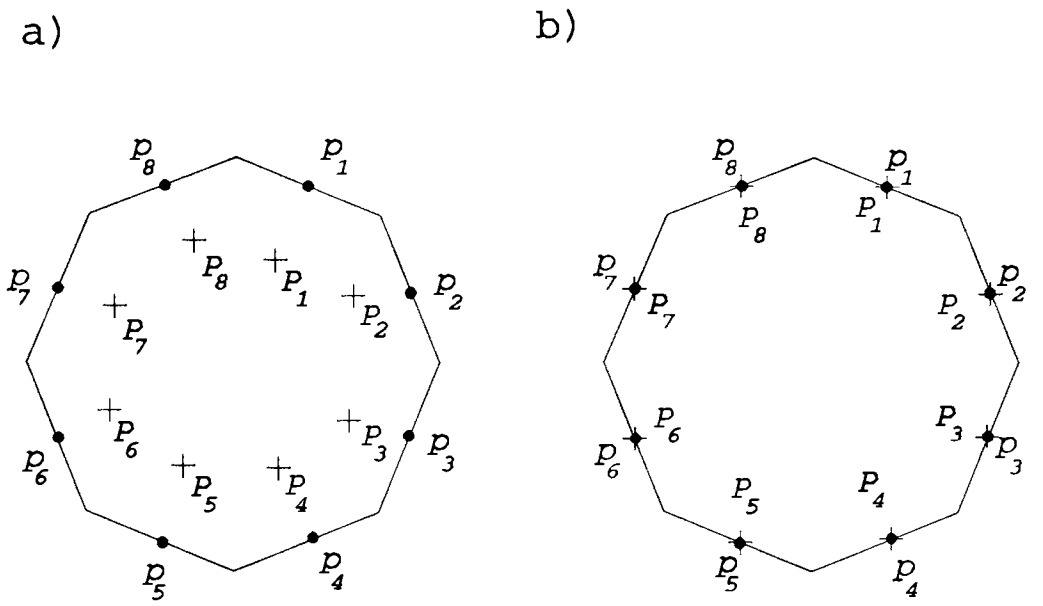

Figure 4-2. The position of calculation points P_i indicated by + for a) the interior formulation and b) the surface formulation. The nodal points are also shown as bold dots with the nodal pressures indicated.

b) The surface formulation (see Chertock [20]), where the N calculation points are placed at the nodes on the surface of the body, see Figure 4-2 b). Due to the planar geometry of the elements the local solid angle $C(P_i)=2\pi$ at all nodes. Hence, for P placed at node number m equation (4.3) states

$$2\pi p_m = p_1 h_{m1} + p_2 h_{m2} + \cdots + p_m h_{mm} + \cdots + p_N h_{mN} \ . \qquad (4.6)$$

The resulting matrix formulation is obtained by placing the N calculation points at the N nodes in the centre of the N elements:

$$(\boldsymbol{H}-2\pi \boldsymbol{I}_N)\boldsymbol{p} = -4\pi \boldsymbol{p}^I \ , \qquad (4.7)$$

where $\boldsymbol{I}_N$ is the N-by-N identity matrix. The symbols in equation (4.7) are similar to the symbols of equation (4.5) although the elements of the $\boldsymbol{H}$ matrix are not identical.

In order to be able to treat radiation problems an approach similar to the one outlined above may be used to discretize the surface integral concerning the normal velocity i.e. the second term of the integral in equation (2.26). Defining the normal velocity at the same nodes as for the pressure, and using the same surface mesh yields the following matrix equation for the discretized problem:

$$\begin{aligned} & 2\pi \boldsymbol{I}\boldsymbol{p} = \boldsymbol{H}\boldsymbol{p} + \boldsymbol{G}\boldsymbol{v} + 4\pi \boldsymbol{p}^I \\ \Updownarrow & \\ & (\boldsymbol{H}-2\pi \boldsymbol{I}_N)\boldsymbol{p} = \boldsymbol{G}\boldsymbol{v} + 4\pi \boldsymbol{p}^I \ , \end{aligned} \qquad (4.8)$$

valid for the surface formulation. Here the element g_{ij} of the matrix $\boldsymbol{G}$ is the integral of the function $ikz_0 G(R)$ over the j'th element with respect to the i'th calculation point. For the interior formulation a similar equation arises with the left-hand side of equation (4.8) replaced by zero. Note that the matrices $\boldsymbol{H}$ and $\boldsymbol{G}$ also can be interpreted as integral operators that exactly represent equation (2.26) [41,76]. Scattering from bodies with a finite surface impedance may be treated using the impedance relation $\boldsymbol{p} = -\boldsymbol{Z}\boldsymbol{v}$, where $\boldsymbol{Z}$ is the impedance matrix -

the negative sign is due to the fact, that the velocity is calculated along the outward normal to the surface. For a locally reacting surface Z has non-zero elements in the diagonal only. In all these cases the matrix equation (4.8) may be transformed into the familiar system of N equations with N unknowns by specifing the boundary conditions and, if desired, the incoming wave.

Thus Helmholtz integral equation may be treated numerically by dividing the body into small elements. On each element the pressure and the normal velocity are assumed to be constant, so that the unknown continuous pressure distribution is replaced by a finite number (N) of nodal values. The N unknown pressures are then matched with N equations by evaluating the integral equation at N calculation points (also termed collocation points) either inside the body or on the surface of the body.

4.2 A DISCUSSION OF THE SURFACE FORMULATION AND THE INTERIOR FORMULATION

The major disadvantage of the surface formulation is concerned with the evaluation of the elements in the diagonal of the matrices H and G. Since the calculation point is placed on the surface of the body the Green's function and its normal derivative become singular in these integrals. Analytically there is no problem, since the integrals are integrable in the normal sence, but as will be demonstrated in paragraph 4.3.4 standard numerical methods of integration has problems with singular integrals. Hence, special care must be taken when evaluating these integrals as described in references [8,29, 75,81]. The advantage of the surface formulation is due to the 2π terms, which are to be subtracted in the diagonal of the H matrix of equation (4.7). As the mesh is refined, the elements of H decrese towards zero and hence the resulting matrix $H-2\pi I$ to be inverted tends to be increasingly more diagonal dominant. This is a very desirable behaviour from a computational point of view.

The interior formulation has no problems with singularities since the calculation points are placed inside the surface, but

consequently the 2π terms in the diagonal of the resulting matrix to be inverted are missing. In order to still maintain a diagonal dominance of the matrix H in equation (4.5), the calculation points are usually placed on some related surface inside S as sketched in Figure 4-3 a). These formulations are in the following referred to as 'related interior' formulations [27,30,102]. The problem with these formulations emerges with the selection of calculation points. If two calculation points are placed at the same location, the resulting two equations (of equation (4.4)) are identical, and the resulting matrix is singular and cannot be inverted. Similarly, if two calculation points are placed close to one another, the two resulting equations are almost identical and the resulting matrix almost singular. For slender bodies or bodies having sharp edges it is difficult to choose well spaced calculation points as illustrated in Figure 4-3 b).

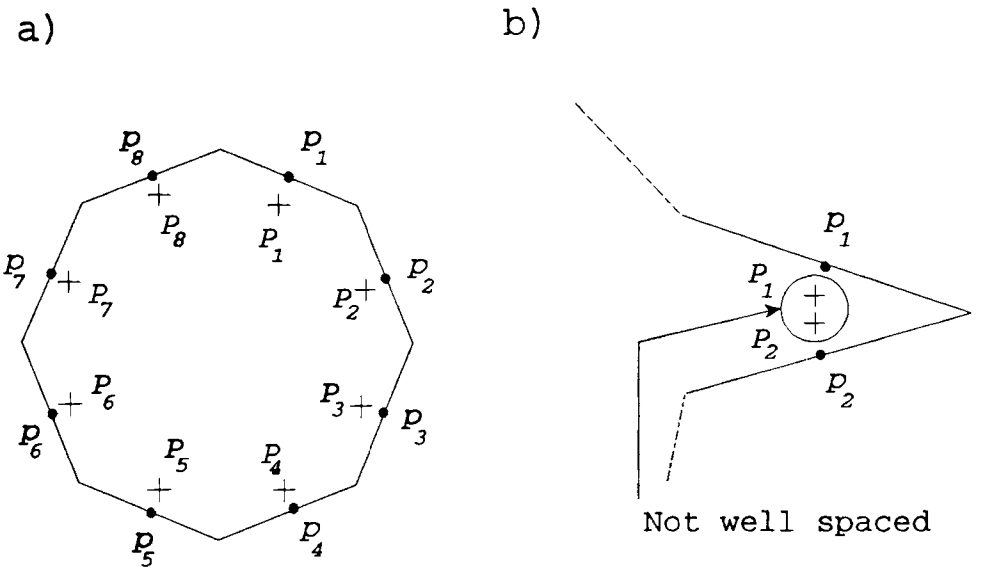

Figure 4-3. The related interior approach. a) The calculation points are placed on a related surface near the nodes. b) Body with a sharp corner resulting in closely spaced calculation points.

For the resons stated above, the author prefers the surface formulation - it also seems to be the most popular formulation when reviewing the literature [3,6,18-22,31,35-38,42,44,54-55, 59,61-63,78-90,93,97-101,105-110].

4.3 NUMERICAL INTEGRATION AND THE CONCEPT OF ORDER

As it has been demonstrated in section 4.1, the numerical solution of Helmholtz integral equation may be divided into two major tasks: Numerical integration over the surface of the body in order to obtain the elements in the H and G matrices, and solution of the resulting system of linear equations. Hence numerical integration is an important part of the total numerical solution, and is in fact often the most time consuming part of the total solution. Furthermore, some of the concepts of numerical integration may be used to explain the reasons for using more advanced functions to represent the variation of the pressure and the normal velocity than the constant value assumed in section 4.1.

4.3.1 THE LEFT RIEMAN SUM

Consider the numerical evaluation of the integral

$$\int_a^b f(x)\,dx \ , \tag{4.9}$$

where $f(x)$ is a known function. Normally, a solution is desired which is suffiently accurate and obtained with as few evaluations of $f(x)$ as possible, since the computational time comsumption almost always lies in the evaluation of $f(x)$. For a simple numerical evaluation of equation (4.9) the interval [a,b] is divided into n small, equally sized elements of length $h=(a-b)/n$, as shown in Figure 4-4 a). The left Riemann sum is defined as the sum of the areas of the rectangular boxes with the height equal to the functions value in the start of each small interval and the width $h=(b-a)/n$:

$$R_n^L = h\sum_{s=0}^{n-1} f(a+sh) \ . \tag{4.10}$$

In order to investigate the convergence of the equation (4.10) it is assumed that $f\in C^1$, where C^1 is the set of functions for which the first derivative exists and is continuous. Consider the first element [a,a+h]; Taylor's formula for f states:

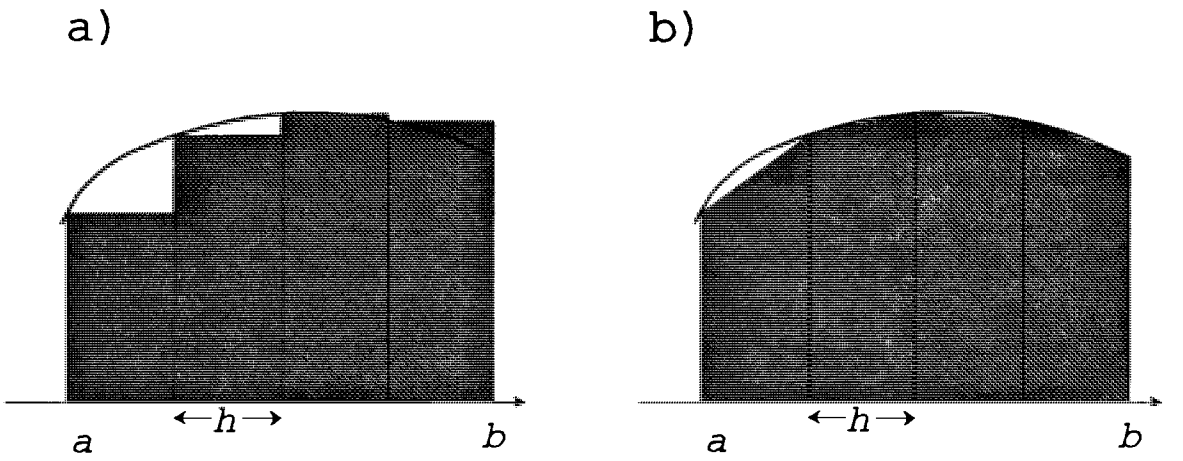

Figure 4-4. Numerical integration as a sum of areas. a) The left Rieman sum; b) The trapeziodal rule

$$f(x) = f(a) + (x-a)\,f'(\xi) \;;\quad a<\xi<a+h \;, \tag{4.11}$$

where f' denotes df/dx, and ξ is an unknown point in the interval. Integrating equation (4.11) over the interval $[a,a+h]$ then yields

$$\begin{aligned}\int_a^{a+h} f(x)\,dx &= \int_a^{a+h} f(a) + (a-h)\,f'(\xi)\,dx \\ &= hf(a) + \frac{h^2}{2} f'(\xi) \;.\end{aligned} \tag{4.12}$$

Adding n terms of this kind yields the integral over the entire interval $[a,b]$:

$$\int_a^b f(x)\,dx = h\sum_{s=0}^{n-1} f(a+sh) + h\,\frac{b-a}{2}\,f'(\xi_n) \;. \tag{4.13}$$

Hence equation (4.10) calculates the desired integral with a certain error given by the difference between equations (4.13) and (4.10). This error is termed the truncation error since it is made by truncating the Taylor series for $f(x)$ after a number of terms, which in this case is one. If $f'(x)$ is sufficiently smooth, the truncation error tends to zero asymptotically like h or $1/n$ when n tends to infinity. The left Rieman sum is said to be an integration formula of order one (q=1), since a reduc-

tion of the element length from h to $h/2$ halves the truncation error, i.e. $err_{2n}/err_n=(1/2)^q=1/2$ for $q=1$.

4.3.2 THE TRAPEZIODAL RULE

In order to obtain faster convergence one could consider the trapezoidal rule. In this case the function is approximated by a straight line between the values of the endpoints of each element as shown in Figure 4-4 b). Hence, the integral is approximated by a sum of areas of trapezoids, which gives the formula its name. For the trapezoidal rule the following relation can be obtained [14]:

$$\int_a^b f(x)dx = h\left[\frac{1}{2}(f(a)+f(b))+\sum_{s=1}^{n-1} f(a+sh)\right]-h^2\frac{b-a}{12}f''(\xi_n) \quad , \tag{4.14}$$

where it is assumed that $f\in C^2$. The order q of the trapeziodal rule is two since if h is reduced to $h/2$ the truncation error reduced to $(1/2)^2 = 1/4$.

Roughly, these numerical integration formulas can be said to be constructed by dividing the interval to be integrated into elements. The function is then interpolated over each element by a polynomial, which may be integrated analytically. For the left Rieman sum the interpolation function is a constant, and for the trapeziodal rule the interpolation function is a first order polynomial. Generally, if $f \in C^\infty$, an interpolation function of order l takes into account $l+1$ terms of the function's Taylor series, resulting in an integration formula of order $l+1$. However, using second order interpolation functions, which gives Simpson's rule, one should expect a formula of order three, but due to a fortunate cancellation of third order terms, Simpsons formula is of order four.

4.3.3 A SIMPLE EXAMPLE

Consider the numerical evaluation of the integral

$$\int_1^4 \sqrt{x}\, dx = \frac{14}{3} . \tag{4.15}$$

Clearly, $\sqrt{x}$ is C^∞ in the interval [1,4]. Table 1 shows the error made by the left Rieman sum, the trapeziod rule and Simpsons rule for different element sizes. The results are shown in 15 digits precision - the machine precision is about 10^{-19}. For each row in table 1 the number of elements n are doubled, and hence the order of the method may be estimated by taking the ratio of the error of two succeeding rows err_{2n}/err_n, this ratio equals $(1/2)^{q_e}$, where q_e is the estimate of the order of the numerical integration formula. It is evident that the formulas stabilize on a constant value of the order, which agrees very well with the theoretical value - for the first coarse divisions the assumption of smoothness of the first derivative, which is not taken into account by the formula, is not met, and hence the estimated order differs from the theoretical.

i	Rieman sum	estimated order for Riemam sum	Trapeziodal rule	estimated order for Trapezio-dal rule	Simpsons rule	estimated order for Simpsons rule
1	1,666666666666667		0,166666666666667		0,004389006498287	
2	0,794958421540382	1,06801	0,044958421540382	1,89030	0,000445958360282	3,29891
4	0,386574074155307	1,04013	0,011574074155307	1,95769	0,000035292872308	3,65946
8	0,190419988193058	1,02156	0,002919988193058	1,98686	0,000002407760470	3,87361
16	0,094481802868617	1,01108	0,000731802868617	1,99644	0,000000154465166	3,96234
32	0,047058066566029	1,00559	0,000183066566029	1,99909	0,000000009721116	3,99002
64	0,023483273932344	1,00281	0,000045773932344	1,99977	0,000000000608639	3,99746
128	0,011730193939565	1,00141	0,000011443939565	1,99994	0,000000000038057	3,99936
256	0,005862236013434	1,00070	0,000002861013434	1,99999	0,000000000002379	3,99984
512	0,002930402755143	1,00035	0,000000715255143	2,00000	0,000000000000149	3,99997
1024	0,001465022563897	1,00018	0,000000178813897	2,00000	0,000000000000009	3,99945
2048	0,000732466578481	1,00009	0,000000044703481	2,00000	0,000000000000001	3,99752
4096	0,000366222113371	1,00004	0,000000011175871	2,00000	0,000000000000000	
8192	0,000183108262718	1,00002	0,000000002793968	2,00000	0,000000000000000	

Table 1. Error made by various numerical integration formulas. The estimated order is also shown.

Another way of showing the convergence of numerical integration formulas is to plot the error as a function of the number of function evaluations in double logaritmic scale, see Figure 4-5. The order q_e may then be estimated as the slope of the curve.

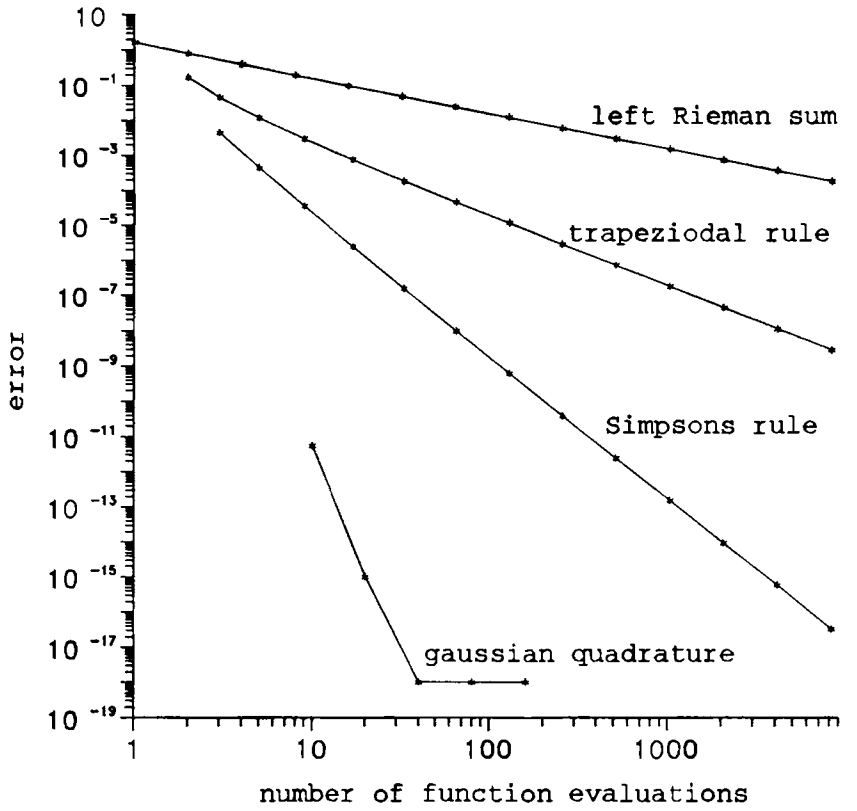

Figure 4-5. The error *vs.* number of function evaluations of various numerical integration formulas.

It is evident from Figure 4-5 that Simpsons rule performs better than both the trapeziodal rule and the left Rieman sum in evaluating the integral of equation (4.15). Due to the high order of Simpsons rule compared to the order of the trapeziodal rule or the left Rieman sum, the superiority of Simpsons rule becomes increasingly pronounced as the demand of accuracy is raised.

The numerical integration formulas investigated so far are all based on equally spaced abscissas. Generally, when using a polynomial of order l requiring about l evaluations of the function per element, a numerical integration formula of order l+1 is obtained. Now, if we allow for arbitrarily spaced

abscissas for evaluation of the function as well, twice the degree of freedom is obtained. In this case it may be shown [96] that a formula using l function evaluations per element has the order $2l$. These formulas are called Gaussian quadrature formulas, and the most common of these formulas is the Gauss-Legendre quadrature:

$$\int_a^b f(x)\,dx = \sum_{i=1}^{l} w_i f(x_i) \quad . \tag{4.16}$$

Tables over the abscissas x_i and weights w_i can be found in e.g. references [8,96]. The abscissas are also termed the Gauss points. The error made when using a 10 point Gauss-Legrendre quadrature (in the following often shortened to Gaussian quadrature) for the integral in equation (4.15) is also plotted in Figure 4-5, and it is evident that this formula performs far better than the other formulas considered. For a 10 point Gauss-Legendre formula the order is 20 (!), but the formula seldom behaves that well, since the assumption of a smooth 21st derivative is seldom met. Furthermore, when increasing the number of elements the truncation error made by this formula quickly becomes less than the machine precision and hence the performance is limited by round-off errors. In Figure 4-5 round-off errors is seen to be dominating for more than 40 function evaluations.

Another advantage associated with Gauss-Legendre quadrature is that the function to be integrated is not evaluated at the endpoints of the interval. The Gauss-Legendre quadrature formula is therefore called an open formula, whereas formulas that do require the function to be evaluated at the endpoints, such as the trapeziodal rule and Simpsons rule, are termed closed formulas. If the Gauss-Legendra formula with an even number of points (like the 10 point formula) is chosen, the function is neither evaluated at the midpoint of the interval. These properties become important when the function to be evaluated is singular or undefined at the midpoint or endpoints of the interval.

4.3.4 INTEGRALS OF SINGULAR FUNCTIONS

The integral

$$\int_0^1 \sqrt{x}\,dx = \frac{2}{3} \tag{4.17}$$

is singular, since $d(\sqrt{x})/dx=1/(2\sqrt{x})$ goes towards infinity as x goes towards zero. The error made by the various formulations *vs.* the number of function evaluations is shown in Figure 4-6.

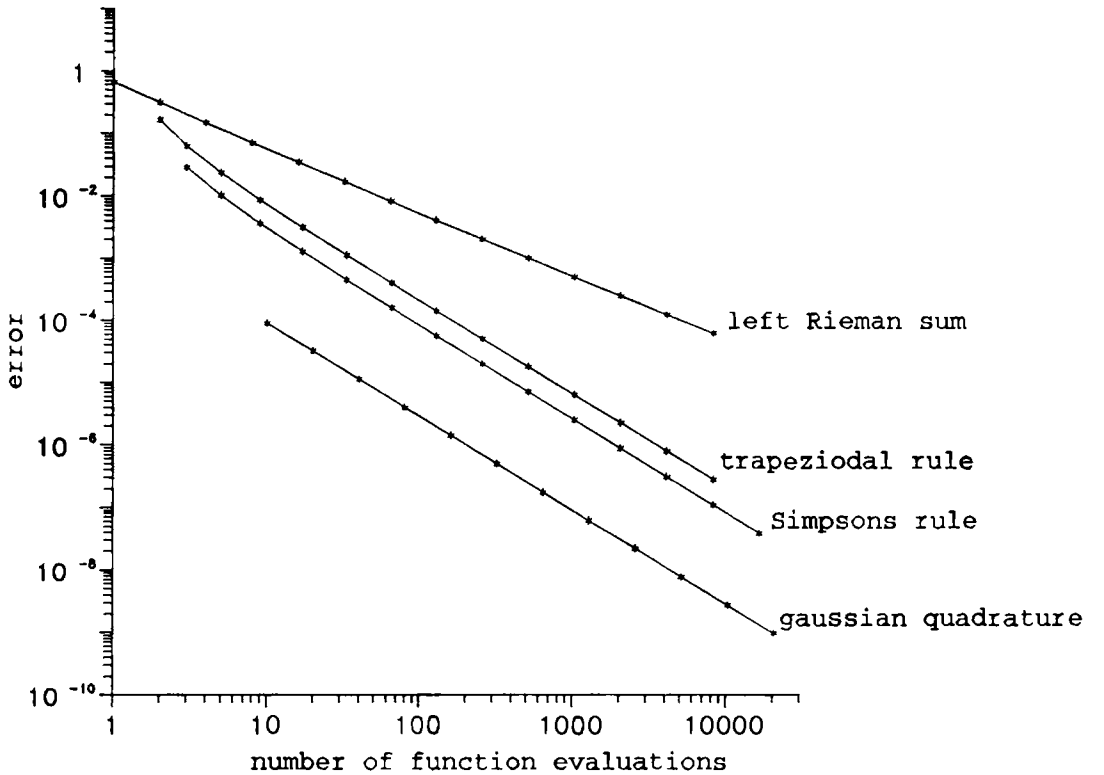

Figure 4-6. The error *vs.* number of function evaluations when the function to be integrated contains a singularity.

In this case we find that the high order formulas do not converge as quickly as they did for the non-singular integral in equation (4.15). Although the error made for a given number of function evaluations is still smaller when using Gaussian quadrature than when using e.g. Simpsons rule, the slope of the curves for the trapeziodal rule, Simpsons rule and Gaussian quadrature is the same. Hence the main benefit of using a high order formula has vanished. The slope of the curves for the trapeziodal rule, Simpsons rule and Gaussian quadrature is

3/2=1/2+1, which corresponds to the fact that the function has a singularity of order 1/2 in its first derivative. Thus it is seen that for these numerical integration formulas the convergence is limited by singularities of the function, whereas the limiting factor of the left Rieman sum still is the order of the integration formula since the order of this formula is less than 3/2.

It can be seen from Figure 4-6 that the Gauss-Legendre quadrature formula still performs best in the singular case although the order benefit is destroyed. It can be shown [96] that the Gauss-Legendre quadrature formula will perform at least as good as any other formula with the same number of function evaluations, unless the formula is specially designed to deal with the singularity in question.

4.3.5 CONCLUDING REMARKS

Numerical integration of a known function is carried out by dividing the integration interval into small elements. For each element the function is evaluated at a finite number of points, and in between these points the function is approximated by an interpolation function. Thus the integral is approximated by a sum of products of the function evaluated at certain points and some weights. The weights are determined by the element length and the interpolation function.

If one uses an advanced interpolation function, a high order formula is obtained. However, a high order formula corresponds to high accuracy only if the function to be integrated is sufficiently smooth.

4.4 IMPLEMENTATION OF THE AXISYMMETRIC INTEGRAL EQUATION FORMULATION

As was shown in chapter 3, the surface integral of the Helmholtz integral equation may be reduced to a line integral over the generator of the body and an integral over the angle of revolution. Since the angular dependance of the pressure and normal velocity could be described by their values on the generator due to the expansion in a cosine series, only the integral over the generator has to be discretized. The approach using constant elements would be to divide the generator into linear elements and place the nodes in the centre of each element, as sketched in Figure 4-2. However, the discussion in section 4.3 suggests a more advenced numerical treatment of the integral in equation (3.36). In this section three numerical implementations of equation (3.36) will be presented - one using linear interpolation functions, one using quadratic interpolation functions, and one using a combination of linear and quadratic elements. It should be noted that two fundamentally different types of interpolation are made in the numerical treatment of equation (3.36). The first type concerns the interpolation of the pressure and the normal velocity between the nodes. The second type of interpolation concerns the geometry of the body; in practice the body is not described as a mathematical formula (or curve) but as a set of geometrical points: the nodes. In between these geometrical nodes the geometry is approximated with interpolation functions analogous to the interpolation of the pressure and the normal velocity. For this reason the interpolation functions are often referred to as shape functions.

4.4.1 LINEAR ELEMENTS

Consider a linear variation of the pressure and the normal velocity over each line element of the generator of the body. A body having N elements then has $M=N+1$ nodes, as sketched in Figure 4-7 a). Thus linear shape functions are used to represent both the geometry and the acoustic variables. Dividing the generator of the body into linear elements allows equation

(3.36) to be approximated by

$$C(P)p_m(P) \approx \sum_{j=1}^{N} \left[\int_{L_j} p_m(Q) F^B(P,Q,m)\, dL_Q \right] + ikz_0 \sum_{j=1}^{N} \left[\int_{L_j} v_m(Q) F^A(P,Q,m)\, dL_Q \right] + 4\pi p_m^I(P) . \qquad (4.18)$$

The procedure is then to put p_m and v_m outside the integration with respect to L.

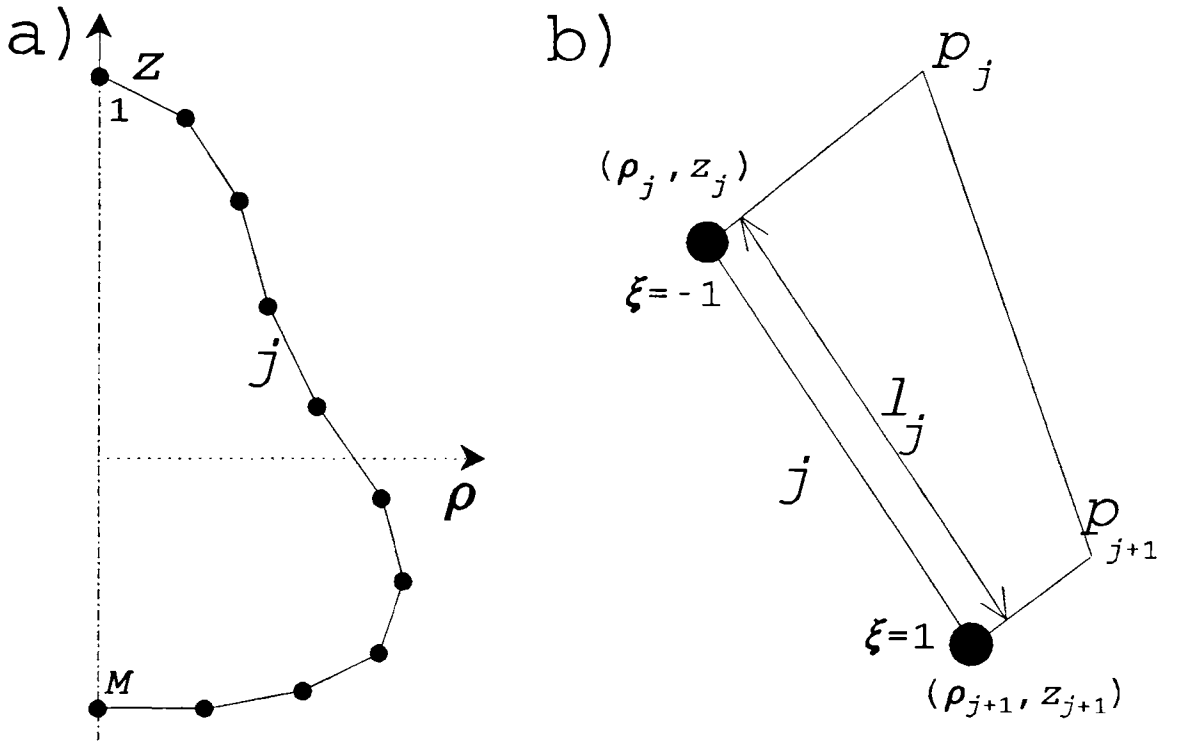

Figure 4-7. Discretization of the generator of an axisymmetric body into linear elements. The z-axis is the axis of revolution. a) Total geometry with element number j indicated. b) Definition of local geometry for element number j.

Consider the first integral on the right-hand side of equation (4.18), where i is associated with the collocation point P:

$$\int_{L_j} p_m(Q) F^B(P_i,Q,m)\ \mathrm{d}L_j$$
$$= \int_{(\rho_j, z_j)}^{(\rho_{j+1}, z_{j+1})} p_m(Q) F^B(P_i,Q,m)\ \mathrm{d}L_j\ . \tag{4.19}$$

Introducing the linear shape functions

$$\phi_1 = \frac{1-\xi}{2}\ ,\quad \phi_2 = \frac{1+\xi}{2}\ ;\ \xi\in[-1,1] \tag{4.20}$$

allows the local geometry to be defined as

$$\begin{aligned} \rho(\xi) &= \rho_j\phi_1(\xi) + \rho_{j+1}\phi_2(\xi) \\ z(\xi) &= z_j\phi_1(\xi) + z_{j+1}\phi_2(\xi)\ . \end{aligned} \tag{4.21}$$

The jacobian of this transformation $J(\xi)=\sqrt{(\partial\rho/\partial\xi)^2 + (\partial z/\partial\xi)^2}$ is $J(\xi)=L_j/2$, i.e. the ratio between the lengths of the integration intervals in the two domains. The pressure is interpolated using the same shape function, as seen Figure 4-7 b), so that

$$p(\xi) = p_j\phi_1(\xi) + p_{j+1}\phi_2(\xi), \tag{4.22}$$

where the expansion index m is omitted for convenience. It is now possible to express the integral of equation (4.19) in terms of the local coordinate ξ:

$$\begin{aligned} &\int_{L_j} p(Q) F^B(P_i,Q,m)\ \mathrm{d}L_j \\ &= \int_{-1}^{1} \left(p_j(\xi)\phi_1(\xi) + p_{j+1}(\xi)\phi_2(\xi)\right) F^B(P_i,\xi,m)\,\frac{L_j}{2}\,d\xi \\ &= p_j h_{ij}^1 + p_{j+1} h_{ij}^2\ , \end{aligned} \tag{4.23}$$

where

$$\begin{aligned} h_{ij}^1 &= \int_{-1}^{1} \phi_1(\xi)\, F^B(P_i,\xi,m)\,\frac{L_j}{2}\ \mathrm{d}\xi \\ h_{ij}^2 &= \int_{-1}^{1} \phi_2(\xi)\, F^B(P_i,\xi,m)\,\frac{L_j}{2}\ \mathrm{d}\xi\ . \end{aligned} \tag{4.24}$$

It should be noted that the functions to be evaluated in the

integrals h_{ij}^1 and h_{ij}^2 are almost identical. They consist of a shape function (either ϕ_1 or ϕ_2) which is fast to evaluate times a function F^B. F^B is quite computationally intensive since this function contains an integral over the angle of revolution as well as the evaluation of elliptic integrals. Hence, it is advantageous to evaluate the integrals h_{ij}^1 and h_{ij}^2 simultaneously reusing the evaluations of F^B. It may also be noted that when using the open Gaussian quadrature formula, the function F^B is not required at the nodal points (the endpoints of the integration interval), where it may be singular due to the singularity in the Green's function.

The integrals containing v_m are handled analogously. Considering element number j, the integral in the second term of equation (4.18) can be transformed to

$$\begin{aligned}
&\int_{L_j} v(Q) F^A(P_i,Q,m)\, dL_j \\
&= \int_{-1}^{1} \left(v_j(\xi)\phi_1(\xi) + v_{j+1}(\xi)\phi_2(\xi)\right) F^A(P_i,\xi,m) \frac{L_j}{2} d\xi \\
&= v_j g_{ij}^1 + v_{j+1} g_{ij}^2 ,
\end{aligned} \tag{4.25}$$

where the expansion index m is omitted, and

$$\begin{aligned}
g_{ij}^1 &= \int_{-1}^{1} \phi_1(\xi) F^A(P_i,\xi,m) \frac{L_j}{2}\, d\xi \\
g_{ij}^2 &= \int_{-1}^{1} \phi_2(\xi) F^A(P_i,\xi,m) \frac{L_j}{2}\, d\xi .
\end{aligned} \tag{4.26}$$

For the i'th calculation point equation (4.18) is now approximated by (still with the index m omitted)

$$\begin{aligned}
C_i p_i = {} & p_1 h_{i1}^1 + p_2 (h_{i1}^2 + h_{i2}^1) + \cdots + p_j (h_{ij-1}^2 + h_{ij}^1) + \cdots + p_M h_{iN}^2) \\
& ikz_0 \left(v_1 g_{i1}^1 + v_2 (g_{i1}^2 + g_{i2}^1) + \cdots + v_j (g_{ij-1}^2 + g_{ij}^1) + \cdots + v_M g_{iN}^2\right) \\
& + 4\pi p_i^I ,
\end{aligned} \tag{4.27}$$

since the pressure p_j and the normal velocity v_j at node j contributes to the j-1'st element and the j'th element. Using M

calculation points placed at the M nodes allows a matrix equation to be set up:

$$\boldsymbol{C}\,\boldsymbol{p}_m = \boldsymbol{H}_m\boldsymbol{p}_m + \boldsymbol{G}_m\boldsymbol{v}_m + 4\pi\,\boldsymbol{p}_m^I\,, \tag{4.28}$$

where m is the expansion index of equation (4.18).

The matrices in equation (4.28) are defined as follows:

$$\boldsymbol{C} = \begin{bmatrix} C_1 & 0 & \cdots & & & 0 \\ \vdots & & & & & \vdots \\ 0 & \cdots & 0 & C_i & 0 \cdots & 0 \\ \vdots & & & & & \vdots \\ 0 & \cdots & & & 0 & C_M \end{bmatrix}, \tag{4.29}$$

$$\boldsymbol{H}_m = \begin{bmatrix} h_{11}^1 & h_{11}^2+h_{12}^1 & \cdots & h_{1N-1}^2+h_{1N}^1 & h_{1N}^2 \\ \vdots & & & & \vdots \\ h_{i1}^1 & h_{i1}^2+h_{i2}^1 & \cdots & h_{iN-1}^2+h_{iN}^1 & h_{iN}^2 \\ \vdots & & & & \vdots \\ h_{M1}^1 & h_{M1}^2+h_{M2}^1 & \cdots & h_{MN-1}^2+h_{MN}^1 & h_{MN}^2 \end{bmatrix}, \tag{4.30}$$

and

$$\boldsymbol{G}_m = \begin{bmatrix} g_{11}^1 & g_{11}^2+g_{12}^1 & \cdots & g_{1N-1}^2+g_{1N}^1 & g_{1N}^2 \\ \vdots & & & & \vdots \\ g_{i1}^1 & g_{i1}^2+g_{i2}^1 & \cdots & g_{iN-1}^2+g_{iN}^1 & g_{iN}^2 \\ \vdots & & & & \vdots \\ g_{M1}^1 & g_{M1}^2+g_{M2}^1 & \cdots & g_{MN-1}^2+g_{MN}^1 & g_{MN}^2 \end{bmatrix}. \tag{4.31}$$

By introducing the boundary conditions, the matrix equation (4.28) is transformed into the familiar set of equations:

$$\boldsymbol{A}_m\boldsymbol{x}_m = \boldsymbol{y}_m\,, \tag{4.32}$$

where $\boldsymbol{x}_m$ is the unknown vector and $\boldsymbol{y}_m$ is the known vector. For the problem of scattering from a rigid surface $\boldsymbol{A}_m$ equals C-$\boldsymbol{H}_m$

of equation (4.30) and y_m equals p_m^I, and for a radiation problem where v_m is known, A_m equals $C-H_m$ and y_m equals G_m of equation (4.31) times v_m: $y_m = G_m v_m$. In both these cases x_m equals p_m.

4.4.2 QUADRATIC ELEMENTS

Continuing the sofistication process of the numerical approximation, quadratic elements are now considered. For each element three nodes are now required to determine the variation of the geometry and the acoustic variables. Quadratic elements are introduced not only in order to obtain fast convergence of the method when the mesh size is refined, but also because quadratic elements are frequently used in finite element calculations. The link between finite element models and boundary element models is easily acknowledged when the same shape functions are used for both models [35]. Hence, the quadratic elements are also introduced to make the boundary element model compatible with finite element models. Consider now a body divided into N elements as sketched in Figure 4-8 a). The number of nodes is $M=2N+1$.

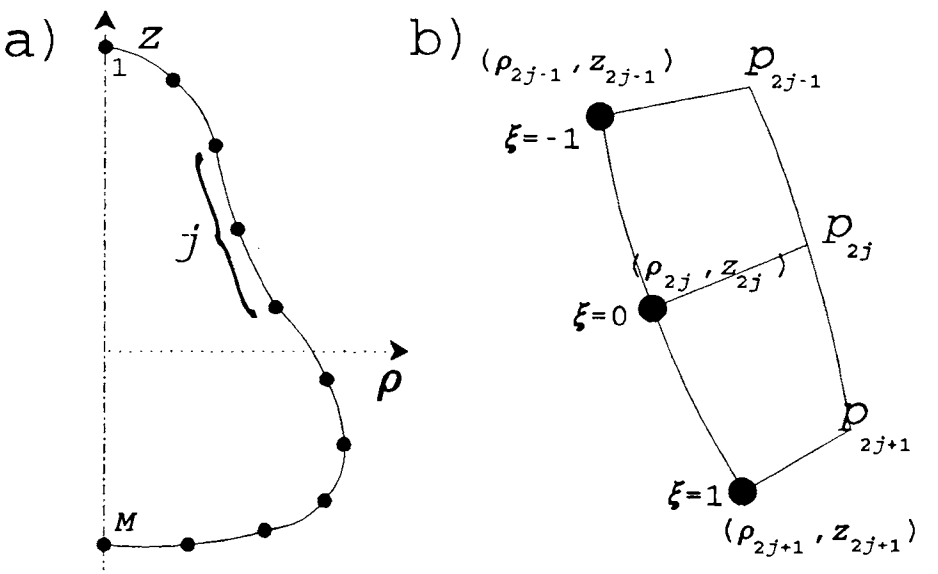

Figure 4-8. Discretization of the generator of an axisymmetric body into quadratic elements. The z-axis is the axis of revolution. a) Total geometry with the j'th element indicated. b) Definition of local geometry for the j'th element.

Clearly, the quadratic shape functions represent a curved geometry better than the linear shape functions. Again, the integral over the generator is divided into a sum of integrals over each element as in equation (4.18), but for the same number of nodes the 'quadratic model' has only half the elements of the 'linear model'. The integral over element number j with respect to collocation point i now states

$$\begin{aligned}&\int_{L_j} p_m(Q) F^B(P_i,Q,m)\ \mathrm{d}L_j \\ &= \int_{(\rho_{2j-1},z_{2j-1})}^{(\rho_{2j+1},z_{2j+1})} p_m(Q) F^B(P_i,Q,m)\ \mathrm{d}L_j\ .\end{aligned} \tag{4.33}$$

The shape functions for quadratic elements are [8,82]:

$$\phi_1 = \frac{\xi(\xi-1)}{2}\ ,\ \phi_2 = 1-\xi^2\ ,\ \phi_3 = \frac{\xi(\xi+1)}{2}\ ,\ \xi\in[-1,1]\ . \tag{4.34}$$

Thus the local geometry, as seen in Figure 4-8 b) may now be described by

$$\begin{aligned}\rho(\xi) &= \rho_{2j-1}\phi_1(\xi)+\rho_{2j}\phi_2(\xi)+\rho_{2j+1}\phi_3(\xi) \\ z(\xi) &= z_{2j-1}\phi_1(\xi)+z_{2j}\phi_2(\xi)+z_{2j+1}\phi_3(\xi)\ .\end{aligned} \tag{4.35}$$

The jacobian of this transformation $J(\xi)=\sqrt{(\partial\rho/\partial\xi)^2+(\partial z/\partial\xi)^2}$ involves the derivatives of the shape functions:

$$\begin{aligned}\frac{\partial\rho}{\partial\xi} &= \rho_{2j-1}(\xi-\tfrac{1}{2})-2\rho_{2j}\xi+\rho_{2j+1}(\xi+\tfrac{1}{2}) \\ \frac{\partial z}{\partial\xi} &= z_{2j-1}(\xi-\tfrac{1}{2})-2z_{2j}\xi+z_{2j+1}(\xi+\tfrac{1}{2})\ .\end{aligned} \tag{4.36}$$

Note that for quadratic elements the unit normal vector $\boldsymbol{n}$ also varies with ξ. If the nodes are numbered clock-wise $\boldsymbol{n}$ may be found from the (ρ,z) coordinates by

$$\boldsymbol{n} = \left(-\frac{\mathrm{d}z}{\mathrm{d}\xi}, \frac{\mathrm{d}\rho}{\mathrm{d}\xi}\right)\ . \tag{4.37}$$

For counter clock-wise numbering the sign of the right side must be changed. For the linear elements described in the above paragraph the normal vector is constant within each element.

Using the same shape functions for the pressure:

$$p(\xi) = p_{2j-1}\phi_1(\xi) + p_{2j}\phi_2(\xi) + p_{2j+1}\phi_3(\xi) \ , \tag{4.38}$$

where the expansion index m is omitted for convenience, allows equation (4.33) to be rewritten as

$$\begin{aligned} &\int_{L_j} p(Q) F^B(P_i,Q,m)\ \mathrm{d}L_j \\ &= p_{2j-1}h^1_{ij} + p_{2j}h^2_{ij} + p_{2j+1}h^3_{ij} \ , \end{aligned} \tag{4.39}$$

where

$$\begin{aligned} h^1_{ij} &= \int_{-1}^{1} \phi_1(\xi) F^B(P_i,\xi,m) J(\xi)\mathrm{d}\xi \\ h^2_{ij} &= \int_{-1}^{1} \phi_1(\xi) F^B(P_i,\xi,m) J(\xi)\mathrm{d}\xi \\ h^3_{ij} &= \int_{-1}^{1} \phi_3(\xi) F^B(P_i,\xi,m) J(\xi)\mathrm{d}\xi \ . \end{aligned} \tag{4.40a,b,c}$$

Once again a large amount of computational time may be saved by reusing the evaluation of F^B when evaluating the integrals of equations (4.40a,b,c). Note that a Gaussian quadrature formula of even order should be used to evaluate the integrals of equations (4.40a,b,c) since then F^B is not required for either ξ=-1, ξ=0 nor ξ=1, where F^B may be undefined due to the singularity in Green's function.

The integrals containing v_m are handled analogously, and placing M collocation points on the M nodes allows a matrix equation similar to equation (4.18) to be set up:

$$C p_m = H_m p_m + G_m v_m + 4\pi p^I_m \ , \tag{4.41}$$

where m is the expansion index of equation (4.18). The matrices of equation (4.41) are defined as follows (note that the middle node corresponding to ξ=0 is in contact with only one element):

$$C = \begin{bmatrix} C_1 & 0 & \cdots & & & 0 \\ \vdots & & & & & \vdots \\ 0 & \cdots & 0 & C_i & 0 & \cdots & 0 \\ \vdots & & & & & & \vdots \\ 0 & \cdots & & & & 0 & C_M \end{bmatrix}, \tag{4.42}$$

$$H_m = \begin{bmatrix} h_{11}^1 & h_{11}^2 & h_{11}^3+h_{12}^1 & h_{12}^2 & \cdots & h_{1N-1}^3+h_{1N}^1 & h_{1N}^2 & h_{1N}^3 \\ \vdots & & & & & & & \\ h_{i1}^1 & h_{i1}^2 & h_{i1}^3+h_{i2}^1 & h_{i2}^2 & \cdots & h_{iN-1}^3+h_{iN}^1 & h_{iN}^2 & h_{iN}^3 \\ \vdots & & & & & & & \\ h_{M1}^1 & h_{M1}^2 & h_{M1}^3+h_{M2}^1 & h_{M2}^2 & \cdots & h_{MN-1}^3+h_{MN}^1 & h_{MN}^2 & h_{MN}^3 \end{bmatrix}, \tag{4.43}$$

and

$$G_m = \begin{bmatrix} g_{11}^1 & g_{11}^2 & g_{11}^3+g_{12}^1 & g_{12}^2 & \cdots & g_{1N-1}^3+g_{1N}^1 & g_{1N}^2 & g_{1N}^3 \\ \vdots & & & & & & & \\ g_{i1}^1 & g_{i1}^2 & g_{i1}^3+g_{i2}^1 & g_{i2}^2 & \cdots & g_{iN-1}^3+g_{iN}^1 & g_{iN}^2 & g_{iN}^3 \\ \vdots & & & & & & & \\ g_{M1}^1 & g_{M1}^2 & g_{M1}^3+g_{M2}^1 & g_{M2}^2 & \cdots & g_{MN-1}^3+g_{MN}^1 & g_{MN}^2 & g_{MN}^3 \end{bmatrix}. \tag{4.44}$$

The matrix equation (4.41) is transformed into the familiar set of equations by applying the boundary conditions.

4.4.3. SUPERPARAMETRIC ELEMENTS

If the same shape functions are used for discretizing both the geometry and the acoustic variables the elements are termed 'isoparametric'. This is the case for the linear elements described in paragraph 4.4.1 and the quadratic elements described in paragraph 4.4.2. Isoparametric elements is by far the most well known element type in boundary element method formulations for acoustics. In fact, the use of non-isoparametric formulation for acoustics has not been reported in the litterature as far as the author knows. However, as the isoparametric quadratic formulation was tested for radiation problems some annoying fluctuations of the solution was observed, which does not occur using isoparametric linear

elements. This is described in paragraph 4.4.4. In order to avoid these fluctuations a superparametric formulation was developed. The term superparametric elements is adapted from finite elements theory [32]. The superparametric formulation uses quadratic shape functions for the geometry and linear shape functions for the acoustic variables. Hence, the mid-element node corresponding to $\xi=0$ of the quadratic element, seen in Figure 4-8 b) is a geometrical node only, whereas the 'interelement' nodes corresponding to $\xi=-1$ and $\xi=1$ are both geometrical and acoustical nodes. Besides from avoiding the annoying fluctuation problem already mentioned the benefit of the superparametric formulation is its ability to represent a curved geometry with the accuracy of the quadratic elements while maintaining the fewer unknown pressures or normal velocities from the linear element formulation.

4.4.4 THE PRESSURE ON A PULSATING SPHERE

Consider the problem of radiation from a pulsating sphere. Analytically, the pressure is constant on the surface of the sphere. Figure 4-9 shows the deviation from the analytical result of the numerically evaluated pressure on the surface of the sphere, calculated using 21 nodes for the unknown pressure. Results are shown for the isoparametric quadratic formulation, the isoparametric linear formulation and the superparametric formulation. The error is calculated as the deviation from the analytical solution in percent with respect to the analytical solution. Figure 4-9 shows that the error of the isoparametric quadratic formulation is fluctuating, whereas the error made by the isoparametric linear formulation and the superparametric formulation remain almost constant as functions of the node number. This fluctuating nature of the error was also observed for other radiation problems when using the isoparametric quadratic model. For scattering problems a fluctuating error was also found when using the exact solid angle for the $C(P)$'s of equation (4.42). However, if the approximate numerical expression for the solid angles, equation (3.37), was used, the error became smooth as a function of the node number. The

author has not yet found an explation for this behaviour. Clearly, if calculating e.g. the radiated acoustic power, the resulting error would not be as large as the error observed for the pressure at each node, since in this case the error at each node would 'cancel out' to some extent. However, the error would still be unexpectedly large compared to the less sofisticated superparametric formulation.

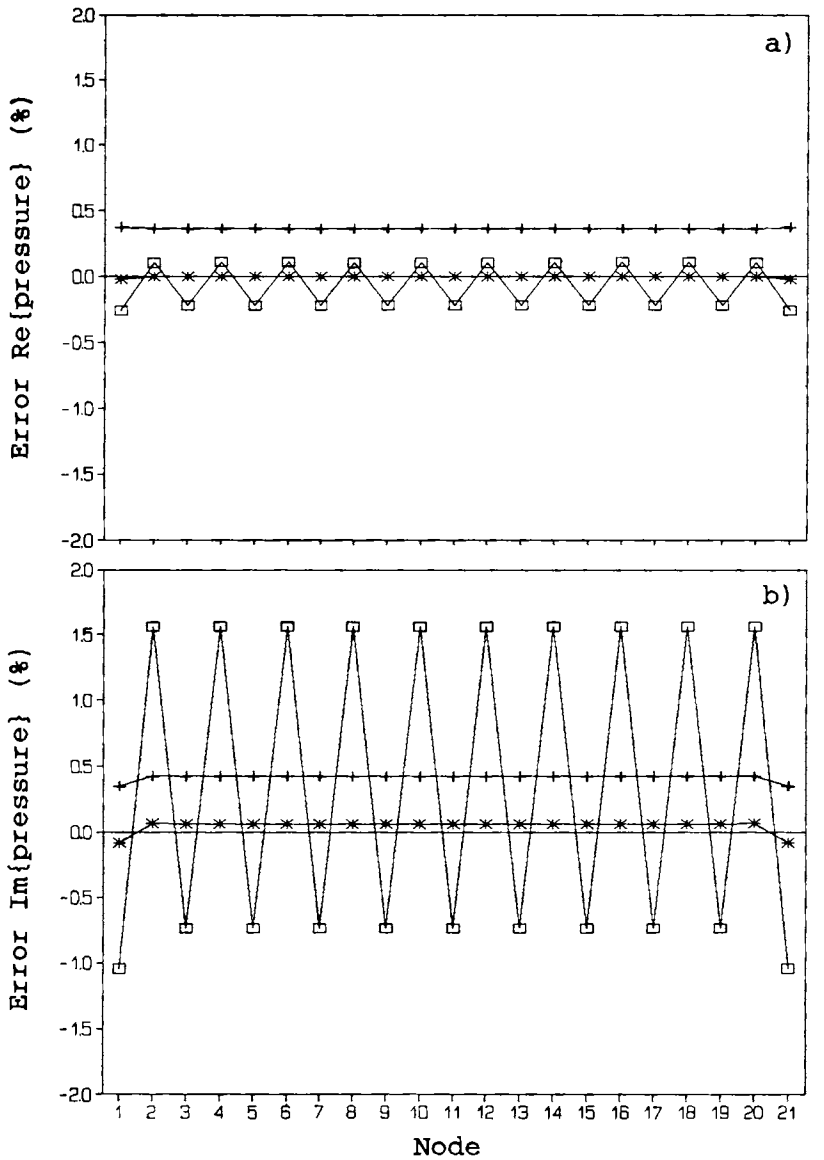

Figure 4-9. Error made by the three formulations when calculating the pressure on a pulsating sphere at ka=1 .——□——, isoparametric quadratic formulation; ——+——, isoparametric linear formulation; ——*——, superparametric formulation.

4.4.5 DISCONTINUOUS VELOCITY DISTRIBUTION

For a number of applications a discontinuous velocity distribution is specified e.g. when radiation from a baffled piston is considered. Moreover, when discretizing a curved body a unique normal vector does seldom exist at a node in contact with two elements, as seen in Figure 4-10. Hence, the normal velocity will not be uniquely given at these nodes. This problem may be handled by introducing two normal velocities for the nodes in contact with two elements as sketched in Figure 4-10, each being the normal velocity with respect to the unit normal vector taken to the limit $\xi=-1$ or $\xi=1$ of the element in question. Consider as an example quadratic elements. Node number $2j+1$ connects element number j and element number $j+1$. Now, the normal velocity v_{2j+1} of node $2j+1$ is divided into two normal velocities v^{-}_{2j+1} corresponding to element number j and v^{+}_{2j+1} corresponding to element number $j+1$. Hence, for quadratic elements $3N$ normal velocities are specified. The G_m matrix of equation (4.44) shold then be modified to a matrix of $3N$ columns (the number of rows should still be M):

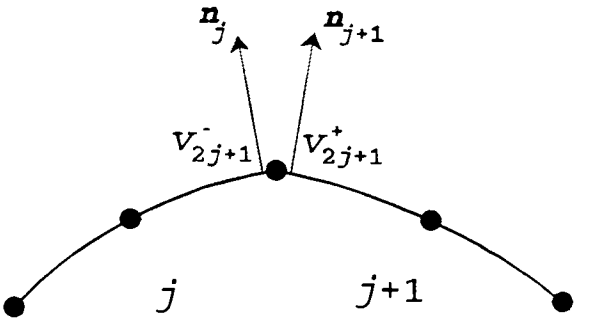

Figure 4-10. A discretized body with nonunique normal vector.

$$G_m = \begin{bmatrix} g^1_{11} & g^2_{11} & g^3_{11} & g^1_{12} & \cdots & g^3_{1N-1} & g^1_{1N} & g^2_{1N} & g^3_{1N} \\ \vdots & & & & & & & & \\ g^1_{i1} & g^2_{i1} & g^3_{i1} & g^1_{i2} & \cdots & g^3_{iN-1} & g^1_{iN} & g^2_{iN} & g^3_{iN} \\ \vdots & & & & & & & & \\ g^1_{M1} & g^2_{M1} & g^3_{M1} & g^1_{M2} & \cdots & g^3_{MN-1} & g^1_{MN} & g^2_{MN} & g^3_{MN} \end{bmatrix}, \qquad (4.45)$$

so the product $G_m v_m$ is still a vector of M elements. Clearly, any radiation problem with a unique velocity distribution may be treated using this more general approach.

For linear elements an analogous approach may be used. In this case the G_m matrix consists of $2N$ columns and M rows.

4.5 TEST CASES

To verify the axisymmetric integral equation formulation desbribed in chapter 3 and to demonstrate its advantages a number of test cases have been run using linear elements. Scattering as well as sound radiation has been tested.

4.5.1. APPLICATIONS TO SCATTERING

The first test case is the scattering of a plane wave by a rigid sphere of radius a. Since the sphere is axisymmetric with respect to the z-axis, the plane wave is supposed to be travelling along the negative ρ-axis in order to involve all terms in the cosine expansion of equation (3.5).

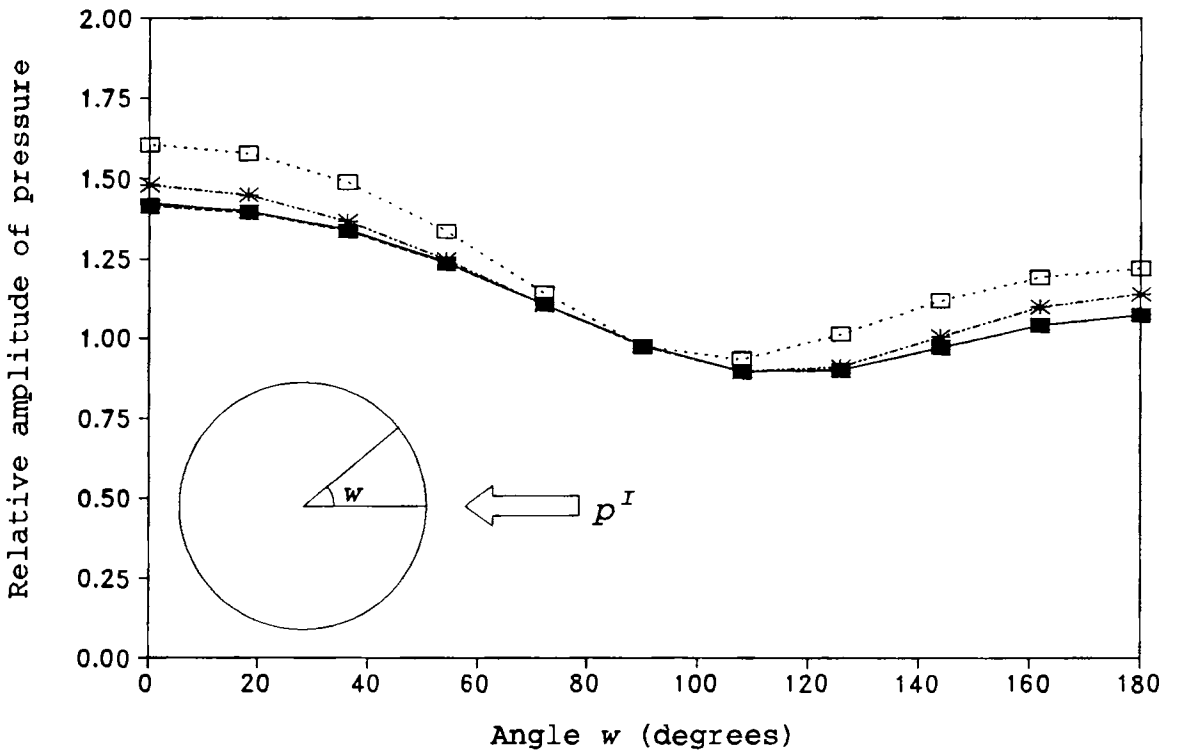

Figure 4-11. Pressure on the surface of a sphere when scattering of a plane incoming wave for ka=1 is considered. ————, analytical solution; ····□····, boundary element calculation, 2 terms;·-···-*-···-·, boundary element calculation, 3 terms;----■----, boundary element calculation, 4 terms.

Figure 4-11 shows the modulus of the complex pressure on the surface of the sphere as a function of the angle defined in the small inset in the figure for the case ka=1.

The generator is modelled by 11 nodes, and the pressure calculated by truncating the sum (3.38) at m=1, m=2 and m=3, is shown compared to the analytical solution. It is apparent that 4 terms are sufficient to describe the sound field accurately at this frequency.

In order to observe the effect of an increased frequency the problem was also run for ka=5 and modelling the generator by 26 nodes. Figure 4-12 shows the calculated pressure obtained by truncating the sum (3.38) at m=6, m=7 and m=8.

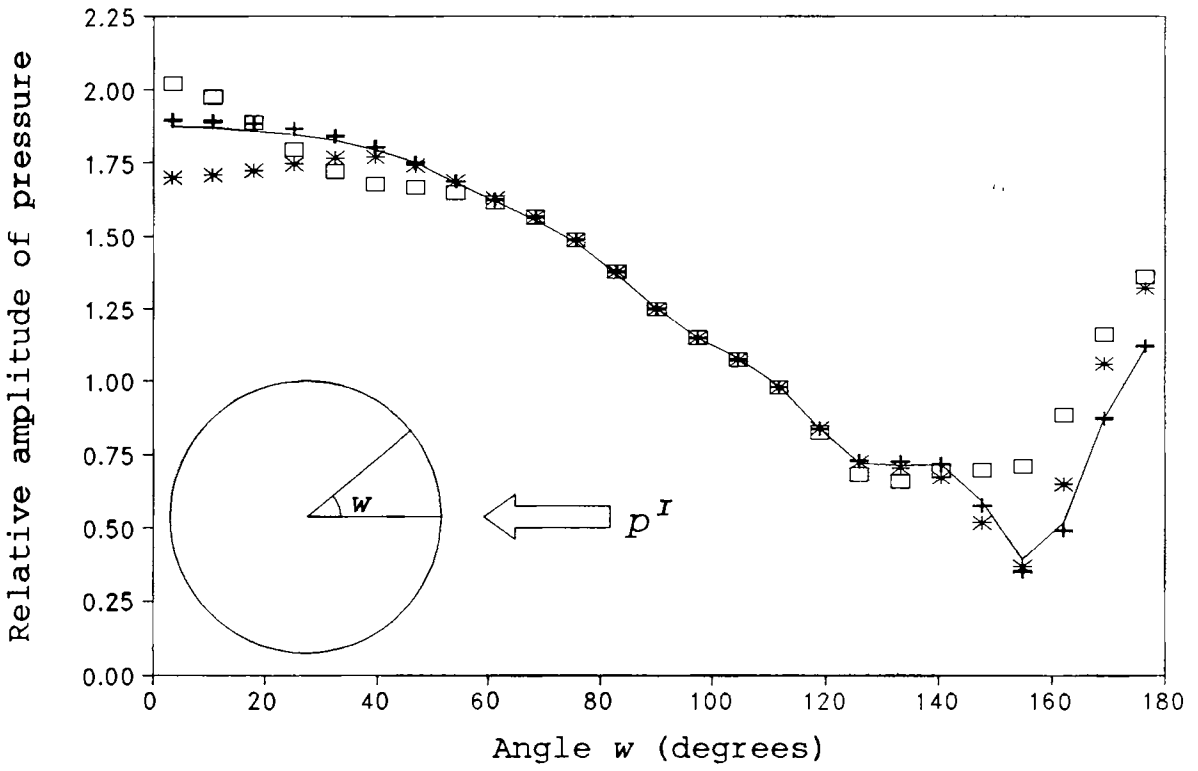

Figure 4-12. Pressure on the surface of a sphere when scattering of a plane incoming wave for ka=5 is considered.————, analytical solution; □, boundary element calculation, 6 terms; *, boundary element calculation, 7 terms; +, boundary element calculation, 8 terms.

At this frequency 8 terms must be calculated in order to obtain an accurate solution; adding more terms does not improve the accuracy significantly. In order to obtain a better accuracy the discretization must be refined. It may also be noted that at high frequencies the integral of revolution F_1^A becomes strongly oscillating, and hence the numerical integration of this integral must be refined.

The second test case concerns the scattering of a plane wave from two rigid spheres, where the axis of symmetry is parallel to the wavefront of the incoming wave. The two spheres both have radius a and the distance between their centres is d=5a. The problem was run for ka=1 using a 16 node discretization for each sphere.

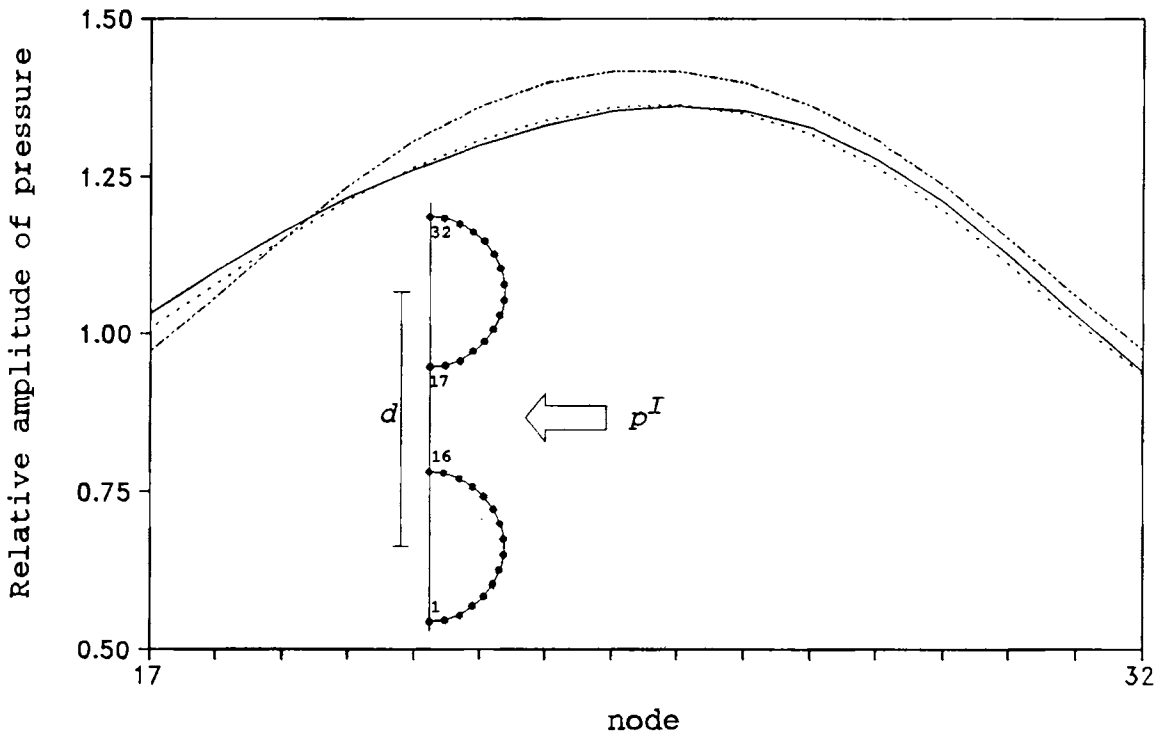

Figure 4-13. Pressure on the surface of the upper sphere when scattering of a plane incoming wave by 2 spheres for ka=1 and d=5a is considered.————, boundary element calculation; ·····, approximative analytical; ·-·-·-·-·, 1 sphere.

Figure 4-13 shows the pressure on the surface of the upper sphere obtained by the boundary element formulation truncating the cosine expansion at m=3 (the fifth term (m=4) was found to be negligible) as a function of node number as shown in the inset in Figure 4-13. Due to symmetry, the pressure on the lower sphere is not shown.

The boundary element solution is compared to the analytical solution of scattering by one sphere only, and to an approximative solution formed by adding the scattered field by the lower sphere, in the absence of the upper, to the field on the surface of the upper sphere in the absence of the lower. A similar way of obtaining an approximative solution has been used in reference [82]. The approximate solution is expected to be accurate at low frequencies and for large distances between the spheres as in the present case.

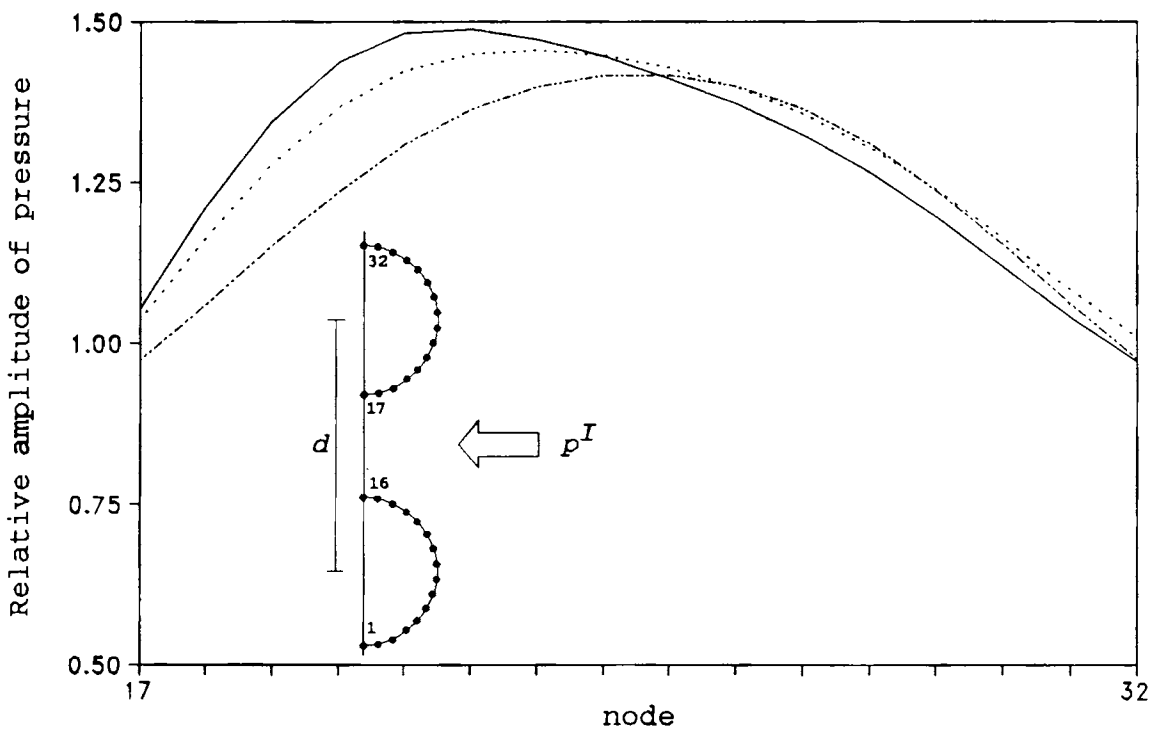

Figure 4-14. Pressure on the surface of the upper sphere when scattering of a plane incoming wave by 2 spheres for ka=1 and d=3a is considered. ————, boundary element calculation; ·····, approximative analytical; ·-·-·-·-·, 1 sphere.

As the spheres become more closely spaced, the interacting scattering effect becomes more significant. Figure 4-14 shows the same results as seen in Figure 4-13, for the frequency ka=1 but for a distance between the spheres of only d=3a which means that the distance between the surfaces of the spheres is now only one radius.

In this case the boundary element solution formed by 4 terms of the cosine expansion (the fifth being negligible) differs more significantly from the approximate solution, although the approximate solution still provides a general image of the sound field.

4.5.2 APPLICATION TO RADIATION

As an example of the application of this formulation to radiation, the radiation from a vibrating sphere centered at (0,0,0) is considered.

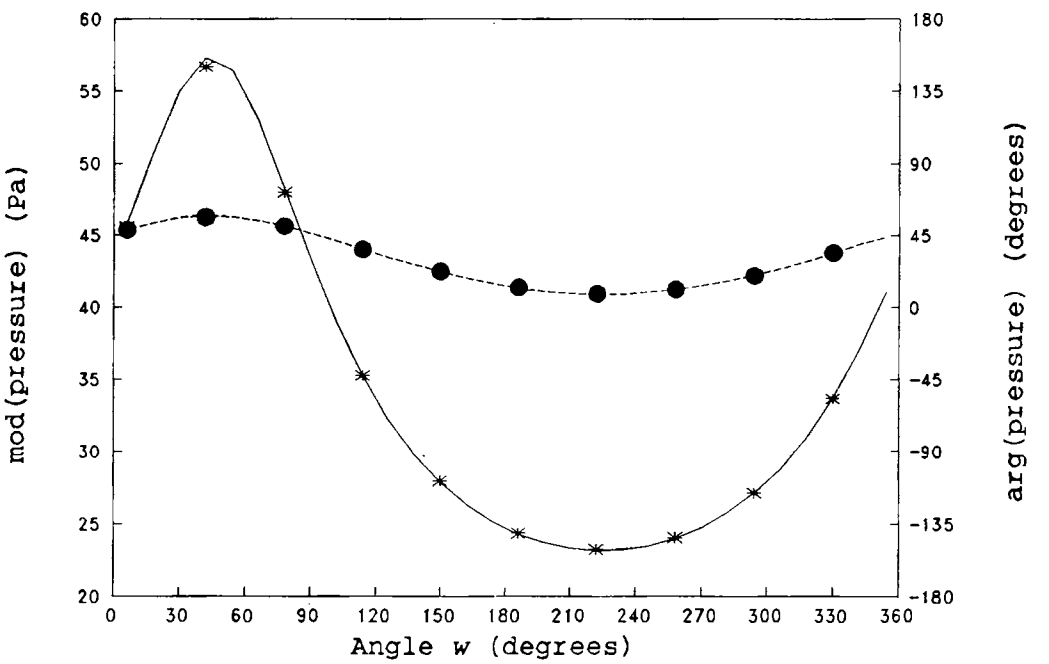

Figure 4-15. Pressure on the surface of a vibrating sphere for ka=1. ————, mod(pressure) analytical; --------, arg(pressure) analytical; *, mod(pressure) boundary element calculation; ●, arg(pressure) boundary element calculation.

In order to involve all terms in the cosine expansion, the normal velocity of the surface of the sphere is determined by

equating it with the velocity produced by a monopole q of unit strength (1 m^3/s) placed at $(\rho_q, z_q, \theta_q)=(0.3, 0.3, 0)$. This method of generating the surface velocity of a sphere has been used in e.g. reference [78]. The boundary element formulation now produces a solution to this radiation problem, and this solution may now be compared to the analytical solution of the monopole case. Figure 4-15 shows the pressure on the surface of the sphere as a function of the angle w to the ρ-axis for ka=1, using a 16 node discretization. Good agreement is found using four terms of the cosine expansion.

Finer discretization must be used to obtain a more accurate solution, since adding more terms of the cosine expansion does not improve the result at this frequency.

As a final testcase for radiation, the above problem was run for ka=2. Figure 4-16 shows that 4 terms of the cosine expansion still suffice to accurately predict the pressure on the surface of the sphere. However, finer discretization had to be used in order to calculate accurate values - in this case 30 nodes were used.

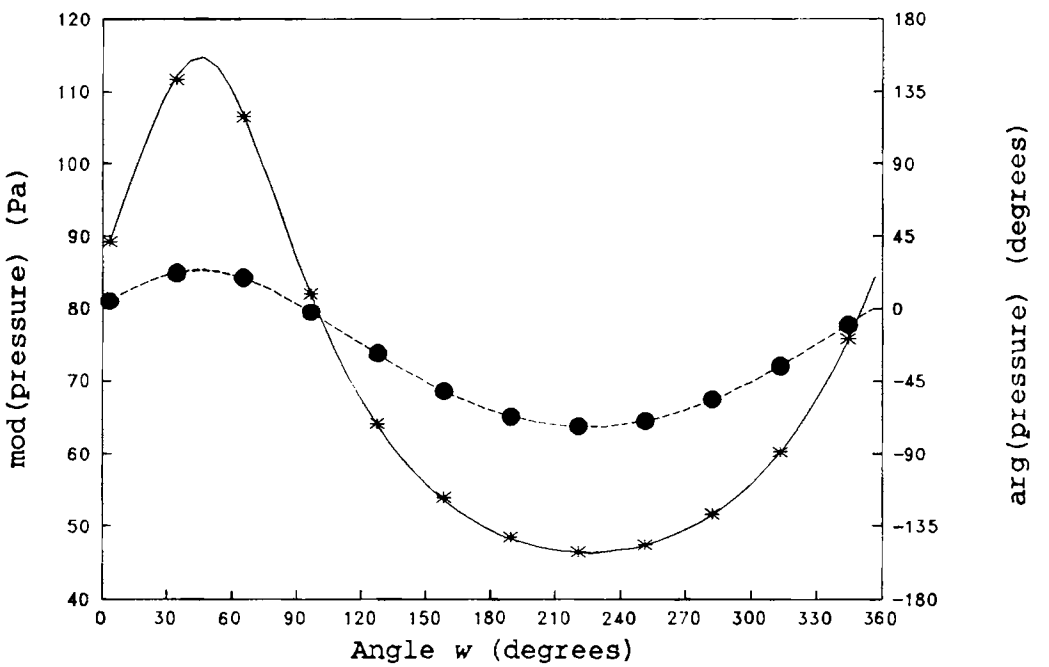

Figure 4-16. Pressure on the surface of a vibrating sphere for ka=2. ————, mod(pressure) analytical;--------, arg(pressure) analytical; *, mod(pressure) boundary element calculation; ●, arg(pressure) boundary element calculation.

4.5.3 CONCLUDING REMARKS

The axisymmetric integral equation formulation for non-axisymmetric boundary conditions has been tested for radiation and scattering problems. For the problems considered only relatively few terms of the cosine expansion were required in order to obtain an accurate solution. Hence, the axisymmetric formulation requires much less calculation time and much less storage than a full three-dimensional numerical solution of the same problem - a comparison between the axisymmetric formulation and a three-dimensional formulation is given in paragraph 4.7.10. Further problems solved with the axisymmetric formulation using linear and quadratic elements are presented in chapters 7 and 8.

4.6 CONVERGENCE

In this section the convergence of the axisymmetric formulations using isoparametric linear, isoparametric quadratic and superparametric elements will be discussed. Unfortunately, this situation is much less straightforward compared to the discussion of convergence of numerical integration formulas in section 4.3, and in the literature only a few studys of convergence has been reported [59,99] In a boundary element formulation several approximations are made:

a) The geometrical shape of the body is approximated using shape functions.
b) The acoustic variables are approximated using shape functions.
c) Numerical integrations of 'influence functions' are carried out.
d) The unknown acoustic variable are found numerically by solving a set of linear equations.

Suppose that the round-off errors made by solving the set of equations and the error made by the numerical integration are insignificant compared to the errors due to the first two approximations. For the 10 point guassian quadrature formula used here, this is indeed true. In fact, in order to optimize the formulation with respect to calculation time a more coarse

numerical integration formula should be used. In the test cases considered in the following, the frequency and body shape is chosen so that the resulting system of equations is well conditioned. Hence, round-off errors due to the numerical solution of the set of equations are negligible.

Under these assumptions only the approximations related to the geometry and the acoustic variables are considered. If scattering from a rigid body is considered, only the pressure is discretized, since the normal velocity is zero, whereas radiation problems involve discretization of the normal velocity as well. For this reason, the following discussion is divided into scattering and radiation problems.

The error made by discretizing the geometry corresponds to the difference between the solution of two problems. The first of these problems is the problem involving the 'real' body, and the second problem is the one where the body is subsituted with the discretized body as modelled by the shape functions. The behavior of this error is difficult to predict - it depends on the frequency, the shape of the body, and on the boundary conditions.

The error due to the discretization of the acoustic variables should be comparable to the error made when interpolating a known function, which is to be integrated - i.e. similar to the error under study in section 4.3. In order for the problems considered here to resemble the situation described in section 4.3 as most as possible, the generator of the body is divided into elements of equal length. In practice elements of equal lenght would not be the optimum choice, and for several problems such a division of the geometry would not even exist. For an optimal calculation (accuracy *vs.* calculation time) small elements should be used where the geometry or the acoustic variables vary quickly, whereas large elements should be used where the variation of these quantities is slow.

All in all, the curves presented in this section are expected to be straight lines in a double logarithmic coordinate system corresponding to an error proportional to h^q, where q is the order of the formulation. However, becaurse of

the unpredictable behaviour of the error due to the geometrical discretization, the curves might not be straight if this error is dominating.

4.6.1 SCATTERING BY A RIGID SPHERE

In Figure 4-17 scattering by a rigid sphere is considered. In order to compare the three formulations, the error is shown as a function of the number M of acoustical nodes. For the isoparametric quadratic formulation the number of acoustical nodes equals $2N+1$, where N is the number of elements. For both the isoparametric linear formulation and the superparametric formulation the number of nodes equals $N+1$. Since the time used for setting up the set of equations is proportional to $M \cdot N$, the time used for setting up the set of equations is less for the isoparametric quadratic formulation than for the isoparametric linear formulation and the superparametric formulation. However, the storage required for the set of equations and the time spend on solving the set of equations are the same in all three cases. For large M the total time used by all three formulations is dominated by the solution of the system of equations, since the time spend on matrix inversion grows as M^3. For these reasons the author finds that the comparison between the three formulations is most fairly based on the number of unknowns M. The error is calculated as the length of the residual vector, which contains the difference between the analytical solution and the boundary element solution. Hence, when increasing the number of nodes, the number of terms in this error measure is also increased. Clearly, for each node the error is less than the error shown in Figure 4-17, but the error is generally not uniformly distributed over the nodes. This way of showing the error is a 'worst-case' method - the aforementioned fluctuating error of the isoparametric quadratic formulation for radiation is fully included, for instance. Figure 4-17 shows the error measure of the three formulations as functions of the number of acoustical nodes for $ka=1$, where a is the radius of the sphere. The incoming plane wave is of magnitude one (dimensionless for convenience). The figure shows

that the isoparametric formulation converges faster than the isoparametric linear formulation and also faster than the superparametric formulation.

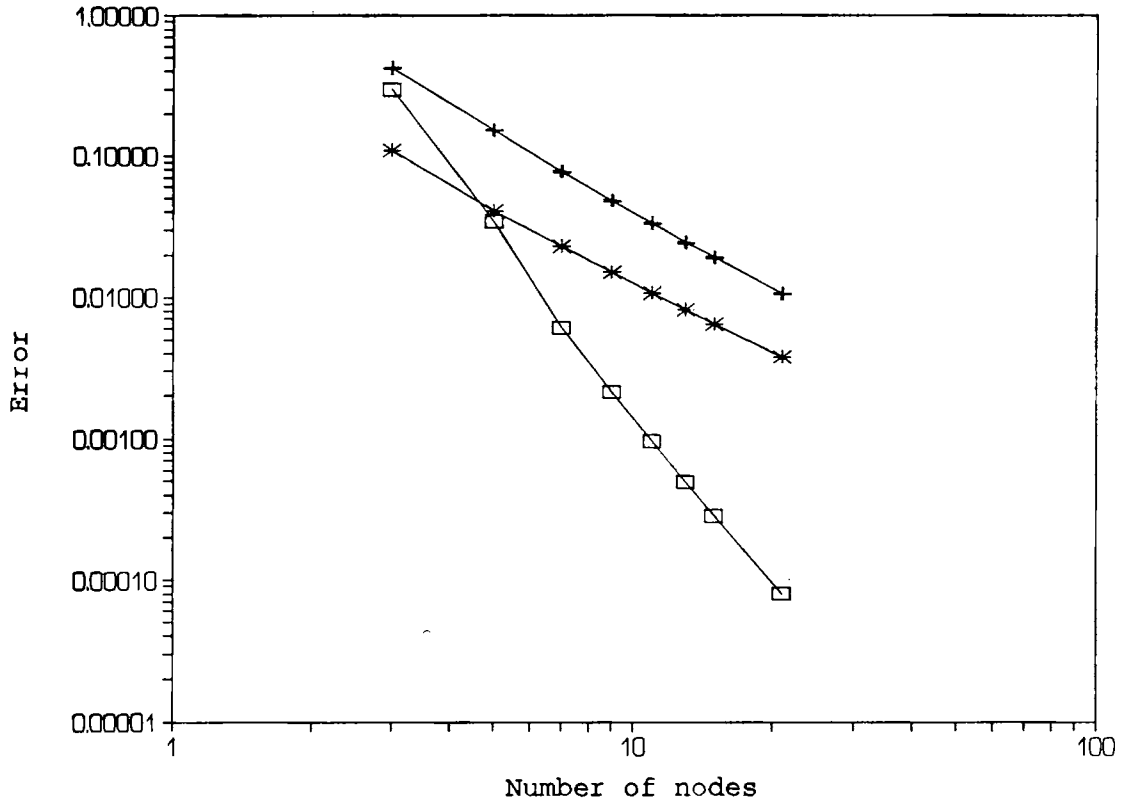

Figure 4-17. Error made by the three different boundary element formulations for scattering by a rigid sphere at *ka*=1. ——□——, isoparametric quadratic formulation; ——+——, isoparametric linear formulation; ——*——, superparametric formulation.

The slope of the curve for the isoparametric quadratic formulation is around -4, whereas the slope for both the isoparametric linear formulation and the superparametric formulation is around -2. Since for scattering by a rigid sphere both the geometry and the pressure on the surface of the sphere have smooth high order derivatives, the convergence obtained here is expected to be close to the best possible.

When using isoparametric quadratic elements a rule of thumb is to choose the element size to be about half of the wavelength [107]. For the problem considered in Figure 4-17 this

discretization corresponds to 3 nodes, and the error found using the isoparametric quadratic formulation is 0.3. Note that the error is the squareroot of the sum of the squares of the error at each node. For the superparametric formulation the error using 3 nodes is 0.1, and for the isoparametric linear formulation the error using 3 nodes is 0.4. Hence, for this very coarse discretization the superparametric formulation performs best, whereas the isoparametric quadratic formulation performes best for finer discretizations.

4.6.2 SCATTERING BY A RIGID CIRCULAR CYLINDER

In order to investigate the effect of discretizing the acoustic variables only, scattering by a rigid cylinder is now considered. In this case the geometry is completely described using 4 equally sized elements, as sketched in Figure 4-18. The length of the cylinder equals its diameter. Unfortunately, an analytical solution of this problem does not exist. Hence, the 'analytical' solution was produced as the boundary element solution with a very fine grid - the grid was refined until the difference between two calculations was negligible compared to the accuracy obtained by the coarse division of the generator of the cylinder, used here to examine the convergence properties. Thus the 'analytical' solution is a boundary element solution using 160 isoparametric quadratic elements (321 nodes). Figure 4-19 shows the error made by the three formulations for the case of scattering by the rigid cylinder at ka=1. The incoming plane wave is again of magnitude one (dimensionless for convenience). Still, it appears that the isopametric quadratic formulation performes best. The curves for the isoparametric linear formulation and for the super-

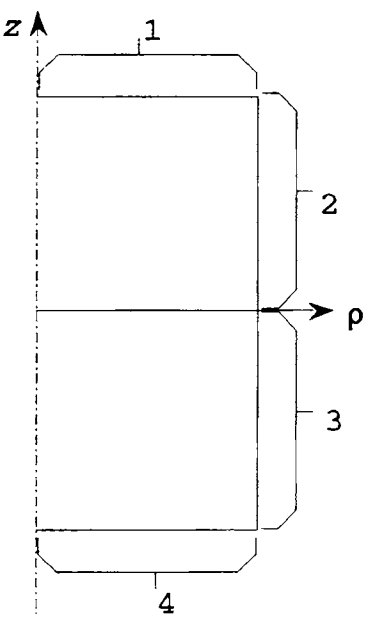

Figure 4-18. The generator of a cylinder divided into 4 elements.

parametric formulation coincide. This is not unexpected, since the superparametric formulation may be regarded as a linear formulation with improved geometric interpolation. In the case of a circular cylinder, the generator consists of straight lines, which means that the improvement with respect to geometry has vanished.

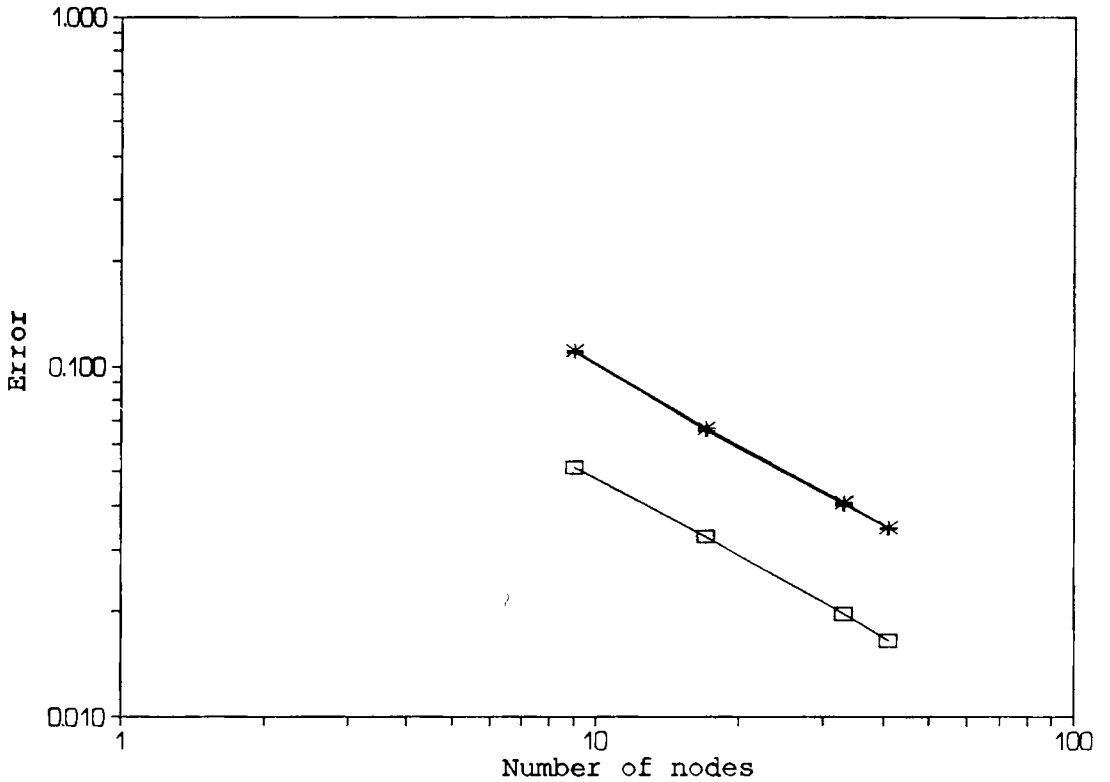

Figure 4-19. Error made by the three different boundary element formulations for scattering by a rigid cylinder at ka=1. ——□——, isoparametric quadratic formulation; ——+——, isoparametric linear formulation; ——*——, superparametric formulation.

The most noticeable feature of Figure 4-19 is the fact that all the curves have the same slope, which is around -0.7. This is probably due to the sharp edge of the cylinder, which theoretically causes the particle velocity to be infinite near the edge. In practice the particle velocity would be finite due to the viscosity of the fluid, of course. The asymptotic behaviour of the pressure near an edge may be found by the

following loose study. Consider the sound field near the edge of the cylinder. For the diffraction problem, the term of interest is kr, where r is the distance from the edge. Now, for any finite frequency kr tends to zero when r tends to zero, but since the diffraction problem is only governed by kr it is mathematically legitimate to keep r constant and let k tend to zero instead, and still draw the same conclusions from the approximative study. Hence, in the limit of small r Laplace's equation may be used. For Laplace's equation, traditionally used in the limit of small k, it is well known [58, p.69] that an edge of angle $3\pi/2$ produces a $r^{-1/3}$ behavior of the flow velocity at the edge - the general rule is that an angle α produces a $r^{\pi/\alpha-1}$ behavior of the flow velocity. Hence, the particle velocity tends to infinite as r tends to zero. The well known $r^{-1/2}$ behaveior of the particle velocity near the edge of a thin screen [69, p.505,108-109] may also be explained in this way.

From the analysis of numerical integration it became clear that a singularity in a function would destroy the main benefit of a high order method, and this is what the author assumes is the reason for the behaveior of the curves in Figure 4-19. The case of scattering by a rigid cylinder is reconsidered in paragraph 9.1.2.

In fact, also the sphere has edges when modelled as discussed in paragraph 4.4.5. However, since the order of the singularity depends of the opening angle, the singularities are so weak in this case that the benefit of a high order formulation is not destroyed. The problem of singularity may also be seen immediately from equation (3.1), where $\partial G(R)/\partial n$ occurs - clearly the normal vector n is not defined at the edge of the cylinder. In fact the assumptions for setting up Helmholtz integral equation has been violated by the introduction of these discontinuities - the reason why the theory still works is that it is only violated in a region of vanishing area.

As an example, consider the most coarse mesh used in the calculations presented in Figure 4-19. This mesh consists of 9 acoustical nodes, which for the isoparametric quadratic for-

mulation corresponds to about 3 elements per wavelength at *ka*=1. The error made by the isoparametric quadratic formulation for this mesh is about 0.05. In order to obtain the same precision with the isoparametric linear model or the superparametric model about 25 nodes must be used.

4.6.3 RADIATION FROM A PULSATING SPHERE

When radiation from a pulsating sphere is considered, both the pressure and, of course, the normal velocity are constant on the surface of the sphere. Hence this test case should isolate the approximation made with respect to the geometry. Figure 4-20 shows the error made by the three formulations for *ka*=1. The magnitude of the pressure on the surface of the sphere is in this case about 33 Pa, and the errors shown should, of course, be compared to this number. The fluctuating error of the isoparametric quadratic formulation is again fully included, which means that if e.g. the radiated acoustic power was calculated the error would be smaller.

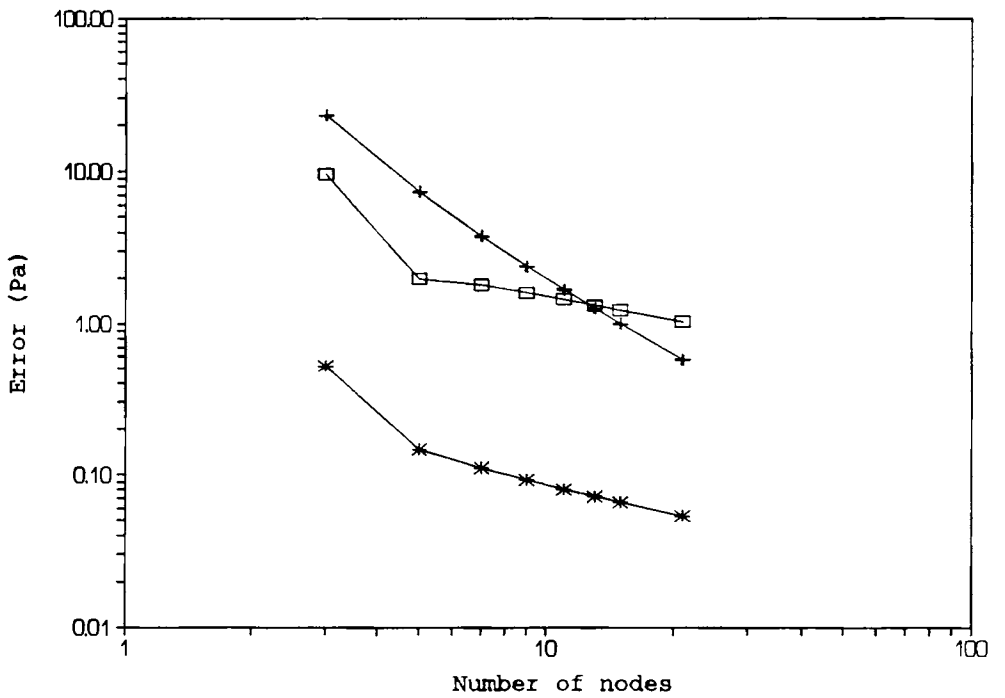

Figure 4-20. Error made by the three different boundary element formulations for radiation from a pulsating sphere at *ka*=1. ——□——, isoparametric quadratic formulation; ——+——, isoparametric linear formulation; ——*——, superparametric formulation.

For the isoparametric quadratic and the superparametric formulations the error is significantly reduced when refining the mesh from 3 to 5 acoustical nodes. Further refinement of the mesh does not improve the accuracy very much - the slope of the curves for a large number of nodes is around -0.5 for the isoparametric quadratic formulation and -0.75 for the superparametric formulation. For the isoparametric linear formulation the curve has a slight arch. At three nodes the slope is around -2, but at 21 nodes the slope is around -1.5. Hence, the convergence declines as the number of nodes increases. For this reason it is not expected that the isoparametric linear formulation will perform better than the superparametric for a very large number of nodes, although extrapolation of the curves in figure 4-20 could indicate that this was the case. Clearly, the superparametric formulation performs far better than the isoparametric quadratic formulation and the isoparametric linear formulation. The error for 3 nodes, which corresponds to an element length equal to half a wavelength for the quadratic formulation, is about 0.5 Pa for the superparametric formulation. For the isoparametric quadratic formulation the error is about 9.5 Pa, which corresponds to an average of 3 Pa or 10 % of the analytically calculated pressure at each node. For the isoparametric linear formulation the error is about 23 Pa.

4.6.4 RADIATION FROM A VIBRATING CYLINDER

In order to investigate the effect of discretizing the acoustic variables only, radiation from a cylinder is now considered. The normal velocity of the surface was determined by equating it with the velocity produced by a monopole q of strength one (1 m^3/s) placed at the centre of the cylinder $(\rho_q, z_q, \theta_q) = (0,0,0)$. This method for generating a surface velocity for an arbitrary shape was also used in paragraph 4.5.2 and is sometimes termed a One Point Source test [78]. The solution for the pressure on the surface of the cylinder calculated by the boundary element formulations, for this prescribed velocity distribution and with the monopole removed,

may then be compared to the pressure due to the monopole at (0,0,0) with the cylinder removed, where the latter case, of course, can be evaluated analytically. Figure 4-21 shows the error made by the three formulations for a cylinder, with its length equal to its diameter, at ka=1.

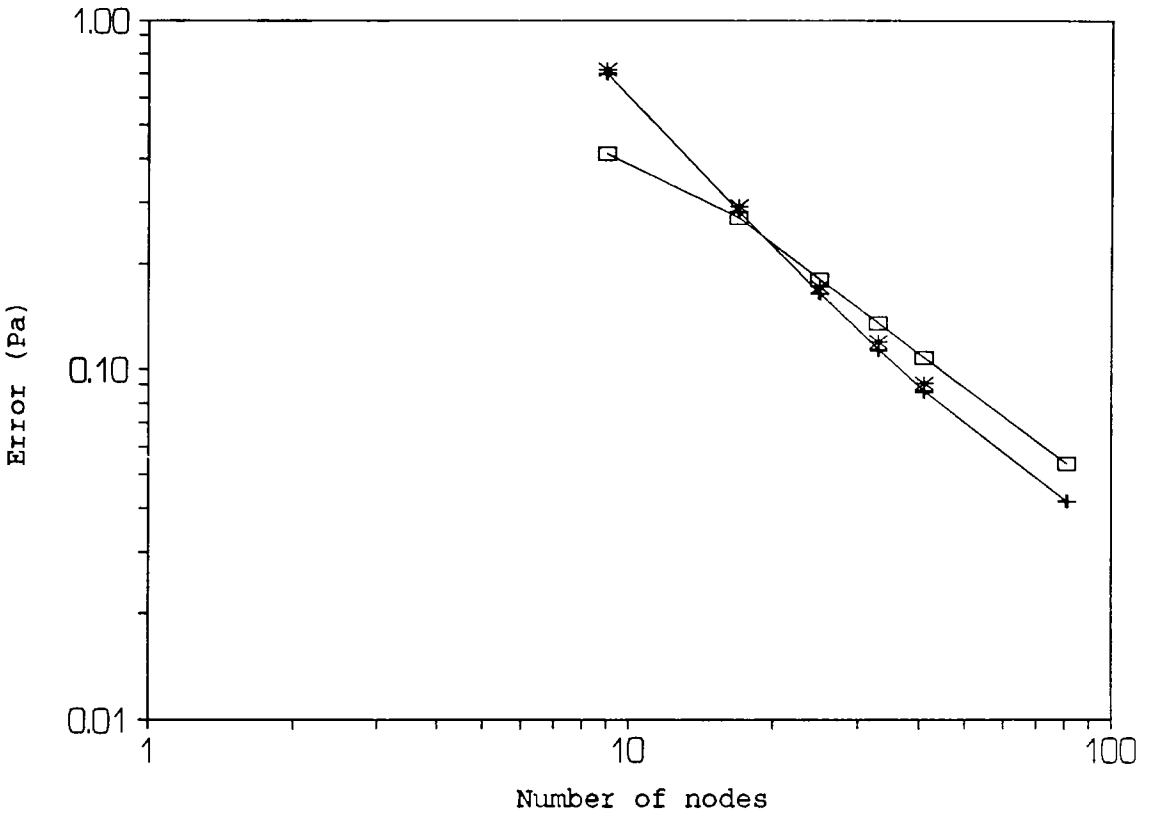

Figure 4-21. Error made by the three different boundary element formulations for radiation from a vibrating cylinder at ka=1. ——□——, isoparametric quadratic formulation; ——+——, isoparametric linear formulation; ——*——, superparametric formulation.

Again the edges of the cylinder seems to destroy the benefit of using a high order formulation, since it is seen that the slope of all three curves at large node numbers is around -1. For the most coarse discretization with 9 nodes, which corresponds to about three elements per wavelength, the error made by the isoparametric quadratic formulation is about 0.4 Pa. The analytical solution for the pressure on the surface of the cylinder varies from 23 Pa to 33 Pa. Again the curves

for the isoparametric linear formulation and the superparametric formulation coincide due to the linear geometry. With 9 nodes the error made by these formulations is about 0.7 Pa. However, for more than 17 nodes the isoparametric linear formulation and the superparametric formulation performs slightly better than the isoparametric quadratic formulation.

4.6.5 QUARTER-POINT TECHNIQUE

In paragraph 6.4.2 it was demonstrated that the benefit with respect to convergence of using the high order quadratic shape functions was destroyed in the case of scattering of a plane wave by a rigid cylinder. It was justified that in this case the tangential flow velocity had a $r^{-1/3}$ behavior near the edge of the cylinder. Hence, it was assumed that this singularity in the flow velocity destroyed the benefit of the high order formula. Recently Wu and Wan [108-109] has adopted the so-called quarter-point technique from the finite element method in order to efficiently handle the $r^{-1/2}$ singularity of the flow velocity near a knife edge. It this case the pressure has a $r^{1/2}$ behavior near the edge. Now suppose that the squareroot function is to be approximated by the quadratic shape functions. The normal approach described in paragraph 4.4.2 approximates the function by its values at the two endpoints and the midpoint of the interval, as shown in Figure 4-22 a). It can be seen in Figure 4-22 a) that when using the normal technique, the shape functions approximate the squareroot poorly. The quarter-point technique displaces the mid-element node to a position, where the distance to the singularity is one quarter of the lenght of the element. It can be seen in Figure 4-22 b) that when using this technique, the shape functions exactly model the squareroot function - in fact the two curves exactly coincides. It was shown in the paper by Wu and Wan [108] that the accuracy of the boundary element calculations was dramatically improved when using this quarter-point technique.

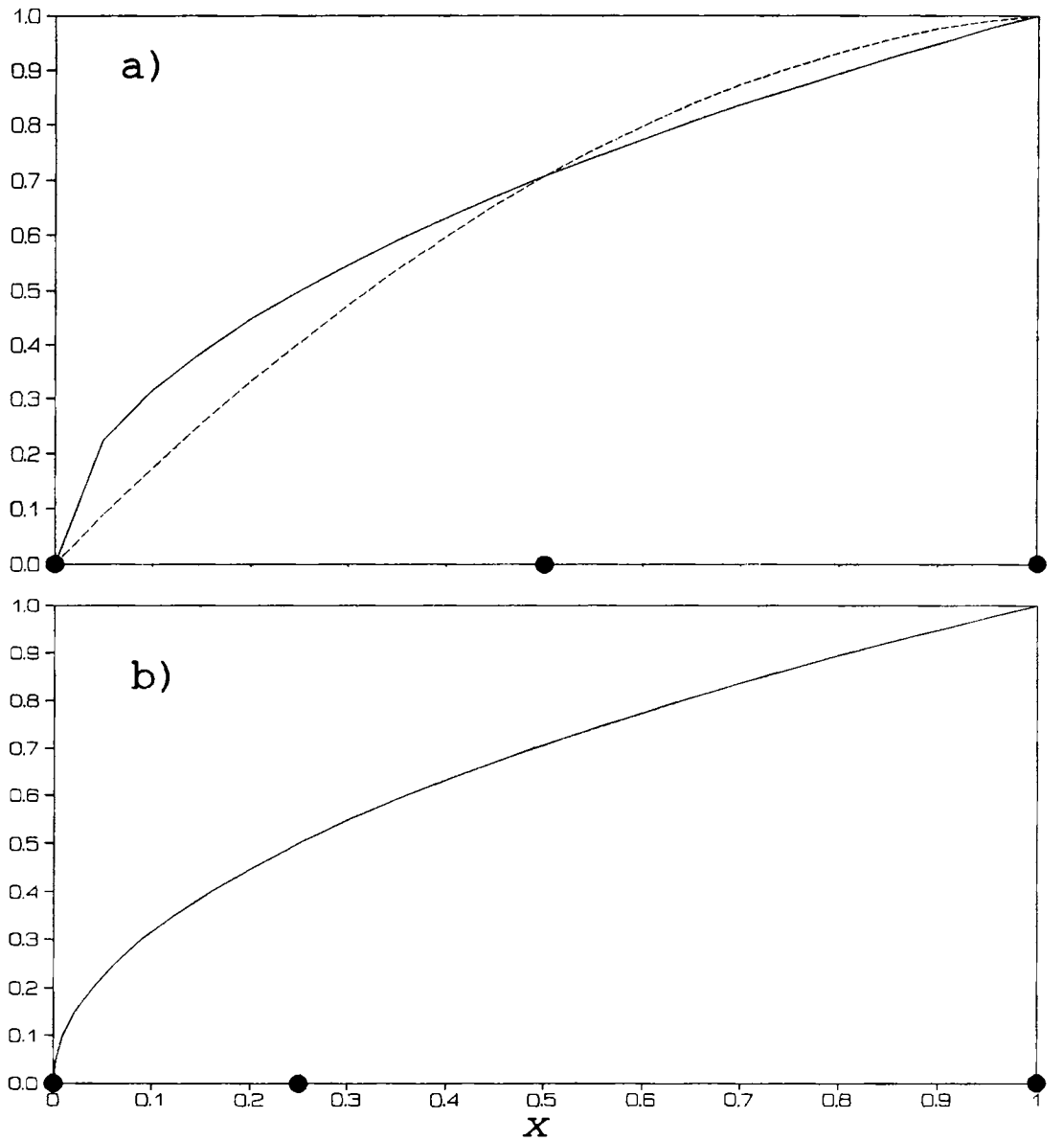

Figure 4-22. Approximation of the squareroot function by quadratic shape functions. a) normal technique; b) quarter-point technique. ————, squareroot function; --------, approximation by quadratic shape functions. The nodal points are indicated with bold dots on the x-axis.

Thus the idea of using a similar technique to model the $r^{2/3}$ behavior of the pressure near the edge of the cylinder suggests itself. In order to do this, the $r^{2/3}$ function was plotted and the mid-element node was displaced in order to obtain a good approximation of the $r^{2/3}$ function near r=0. After a few attemp it was found that if the mid-element node was placed at a distance of 0.275 times the element length to the singularity,

a good approximation of the $r^{2/3}$ function was obtained as shown in Figure 4-23. Note, however, that the $r^{2/3}$ function is not exactly represented by the shape functions, as was the case for the squareroot function.

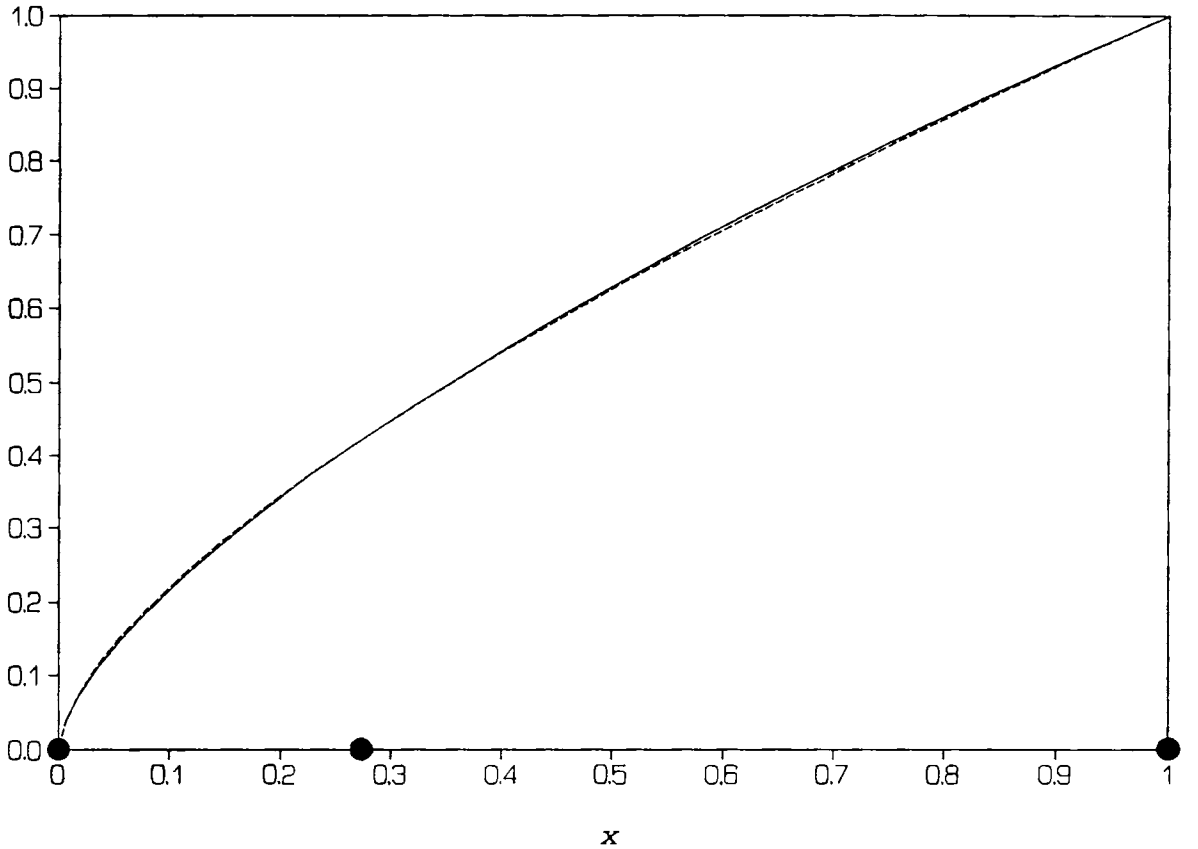

Figure 4-23. Approximation of the $r^{2/3}$ function by quadratic shape functions. ————, $r^{2/3}$ function; --------, approximation by quadratic shape functions. The nodal points are indicated with bold dots on the x-axis.

The problem of scattering of a plane wave of unit magnitude by a rigid cylinder at ka=1 was then re-calculated using this generalized quarter-point technique. Figure 4-24 show the error of the original implementation using normal isoparametric quadratic elements and the error of the new implementation using isoparametric quadratic elements and the generalized quarter-point technique. The error is the length of the residual vector, which contains the difference between the 'analytical' solution and the calculated solution at the two 'end-element' nodes. The reason for not including the mid-element

node was simply that the 'analytical' solution not readily produces a value at this node. The 'analytical' solution was the fine-meshed boundary element calculation also used in paragraph 4.6.2.

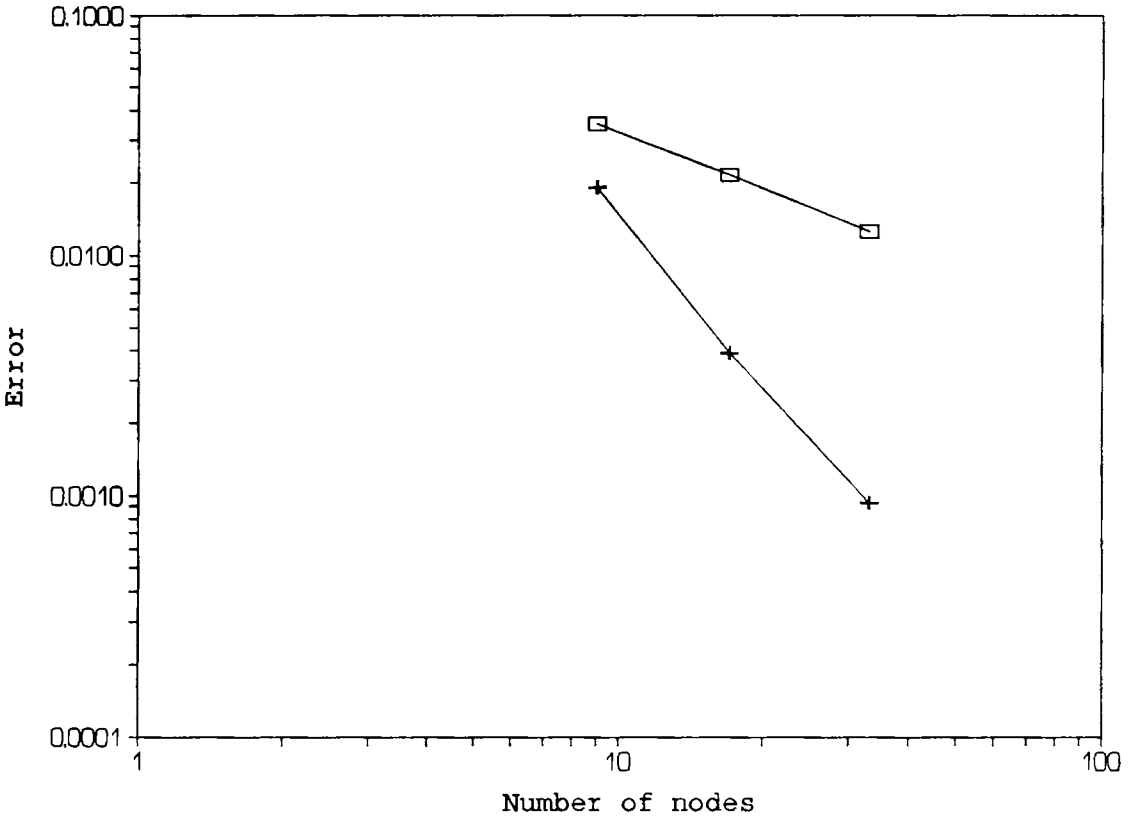

Figure 4-24. Error made by the two boundary element formulations for scattering by a rigid cylinder at ka=1. ——□——, normal isoparametric quadratic formulation; ——+——, generalized quarter-point formulation.

It can be seen from Figure 4-24 that the formulation using the generalized quarter-point technique produces a much more accurate result than the normal formulation. Moreover, the generalized quarter-point technique seems to restore the high convergence rate of the isoparametric quadratic formulation. The author expects that any scattering problem with a singularity due to an edge, can be modelled accurately by an adequate placement of the mid-element node.

4.6.6 CONCLUDING REMARKS

The convergence of the three boundary element formulations for the axisymmetric integral equation has been examined in four test cases. The test cases chosen should throw light on the effect of the approximations made regarding the geometry and the acoustic variables. The results presented here are mainly of theoretical interest, since an optimized formulation for practical use would be carried out with a more coarse integration over each element, so that the error due to this integration could not be neglected. Moreover, a pratical formulation would not use equally sized elements, as used for these test cases.

However, the test cases presented here may serve as an instrument to compare different boundary element formulations. It must be admitted that the calculations presented in this section merely outlines the topic of convergence, and some of the complications, which arise when this topic is examined. Much further theoretical work and further test cases should be made in order to investigate convergence of boundary element formulations adequately. It would also be interesting to evaluate the ability of different methods to overcome the non-uniqueness problem with respect to convergence, in a much more systematic manner than it has been done until now in the literature. The non-uniqueness problem is presented in chapter 5.

Finally, a generalized quarter-point technique was used to model the $r^{2/3}$ behaviour of the pressure near the edge of a rigid cylinder when scattering an incoming plane wave. The generalized quarter-point technique improves the accuracy of the isoparametric formulation significantly and restores the high convergence rate of this formulation.

4.7 IMPLEMENTATION OF THE THREE-DIMENSIONAL FORMULATION

A simple implementation of the Helmholtz integral equation for three-dimensional problems using constant elements has been outlined in section 4.1. In this section the more advanced approaches, using elements corresponding to linear and quadratic shape functions, will be described [8,9,80,112]. Usually two types of elements are used: triangular and quadrilateral elements. The transformation of the three-dimensional Helmholtz integral equation into a set of linear equations will not be described as detailed as for the axisymmetric formulation, since the general ideas are the same. Thus, the elements of the difference formulations and the corresponding shape functions will merely be listed, and some comments on the transformation to a set of linear equations will be given. A three-dimensional boundary element formulation has been implemented using superparametric elements, and test cases for this implementation will be presented.

4.7.1 LINEAR TRIANGULAR ELEMENTS

If the geometry is assumed to vary linearly between the nodes, the global coordinates (x,y,z) are connected to the local coordinates of the elements as follows:

$$\begin{aligned} x &= x_1\xi_1 + x_2\xi_2 + x_3\xi_3 \ , \\ y &= y_1\xi_1 + y_2\xi_2 + y_3\xi_3 \ , \\ z &= z_1\xi_1 + z_2\xi_2 + z_3\xi_3 \ . \end{aligned} \tag{4.46}$$

Here $\xi_3=1-\xi_1-\xi_2$, and the indices for the global coordinates refer to the local node numbering defined in Figure 4-25. Clearly ξ_1 and ξ_2 suffices in order to describe the planar triangular geometry - the reason for defining the dependant third coordinate ξ_3 is that the resulting equations then become neatly symmetric with respect to the ξ's. Thus the shape functions for this case are simply

$$N_1(\xi_1,\xi_2,\xi_3) = \xi_1 ,$$
$$N_2(\xi_1,\xi_2,\xi_3) = \xi_2 , \qquad (4.47a,b,c)$$
$$N_3(\xi_1,\xi_2,\xi_3) = \xi_3 ,$$

and the planar element described by the three sets of global coordinates (x_1,y_1,z_1), (x_2,y_2,z_2), and (x_3,y_3,z_3) is transformed into a planar triangular element in a (ξ_1,ξ_2,ξ_3) system, as sketched in Figures 4-25 a) and 4-25 b). The (ξ_1,ξ_2,ξ_3) system is the well-known area-coordinate system frequently used in finite element methods, from where the term 'parent element' for the element in Figure 4-25 b) is also adopted. The Jacobian of this transformation equals the ratio between the areas of the triangles, which is $2A$, where A is the area of the element in Figure 4-25 a). Note that the parent element is shown in a way that underlines the symmetry with respect to the ξ's and not in a right-angled coordinate system, and that the area of the parent element actually is 1/2.

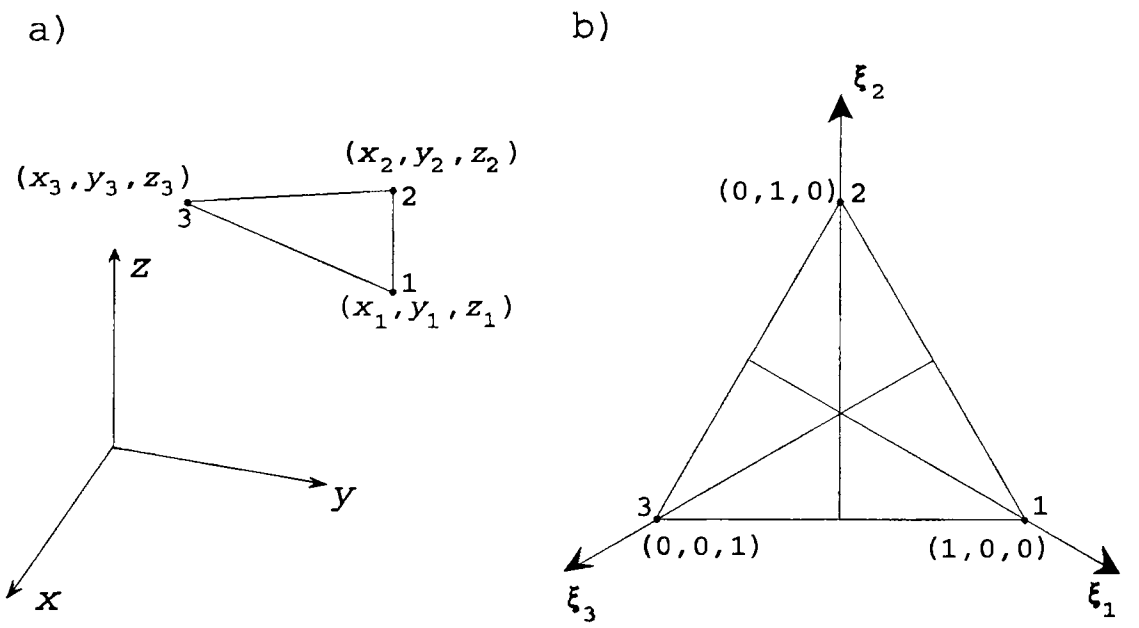

Figure 4-25. Transformation of a planar triangular element to its corresponding parent element. a) The planar element in the global coordinate system with local numbering of the nodes indicated. b) Corresponding parent element in local coordinate system with local node numbers indicated.

The pressure and the normal velocity may be expressed by the same shape functions:

$$p(\xi_1,\xi_2,\xi_3) = \sum_{\alpha=1}^{3} N_\alpha(\xi_1,\xi_2,\xi_3)\, p_\alpha \ , \tag{4.48}$$

and

$$v(\xi_1,\xi_2,\xi_3) = \sum_{\alpha=1}^{3} N_\alpha(\xi_1,\xi_2,\xi_3)\, v_\alpha \ . \tag{4.49}$$

In this case the element above is termed isoparametric linear triangular element.

4.7.2 QUADRATIC TRIANGULAR ELEMENTS

If a quadratic variation of the geometry is assumed 6 nodes are required to describe the geometry. Figure 4-26 shows the transformation from the global coordinate system to the local coordinate system in this case.

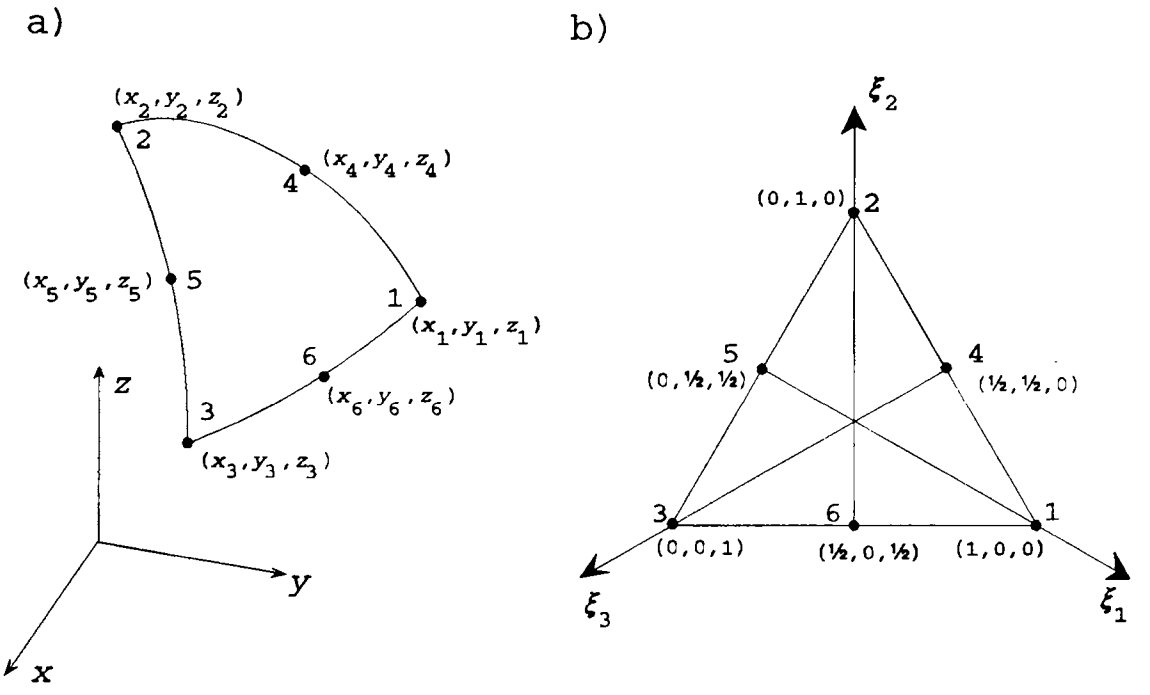

Figure 4-26. Transformation of a curved triangular element to its corresponding parent element. a) The curved element in the global coordinate system with local numbering of the nodes indicated. b) Corresponding parent element in local coordinate system with local node numbers indicated.

The shape functions of this transformation are:

$$\begin{aligned} N_1(\xi_1,\xi_2,\xi_3) &= \xi_1(2\xi_1-1), \\ N_2(\xi_1,\xi_2,\xi_3) &= \xi_2(2\xi_2-1), \\ N_3(\xi_1,\xi_2,\xi_3) &= \xi_3(2\xi_3-1), \\ N_4(\xi_1,\xi_2,\xi_3) &= 4\xi_1\xi_2, \\ N_5(\xi_1,\xi_2,\xi_3) &= 4\xi_2\xi_3, \\ N_6(\xi_1,\xi_2,\xi_3) &= 4\xi_1\xi_3, \end{aligned} \qquad (4.50a\text{-}f)$$

where $\xi_3=1-\xi_1-\xi_2$. This leads to the following expression for the global coordinates for a point of the element, as a function of the local coordinates (ξ_1,ξ_2,ξ_3):

$$\begin{aligned} x(\xi_1,\xi_2,\xi_3) &= \sum_{\alpha=1}^{6} N_\alpha(\xi_1,\xi_2,\xi_3)\, x_\alpha , \\ y(\xi_1,\xi_2,\xi_3) &= \sum_{\alpha=1}^{6} N_\alpha(\xi_1,\xi_2,\xi_3)\, y_\alpha , \\ z(\xi_1,\xi_2,\xi_3) &= \sum_{\alpha=1}^{6} N_\alpha(\xi_1,\xi_2,\xi_3)\, z_\alpha . \end{aligned} \qquad (4.51a,b,c)$$

The Jacobian of this transformation is

$$J(\xi_1,\xi_2,\xi_3) = \| (\partial r/\partial\xi_1)\times(\partial r/\partial\xi_2) \|_2 , \qquad (4.52)$$

where $r=(x,y,z)$. Note that the Jacobian is the lenght of the normal vector:

$$n = \frac{\partial r}{\partial \xi_1}\times\frac{\partial r}{\partial \xi_2} , \qquad (4.53)$$

which is also needed to construct the normal derivative of Green's function.

The pressure and normal velocity are approximated using the same shape functions:

$$p(\xi_1,\xi_2,\xi_3) = \sum_{\alpha=1}^{6} N_\alpha(\xi_1,\xi_2,\xi_3)\, p_\alpha \ , \qquad (4.54)$$

and

$$v(\xi_1,\xi_2,\xi_3) = \sum_{\alpha=1}^{6} N_\alpha(\xi_1,\xi_2,\xi_3)\, v_\alpha \ . \qquad (4.55)$$

Thus, an isoparametric quadratic triangular element has been obtained.

4.7.3 LINEAR QUADRILATERAL ELEMENTS

Consider the transformation of a plane quadrilateral element to its parent element as sketched in Figure 4-27.

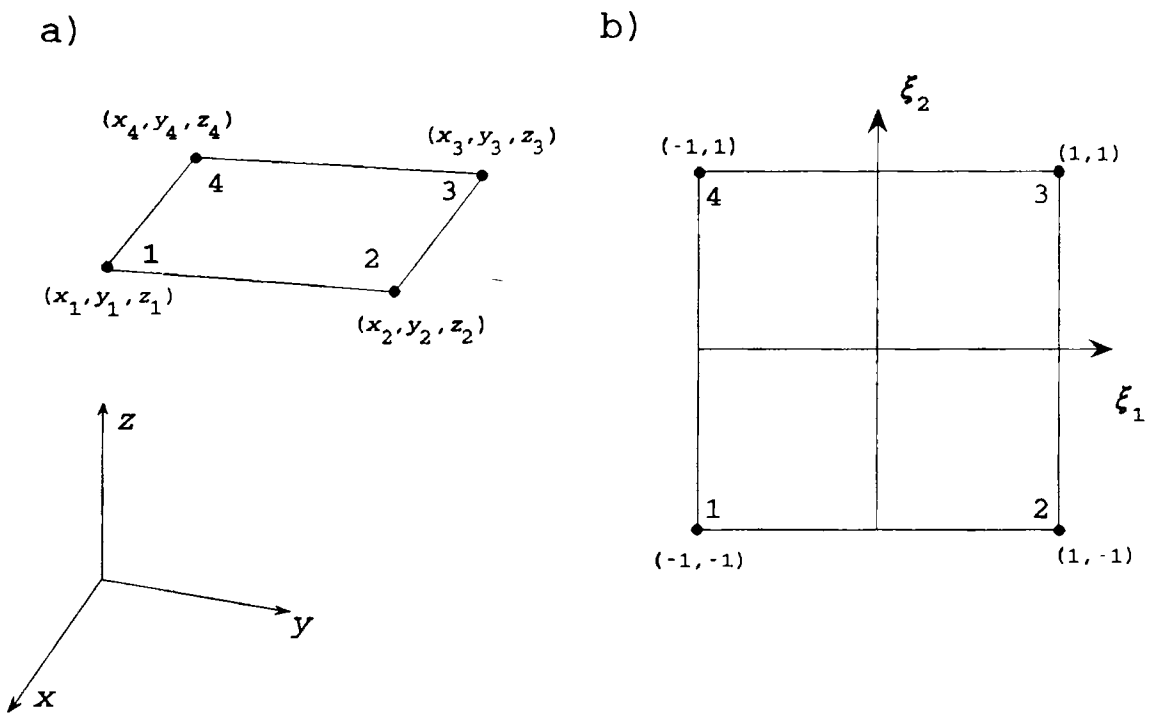

Figure 4-27. Transformation of a planar quadrilateral element to its corresponding parent element. a) The planar element in the global coordinate system with local numbering of the nodes indicated. b) Corresponding parent element in local coordinate system with local node numbers indicated.

The shape functions of this transformation are:

$$
\begin{aligned}
N_1(\xi_1,\xi_2) &= \tfrac{1}{4}(1-\xi_1)(1-\xi_2) \ , \\
N_2(\xi_1,\xi_2) &= \tfrac{1}{4}(1+\xi_1)(1-\xi_2) \ , \\
N_3(\xi_1,\xi_2) &= \tfrac{1}{4}(1+\xi_1)(1+\xi_2) \ , \\
N_4(\xi_1,\xi_2) &= \tfrac{1}{4}(1-\xi_1)(1+\xi_2) \ ,
\end{aligned}
\qquad (4.56a\text{-}d)
$$

which leads to the following expression for the global coordinates for a point on the element in terms of the local coordinates:

$$
\begin{aligned}
x(\xi_1,\xi_2) &= \sum_{\alpha=1}^{4} N_\alpha(\xi_1,\xi_2)\, x_\alpha \ , \\
y(\xi_1,\xi_2) &= \sum_{\alpha=1}^{4} N_\alpha(\xi_1,\xi_2)\, y_\alpha \ , \\
z(\xi_1,\xi_2) &= \sum_{\alpha=1}^{4} N_\alpha(\xi_1,\xi_2)\, z_\alpha \ .
\end{aligned}
\qquad (4.57a,b,c)
$$

The Jacobian of this transformation equals $A/4$, where A is the area of the element in Figure 4-27 a). In order to obtain an isoparametric linear quadrilateral element, the pressure and normal velocity are approximated using the same shape functions:

$$
p(\xi_1,\xi_2) = \sum_{\alpha=1}^{4} N_\alpha(\xi_1,\xi_2)\, p_\alpha \ , \qquad (4.58)
$$

and

$$
v(\xi_1,\xi_2) = \sum_{\alpha=1}^{4} N_\alpha(\xi_1,\xi_2)\, v_\alpha \ . \qquad (4.59)
$$

Note that the unit normal vector is constant within each element.

4.7.4 QUADRATIC QUADRILATERAL ELEMENTS

Finally, the quadratic quadrilateral element is considered. In this case the geometry is assumed to vary in a quadratic

manner over each element. Now 8 nodes are needed for a description of the geometry, as sketched in Figure 4-28.

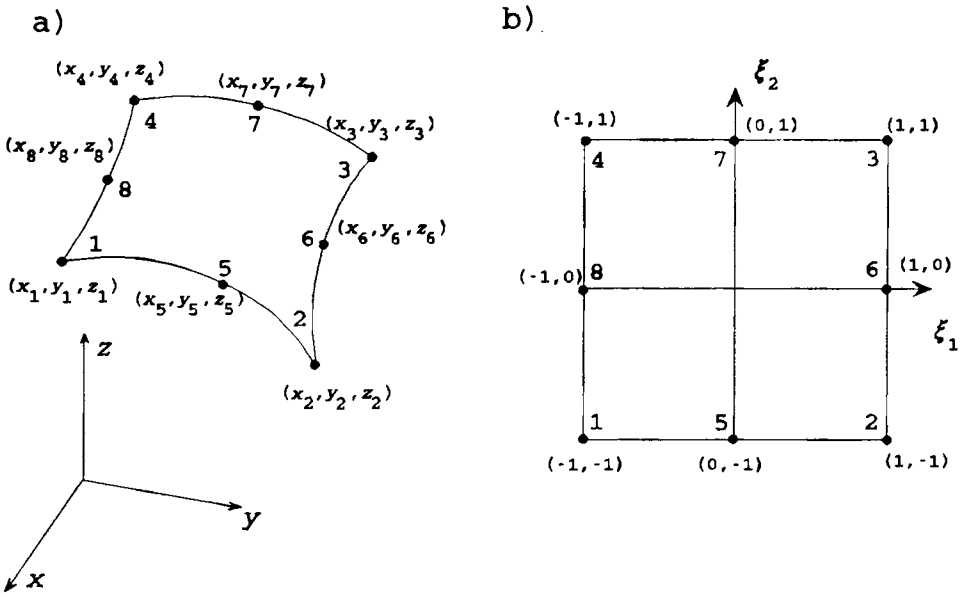

Figure 4-28. Transformation of a curved quadrilateral element to its corresponding parent element. a) The curved element in the global coordinate system with local numbering of the nodes indicated. b) Corresponding parent element in local coordinate system with local node numbers indicated.

The shape functions of this transformation are:

$$N_1(\xi_1,\xi_2) = \tfrac{1}{4}(1-\xi_1)(1-\xi_2)(-\xi_1-\xi_2-1),$$

$$N_2(\xi_1,\xi_2) = \tfrac{1}{4}(1+\xi_1)(1-\xi_2)(\xi_1-\xi_2-1),$$

$$N_3(\xi_1,\xi_2) = \tfrac{1}{4}(1+\xi_1)(1+\xi_2)(\xi_1+\xi_2-1),$$

$$N_4(\xi_1,\xi_2) = \tfrac{1}{4}(1-\xi_1)(1+\xi_2)(-\xi_1+\xi_2-1),$$

$$N_5(\xi_1,\xi_2) = \tfrac{1}{2}(1-\xi_1^2)(1-\xi_2),$$

$$N_6(\xi_1,\xi_2) = \tfrac{1}{2}(1-\xi_2^2)(1+\xi_1),$$

$$N_7(\xi_1,\xi_2) = \tfrac{1}{2}(1-\xi_1^2)(1+\xi_2),$$

$$N_8(\xi_1,\xi_2) = \tfrac{1}{2}(1-\xi_2^2)(1-\xi_1). \qquad (4.60a\text{-}h)$$

In this case the global coordinates of a point on the element is related to the local coordinates as follows:

$$x(\xi_1,\xi_2) = \sum_{\alpha=1}^{8} N_\alpha(\xi_1,\xi_2)\, x_\alpha \,,$$

$$y(\xi_1,\xi_2) = \sum_{\alpha=1}^{8} N_\alpha(\xi_1,\xi_2)\, y_\alpha \,, \qquad (4.61a,b,c)$$

$$z(\xi_1,\xi_2) = \sum_{\alpha=1}^{8} N_\alpha(\xi_1,\xi_2)\, z_\alpha \,.$$

As was also the case for the quadratic triangular elements, the Jacobian is the lenght of the normal vector $\boldsymbol{n}$:

$$\boldsymbol{n} = \frac{\partial \boldsymbol{r}}{\partial \xi_1} \times \frac{\partial \boldsymbol{r}}{\partial \xi_2} \,, \qquad (4.62)$$

where $\boldsymbol{r}=(x,y,z)$. If now the pressure and normal velocity are expressed using the same shape functions:

$$p(\xi_1,\xi_2) = \sum_{\alpha=1}^{8} N_\alpha(\xi_1,\xi_2)\, p_\alpha \,, \qquad (4.63)$$

and

$$v(\xi_1,\xi_2) = \sum_{\alpha=1}^{8} N_\alpha(\xi_1,\xi_2)\, v_\alpha \,, \qquad (4.64)$$

an isoparametric quadratic quadrilateral element has been obtained.

4.7.5 SUPERPARAMETRIC TRIANGULAR ELEMENTS

If the shape functions used to approximate the body are of a higher order than the shape functions used to approximate the acoustics variables, the elements are termed superparametric [32]. Conversely, if the shape functions for the geometry are of a lower order than the shape functions of the acoustics variables, the elements are termed subparametric. In order to obtain superparametric elements, quadratic shape functions (equations (4.50a-f), (4.51a,b,c), (4.52), and (4.51)) are used to discretize the geometry, whereas linear shape functions

(equations (4.48) and (4.49)) are used to discretize the acoustic variables.

As the quadratic shape functions was implemented for acoustic boundary element computations [80,81] it was stated that the main benefit of using these elements was the ability of the quadratic elements to represent curved surfaces, whereas the benefit of a better representation of the acoustic variables was less significant. Furthermore, it was found in section 4.6, where convergence of the axisymmetric formulations was discussed, that singularities often caused the pressure to be only continuous. This destroys the main benefit of using high order shape functions, the benefit being faster convergence than obtained when using shape functions of lower order. Finally, since all programming of this project was carried out on a regular personal computer, it was important to use as few acoustical nodes as possible when calculating three-dimensional problems, in order to keep the sizes of the resulting matrices to within resonable limits. It was also found in section 4.6 that the error made by the axisymmetric superparametric formulation in three of the four test cases was smaller than, or of the same magnitude, as the error made by both the isoparametric linear formulation and the isoparametric quadratic formulation.

4.7.6 NUMBERING OF NODES

For the reasons outlined above a superparametric triangular formulation was implemented for calculating three-dimensional problems.

When discretizing a three-dimensional problem, the relation between local and global node numbers are not as simple as when discretizing the generator of an axisymmetric body. Fortunately, the numbering of nodes is not as critical for boundary element formulations as it is for the finite element method, where correct numbering is vital for the bandwidth of the resulting matrices and thus for the efficiency of the method. For boundary element calculations the resultating matrices are generally fully populated (all elements are non-zero), and the problem of reducing the bandwidth does nor occur.

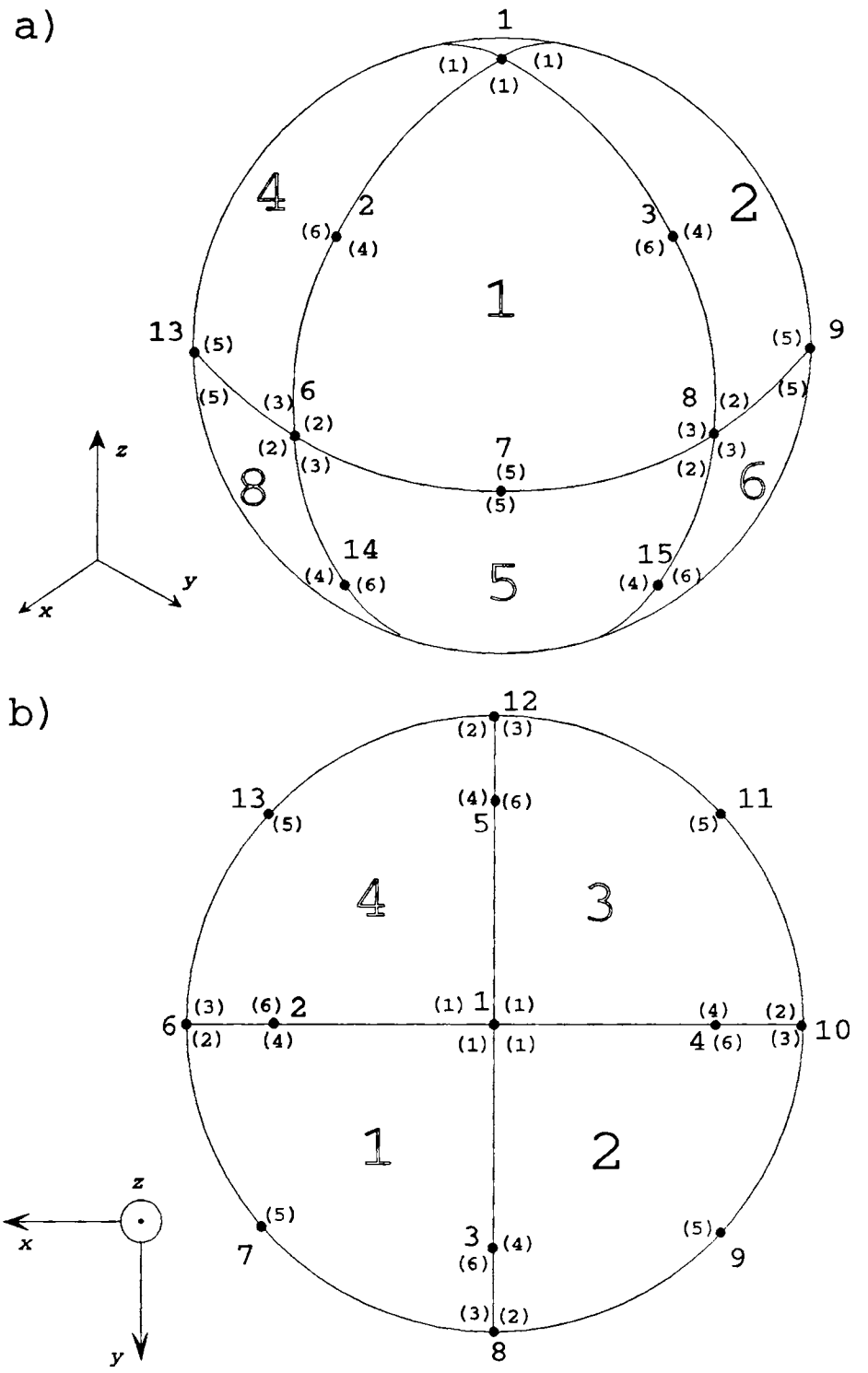

Figure 4-29. Discretization of a sphere of radius one into 8 quadratic triangular elements. a) Perspective view. b) Upper hemisphere. The large number in the centre of each element is the element number, the normal sized numbers are the global node numbers, and the small numbers in brackets are the local node numbers.

As an example of how the data structures needed to describe the geometry are defined, and how the relation between local and global numbering of the nodes is obtained the discretization of a sphere is considered. Figure 4-29 a) shows the discretization of a sphere of radius one into 8 quadratic triangular elements, and Figure 4-29 b) shows the upper hemisphere. With the numbering indicated in Figure 4-29 the global (x,y,z)-coordinates of the geometrical nodes are listed in Table 2.

Global node number	x	y	z
1	0	0	1
2	0,7071	0	0,7071
3	0	0,7071	0,7071
4	-0,7071	0	0,7071
5	0	-0,7071	0,7071
6	1	0	0
7	0,7071	0,7071	0
8	0	1	0
9	-0,7071	0,7071	0
10	-1	0	0
11	-0,7071	-0,7071	0
12	0	-1	0
13	0,7071	-0,7071	0
14	0,7071	0	-0,7071
15	0	0,7071	-0,7071
16	-0,7071	0	-0,7071
17	0	-0,7071	-0,7071
18	0	0	-1

Table 2. The global coordinates of the global geometrical nodes

A data structure is now needed which connects the local node number of each element to the global node number. An

example of this data structure for the sphere shown in Figure 4-29 is shown in Table 3. The table is read in the following way: For the 4'th local node of the 5'th element the global node number is 15, for instance.

element number	local node 1	local node 2	local node 3	local node 4	local node 5	local node 6
1	1	6	8	2	7	3
2	1	8	10	3	9	4
3	1	10	12	4	11	5
4	1	12	6	5	13	2
5	18	8	6	15	7	14
6	18	10	8	16	9	15
7	18	12	10	17	11	16
8	18	6	12	14	13	17

Table 3. The global node numbers *vs.* the local node number and the element number.

For the superparametric formulation not all geometrical nodes are acoustical nodes as well - only the local geometrical nodes 1, 2 , and 3 of figure 4-29 b) are also acoustical nodes. For the discretized sphere in figure 4-29 there are 6 acoustical nodes with the global geometrical node numbers {1,6,8,10, 12,18}. Hence, for the superparametric formulation a further data structure must be defined, which establishes the relationship between the global geometrical node number and the global acoustical node number. This data structure, for the example of the sphere, is listed in Table 4.

In order to find the global (x,y,z) coordinates needed to calculate the source-receiver distance R of Green's function and its derivative, as a function of the integration variables ξ_1, ξ_2 and the dependent coordinate ξ_3, the procedure is: Relate the local node number of the geometrical node to its global node number by a look-up in Table 3 and then find its global coordinates through Table 2.

Global acoustical node number	1	2	3	4	5	6
Global geometrical node number	1	6	8	10	12	18

Table 4. Relation between the global acoustical node number and the global geometrical node number.

The procedure for setting up the set of linear equations is as follows: Place the collocation point number i at the i'th acoustical node to form the i'th row of the 'influence' matrices $\boldsymbol{H}$ and $\boldsymbol{G}$ of equation (4.8). For each element a numerical integration of the 'influence' functions is carried out and the result is referred to the corresponding local acoustical nodes (i.e. the local geometrical nodes 1, 2, and 3) through the acoustical shape functions of equations (4.48) and (4.49). The results of the integrations are referred to the global acoustical nodes through look-ups in Tables 3 and 4 and placed in the corresponding columns of the $\boldsymbol{H}$ and $\boldsymbol{G}$ matrices.

4.7.7 NUMERICAL INTEGRATION OF TRIANGULAR ELEMENTS

For the triangular elements in Figures 4-25 b) and 4-26 b) special numerical integration formulas are given [8,112]. The formula used here is of order 6. The integration points and the corresponding weights is shown in Figure 4-30.

Note that the weights listed in Figure 4-30 adds up to one, and hence the result of the integration should be multiplied by the area of the triangle (1/2 for the triangular parent element).

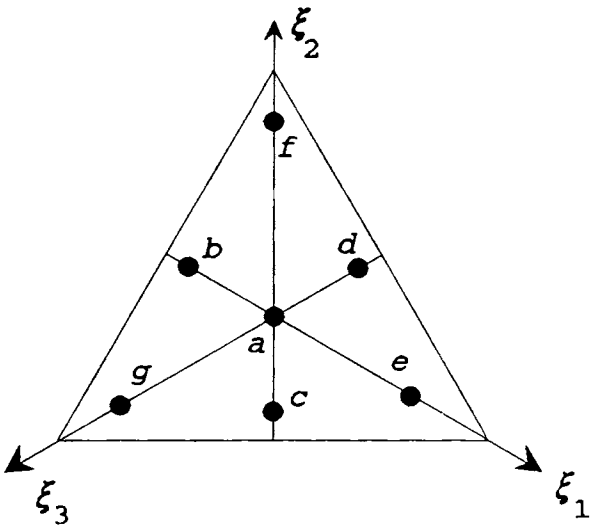

Points	(ξ_1, ξ_2, ξ_3)	Weights
a	(1/3,1/3,1/3)	0.2250000000
b	$(\alpha_1, \beta_1, \beta_1)$	0.1323941527
c	$(\beta_1, \alpha_1, \beta_1)$	0.1323941527
d	$(\beta_1, \beta_1, \alpha_1)$	0.1323941527
e	$(\alpha_2, \beta_2, \beta_2)$	0.1259391805
f	$(\beta_2, \alpha_2, \beta_2)$	0.1259391805
g	$(\beta_2, \beta_2, \alpha_2)$	0.1259391805

with

$\alpha_1 = 0.0597158717$

$\beta_1 = 0.4701420641$

$\alpha_2 = 0.7974269853$

$\beta_2 = 0.1012865073$

Figure 4-30. Numerical integration formula for triangle. The Gauss points and the corresponding weights are also listed.

4.7.8 NUMERICAL INTEGRATION OF QUADRILATERAL ELEMENTS

For the quadrilateral parent elements of Figures 4-27 b) and 4-28 b) numerical integration of a function f may be carried out by combining two one-dimensional Guassian quadrature formulas:

$$\int_{-1}^{1}\int_{-1}^{1} f(\xi_1,\xi_2)\, d\xi_1\, d\xi_2 \approx \sum_{j=1}^{J}\sum_{i=1}^{I} f(x_i,x_j) w_i w_j \,. \qquad (4.65)$$

Here the Gauss points (x_i and x_j) and weights (w_i and w_j) of the one-dimensional formula discussed in paragraph 4.3.3 are used.

4.7.9 SINGULAR INTEGRALS

For the integration over the elements in contact with the collocation point, special care must be taken since the Green's function and its normal derivative contain singularities of order $1/R$ [75,81].

In reference [75] these integrals were handled by intro-

ducing a local polar coordinate system (r,θ), such that the singularity was placed in r=0. In this way the singularity is neutralized due to the factor r in the Jacobian of the transformation. In references [8, 29] specialized numerical integration formulas for triangles and quadrangles with an $1/R$ singularity is given. In the present work the idea due to Rizzo and Shippy [75] has been used, and the technique will hence be outlined, for the case of a singularity at the corner of a triangle.

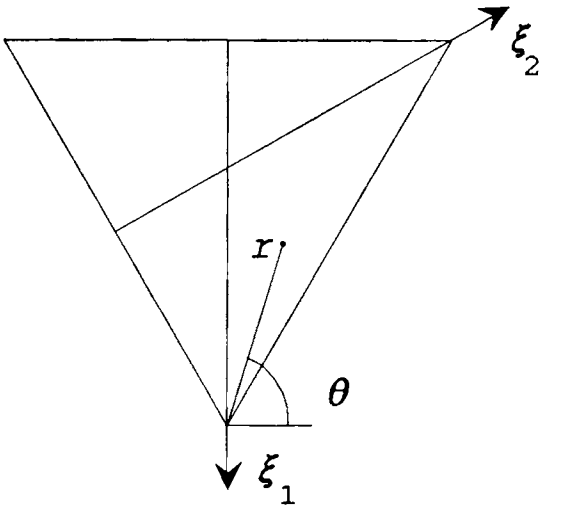

Figure 4-31. Definition of local polar coordinate system for a triangular element with a singularity at the local node number 1.

Consider the triangular parent element of Figures 4-25 b) and 4-26 b). If the singularity is placed at the local node number 1, the polar coordinate system (r,θ) should be placed so that r=0 at the singularity as sketched in Figure 4-31. For this transformation

$$\xi_1 = 1-r\sin\theta \quad \text{,and} \quad \xi_2 = \frac{\sqrt{3}}{2} r\cos\theta + \frac{1}{2} r\sin\theta \qquad (4.66)$$

is found. The Jacobian of this transformation equals $\sqrt{3}/2\ r$. Note that mathematically this transformation is illegal due to the singularity of the function to be integrated, but this may be handled by excluding a small area of radius ϵ around the singularity and then let ϵ tend to zero. Thus the integral of the singular function f is transformed as follows:

$$\int_{S_j} f(\xi_1,\xi_2)\ d\xi_1 d\xi_2 = \int_{\pi/3}^{2\pi/3} \int_0^{1/r\sin\theta} f(r,\theta) \frac{\sqrt{3}}{2} r\, dr\, d\theta \quad , (4.67)$$

and thereby the $1/R$ singularity of f is neutralized by the

Jabobian of the transformation. The two-dimensional integral on the right-hand side of equation (4.67) may be solved numerically by combining two one-dimensional Gaussian quadrature formulas as described in paragraph 4.7.8. Note that this method of numerically integrating the right side of equation (4.67) also has the advantage of close spacing of the Gauss points near the singularity as sketched in Figure 4-32.

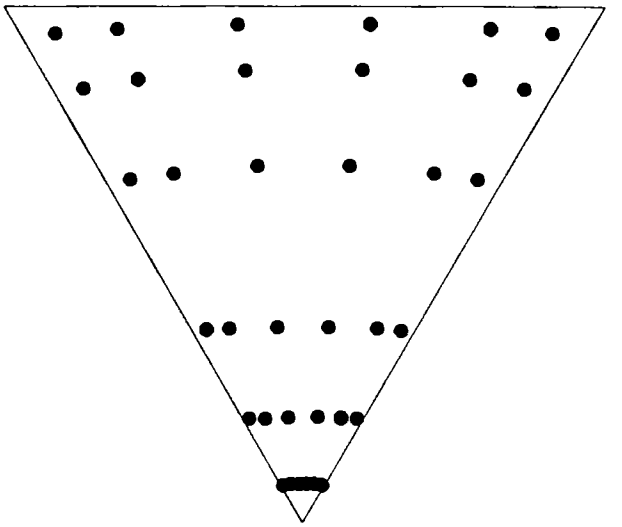

Figure 4-32. Gauss points for the element in Figure 4-31 using two one-dimensional 6 point Gaussian quadrature formulas.

Due to the symmetry of the ξ's, the transformations in the cases where the singularity is placed at either local node 2 or 3 are easily found by suitable rotation of ξ_1, ξ_2, and ξ_3 in equations (4.66) and (4.67).

4.7.10 TEST CASES

For the superparametric triangular model a few test cases has been calculated. The test cases all concern the very familiar case of scattering by a rigid sphere and they are compared to an analytical solution and to the superparametric axisymmetric formulation described in paragraph 4.4.3. The reason for not testing the three-dimensional formulation for a more complicated body shape is that the surface mesh is generated 'by hand' since at this moment no 'pre-processor' for generating the mesh is avaliable. Hence, at this stage, mesh generating is a quite time consuming task, and further verification of the three-dimensional formulation was not carried out.

Figure 4-33 a)-c) shows the pressure on the surface of a rigid sphere exposed to a plane wave of magnitude one (dimensionless for convenience) as functions of the angle

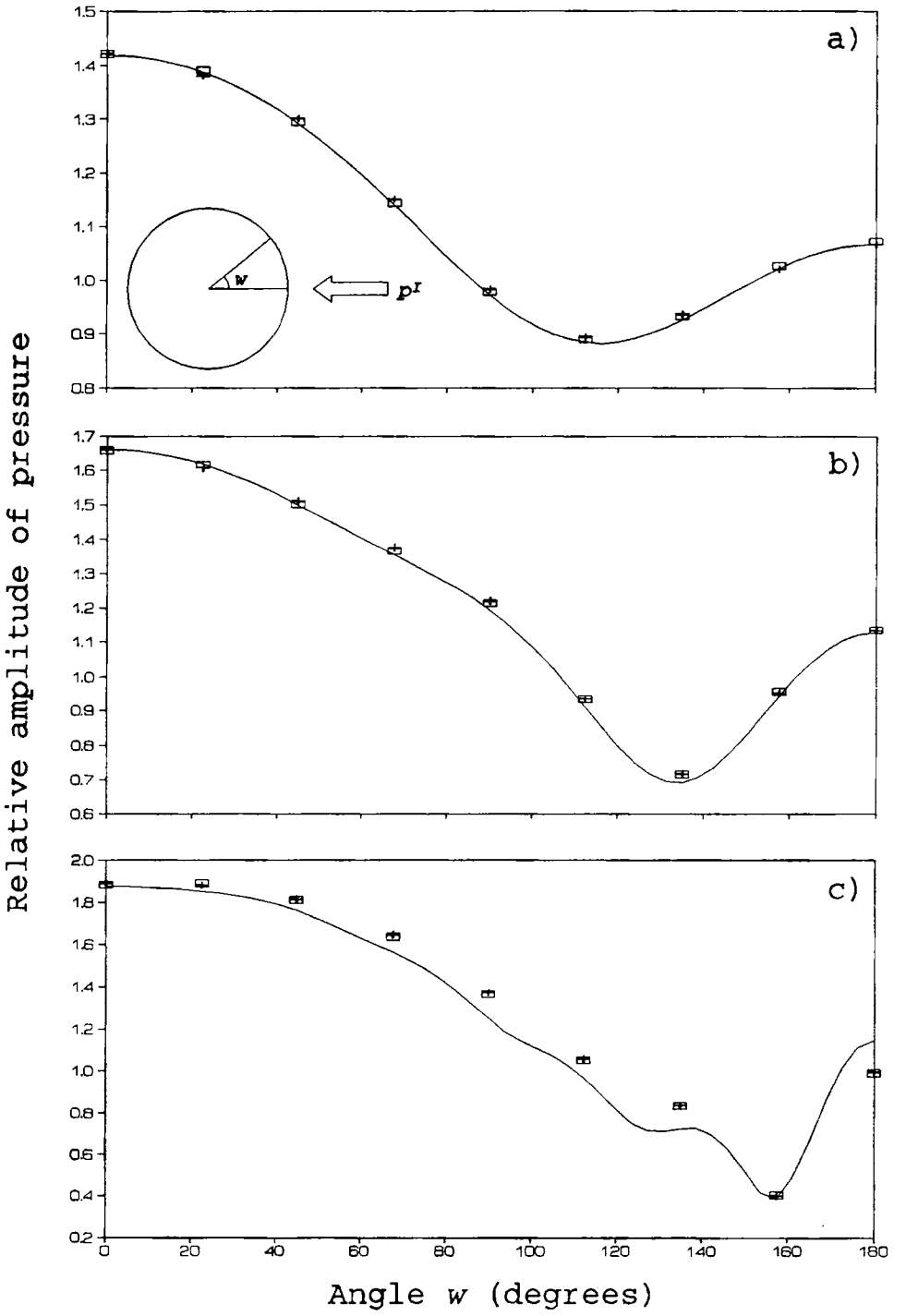

Figure 4-33. Pressure on the surface of a sphere of radius *a* when scattering of a plane incoming wave is considered. a) *ka*=1, b) *ka*=2, c) *ka*=5. ————, analytical solution; □, superparametric axisymmetric formulation; +, superparametric three-dimensional formulation.

defined in the small inset in Figure 4-33 a). The test cases were run for ka=1 (Figure 4-33 a)), ka=2 (Figure 4-33 b)), and ka=5 (Figure 4-33 c)), where a is the radius of the sphere. In the figures three curves are shown: the analytical solution, the boundary element solution obtained by the superparametric axisymmetric formulation, and the boundary element solution obtained by the superparametric three-dimensional formulation. For the superparametric axisymmetric formulation 8 quadratic elements were used to model the generator of the sphere corresponding to 9 acoustical nodes on the generator. The superparametric three-dimensional formulation used 168 quadratic triangular elements, which corresponds to 86 acoustical nodes. The acoustical nodes were placed in a manner, such that there were 9 acoustical nodes on the generator of the sphere for the three-dimensional formulation as well. Hence, the element size of the three-dimensional formulation is approximately equal to the element size of the axisymmetric formulation. The ratio of elements per wavelength is 16 for ka=1, 8 for ka=2, and 3 for ka=5. The figure shows that the results obtained by the axisymmetric formulation and the three-dimensional formulation are almost identical. Hence, it is concluded that the error made by the superparametric three-dimensional formulation for a given number of elements per wavelength is of the same size as the error made by the superparametric axisymmetric formulation for the same number of elements per wavelength. This indicates that the experience of accuracy *vs.* mesh fineness acquired in the case of the superparametric axisymmetric formulation can be transferred to the case of the superparametric three-dimensional formulation.

For the highest frequency corresponding to ka=5 the maximum deviation between the analytical solution and the two boundary element calculations is about 0.15, or 15% of the magnitude of the incoming sound wave. The computation time used by the two numerical formulations for each frequency was about 560 seconds for the three-dimensional formulation and about 6 seconds for the axisymmetric formulation (on a personal computer with a 33 MHz 80486 Intel processor). This underlines the advantage of

using the axisymmetric formulation instead of the three-dimentional formulation when problems with rotational symmetry are studied. In paragraph 4.5.1 it was found that 8 terms of the cosine expansion sufficed for an accurate prediction of the pressure on the surface of the sphere at ka=5 when the plane wave was supposed to travel along the negative ρ-axis, which is the situation requiring most cosine terms for a given frequency. Hence, the total time consumed by solving such a problem with the superparametric axisymmetric formulation would be about 8·6=48 seconds, which still is much less than the 560 seconds used in the full three-dimensional case.

4.7.11 CONCLUDING REMARKS

In section 4.7 the most common element types for three-dimensional formulations have been presented along with numerical integration schemes for these elements. Some comments concerning the practical implementation of the method were given in paragraph 4.7.6. A superparametric three-dimensional formulation using triangular elements was implemented and tested for a few test cases. The singular integrals were handled by changing to a local polar coordinate system as suggested by Rizzo and Shippy [75]. The use of superparametric elements for three-dimensional formulations in acoustics has not previously been reported in the literature, as far as the author knows. The three-dimentional formulation has been compared to the axisymmetric formulation in terms of accuracy *vs.* computation time, and the benefit of making use of axisymmetry, when possible, was underlined.

5. THE NON-UNIQUENESS PROBLEM

H.A.Schencks paper of 1967 [78] is perhaps the most cited paper in the literature on the boundary element method in acoustics. In his paper Schenck demonstrate how the simple source formulation breaks down at certain characteristic frequencies for exterior acoustics radiation problems. He also proves that at the same frequencies the surface Helmholtz integral equation formulation described in section 4.1 fails to obtain a unique solution. Finally he proposes a Combined Helmholtz Integral Equation Formulation, CHIEF, which can overcome this problem, which is termed the non-uniqueness problem. This combined formulation is described in section 5.2. Since the paper by Schenck the non-uniqueness problem has frequently been adressed in the literature [10,13,21-22,28,30, 34,36-37,41-43,48,50,56,62-63,68,73-74,76,79,83-84,89,91,100-107,111].

The non-uniqueness problem is a purely mathematical problem, inherent in the surface Helmholtz integral equation (equation (2.26) with P on the surface S), and was originally pointed out by Lamb [58, p.500]. Hence, the problem is not connected to any particular numerical implementation, but occurs regardless of the choice of e.g. shape functions. It was shown by Schenck, that the characteristics frequencies for a given exterior radiation problem (i.e. an exterior Neumann boundary value problem) are the eigenfrequencies of the related interior problem with the same body shape, when the pressure is required to be zero on the inner side of the surface S (i.e. an interior Dirichlet problem). For this reason the characteristic frequencies are also termed fictitious eigenfrequencies [80, 91].

Later a more intuitive explanation has been given by Wu and Seybert [107] using the classical double-layer formulation [13]

$$4\pi p(P) = \int_S \frac{\partial G(P,Q)}{\partial n} \mu(Q)\, dS \,, \qquad (5.1)$$

where $\boldsymbol{n}$ is the outward normal, and μ is the initially unknown 'dipole' distribution on the surface S. In reference [107] it

was shown that when equation (5.1) was brought to the form required to solve the interior Dirichlet problem, it became of the same form as the Helmholtz integral equation for exterior Neumann problems. Since the solution of the interior Dirichlet problem has eigenfrequencies, where the solution is not unique, the exterior Helmholtz integral equation shares these eigenfrequencies, although physically no resonances occur for the exterior problem.

In the same paper it was finally made clear, that the characteristic frequencies of the Helmholtz integral equation for an exterior Dirichlet problem are the eigenfrequencies of the corresponding interior Dirichlet problem as well, and not the eigenfrequencies of the corresponding interior Neumann problem, as stated in some of the literature.

As explained in more detail in section 5.2, the combined formulation suggested by Schenck overcomes the non-uniqueness problem by adding additional constraints to the original system of equations, and thus the correct, unique solution is obtained. For the simple source formulation the 'breakdown' can not be repaired, since the solution produced by this formulation at characteristic frequencies is wrong, and not just non--unique.

The non-uniqueness problem occurs for exterior problems only. For interior problems all eigenfrequencies found by the numerical solution are the 'real' eigenfrequencies of the shape.

The theory behind the non-uniqueness problem is quite complicated, and in the following an intuitive explanation of this problem using terms from active sound control will be given. The author has found this analogy useful in order to grasp at least some of the essence of the non-uniqueness problem.

5.1 ACTIVE CONTROL RELATED EXPLANATION OF THE NON-UNIQUENESS PROBLEM

As stated above the non-uniqueness problem is independent of the actual numerical implementation, since the problem is

connected to the description of the sound field by means of an integral equation, where the integral is over the surface of the body. Hence, the following analogy will be exemplified in a constant element environment for simplicity. It must be emphasized that the explanation given here merely is an analogy and that the explanation is not mathematically waterproof.

Consider a constant element implementation of Helmholtz integral equation as outlined in section 4.1. The strengths of the sources on the boundary are determined by the boundary conditions. One of the most prominent features of the Helmholtz integral equation is the fact that the relationship between the sources and the boundary conditions implies, that for a valid solution a null-field inside the body is obtained. Note again, that the simple source formulation for which the null-field could not be obtained inside the surface as discussed in section 2.4, breaks irrepairably down at the characteristic frequencies.

If the exterior Helmholtz integral equation (2.26) is divided by 4π

$$\alpha p(P) = \frac{1}{4\pi}\int_S \left(p(Q)\frac{\partial G(R)}{\partial n} + ikz_0 v(Q) G(R) \right) dS + p^I(P) \qquad (5.1)$$

is obtained. Here all symbols are as defined in equation (2.26), and

$$\alpha = \begin{cases} 0 \ ; \ P \text{ inside } S \\ 1 \ ; \ P \text{ outside } S \\ 1/2 \ ; \ P \text{ on } S \text{ (for smooth boundary)} \end{cases} . \qquad (5.2)$$

If both the pressure $p(Q)$ and the normal velocity $v(Q)$ are known, the right-hand side of equation (5.1) defines an operator with the property of producing a null-field inside the boundary S. In the following this operator is termed the Helmholtz integral operator. The null-field property was required for a formulation satisfying Huygens' principle, as discussed in section 2.4. Note that the operator is discontinuous as a function of the observation point P. The null-field

inside the body is only obtained exactly with an infinite number of sources on the boundary. For a finite number of sources the null-field may be obtained approximately, and the deviation from the exact null-field tends to zero as the number of nodes tends to infinity. This is consistent with the behaviour of the sound field outside the body, where it was found that the error decreases as the number of elements is increased. As a rule of thumb two isoparametric quadratic elements per wavelength are suggested [107]. It appears that there is a close relation between the deviation from a null-field inside the body and the error made when predicting the sound field outside the body. Actually, it has been suggested [83] that the deviation from a null-field *inside* a body should be used as a quality indicator for a calculation of the sound field *outside* the body. Consider as an example the familiar case of scattering of a plane wave of magnitude one by a rigid sphere of radius a at $ka=2$, which is well below the first characteristic frequency of the sound field within sphere. Figure 5-1 shows the value of the right-hand side of equation (5.1) as a function of the position of the observation point P as defined in the small inset in Figure 5-1. The curves shown in Figure 5-1 are found by quadrature of the right-hand side of equation (5.1), where the pressure has been as found approximately by the boundary element formulation. For these calculations the axisymmetric isoparametric quadratic formulation was used. The dashed curve corresponds to two elements per wavelength, whereas the solid curve corresponds to four elements per wavelength. The curves in Figure 5-1 show that the null-field is obtained approximately for a finite number of nodes. The deviation from an exact null-field is less that 0.12 for the discretization using two elements per wavelength and less than 0.01 for the discretization using four elements per wavelength. Note that in an interval close to the surface of the sphere both curves show larger errors. This is due to the finite number of nodes. As the number of elements per wavelength is increased this interval becomes narrower.

Hence, although the analogy presented in the following is

based in the limit of an infinite number of sources, the results are approximately true for a finite number of sources, if the number of sources per wavelength is sufficiently large. One result of these approximations is that the boundary element coefficient matrix becomes not exactly singular, but only almost singular at the characteristic frequencies [34].

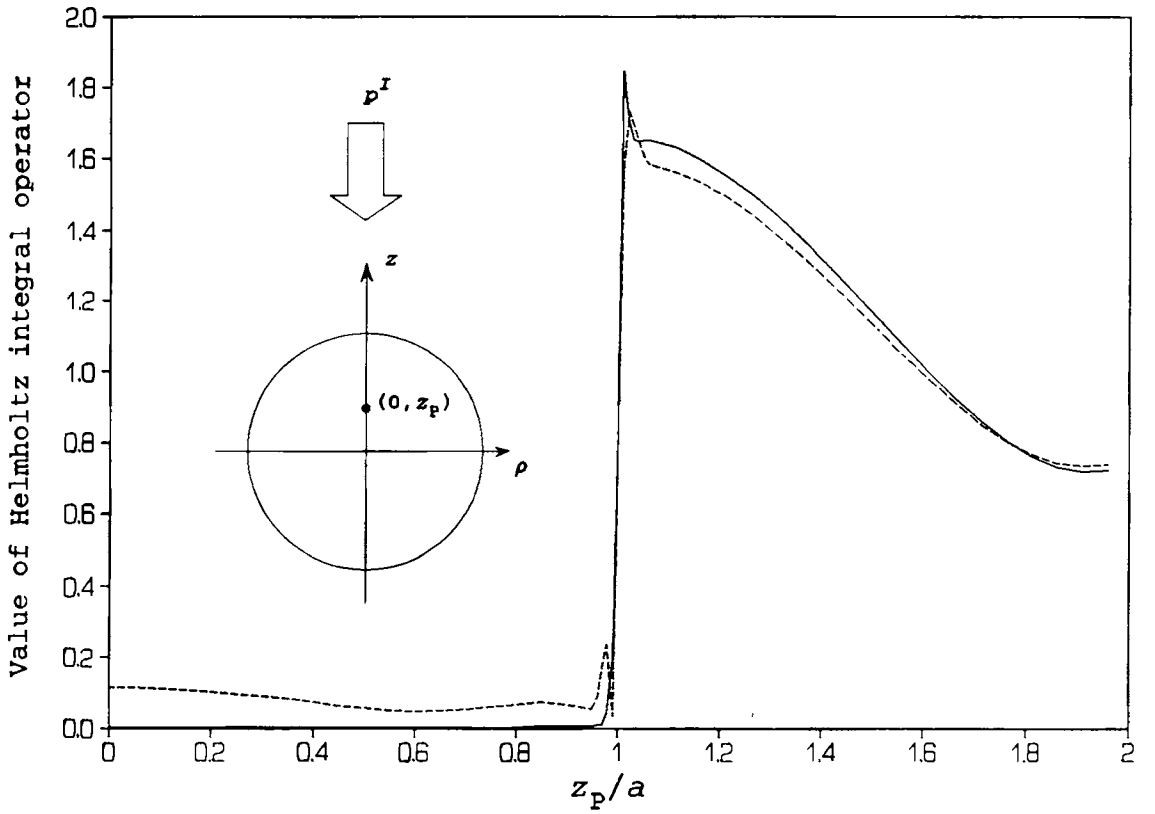

Figure 5-1. Magnitude of the Helmholtz integral operator for the case of scattering of a plane wave by a rigid sphere at ka=2. ------, two elements per wavelength; ———, four elements per wavelength.

For the active control analogy the nodal points are associated with the secondary sources, whereas the calculation points are associated with the error microphones. As an example, consider the case sketched in Figure 5-2 a). The sketch uses M=8 secondary sources but keep the the limit of an infinite number of sources in mind. At a non-characteristic frequency the same number of error microphones should be placed at different locations inside S in order to ensure the desired

null-field overall inside S. For the surface formulation the error microphones are placed so that the field is controlled on the inner surface of S as sketched in Figure 5-2 a), and for the 'related interior' formulation described in section 4.2 the error microphones are placed on a related surface inside S as sketched in Figure 5-2 b). Now, at a characteristic frequency a field exists which has zero pressure at all error microphones, but not null inside all of S.

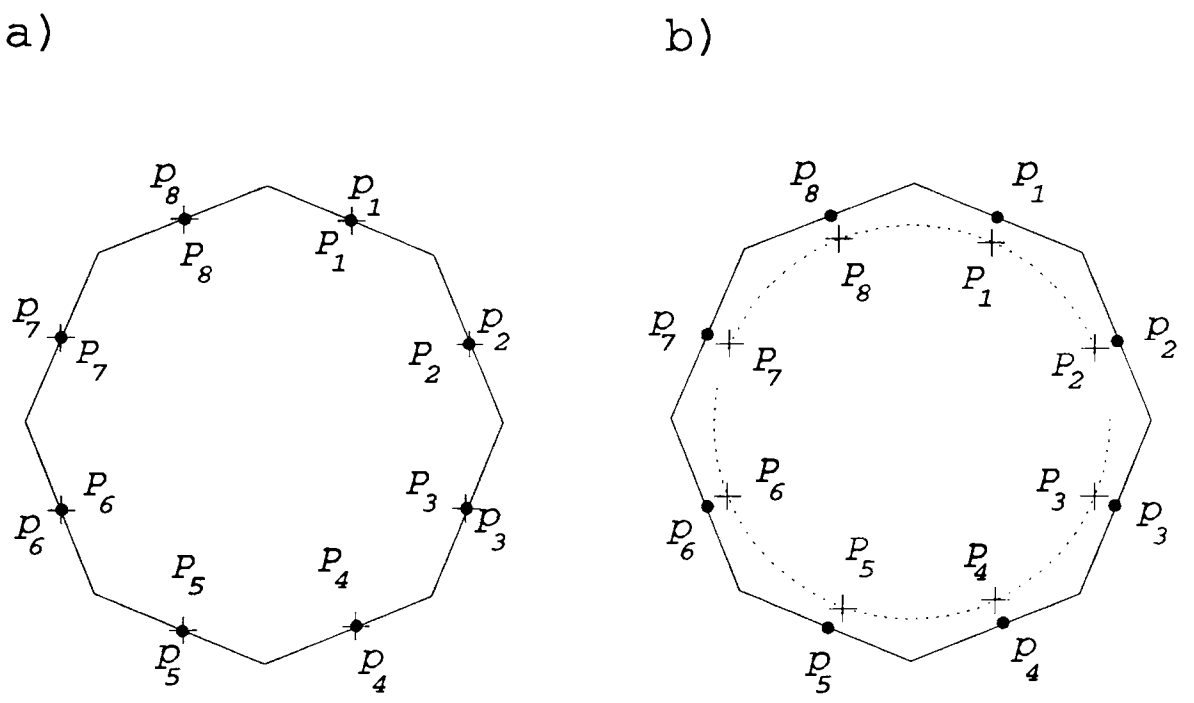

Figure 5-2. Position of the error microphones for the case of a discretized sphere with 8 sources. a) surface formulation; b) 'related interior' formulation; the dotted curve indicates the related boundary.

5.1.1 THE SURFACE FORMULATION

For the surface formulation an example of this is shown in Figure 5-3, where scattering of a plane wave by a rigid sphere at ka=3.1416, which is very close to the first characteristic frequency at $ka=\pi$. Figure 5-3 shows the value of the Helmholtz integral operator as a function of the observation point z_p as defined in the inset of Figure 5-1 when the pressures found by the standard Helmholtz integral equation are inserted. In the following the term standard Helmholtz integral equation is used

for the original approach in order to distinguish from the modified approaches presented in the next three sections. For this calculation 10 isoparametric quadratic elements were used to model the generator of the sphere. At ka=3.1416 this corresponds to about 6.4 elements per wavelength, which at a non-characteristic frequency should give a very small deviation from the desired null-field as demonstrated in Figure 5-1.

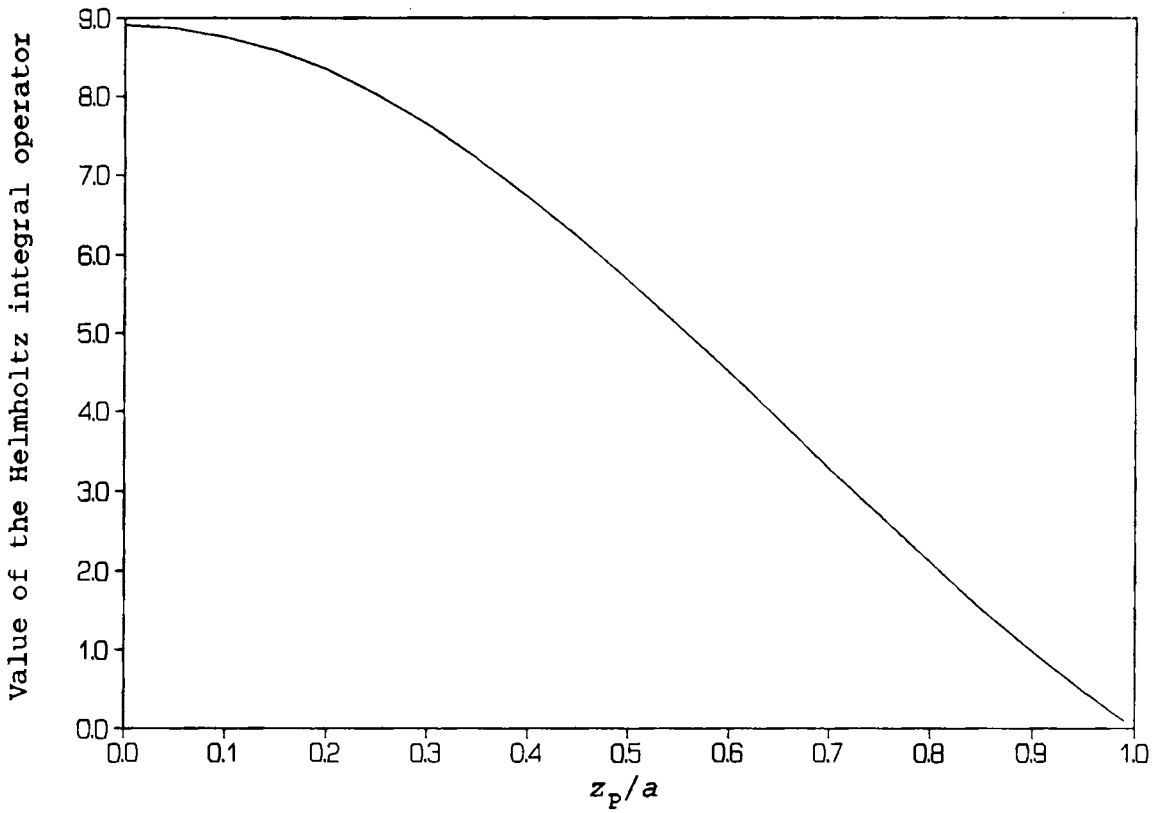

Figure 5-3. Magnitude of the Helmholtz integral operator for the case of scattering of a plane wave by a rigid sphere at ka=3.1416. Definitions as in Figure 5-1.

However, the desired null-field is not obtained inside S, as seen in Figure 5-3 although the field is approximately null on the inner surface of the sphere. At this frequency the pressure calculated by the boundary element formulation on the outer surface has a large error, as can be seen from the results of calculations shown in section 5.5.

The next eigenfrequency corresponding to a rotationally symmetric eigenmode occurs at $ka=2\pi$. At this frequency the

eigenmode of the interior problem has a nodal surface, which is a sphere with the same centre as the sphere defining the problem but with the radius $a/2$. As shown in Figure 5-4 this nodal sphere is also found when evaluating the right-hand side of equation (5.1) for P inside S at ka=6.2832, which is very close to $ka=2\pi$.

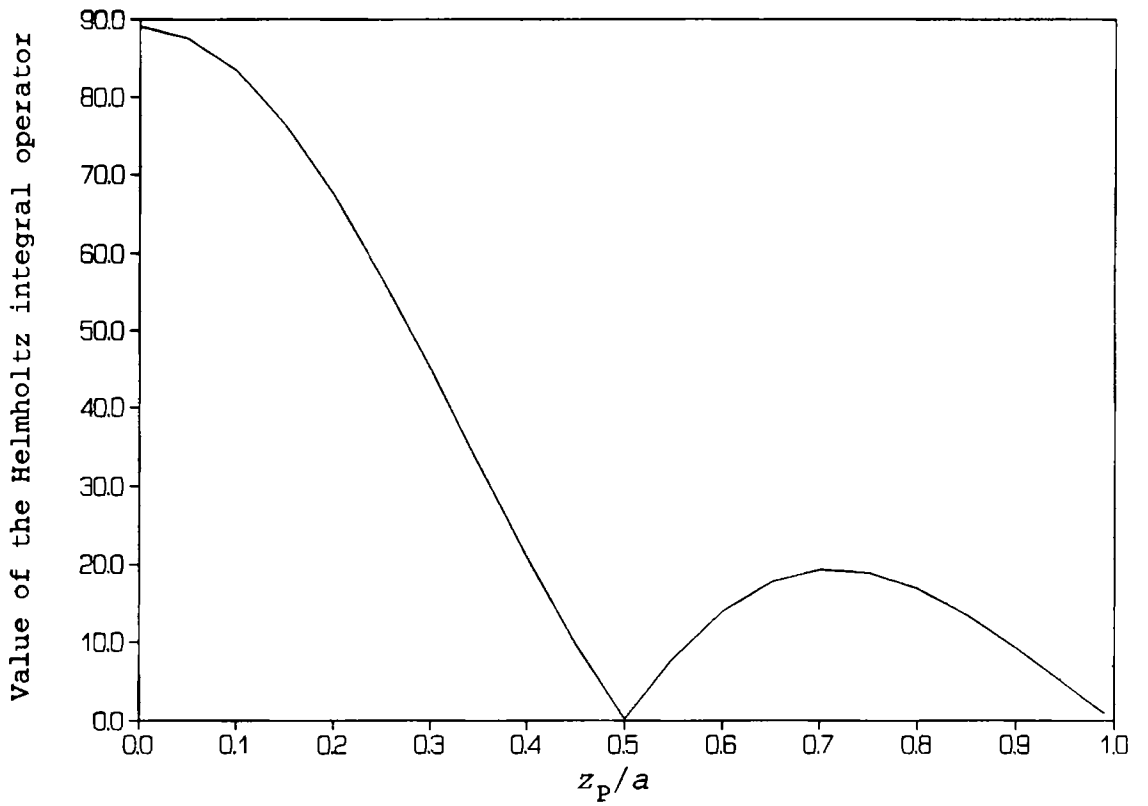

Figure 5-4. As Figure 5-3 but for ka=6.2832.

5.1.2 THE 'RELATED INTERIOR' FORMULATION

The analogy from active control may also be used to explain the failure of the 'related interior' formulation. In this case the error microphones are placed on a related surface inside S. Consider again scattering of a plane wave from a rigid sphere as an example. For this problem a calculation (results not shown) was carried out at ka=3.1416, where the retracted surface was a sphere with the same centre as the original sphere but with the radius a_1=0.9. This calculation was in excellent agreement with the analytical solution. However, at

ka=3.4906585 ($\approx\pi/0.9$) a large error occur as shown in Figure 5-5. Figure 5-5 shows the magnitude of the pressure on the surface of the sphere for this frequency as a function of the angle defined in the small inset in the figure. The generator of the sphere was modelled by 10 isoparametric quadratic elements in an axisymmetric formulation. The incoming plane wave has the dimensionless magnitude one.

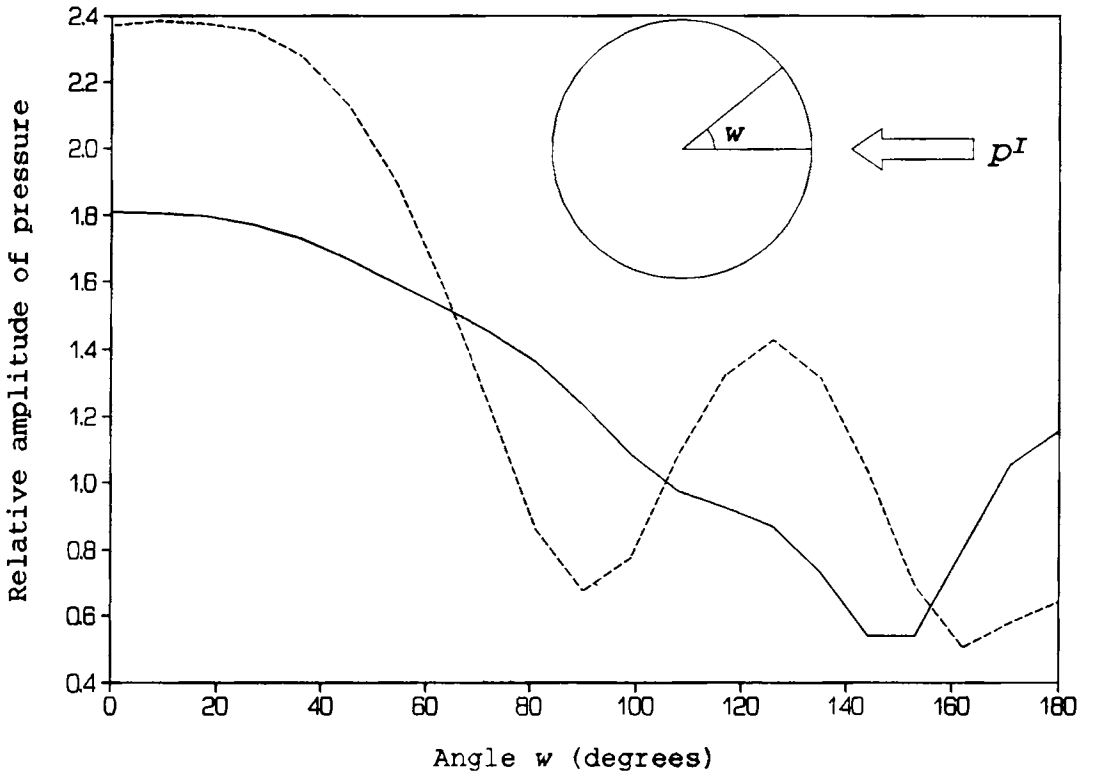

Figure 5-5. Pressure on the surface of a sphere of radius a when scattering of a plane incoming wave at $ka\approx\pi/0.9$ is considered. ————, analytical solution; --------, 'related interior' boundary element calculation, with radius of related surface a_1=0.9. The observation angle w is defined in the small inset.

For this case the value of the Helmholtz integral operator is shown in Figure 5-6. It can be seen from Figure 5-6 that in this case the null-field is obtained on the surface of the related interior sphere, whereas the field is not null elsewhere inside S. Thus by using this analogy it is expected that the retracted formulation for exterior problems has non-unique

solutions at the eigenfrequencies of the corresponding Dirichlet problem involving the related surface [102]. However, since the user has the freedom of choosing the related surface, the characteristic frequencies may be known *a priori*. Unfortunately, the 'related interior' formulation suffers from an undesirable behaviour from a computational point of view, as discussed in section 4.2.

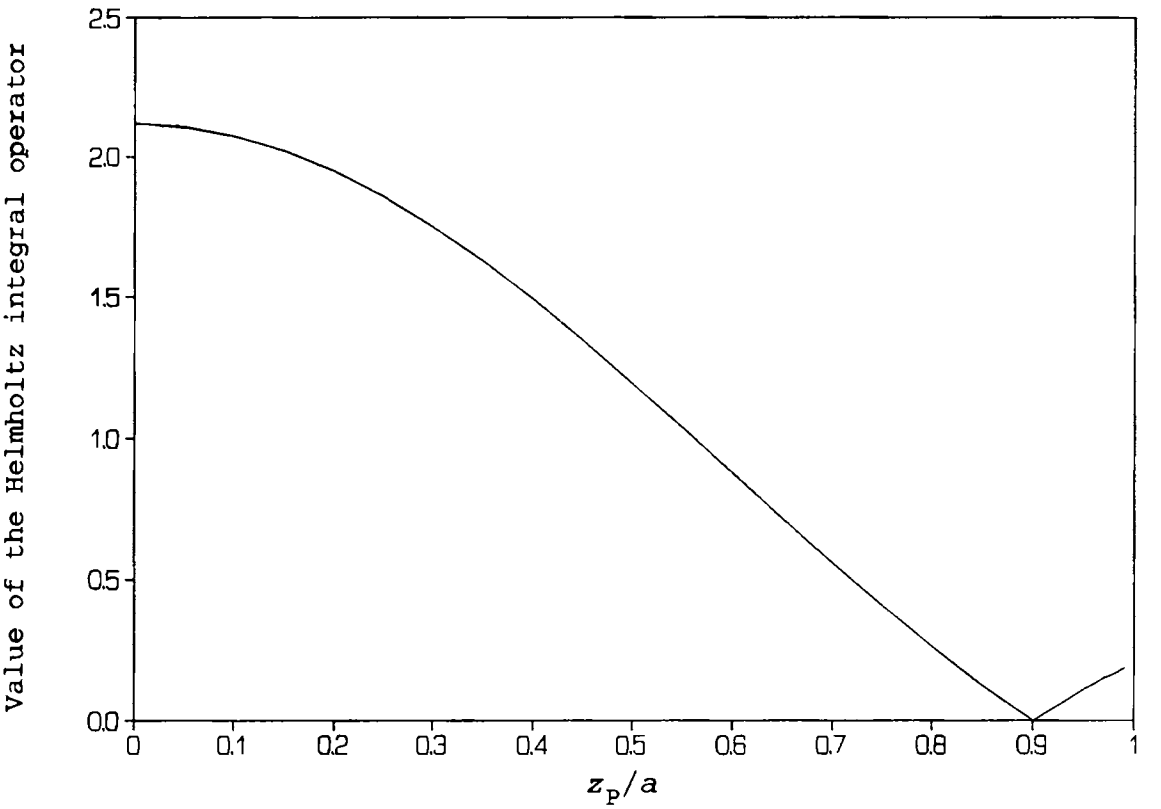

Figure 5-6. Magnitude of the Helmholtz integral operator for the case of scattering of a plane wave by a rigid sphere at $ka \approx \pi/0.9$ using a 'related interior' boundary element formulation. Definitions as shown in the inset of Figure 5-1.

5.1.3 CONCLUDING REMARKS

To conclude this section the analogy to active control is outlined: The Helmholtz integral equation for exterior problems has the property of creating a null-field inside the body of interest. However, at certain characteristic frequencies the interior field may be zero at all the calculation points, although the field is non-zero elsewhere. This also explains

why fictitious eigenfrequencies does not occur for interior problems, since in this case a null-field on the outer surface ensures a null-field overall outside S. In the next section it will be shown how this analogy may also be used to explain the problem of how to choose the so-called CHIEF points.

5.2 THE COMBINED HELMHOLTZ INTEGRAL EQUATION FORMULATION

The Combined Helmholtz Integral Equation Formulation (CHIEF) proposed by Schenck [78] combines the surface Helmholtz integral formulation with the interior Helmholtz integral formulation. The idea is to add a relatively small number of extra equations to the quadratic set of linear equations obtained by the surface Helmholtz integral formulation for the exterior problem. An extra equation is provided by requiring the interior formulation to be satisfied at an interior point. These points are termed CHIEF points. Using the active control analogy, the procedure is to place additional error microphones inside S in order to ensure a null-field overall inside S. This analogy also demonstrates the main problem using the CHIEF method: If the CHIEF point is placed on a nodal surface inside S, for instance at $(\rho,z_p) = (0,0.5)$ for the case considered in Figure 5-4, no additional constraint is obtained, and a non-zero field may still exist inside S. A numerical demonstration of this will be given in section 5.5. The term 'a good CHIEF point' is used for a CHIEF point, which really add an additional constraint to the original system of equations, whereas the term 'a bad CHIEF point' is used for a CHIEF point, which does not add an additional constraint to the original system of equations.

Thus, there are two main problems using the CHIEF method:

a) the determination of the number of good CHIEF points needed to ensure a unique solution,
b) and how to choose good CHIEF points.

The problem of choosing good CHIEF points is coplicated by the fact that at higher frequencies the nodal surfaces of the corresponding interior problem generally are closely spaced.

Normally, the approach would be to distribute a number of

CHIEF points arbitrarily inside S hoping, that a sufficient number of CHIEF points will turn out as good. The resulting overdetermined set of equations is then solved in the least squares sense. The least squares solution of an overdetermined set of equations is discussed in chapter 6. The quality of the solution obtained may be estimated either by examining the Helmholtz integral operator [83] or the condition number of the coefficient matrix. The condition number is introduced in section 6.2.

5.3 THE BURTON AND MILLER METHOD

Due to the above mentioned problems with the CHIEF method, several authors have adopted the Burton and Miller integral equation formulation [13]. The approach is to combine the Helmholtz integral equation with its normal derivative taken at P:

$$C(P)\frac{\partial p(P)}{\partial n_P} = \int_S \left[p(Q)\frac{\partial^2 G(R)}{\partial n_P n_Q} + ikz_0 v(Q)\frac{\partial G(R)}{\partial n_P} \right] dS + 4\pi \frac{\partial p^I(P)}{\partial n_P} , \tag{5.3}$$

where n_P is the unit normal vector at P, and all other symbols are as defined in equation (2.26). Thus, equation (5.3) is multiplied with a constant and added to equation (2.26). The multiplicative constant has been a matter of interest [62,63, 97]. For real wave numbers it has been found [63,73] that the imaginary value i/k produces good results.

The main problem with the application of equation (5.3) for numerical calculations is that equation (5.3) contains a integral with a high order singularity. The evaluation of this so-called hypersingular integral is computational inefficient [13,22], and some regularization techniques are suitable for planar elements only [62,97]. For higher order elements certain conditions on the smoothness of the acoustic variables must be assumed *a priori* as explained in details in Chien [22]. In order to satisfy these conditions the collocation points must usually be placed inside each element [106], where the normal derivative of equation (5.3) is unique. (As discussed in paragraph 4.4.5 the normal direction is seldom unique at the

intersection of two or several elements.) For three-dimensional implementations all this leads to a much larger amount of consumed time and storage. Recently a 'truncated' implementation of the Burton and Miller method has been reported [36-37]. Here equation (5.3) was only applied at the local origins of quadratic isoparametric elements, where the normal direction is unique. Hence, the extra amount of work for this 'truncated' Burton and Miller formulation, which seems to be adequate to ensure uniqueness, was only about 35% compared to the standard surface Helmholtz integral formulation [37].

In order to conclude the discussion above it may be stated that although the Burton and Miller method may be proven to be a theoretically robust formulation for all frequencies [13,111] it is neither computationally efficient nor easy to implement in practice. However, it should be noted that equation (5.3) is the preferable method for calculating radiation and scattering for thin-walled shapes [54,60,108], since the standard surface Helmholtz integral equation method can not be applied directly in this case.

The Burton and Miller method has not been examined in this study.

5.4 OTHER METHODS TO OVERCOME THE NON-UNIQUENESS PROBLEM

In this section some of the other methods of dealing with the nouniqueness problem will be outlined. Alternative numerical formulations, which are not based on a direct solution of the Helmholtz integral equation have been proposed [43,47,57, 66,104]. The idea of these methods is generally to place a number of sources inside the body, and then to determine the strength of these sources by matching the boundary conditions in a variational sence on the surface S. The problem of applying these methods to general shapes lies in the selection of the source points. Furthermore, these methods are not suited for slender bodies or bodies having sharp edges and/or corners, and they often have the same undesirable computational characteristics of the interior Helmholtz integral equation formulation discussed in section 4.2, due to the lack of diagonal

dominance in the resulting matrix of coefficients [47,78,94]. The author finds that a more comprehensive description of these methods is beyond the scope of this text. Hence, only formulations based on the Helmholtz integral equation are outlined in the following.

In a formulation due to Piaszyk and Klosner [68] a CHIEF point is placed *outside* the surface. Since the exterior field is unknown at the outset, this approach requires an iterative procedure to obtain a solution. The convergence of this procedure was not proved rigorously. Another CHIEF method known as the 'enhanced' CHIEF method [89] or as SuperCHIEF [79] requires not only the original CHIEF equation to be satisfied inside S but also its derivatives. The 'enhanced CHIEF method uses first order derivatives, whereas the SuperCHIEF method used higher order derivatives. However, if the 'enhanced' CHIEF point falls on the intersection of two nodal surfaces no additional constraint is obtained [107]. Finally, a CHIEF method that requires the CHIEF equation and its normal derivatives to be zero in a small interior region rather than at a point has been suggested [107]. This method is expected to eliminate the non-uniqueness problem, since for the corresponding interior problem only, the desired null solution has nodal 'blocks'. This method has been termed the CHIEF-block method.

At the other end of the spectrum Cunefare, Koopmann, and Brod [30] has suggested a variant of the Burton and Miller method, in which all calculation points are placed inside the body. The advantage of this scheme is that the hypersingular integral is avoided, since in this case the integration point Q never encounters the calculation point P. This 'interior Burton and Miller approach' was termed CHI for Coupled Helmholtz Integrals. Unfortunately, this method suffers from the well known undesirable computational characteristic: lack of diagonal dominance of the coefficient matrix, and the formulation encounters difficulties when applied to slender bodies or bodies with sharp edges.

Finally, Ursell [103] modified the Green's function such that uniqueness was ensured. However, this approach gives rise

to an infinite series which converged slowly at high frequencies. Jones [48] replaced the infinite series with a finite, but uniqueness could then be guaranteed only in a range of frequencies.

5.5 A BRIEF NUMERICAL STUDY OF THE CHIEF METHOD

Analytically, the characteristic frequencies exist at a discrete set of frequencies only, and the problem of characteristic frequencies would not be severe if this was the case for the numerical implementation as well. However, due the numerical approximation, the standard surface Helmholtz integral equation formulation encounters problems in a range of frequencies around a characteristic frequency. In this frequency band the solution produced by the standard surface Helmholtz integral equation formulation is largely in error.

Consider as an example scattering of a plane wave by a rigid sphere of radius a near $ka=\pi$, which is the first characteristic frequency for the sphere. The plane wave has the dimensionless magnitude one. Figure 5-7 shows the error made by the standard formulation compared to the error made by the CHIEF method with one CHIEF point in the centre of the sphere. The error is calculated as the length of the residual vector as defined in paragraph 4.6.1. For these calculations the axisymmetric integral equation formulation was used. In Figure 5-7 three cases are considered: the CHIEF method using 4 isoparametric elements to model the generator of the sphere, the standard formulation using 4 isoparametric elements to model the generator, and the standard formulation with 6 isoparametric elements on the generator. Note that using 4 elements corresponds to about 2,5 elements per wavelength, which is close to the recommended discretization for coarse calculations. In this case the CHIEF point is good, and hence this calculation is believed to represent the minimal error that may be obtained with the four element discretization. The two curves for the standard formulations can be used to acces the issue of the bandwidth of characteristic frequencies mentioned. It can be seen that the solution obtained by the two standard

LABORATORIET FOR AKUSTIK

FORTEGNELSE OVER LABORATORIETS UNDERVISNINGSMATERIALE — august 1993

Kursus 5101: Grundkursus i Akustik og Støj

Note nr.				
	D.A. Bies & C.H. Hansen:	Engineering Noise Control, Theory and Practice, 1988 , Polytek. Bogh.		
0101:	F. Ingerslev:	Hæfte I. Det fysiske og psykofysiologiske grundlag, 1982/89, 170 s.	DKK	80,-*)
0102:	-	Hæfte II. Fysisk Akustik, 1985, 63 s.	-	30,-*)
0104:	-	Opgavesamling, 1990, 148 s.	-	70,-*)
0105:	J.H. Rindel:	Hæfte V. Lydisolation, 1987, 97 s.	-	45,-*)
0106:	S.D. Kristensen:	Hæfte VI. Ekstern støj, 1990, 3. udg., 55 s.	-	30,-
0107:	K.B. Rasmussen:	Grundlæggende diffraktionsteori, 1990, 23 s.	-	10,-*)
0108:	J.H. Rindel:	Acoustic Formulas	-	0,-
0109:	-	Engelsk-Dansk akustisk ordliste	-	0,-
Særtryk:	J. Kristensen & J.H. Rindel:	Bygningsakustik, SBI-anvisning 166, 1989, kap. 1 og 4	-	5,-

Kursus 5121: Elektroakustik

Note nr.				
	K. Rasmussen:	Analogier mellem mekaniske, akustiske og elektriske systemer , Polytek. Forlag		
2102:	K. Rasmussen:	Mikrofoner, 1989, 127 s.	DKK	60,-
2103:	A.Th. Christensen:	Den elektrodynamiske højttaler, 1976, 1989, 50 s.	-	25,-
2104:	-	Opgavesamling, 4. udg., inkl. facitliste, 1982, 88 s.	-	45,-
2107:	K. Rasmussen:	Lydfelter, 1992, 148 s.	-	65,-
2108:	T. Poulsen:	Lydopfattelse, 1991, 54 s. foreløbig udgave	-	30,-

Kursus 5122: Videregående Akustik

Note nr.				
2201:	K. Rasmussen:	Klassisk lineær akustik, 1973/81/86, 235 s.	DKK	100,-
2202:	F. Jacobsen:	Akustisk intensitet, 1991, 37 s.	-	20,-
2203:	-	Lydfeltet i et efterklangsrum, 1993, 48 s.	-	25,-
2204:	K. Rasmussen:	Svingende membraner, 1989, 19 s.	-	15,-
2205:	F. Jacobsen:	Lydudbredelse i rør og kanaler, 1993, 71 s.	-	35,-
2206:	K.B. Rasmussen:	Teoretisk beregning af lydudbredelse udendørs, 1991, 47 s.	-	25,-
2207:	F. Jacobsen:	Opgavesamling, 1993, 17 s.	-	5,-

Kursus 5126: Audioteknik

Note nr.				
2601:	K. Rasmussen:	Magnetisk registrering, 1977/82/87, 140 s.	DKK	60,-*)
2602:	-	Mekanisk registrering, 1974/75/80/89, 79 s. uddrag	-	40,-
2604:	K.B. Rasmussen:	Digital lydregistrering: Compact Disc, 1990, 55 s.	-	30,-
2605:	-	Teoretiske overvejelser vedrørende stereo, 1989, 51 s.	-	25,-
2606:	-	Audiosignaler på magnetisk medium, 1991, 68 s.	-	35,-
2607:	-	Teoretiske modeller for højttalere, 1992, 23 s.	-	10,-

Kursus 5131: Akustisk Kommunikation

Note nr.				
3101:	O. Juhl Pedersen:	Ørets indretning og funktion, 1976, 97 s. inkl. appendiks	DKK	40,-
3108:	-	Psykoakustiske målemetoder, 1988, 43 s.	-	25,-
3109:	O. Juhl Pedersen:	Genevirkning af støj, 1982, 54 s.	-	20,-
3110:	O.J.P./T. Poulsen:	Beregning af hørestyrke af stationære lydsignaler, 1983, 24 s.	-	10,-
3111:	T. Poulsen:	Taleforståelighed, 1993, 4. udg., 57 s.	-	30,-
3112:	- :	Høreapparater, 1990, 16 s.	-	5,-
3201:	T. Jacobsen:	Lokalisation af lydsignaler, 1977, 48 s.	-	20,-

Kursus 5142: Bygnings- og Rumakustik

Note nr.				
	J. Kristensen & J.H. Rindel:	Bygningsakustik. SBI-anvisning 166, 1989, Polytek. Bogh.		
4201:	J.H. Rindel:	Hæfte IV. Anvendt rumakustik, 1984/90, 97 s.	DKK	45,-
4202:	-	Notat A. Lydudstråling fra plader, 1979, 37 s.	-	15,-
4204:	-	Notat Z. Anvendt geometrisk diffraktionsteori, 1979, 20 s.	-	8,-*)
4206:	-	Notat C. Lydtransmission - statistisk energianalyse, 1980, 27 s.	-	10,-
4208:	-	Notat S. Stationære lydfelter i rum, 1981, 43 s.	-	20,-
4209:	-	Notat P. Lydrefleksion og -absorption, 1981, 41 s.	-	15,-
4210:	-	Notat R. Lydabsorbenter, 1982, 46 s.	-	20,-

Kursus 5170: Lyd og Vibrationer

Note nr.				
7001:	F. Jacobsen:	Introduktion til anvendt signalanalyse, 1992, ca. 56 s.	DKK	30,-
7011:	M. Ohlrich:	Struktur-transmitteret lyd. Del 1a, 2. udg. 1991, 196 s.	-	85,-
7012:	-	Struktur-transmitteret lyd. Del 1b, 1993, 80 s.	-	40,-
7013:	-	Opgavesamling, 1991, 26 s.	-	10,-

*) ikke obligatorisk

formulations has large errors in a range of frequencies around the characteristic freqiency, and that generally the 4 element model is in more error than the 6 element model. It can also be seen that the actual bandwidth, in which poor solutions are obtained, depends on the accuracy demanded by the user. If, for instance, the user demands the error to be less than 0.3, which is about 3 times the error obtained using the CHIEF method, then the bandwidth of poor solutions is about 0.013 for the 4 element model, and 0.005 for the 6 element model in this case. Thus, the effect of discretization is, that for a coarse discretization a larger error is encountered than for a finer discretization, as also found in [83].

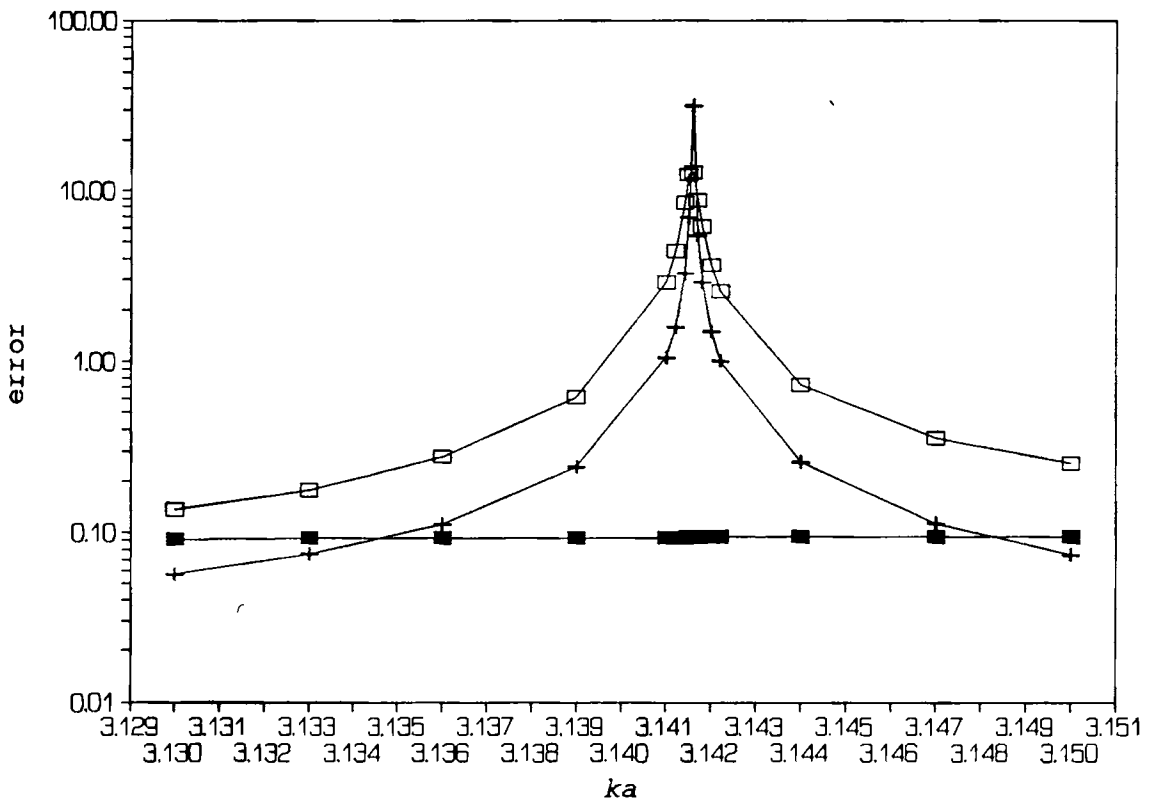

Figure 5-7. Error made by three boundary element calculations in the case of scattering of a plane wave by a rigid sphere near $ka=\pi$. ——■——, CHIEF calculation using 4 quadratic elements; ——□——, standard calculation using 4 quadratic elements; ——+——, standard calculation, using 6 quadratic elements.

In order to observe the effect of the 'sophistication' of the formulations in terms of the order of the shape functions used the same problem was run using the linear elements described in paragraph 4.4.1. Figure 5-8 shows the error made by an isoparametric linear CHIEF, an isoparametric linear standard formulation , and the isoparametric quadratic formulation used in Figure 5-7 as well. For all formulations 13 nodes were used.

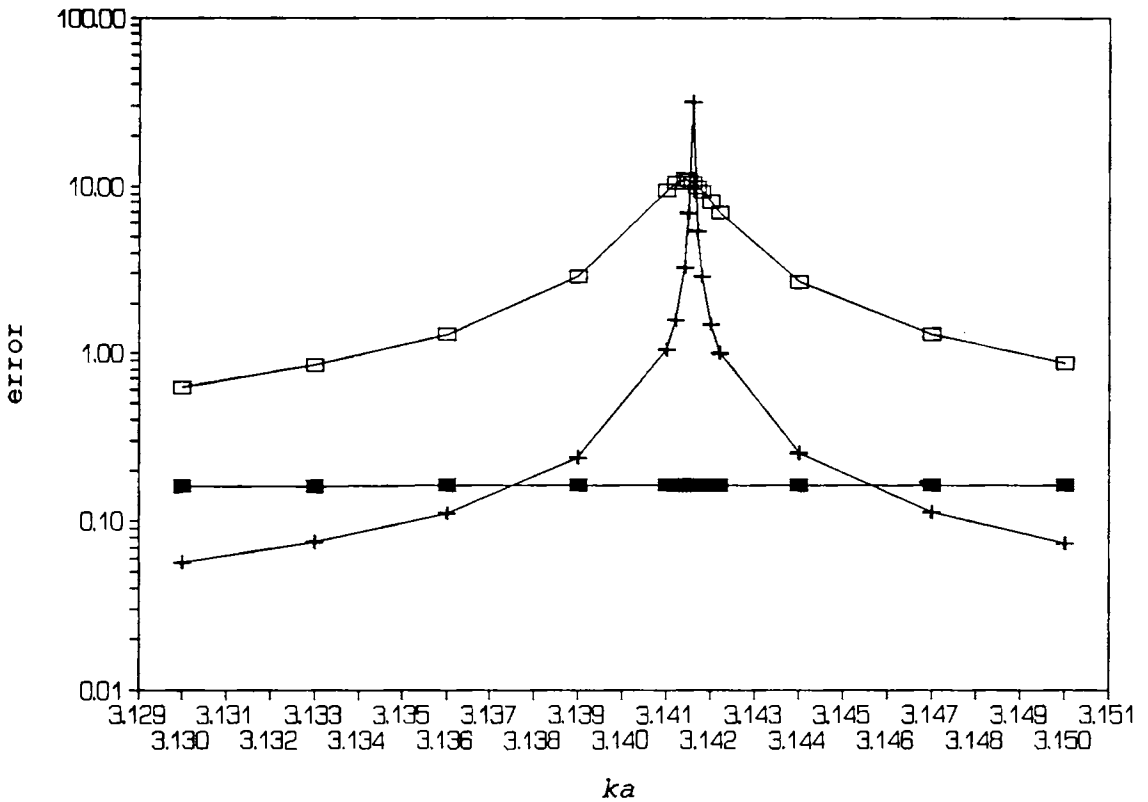

Figure 5-8. Error made by three boundary element calculations in the case of scattering of a plane wave by a rigid sphere near $ka=\pi$. ——■——, CHIEF calculation using 12 linear elements; ——□——, standard calculation using 12 linear elements; ——+——, standard calculation using 6 quadratic elements.

It can be seen from the figure that the conclusions drawn considering the effect of discretization also holds when considering the effect of 'sophistication' of the methods: the more 'sophisticated' standard quadratic formulation performs generally better near a characteristic frequency than the

linear formulation with the same number of nodes.

Similary, the nodal surfaces inside the body has a certain spatial bandwidth due to the numerical modelling. Since an investigation of the spatial bandwidth leads to conclusions analogous to the conclusions drawn for the frequency bandwidth case [83], this effect is merely demonstrated in the case of scattering of a plane wave by a rigid sphere at ka=6.2832, which was the case also considered in Figure 5-4. Figure 5-9 shows the error as a function of the location of the CHIEF point z_p as shown in the inset in the figure. Evidently, the CHIEF point should not be placed near the nodal surface or near the boundary surface. This calculation was carried out using a 29 element isoparametric linear formulation.

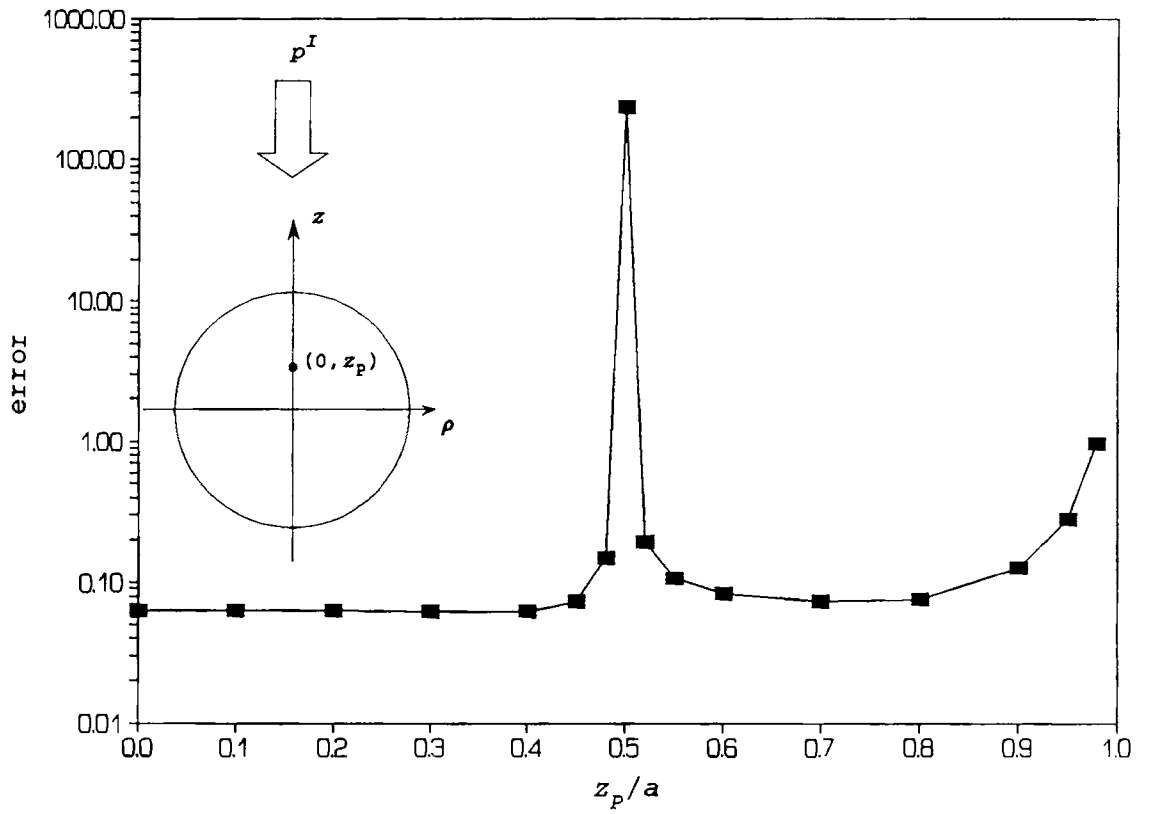

Figure 5-9. Error made by a 30 node isoparametric linear CHIEF calculation in the case of scattering of a plane wave by a rigid sphere at ka=6.2832. The error is shown as a function of the location of the CHIEF point as defined in the inset in Figure 5-1.

To conclude this section it can be stated that due to the numerical treatment, the solution of the standard Helmholtz integral equation fails in a band around the characteristic frequencies. Likewise, a spatial bandwidth is observed for the locations at which the CHIEF points are 'bad'. Although these bands theoretically may be narrowed as much as the user wishes by increasing the number of elements, this strategy to overcome the non-uniqueness problem leads to an enormous amount of time and storage required. The problem of characteristic frequencies and nodal surfaces is further complicated by the fact that at higher frequencies the number of characteristic frequencies per octave increases and the spacing between the nodal surfaces decreases.

6. SOLUTION OF LINEAR ALGEBRAIC EQUATIONS

In chapter 4 the Helmholtz Integral Equation was transformed into the matrix equation

$$(C-H)p = Gv+4\pi p^I \ . \tag{6.1}$$

Thus the distribution of the pressure p and the normal velocity v is replaced by a finite number of nodal values, of which either p or v is known at each node. Alternatively, an impedance relation may be known:

$$p = -Z v \ , \tag{6.2}$$

where Z is an impedance matrix; the negative sign is due to the fact that the velocity is calculated along the outward normal to the surface. For a locally reacting surface Z has values in the diagonal only. Thus, when introducing the boundary conditions, equation (6.1) may be reduced to

$$A^{com} x^{com} = b^{com} \ , \tag{6.3}$$

where A is a $M \times M$ matrix, and x and b are vectors of length M. M is the number of acoustical nodes. The superscript com in equation (6.3) refers to the fact, that the quantities are complex:

$$\begin{aligned} A^{com} &= A^{re} + i A^{im} \ , \\ x^{com} &= x^{re} + i x^{im} \ , \\ b^{com} &= b^{re} + i b^{im} \ . \end{aligned} \tag{6.4a,b,c}$$

The solution of a complex set of equations may either be found using a solution algoritm working with complex numbers or - as is the case in this work - by transformation of the complex set of equations (equation (6.3)) into an equivalent $2M \times 2M$ set of equations

$$\begin{bmatrix} A^{re} & -A^{im} \\ A^{im} & A^{re} \end{bmatrix} \begin{bmatrix} x^{re} \\ x^{im} \end{bmatrix} = \begin{bmatrix} b^{re} \\ b^{im} \end{bmatrix} , \tag{6.5}$$

where all elements are real numbers. Although the latter method requires twice the storage of the former, this method has been

chosen for the present work. This is mainly because many well-documented standard algoritms with program listings for solving a real set of equations are available [33,70], and secondly because handling complex number is quite difficult in Pascal, which is the programming language used in this project.

Keeping the transformation of a complex set of equations (equation (6.3)) into a real set of equations (equation (6.5)) in mind, the real system of equations

$$\boldsymbol{A}\boldsymbol{x} = \boldsymbol{b} \tag{6.6}$$

is considered in the following.

The purpose of this chapter is not to discuss the solution of equation (6.6) in detail. The problem of solving a set of equations is the issue of numerous numerical methods, and are consequently well described in the literature. The author recommends Press *et al.* [70] for a short introduction to the subject, and Golub and Van Loan [39] for a more detailed treatment. In this chapter the three different algoritms used in this project for solving equation (6.6) will merely be outlined. The matrices produced by boundary element formulations are generally neither band limited nor symmetric, and hence general algorithms for solving a set of equations must be used.

The 'text-book' method of solving equation (6.6) is the Gauss-Jordan elimination, which implies the determination of the inverse of $\boldsymbol{A}$ by the means of 'row-operations'. A 'row-operation' is the replacement of a row in $\boldsymbol{A}$ by a linear combination of the row it selv and any other row.

However, a full inversion as obtained using the Gauss-Jordan elimination of $\boldsymbol{A}$ is not required for finding the unknown vector $\boldsymbol{x}$, and hence modern and more efficient methods of solving a set of equations brings $\boldsymbol{A}$ to a form from which the solution of the set of equations is more easily obtained. This process is termed factorization or decomposition of $\boldsymbol{A}$.

The factorization of $\boldsymbol{A}$ is independent of the right-hand side of equation (6.6), and hence the factorization of $\boldsymbol{A}$ may be reused for different right-hand sides. This feature is useful

for several boundary element calculations e.g. solution of scattering problems involving several angles of incidence. Gauss-Jordan elimination requires the right-hand side to be known in advance, and is therefore not suitable for iterative methods, where the right-hand side depends on the result of the previous iteration. Iteration will be used in chapter 7.

Two other operations frequently carried out when solving a linear set of equations numerically are the interchanging of two rows or two columns of $\boldsymbol{A}$. Interchanging two rows of $\boldsymbol{A}$ and the right-hand side of the equation simply corresponds to writing the system of equations in a different order. However, the proper interchanging of rows is vital for the numerical stabitity of the LU factorization to be described in section 6.1, and is termed partial pivoting or row pivoting [70]. For the so-called QR factorization to be described in section 6.3 interchanging of columns - column pivoting - may be performed in order to stabilize the algorithm numerically. In this case the rows of the unknown vector $\boldsymbol{x}$ is interchanged correspondingly, and the solution must be 'unscrambled' to the original order afterwards. For more details about pivoting refer to e.g. Golub [39].

The number of floating point operations (flops) required by an algoritm is often used for measuring the efficiency when comparing different factorization algoritms. A flop is either a multiplication or an addition. Gauss-Jordan elimination of a $N \times N$ matrix requires $2N^3$ flops, for instance.

The most common factorization method used to solve a system of equations is the LU factorization, which will be described in the next section. However, it appears that alternative factorization methods may advantageously be used near a characteristic frequency as will be demonstrated in section 6.4. Two such factorization methods, the singular value decomposition, and the QR factorization, will be outlined in section 6.2 and section 6.3 respectively.

6.1 LU FACTORIZATION

If $\boldsymbol{A}$ is quadratic ($N\times N$) and regular (i.e. not singular) the following factorization can always be made [39]:

$$\boldsymbol{A} = \boldsymbol{L}\boldsymbol{U} \ , \tag{6.7}$$

where $\boldsymbol{L}$ is a lower triangular matrix:

$$\boldsymbol{L} = \begin{bmatrix} 1 & 0 & 0 & 0 \\ l_{21} & 1 & 0 & 0 \\ l_{31} & l_{32} & 1 & 0 \\ l_{41} & l_{42} & l_{43} & 1 \end{bmatrix} , \tag{6.8}$$

and $\boldsymbol{U}$ is an upper triangular matrix:

$$\boldsymbol{U} = \begin{bmatrix} u_{11} & u_{12} & u_{13} & u_{14} \\ 0 & u_{22} & u_{23} & u_{24} \\ 0 & 0 & u_{33} & u_{34} \\ 0 & 0 & 0 & u_{44} \end{bmatrix} . \tag{6.9}$$

The factorization is shown for a 4×4 matrix but is of course general for any $N\times N$ matrix $N=2,3,4,\ldots$

Once the LU factorization of $\boldsymbol{A}$ is performed, the solution of equation (6.6) is easily obtained by the following two steps. First solve

$$\boldsymbol{L}\boldsymbol{y} = \boldsymbol{b} \tag{6.10}$$

and then

$$\boldsymbol{U}\boldsymbol{x} = \boldsymbol{y} \ . \tag{6.11}$$

Equation (6.10) is easily solved by a technique called forward substitution:

$$\begin{aligned} y_1 &= b_1 \\ y_i &= b_i - \sum_{j=1}^{i-1} l_{ij} y_j \end{aligned} \tag{6.12}$$

and equation (6.11) by back substitution:

$$x_N = \frac{y_N}{u_{NN}}$$

$$x_i = \frac{1}{u_{ii}} \left[y_i - \sum_{j=i+1}^{N} u_{ij} x_j \right] . \qquad (6.13)$$

The calculation of L and U requires $2/3N^3$ flops, whereas a total of $2N^2$ flops are required by equations (6.12) and (6.13) for each right-hand side. Hence, for large systems (say, N>100) and relatively few right-hand sides LU factorization is about three times as efficient as Gauss-Jordan elimination.

As stated in chapter 5 a solution to a system with more equations than unknowns might be wanted in order to ensure uniqueness of the solution. In this case the linear least squares solution is of interest. The linear least squares solution is the solution that comes closest to satisfing all equations silmutaneously in the sence that the sum of the squares of the differences between the left and right-hand side of equation (6.6) is minimized. The linear least squares solution may be shown to be the solution of the normal equations:

$$(\boldsymbol{A}^T\boldsymbol{A})\boldsymbol{x} = (\boldsymbol{A}^T\boldsymbol{b}) \ , \qquad (6.14)$$

where $\boldsymbol{A}^T$ denotes the transpose of $\boldsymbol{A}$. However, equation (6.14) is not generally the best way to find least squares solutions [70]. Note that $\boldsymbol{A}^T\boldsymbol{A}$ is symmetric, and hence almost half of the work may be saved in computing $\boldsymbol{A}^T\boldsymbol{A}$. Furthermore, a specialized and time saving factorization scheme, which takes advantage of the symmetry of the matrix may by used to compute the solution to the normal equations. One such method is the Cholesky factorization [39].

6.2 THE SINGULAR VALUE DECOMPOSITION

By the transformation of the integral equation to a linear set of equations the problem of characteristic frequencies appears as an ill-conditioning of the coefficient matrix $\boldsymbol{A}^{com}$. The condition number κ may be roughly described as the factor a

disturbance of an element in the matrix $\boldsymbol{A}^{com}$ or the right-hand side $\boldsymbol{b}^{com}$ may be multiplied with in the solution vector $\boldsymbol{x}^{com}$. Thus the matrix is ill-conditioned if the condition number is large, and if the condition number is infinite the matrix is singular. As the elements of $\boldsymbol{A}^{com}$ are the results of approximations (discretization and numerical integration), the uncertainty related to these elements are usually much larger than the internal machine precision.

In handling singular/ill-conditioned matrices the Singular Value Decomposition (SVD) is often considered the ultimate tool, see e.g. Press et al.[70]. The Singular Value Decomposition of the real square $N \times N$ matrix $\boldsymbol{A}$ of equation (6.6) is defined as

$$\boldsymbol{A} = \boldsymbol{U}\boldsymbol{W}\boldsymbol{V}^T \ . \tag{6.15}$$

This decomposition is always possible [39,70], and programs to perform the SVD are available both for main-frames and for PC's (routines are listed e.g. in Press et al.[70]). The matrices $\boldsymbol{U}$ and $\boldsymbol{V}$ are orthogonal, i.e.

$$\begin{aligned} \sum_{i=1}^{N} u_{ik} u_{in} &= \delta_{kn} \ , \quad && 1 \le k \le N \\ & && 1 \le n \le N \\ \sum_{j=1}^{N} v_{jk} v_{jn} &= \delta_{kn} \ , \quad && 1 \le k \le N \\ & && 1 \le n \le N \end{aligned} \ , \tag{6.16a,b}$$

where u_{ik} denotes the element in row i and column k of matrix $\boldsymbol{U}$, and δ is the Kronecker delta. $\boldsymbol{W}$ is a diagonal matrix, and the values w_{jj} (or shortly w_j) in the diagonal of $\boldsymbol{W}$ are called the singular values. Without loss of generality the columns of the matrices $\boldsymbol{U}$, $\boldsymbol{V}$, and $\boldsymbol{W}$ may be arranged in order of descending w_j's, so that w_1 is the largest element and w_N is the smallest. Since $\boldsymbol{U}$ and $\boldsymbol{V}$ are orthogonal their inverses equal their transposes, and the inverse of $\boldsymbol{A}$ is thus

$$\boldsymbol{A}^{-1} = \boldsymbol{V} \cdot [\mathrm{diag}(1/w_j)] \cdot \boldsymbol{U}^T \ . \tag{6.17}$$

Analytically, this formula behaves well if none of the w_j's are zero, but numerical problems arise if one or several of the

w_j's are small compared to the accuracy of the elements of $\boldsymbol{A}$. The condition number κ of a matrix is defined as the ratio w_1/w_N, and as previously mentioned the matrix is said to be ill-conditioned/singular if this ratio is large/infinite.

In order to investigate the properties of the SVD further, it is convenient to regard $\boldsymbol{A}$ as the matrix of a linear mapping:

$$\boldsymbol{y} = \boldsymbol{A}\boldsymbol{x} \ , \tag{6.18}$$

i.e. the vector $\boldsymbol{x}$ is mapped on to the vector $\boldsymbol{y}$ by equation (6.18). The columns in $\boldsymbol{U}$ and $\boldsymbol{V}$ calculated by a SVD are connected by the simple relation

$$\boldsymbol{A}\boldsymbol{v}_j = w_j\boldsymbol{u}_j \ . \tag{6.19}$$

Any vector $\boldsymbol{x}\in\mathbb{R}^N$ may be expressed by the columns of $\boldsymbol{V}$:

$$\boldsymbol{x} = \xi_1\boldsymbol{v}_1 + \xi_2\boldsymbol{v}_2 + \ldots + \xi_N\boldsymbol{v}_N \ , \tag{6.20}$$

and the vector $\boldsymbol{y}$ onto which $\boldsymbol{x}$ is mapped by equation (6.18) may be expressed using equation (6.19) and equation (6.20):

$$\boldsymbol{y} = \sum_{j=1}^{N} \xi_j w_j \boldsymbol{u}_j \ . \tag{6.21}$$

Considering equation (6.19) the w_j's may thus be regarded as the magnification of the v_j's when mapped onto the corresponding $\boldsymbol{u}_j$'s. Thus the w_j's are, in some sense similar to a transfer function. If $\boldsymbol{A}$ is regular $\boldsymbol{y}$ will go through all possible combinations of the columns of $\boldsymbol{U}$ as $\boldsymbol{x}$ goes through all possible combinations of the columns of $\boldsymbol{V}$, given by equation (6.20). Consequently the columns of $\boldsymbol{V}$ is an orthogonal basis for the solution space of $\boldsymbol{A}$, and the columns of $\boldsymbol{U}$ is an orthogonal basis for the range of $\boldsymbol{A}$. Range refers to what may be reached by the linear mapping defined by $\boldsymbol{A}$.

If $\boldsymbol{A}$ is singular then one or several of the w_j's are zero and the corresponding last column(s) of $\boldsymbol{V}$ are called singular vectors and are by equation (6.19) mapped on to the zero-vector:

$$\boldsymbol{A}\boldsymbol{v}_j = \boldsymbol{0} \ . \tag{6.22}$$

$\boldsymbol{A}$ is R, then the last $N-R$ of the w_j's would be zero. In that case two additional subspaces are needed in the discussion of the mapping. The last N-R columns of $\boldsymbol{V}$ are called the null space of $\boldsymbol{A}$ since they are mapped into the zero-vector, and the corresponding last N-R columns of $\boldsymbol{U}$ are called the orthogonal complement of $\boldsymbol{A}$, since this vector space may not be reached by the mapping defined by equation (6.18). The solution space of $\boldsymbol{A}$ is then spanned by the first R columns of $\boldsymbol{V}$, and the range of $\boldsymbol{A}$ by the first R columns of $\boldsymbol{U}$. These properties are summarized in table 5:

name	basis vectors	dimension
range	$\boldsymbol{u}_1, \boldsymbol{u}_2, .., \boldsymbol{u}_R$	R
orthog. compl.	$\boldsymbol{u}_{R+1}, ..., \boldsymbol{u}_N$	N-R
solution space	$\boldsymbol{v}_1, \boldsymbol{v}_2, ..., \boldsymbol{v}_R$	R
null space	$\boldsymbol{v}_{R+1}, ..., \boldsymbol{v}_N$	N-R

Table 5: The connection between the four fundamental subspaces and the singular value decomposition.

If $\boldsymbol{A}$ is the coefficient matrix of a system of equations to be solved for a known right-hand side $\boldsymbol{b}$, such as

$$\boldsymbol{A}\boldsymbol{x} = \boldsymbol{b} \ , \tag{6.23}$$

then $\boldsymbol{A}$ being singular corresponds to one of two alternatives: Either the system of equations has no solution, which is $\boldsymbol{b}$ is not in the range of $\boldsymbol{A}$, or the system of equations has one or several infinities of solutions, since in this case any combination of the zero-vectors $(\boldsymbol{v}_{R+1}, ..., \boldsymbol{v}_N)$ may be added to a specific solution. In the latter case $\boldsymbol{b}$ is in the range of $\boldsymbol{A}$, and may be expressed as a linear combination of the first R columns of $\boldsymbol{A}$.

Turning now to the BEM, it is a fact that a solution is known to exist at the characteristic frequencies when using the Helmholtz integral equation, which is in contrast to e.g. the simple source formulation [78]. Hence, the latter of the above alternative must be the one encountered in the present case. The number of zero w_j elements is, as previously stated, the

rank deficiency of the matrix $\boldsymbol{A}$ *and is also the number of missing linearly independent equations that must be added in order to obtain a system where the number of linearly independent equations equals the number of unknowns*. Thus the problem is to add additional constraints to the system of equations in order to obtain an unique solution out of the infinity many solutions to the singular system of equations.

Numerically, an exact singular matrix seldom occurs, and in fact it has been proved [34] that an exact singular matrix never occurs in boundary element matrices. However, the situation described above presents it self in the shape of an ill-conditioned matrix. The numerical rank deficiency of a matrix may be defined as the number of w_j's below a certain value. If equation (6.17) is used without modifications at a characteristic frequency, the solution vector may be wandering off towards infinity in a direction of an almost singular vector, or, in the case of a rank deficiency higher than one, any combination of the singular vectors.

Note that the SVD may also be used in the case of an $M \times N$ matrix ($M>N$). In this case $\boldsymbol{U}$ is a $M \times N$ column-orthogonal matrix, and the matrices $\boldsymbol{V}$ and $\boldsymbol{W}$ are both $N \times N$. The solution produced by the SVD is the linear least squares solution. The generalized condition number is still defined as the ratio w_1/w_N. A matrix for which the number of rows does not equal the number of columns is termed a rectangular matrix. In terms of accuracy the SVD is more favourable than the traditional least-squares procedure using $\boldsymbol{A}^T\boldsymbol{A}$, since the matrix $\boldsymbol{A}^T\boldsymbol{A}$ has the condition number κ^2 if the rectangular matrix $\boldsymbol{A}$ has the condition number κ.

As demonstrated above, the singular value decomposition is the ultimate choice in terms of obtaining information about the set of equations. The price payed is in terms of effciency: In order to solve an $N \times N$ system $12 \cdot N^3$ flops are required. It will be demonstrated in section 6.4 that the information useful for boundary element calculations consists of the smallest singular values and the corresponding almost singular vectors. This information may be obtained considerably cheaper in terms of

flops using a superstructure based on the QR-factorization to be described in the next section.

6.3 THE QR-FACTORIZATION

The matrix $\boldsymbol{A}$ of equation (6.6) may also be written as

$$\boldsymbol{A} = \boldsymbol{QR} \ , \tag{6.14}$$

where $\boldsymbol{Q}$ is an orthogonal $N \times N$ matrix and $\boldsymbol{R}$ is upper triangular. Hence, the set of equations can be solved in two steps:

$$\boldsymbol{y} = \boldsymbol{Q}^T \boldsymbol{b} \tag{6.15}$$

and

$$\boldsymbol{Rx} = \boldsymbol{y} \ , \tag{6.26}$$

where backsubstitution as in equation (6.13) is used to solve equation (6.26). The Rank Revealing QR (RRQR) factorization is a special QR factorization, for which the column pivoting is organized in a way which ensures that the numerical rank, and hence ill-conditioning, is revealed by producing good estimates of the smallest singular values. Furthermore, good estimations of the singular vectors are also obtained. The algorithmic details and proofs may be found in [16]. Here it suffices to say that the coefficient matrices produced by the boundary element method are well-suited for the RRQR algorithm, and that in all cases studied by the author, the RRQR factorization has provided qualitatively the same singular values and singular vectors as the singular value decomposition.

However, the RRQR factorization is much more efficient than the singular value decomposition. In order to compute a QR factorization of an $N \times N$ matrix $4/3 \cdot N^3$ flops are required. Although this number of flops is twice the number of flops for the LU-factorization, the QR factorization tends to be as efficient as the LU factorization in practice [39]. This is because the QR algorithm adresses the elements of $\boldsymbol{A}$ in the same order as they are stored in the computer, and thus reduces the memory traffic in the computer. The rank revealing superstructure on

the QR algorithm requires only in the order of N^2 flops for the estimation of each small singular value, and the corresponding singular vector. Hence the extra amount of work due to the rank revealing part is vanishing for large systems of equations with a small rank deficiency, compared to the work of the QR factorization.

If the matrix $\boldsymbol{A}$ is overdetermined ($M \times N$ where $M > N$), the QR factorization produces the linear least squares solution. In this case Q is an $M \times M$ orthogonal matrix and R is an $M \times N$ upper triangular matrix. Both in respect to accuracy and the time consumed, the QR factorization is preferable for solving the linear least squares problem when $M-N$ is small compared to N, as usually is the case for boundary element calculations.

Finally, another important feature of the QR factorization should be mentioned: If the QR factorization of e.g. a square ($N \times N$) system is known, the QR factorization may be updated rather than recalculated if more equations are added to the system [39]. For boundary element calculations this feature is very useful: If ill-conditioning has been found by the RRQR factorization due to the pressence of a nearby characteristic frequency, addition of further equations to the original system of equations will be required. This could be done by the CHIEF method or by a related approach, see sections 5.2 and 5.4. In this case a new QR factorization need not to be calculated from the start. The updating of the QR factorization requires an order less of flops than the QR factorization it self, and hence the time spend to update the QR factorization is vanishing for a large system of equations with a small number of extra equations added, which generally is the case using CHIEF or a related approach.

6.4 USING RANK REVEALING FACTORIZATIONS WITH METHODS TO OVERCOME THE NONUNIQUENESS PROBLEM

In section 5.2 it was concluded that there were two major problems related to the CHIEF method:

a) the determination of the number of good CHIEF points needed to ensure a unique solution,

b) and how to determine whether a CHIEF point is good.

In this section it will be demonstated how both problem may be overcome by the use of rank revealing factorizations. For simplicity the approach will be described using the original CHIEF approach, although the scheme presented here is valid for the enhanced CHIEF [89], the SuperCHIEF [79], and the CHIEF-block [107] methods without modifications. For clarity the theory is described using the singular value decomposition although the rank revealing QR factorization is preferable from a computational point of wiev as discussed in sections 6.2 and 6.3. All calculations presented here has been re-calculated using the RRQR factorization and the same results were found.

6.4.1 USING THE SINGULAR VALUE DECOMPOSITION IN BOUNDARY ELEMEMT CALCULATIONS

The theory for the singular value decomposition in section 6.2 was discussed for the case of a real matrix $\boldsymbol{A}$. The handling of the complex boundary element method (BEM) coefficient matrix in equation (6.3) has been done by rewriting the complex system of equations in equation (6.3) as the real system of equations in equation (6.5). Now, if $\boldsymbol{x}_0=\boldsymbol{x}_0^{re}+i\boldsymbol{x}_0^{im}$ is a singular vector so that

$$\begin{bmatrix} \boldsymbol{A}^{re} & -\boldsymbol{A}^{im} \\ \boldsymbol{A}^{im} & \boldsymbol{A}^{re} \end{bmatrix} \begin{bmatrix} \boldsymbol{x}_0^{re} \\ \boldsymbol{x}_0^{im} \end{bmatrix} = \boldsymbol{0} \,, \tag{6.27}$$

then it immediately follows that $-\boldsymbol{x}_0^{I}+i\boldsymbol{x}_0^{R}$ is a singular vector as well, and this vector is evidently orthogonal to $\boldsymbol{x}_0=\boldsymbol{x}_0^{R}+i\boldsymbol{x}_0^{I}$. It can be shown that the singular values of the matrix in equation (6.5) always appear as pairs of the same value due to the special structure of the $2M$x$2M$ matrix, and

that the two columns in both U and V, corresponding to the two identical w_j's, have the property mentioned above. In the following examples only one value of the pair of w_j's is shown. In order to investigate the behaviour of the singular values (the w_j's) near a fictitious eigenfrequency, the SVD has been performed on the square BEM coefficient matrix in the case of a rigid sphere. The axisymmetry of the geometry in the presented examples has been exploited, and hence the test cases have been calculated by means of an axisymmetric boundary element formulation, where only the generator of the body has been discretized. The generator of the sphere was divided into 19 isoparametric linear elements.

One of the important properties of the SVD is demonstrated in figure 6.1, which shows the singular values of the BEM coefficient matrix in a frequency range near the first characteristic frequency at $ka=\pi$. From the figure it is evident that the first 19 singular values are practically constant in the range of $ka=3.128$ to $ka=3.156$, whereas the last singular value shows a strong dependence of the distance to the characteristic frequency. Since the first singular value w_1 is almost constant in this frequency range, the condition number $\kappa=w_1/w_M$ ($M=20$) is inversely proportional to the last singular value and thus becomes large as the frequency approaches the characteristic frequency. Hence the problem of characteristic frequencies is directly reflected in the last singular value in this case. Since only one singular value becomes small at $ka=\pi$, only one good CHIEF point is needed to add the sufficient constraint to the system of equations. Accordingly, the condition number calculated by the SVD for the overdetermined system of equations, produced by the BEM coefficient matrix with a CHIEF point in the centre of the sphere, is $\kappa=2.6$, which is very close to the best possible theoretical value, unity.

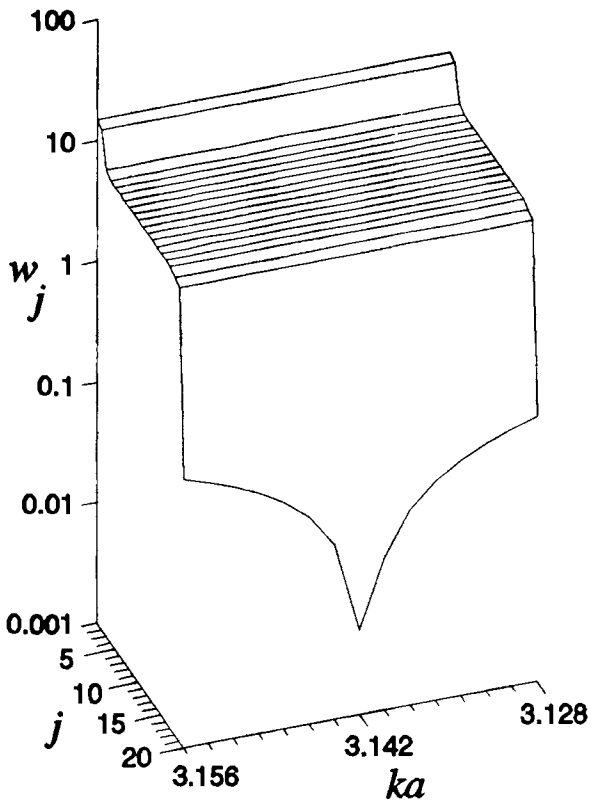

Figure 6.1. The 20 singular values of the boundary element coefficient matrix for a 20 node discretization of a rigid sphere near the first characteristic frequency at $ka=\pi$.

6.4.2 NUMERICAL RANK

As briefly mentioned in section 6.2, an exact singular matrix practically never occurs in boundary element calculations [34]. Instead the problem of characteristic frequencies is reflected in an ill-conditioning of the boundary element coefficient matrix. Hence, a threshold for the w_j's under which the matrix is said to be numerically rank deficient must be chosen. In order to investigate the connection between the smallest singular value and the error made by the BEM formulation without any CHIEF points the following testcase has been calculated. The error made by the isoparametric linear BEM formulation in the case of scattering of a plane wave of unit magnitude by a rigid sphere, and the smallest singular value have been calculated. The results are plotted as functions of the dimensionless wavenumber ka in Figure 6-2.

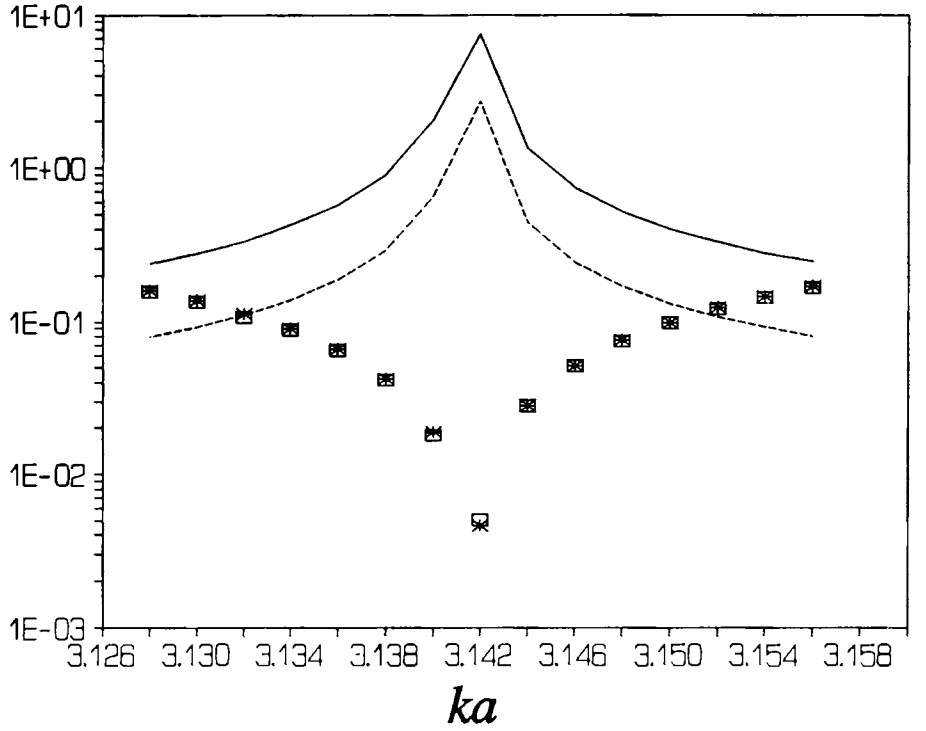

Figure 6-2. Solution error and the smallest singular value near the first characteristic frequency at $ka=\pi$. □, Smallest singular value for 20 node discretization; *, smallest singular value for 40 node discretization; ————, solution error for 20 node discretization; --------, solution error for 40 node discretization.

The error is as usual calculated as the length of the residual vector - the residual vector being the vector containing the difference between the analytical solution and the BEM solution at the nodes. For this figure two BEM calculations have been made: one using a 20 node discretization (the same as used for Figure 6-1), and one using a 40 node discretization.

The figure shows that for both discretizations, the smallest singular values are practically identical, whereas the error depends strongly on the discretization. This may be explained by the close relation between the smallest singular value and the condition number. As mentioned previously, the condition number may be regarded as the 'blow-up' factor for the error due to the approximations made by the BEM formulation, and evidently the degree of approximation is larger for

the 20 node formulation than for the 40 node formulation. Hence, although the smallest singular value is the same in the two situations, the resulting error is not. However, the smallest singular value obviously proves to be a good estimate of the error and thus it is possible to use the smallest singular value as an error indicator. Thus it is possible to choose a threshold for the singular values, and improve the standard BEM formulation e.g. by adding CHIEF points if this threshold is crossed. As mentioned above, the resulting error is not a function of the smallest singular value only, and hence the threshold should be chosen for each actual implementation of the Helmholtz integral equation specifically. For any practical implementation the ratio of wavelength to element could be kept size constant, and the error made by this particular implementation could be examined for cases where the non-uniqueness problem does not occur. The threshold could then be defined by examining the smallest singular value for the implementation as the frequency is moved close to a characteristic frequency. The threshold would then be the largest of the smallest singular values in the band of frequency band where the error is unacceptably high compared to the level found in the first experiment.

6.4.3 ADDING A CHIEF POINT

Once the number of good CHIEF points needed to pick out the correct solution to the problem has been determined by inspecting the singular values of the BEM coefficient matrix, it becomes important to be able to estimate the quality of a CHIEF point. Note that if the complex system of equations has been transformed to a real system by equation (6.5), a CHIEF point provides two independent equations to be satisfied along with the standard BEM coefficient matrix corresponding to the two singular vectors shown to exist in paragraph 6.4.2 for the pair of singular values.

The SVD provides a very good tool for deciding whether a CHIEF point is good: the singular vectors. When a matrix $\boldsymbol{A}$ is rank-one deficient, that is, when the smallest singular value

is zero, any constant times the singular vector may be added to a specific solution without altering the righthand side. Consider for simplicity the real system of equations

$$\boldsymbol{A}\boldsymbol{x} = \boldsymbol{b} \quad (=\boldsymbol{A}(\boldsymbol{x}+t\boldsymbol{x}_0)) \; ; \quad t\in\mathbf{R} \, , \tag{6.28}$$

where $\boldsymbol{x}_0$ is a singular vector. In order to pick out a solution from this infinity of solutions an extra equation may be added by means of a CHIEF point to impose the necessary constraint on the parameter t. This results in a rectangular system of equations. If the extra equation adds the necessary constraint, that is, the CHIEF point is good, then the rectangular system is non-singular. This implies that the singular vector $\boldsymbol{x}_0$ of equation (6.28) is not a singular vector for the rectangular system

$$\begin{bmatrix} \boldsymbol{A} \\ \\ \boldsymbol{a}_{ex}^{T} \end{bmatrix} \boldsymbol{x}_0 \neq \boldsymbol{0} \tag{6.29a}$$

$$\Updownarrow$$

$$\boldsymbol{a}_{ex}^{T} \cdot \boldsymbol{x}_0 \neq 0, \tag{6.29b}$$

since $\boldsymbol{A}\boldsymbol{x}_0 = \boldsymbol{0}$. If equation (6.29b) is true then the rectangular system of equations is non-singular, and the solution may be found as the least-squares solution of the rectangular system. In practice the left-hand side must be greater than a certain threshold, of course.

The lefthand side of equation (6.29b) may be used as a quality indicator of the extra equation, since a small product implies that no additional constraint has been obtained.

The theory described above is also valid for the case of the $2M\times 2M$ real system transformed from the complex BEM coefficient matrix. Here the combination of two singular vectors corresponding to the pair of singular values is to be found from the two extra equations added by a CHIEF point. Due to the special symmetry of the equations, the largest of the dot products of an extra equation and the singular vector may be used as the quality indicator.

In order to test this formulation, the case of scattering of a plane wave by a rigid sphere has been considered at ka=6.2832. This case was also considered in section 5.5, see figure 5-9. The condition number of the BEM coefficient matrix in this case was 12161, where a 30 node linear discretization was used. The solution error has been calculated as the vector containing the difference between the analytical magnitude of the nodal pressures and the magnitude of the nodal pressures calculated by the BEM formulation. At $ka=2\pi$ the interior nodal surface is a sphere with the same centre as the scattering sphere and with the radius $a/2$. Figure 6-3 shows the solution error, and the value of the quality indicator calculated by equation (6.29b), as functions of the z_p-coordinate of the CHIEF point, the ρ-coordinate and the θ-coordinate being zero. The sphere is centred in a cylindrical coordinate system (ρ,θ,z) as usual. It is evident that the quality indicator is very good at monitoring the solution error.

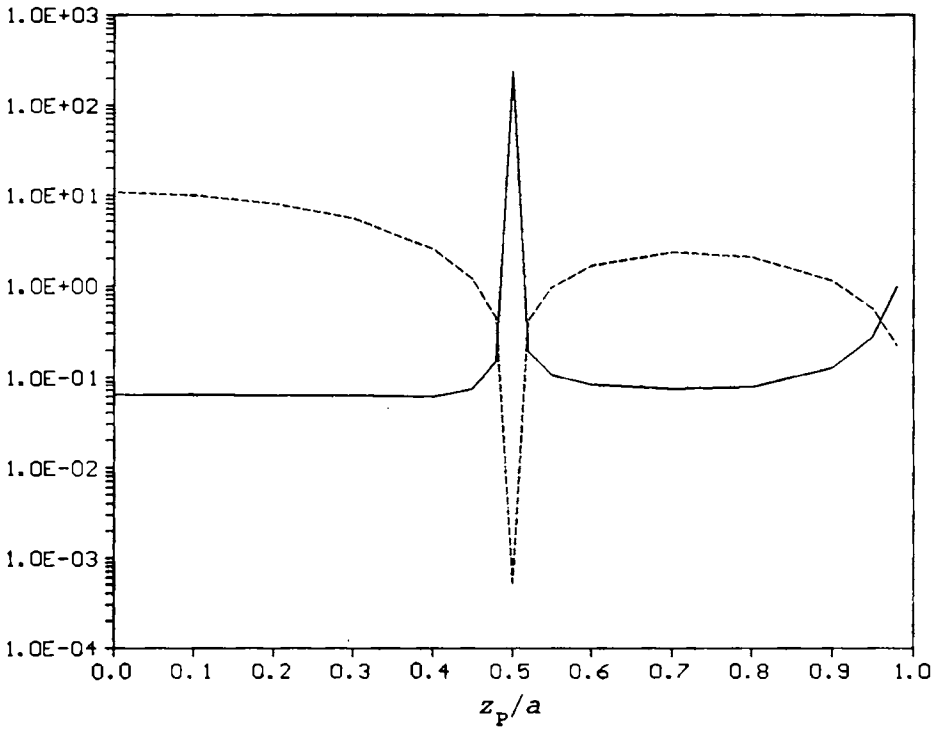

Figure 6-3. Quality indicator and solution error as functions of the z_p-coordinate $(\rho,\theta=0)$ of the CHIEF point for the case of scattering of a plane wave by a rigid sphere at ka=6.2832. The sphere is discretized using 29 isoparametric linear elements.

6.4.4 THE SINGULAR VALUE DECOMPOSITION AT HIGHER FREQUENCIES

At higher frequencies the non-uniqueness problem becomes more severe due to the close spacing of the characteristic frequencies and due to the associated 'bandwidth' as discussed in section 5.5. A situation where the bands of bad solutions no longer are distinct and the solution is corrupted by two or more characteristic frequencies near any chosen frequency may very well be encountered. This situation is reflected in two or more small singular values calculated by the SVD with corresponding singular vectors, and the numerical rank deficiency of the BEM coefficient matrix is thus greater than one. Now, the strategy is to choose a CHIEF point that satisfies equation (6.29b) *for each* singular vector, and thereby decrease the rank deficiency by one in the resulting rectangular matrix. When this has been done for all singular vectors, the resulting rectangular matrix is fully ranked, that is, the rank equals the column dimension, and thus the non-uniqueness problem is solved. Note that each CHIEF point need to concern only *one* singular vector in order to decrease the rank deficiency. Thus it is only required that equation (6.29b) is fulfilled for this particular singular vector, and not for any other singular vector, because they are taken care of by other CHIEF points.

In order to generate a higher rank deficiency, scattering of a plane wave with unit magnitude from a rigid sphere for the characteristic frequency at ka=15.0397 has been considered. The generator of the sphere has been discretized into 79 isoparametric linear elements. In this case two singular values become very small due to the presence of another fictitious eigenfrequency at ka=15.0335, which is reflected in the condition number $\kappa=w_1/w_M=2466$, and the following ratios $w_1/w_{M-1}=310$ and $w_1/w_{M-2}=9.7$. Thus the numerical rank deficiency of the BEM coefficient matrix is two. Figure 6-4 shows the magnitude of the pressure on the surface as a function of the angle defined in the small inset in the figure. It is evident that in this case two 'good' CHIEF points are required to obtain an accurate solution, since the difference between the curves representing the analytical solution and the BEM solution using two CHIEF

points is hardly noticeable. The CHIEF points have been selected with respect to the quality indicator under consideration.

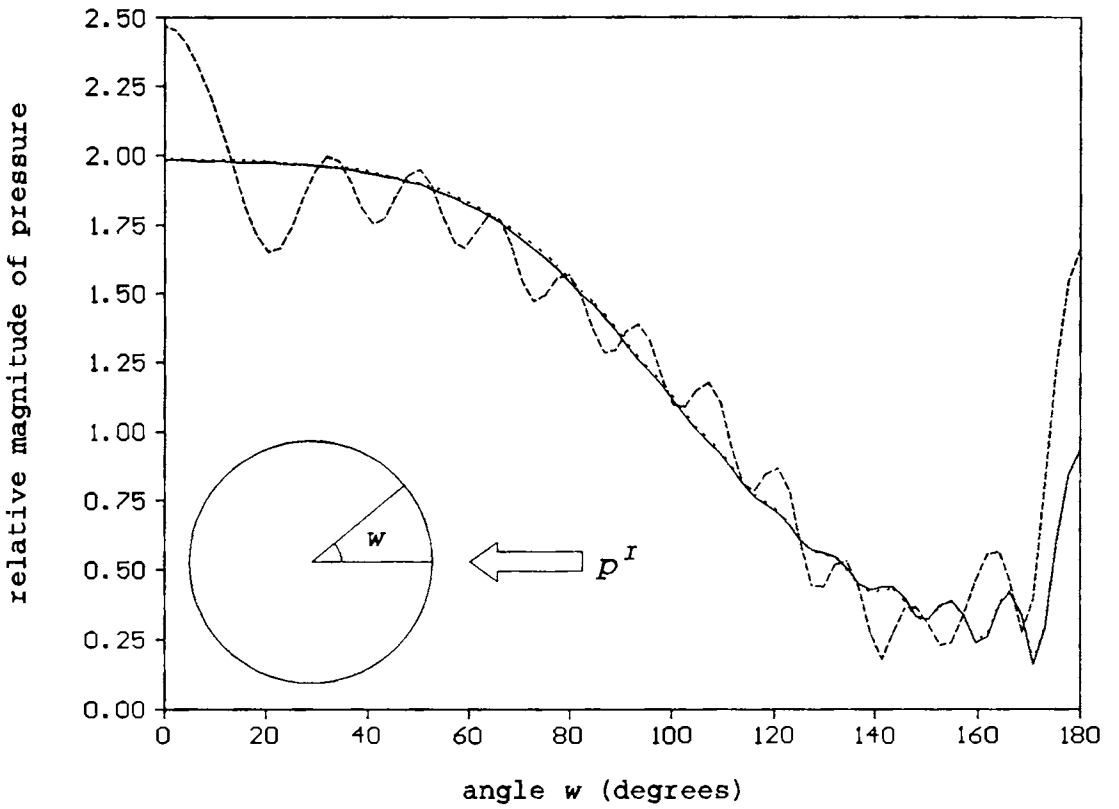

Figure 6-4. Scattering by a rigid sphere at ka=15.0397 where the numerical rank deficiency is two.————, analytical solution; -------, BEM solution using one CHIEF point; ·····, BEM solution using two CHIEF points.

6.4.5 CONCLUDING REMARKS

In this section the non-uniqueness problem of the exterior BEM formulation has been investigated by means of the Singular Value Decomposition (SVD). It has been shown that the rank deficiency of the BEM coefficient matrix at characteristic frequencies may be revealed by the SVD.

Furthermore, it has been shown that due to the 'bandwidth' of the characteristic frequencies the rank deficiency of the BEM coefficient matrix may be greater than one when two or

several characteristic frequencies are near the frequency of interest.

The number of good CHIEF points needed to obtain a unique solution equals the rank deficiency of the BEM coefficient matrix, and it has been shown that by making use of the singular vectors obtained by the SVD the quality of the CHIEF points can be determined reliably.

As mentioned in the beginning of section 6.4, the same information may be obtained using the far more efficient RRQR factorization. The extra cost with respect to computation time comsumed of the RRQR factorization is insignificant compared to the cost of the LU-decomposition, which is the standard method of solving a fully populated set of equations.

This approach may also be applied to more advanced methods to overcome the non-uniqueness problem.

It must be emphasized that the test cases presented in this section concern an axisymmetric model, where the rank deficiency problem is less severe than in a general three-dimensional formulation. However, the method is valid for general three-dimensional formulations as well. A paper describing this work has been accepted for publication [52].

7. APPLICATION OF THE BOUNDARY ELEMENT METHOD TO INVESTIGATION OF STANDARD CONDENSER MICROPHONES

Since 1989 an extensive work on free-field reciprocity calibration has been carried out by The Acoustic Laboratory at the Technical University of Denmark. During this work a number of standard condenser microphones - of types Brüel & Kjaer 4160 and 4180 - have been calibrated with a high degree of accuracy [71]. This work has been organized by the Community Bureau of References under the Commission of the European Communities, and involves four European laboratories with The Acoustics Laboratory as the central laboratory. The purpose of this intercomparison has, among other things, been to obtain the correction curve to be added to the pressure sensitivity for measurements in free-field conditions.

These correction curves are important for e.g. noise measurements, which is a topic of increasing concern. The standard correction curves used today are based on measurements that were carried out more than two decades ago, and they do not meet the requirements to accuracy that is needed nowadays.

The need for standard correction curves is caused by the fact that a free-field calibration is very cumbersome to carry out, whereas pressure calibration may easily be done: In general use it is assumed that the pressure sensitivity of a condenser microphone is independent of the frequency, and hence the microphone may be calibrated at one frequency only, using a pistonphone or a sound level calibrator.

As the experimental accuracy was improved it became apparent that various secondary characteristics associated with the microphones (acoustic centre, acoustic impedance and range of the near field) had to be taken into account in order to increase the accuracy. Furthermore, it is not possible to determine correction curves experimentally for various angles of incidence and for diffuse incidence, with the same high accuracy as for axial incidence. As the axisymmetric integral

equation formulation described in chapter 3 was developed [49, 51], it became obvious to test the boundary element formulation against the experimental data and also to use the boundary element formulation to obtain correction curves for the cases of non-axial incidence. In order to obtain the desired high accuracy the movement of the diaphragm of the microphone had to be taken into account by the means of a coupled structural-acoustical model. The coupled problem is solved by means of a new iterative procedure. Hence the purpose of the present investigation is threefold:

1) To compare the boundary element formulation to very accurate experimental data.
2) To solve the coupled structural-acoustic problem by the means of an iterative procedure.
3) To obtain pressure sensitivity correction curves for various angles of incidence and for a diffuse field.

Furthermore, some quantities of interest for microphone designers and calibration laboratories are examined - these quantities may be determined experimentally only with extreme difficulties.

7.1 NUMERICAL IMPLEMENTATION

Since the microphones B&K 4160 and B&K 4180 to be investigated are almost perfectly axisymmetric, the axisymmetric integral equation formulation developed in chapter 3 are used for the present investigation. Hence, for the following study a boundary element formulation has been made using isoparametric quadratic elements as described in paragraph 4.4.2, for the approximation of equations (3.36) - (3.38). In order to solve the resulting set of equations the LU factorization described in section 6.1 was used. This is because both scattering by different angles of incidence and iteration is used in this study, so that a factorization method that allows the system of equations to be solved efficiently for different right-hand sides may be used with great advantage.

7.2 MICROPHONE CHARACTERISTICS

The free-field correction is defined as the ratio between the free-field and the pressure sensitivity. The pressure sensitivity is the ratio between the magnitudes of the open-circuit voltage and the pressure on the diaphragm when the microphone is exposed to a harmonic sound field in which the pressure is constant over the area of the diaphragm. The technique used for pressure reciprocity calibration of microphones has been developed into a high precision. Exposing the microphone to a freely propagating plane wave allows the free-field sensitivity to be determined as the ratio between the open-circuit voltage and the magnitude of the undisturbed plane wave. Normally zero degree incidence, where the wavefront is parallel to the diaphragm is assumed unless an angle of incidence is specified.

The main component of the free-field correction curve is due to the geometrical shape of the microphone. Investigating this component corresponds to determining the diffraction caused by the microphone when the diaphragm is blocked. Such investigations have been carried out experimentally on scale models of microphones [11,77].

The remaining component is due to the movement of the diaphragm. In normal use of the microphone the sound pressure is measured exactly because it sets the diaphragm of the microphone into movement. Evidently this movement has a certain small effect on the sound field, and hence a coupled structural-acoustical problem arises.

7.2.1 FREE-FIELD CORRECTION CURVE

In order to determine the pressure sensitivity it is necessary to relate the magnitude of the pressure on the membrane to an electrical output. If the diaphragm of a microphone is exposed to a harmonic point force, the electrical output will depend on the location of the point force. At low frequencies the open-circuit voltage will be at a maximum when the point force acts at the centre of the diaphragm, and the voltage will decrease towards zero as the point force moves to

the edge of the diaphragm. Hence a weighting function $f(r)$ must be defined for any arbitrary pressure distribution over the area of the diaphragm. As the open-circuit voltage over a capacitor is proportional to the distance between the electrodes, the weighting function is roughly shaped as the displacement of the diaphragm. Thus assuming that the radius of the diaphragm a equals the radius of the backplate, and using the axisymmetry of the problem, one may express the pressure sensitivity M_p in terms of the displacement of the diaphragm [77]:

$$M_p = c_{mic} \int_0^a f(r)\, r\, dr \tag{7.1}$$

in which

$$f(r) = \frac{J_0(k_1 r) - J_0(k_1 a)}{1 - J_0(k_1 a)} , \tag{7.2}$$

where c_{mic} is a proportionality constant and k_1 is the wave number in the diaphragm material (nickel). The expression for $f(r)$ is the displacement of a plane, stretched membrane in front of a volume [64] when exposed to a constant harmonic pressure over the area of the membrane and neglecting the presence of the backplate. At low frequencies it is possible to approximate equation (7.2) by

$$f(r) = 1-(r^2/a^2) . \tag{7.3}$$

At high frequencies i.e. from the resonance frequency and above, the diaphragm does not behave as a plane, stretched membrane due to the presence of the backplate, and neither equation (7.2) nor (7.3) can be expected to give accurate results. However, the actual displacement of the diaphragm at high frequencies is unknown, and in this study equation (7.3) is used for the weighting function for all frequencies. Hence the present investigation is limited to relatively low frequencies.

Ultimately the membrane problem should be solved numerically including the very complex configuration represented by the

backplate with holes. It would then be possible to express the sound field in terms of eigenfunctions of the membrane problem. Unfortunately, the geometry of this problem is very complex and may not be solved readily; furthermore the actual boundary condition at the edge of the diaphragm is unknown at this level of detail. In this line of thought the present investigation takes into account only the first order effect, by including the first term of the eigenfunction expansion, which is expected to be dominating by far at low frequencies.

When the microphone is exposed to a plane wave of zero degree incidence, the pressure is no longer constant over the area of the diaphragm but varies axisymmetric along the radius of the diaphragm. Defining its value relative to the undisturbed incoming wave as $p(r)$ allows one to establish an equation for the free-field sensitivity:

$$M_f = c_{mic} \operatorname{mod}\left(\int_0^a p(r)\, f(r)\, r \, dr \right) . \tag{7.4}$$

Hence the sound field on the diaphragm is expanded into the eigenfunctions of the diaphragm problem (using only one term and neglecting all others), or explained in a more physical manner: the pressure acts through a certain weighting function.

Thus it is possible to derive an approximate expression for the free-field correction curve by combining equations (7.1) and (7.4):

$$f_c = \frac{\operatorname{mod}\left(\int_0^a p(r)\, f(r)\, r \, dr \right)}{\int_0^a f(r)\, r \, dr} . \tag{7.5}$$

Normally the free-field correction curve is given in a logarithmic scale: $F_c = 20 \log_{10} f_c$.

If the angle of incidence differs from 0 or 180 degrees the pressure on the surface is no longer axisymmetric. In this case the incoming field should be dissolved in terms of eigenfunctions to the membrane problem including non-axisymmetric terms. However, due to the very careful crafting of the microphone and to the geometry of the volume between the diaphragm and the backplate, the diaphragm is very unlikely to

move non-axisymmetric, and even if a non-axisymmetric movement of the diaphragm could be provoked, the electrical output for each such mode would be zero due to cancelation. Hence only the axisymmetric part of the incoming wave contributes to the free-field correction curve. The axisymmetric part of the incident wave $p^I(P)$ is by equation (3.5):

$$p_0^I(P) = \frac{1}{\pi}\int_0^\pi p^I(P)\,\mathrm{d}\theta \ . \tag{7.6}$$

Knowing the free-field correction curve for all angles of incidence makes it is possible to obtain an expression for the case of a microphone placed in a diffuse sound field:

$$f_d^2 = \frac{1}{2}\int_0^\pi f_c^2(\theta)\sin(\theta)\mathrm{d}\theta \ . \tag{7.7}$$

7.2.2 MOVEMENT OF THE DIAPHRAGM

In order to increase the accuracy of the model, the movement of the diaphragm must be taken into account. The movement of the diaphragm corresponds to a finite acoustic impedance of the microphone. From experimental results [71] the acoustic impedance is given in terms of the resonance frequency f_0, the equivalent volume V_{eq} and a loss factor d:

$$Z_a = \frac{\gamma p_s}{i\omega V_{eq}}\left[1 - \left(\frac{f}{f_0}\right)^2 + i\,d\,\frac{f}{f_0}\right], \tag{7.8}$$

where γ=1.4 is the ratio of specific heats and p_s is the reference static pressure (101.325 kPa). The movement of the diaphragm could be taken into account by the means of a coupled structural-acoustic model, but in this study the coupled problem is decoupled at the interacting surface (the diaphragm), so that the structural and the acoustic problem may be handled separately. Defining the complex weighted pressure

$$\bar{p} = \frac{\int_0^a p(r)\,f(r)\,r\,\mathrm{d}r}{\int_0^a f(r)\,r\mathrm{d}r} \ , \tag{7.9}$$

the solution to the coupled problem may be found using an

iterative procedure: First the diaphragm is assumed to be blocked (volume velocity $q_0=0$). This gives rise to a weighed pressure $\overline{p_0}$. Equation (7.8) then gives a first order approximation for the volume velocity $q_1=\overline{p_0}/Z_a$. The corresponding diaphragm velocity is $v_1(r)=2(1-(r/a)^2)q_1/(\pi a^2)$, since the movement of the diaphragm is assumed to be parabolic. Then a combined radiation/scattering problem is solved to obtain a first order weighted pressure $\overline{p_1}$. This gives rise to a second order volume velocity, and so forth. The iteration is stopped when the difference between the modulus of two succeeding weighted pressures is sufficiently small (say, below 0·001 dB).

As another approximation for the movement of the diaphragm, scattering by a body shaped as a microphone may be considered, where the diaphragm is replaced with a locally reacting surface with the admittance:

$$Y_s = 2(1-(r/a)^2)/Z_a/(\pi a^2) \ . \qquad (7.10)$$

The two models would give the same result if the pressure was constant over the area of the diaphragm, since in this case the corresponding particle velocity on the surface would be parabolically shaped as is the displacement of the diaphragm. Hence equation (7.10) is valid at low frequencies.

7.2.3 ACOUSTIC CENTRE

In a reciprocity calibration arrangement the microphones are used as receivers as well as sources. When the microphone is used as a source it is convenient to regard the microphone as a monopole. This simplification is valid at large distances from the microphone. However, the location of this equivalent monopole varies with the frequency, and is not exactly at the surface of the diaphragm. The location of the equivalent monopole for a given microphone and a given frequency is called the acoustic centre of the microphone. For the standard axial incidence arrangement the acoustic centre is located on the axis of the microphone, but for a general angle of observation

the acoustic centre will normally be located off-axis. The position of the acoustic centre is important for the determination of the exact effective distance between the microphones in a reciprocity calibration arrangement, and for the B&K 4160 a standard table is provided [45-46]. Unless specified, the angle of observation is zero degrees (standard axial arrangement) in what follows.

7.3 RESULTS

A number of calculations has been made on the B&K 4160 and the 4180 condenser microphones. For the type 4160 microphone the protection grid was removed. In the free-field reciprocity calibration arrangement at the Acoustics Laboratory, the microphones are mounted on long rods, according to the requirements of reference [46]. Hence the microphones can be assumed to be of semi-infinite shape. However, the BEM used here deals with finite bodies only, and hence the length of the microphones in the BEM code must be so large that the reflection from the end of the microphone is sufficiently small. For this purpose a length of 20 times the radius was found to be sufficient, whereas a length of 10 times the radius, which is approximately the length of a common preamplifier used with the microphones, was found to be too short. The microphones were then terminated with a hemisphere in the code. Figure 7.1 shows the geometry of the microphones as used in the code. All dimensions are in mm.

Since the standard condenser microphone B&K 4160 is more well-known through experiments than the B&K 4180, the results for the B&K 4160 are examined in details, whereas the results for the B&K 4180 are merely listed.

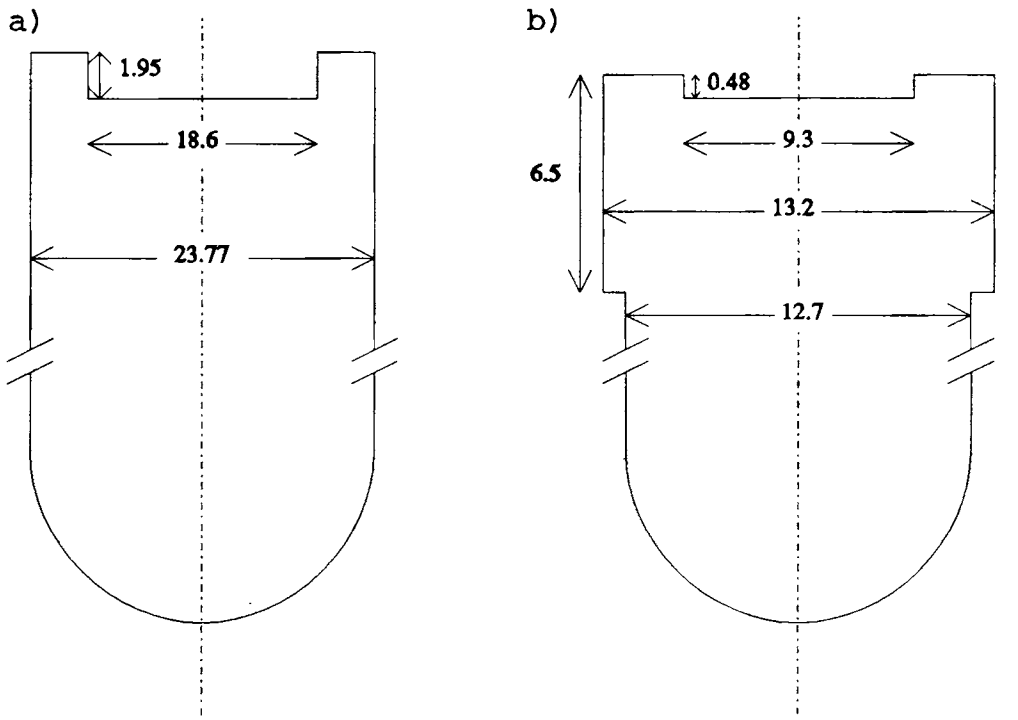

Figure 7-1. Simplified microphone geometry as used in the boundary element model. All dimensions are in mm.
a) B&K 4160; b) B&K 4180

7.3.1 FREE-FIELD CORRECTION CURVES

For the B&K 4160 a series of three calculations was made. For each calculation the mesh size was halved in order to examine the convergence of the method. In this way the calculations were estimated to have converged to within 0·02 dB. The results shown are the ones determined with the finest mesh using 160 elements along the generator of the microphone model. Figure 7-2 shows the free-field correction curves obtained by measurements [71] and by calculation using the structural-acoustical model described in paragraph 7.2.2. The curve provided by Brüel and Kjær [12] is also plotted, but it is hardly distinguishable from the measurements made at The Acoustics Laboratory in the scale of Figure 7-2. For the B&K 4160 an equivalent volume V_{eq} = 150·10^{-9} m^3, a loss factor d=1 and a resonance frequency f_0 = 8000 Hz were used in the model.

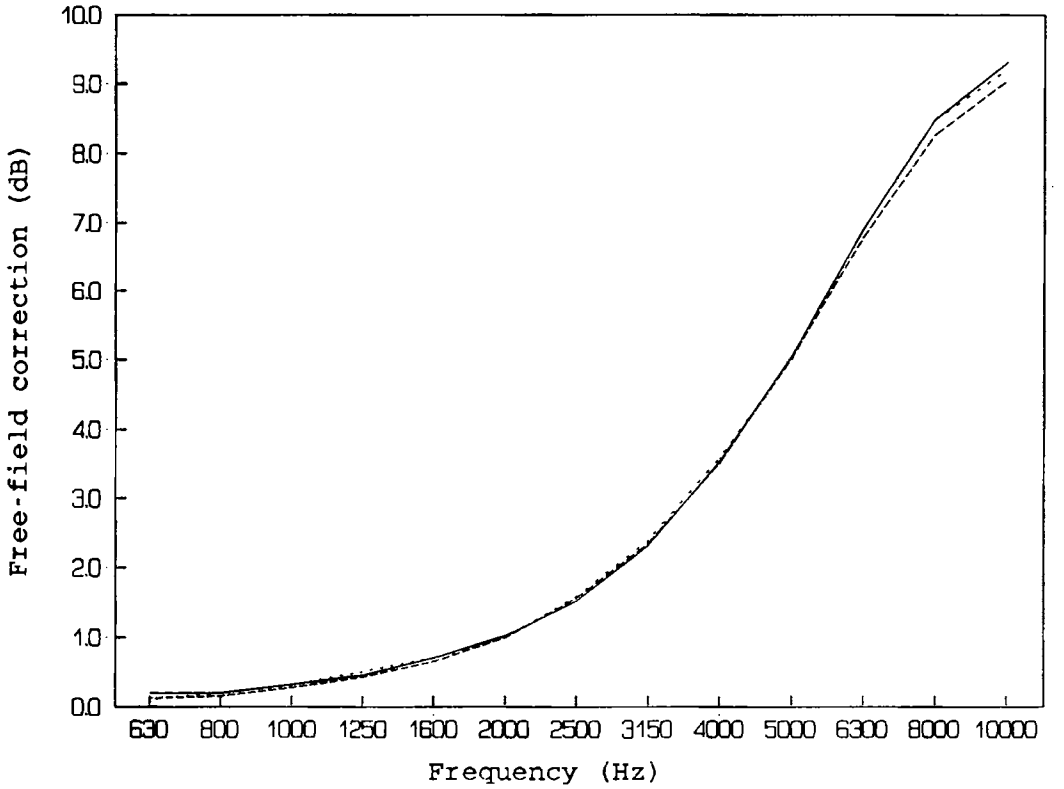

Figure 7-2. The free-field correction for the B&K 4160. ————, measured values; --------, calculated values; ·····, values provided by B&K.

The difference between the three curves in Figure 7-2 is hardly noticeable at most frequencies - it is only at the lowest frequency 630 Hz and at the resonance frequency and above that the difference is large enough to be noticed on the figure. The small difference (0.1 dB) between the results at 630 Hz is probably due to a poor signal-to-noise ratio at low frequencies in the experimental set-up. From 6300 Hz to 10000 Hz the difference between the calculated curve and the measured curve, which coincides with the curve provided by B&K, increases monotonously from 0.1 dB to about 0.3 dB. This difference is believed to be due to the assumption of parabolic movement of the diaphragm, which is probably not valid at these frequencies. However, no better model is available at present. Between 800 Hz and 5000 Hz the agreement is excellent. At these

the total (numerical plus experimental) accuracy.

In Figure 7-3 the ratio between the free-field correction obtained with the structural-acoustical model and that obtained with a rigid model is shown. It can be seen that the movement of the diaphragm has no significance at the lowest frequencies as one would expect, since the acoustic impedance given by equation (7.8) increases towards infinity as the frequency goes towards zero. However, the effect increases with the frequency and is as large as 0.23 dB below the resonance frequency. As this effect is much larger than the deviation between the calculated and the measured free-field correction seen in Figure 7-2 it is concluded that the structural-acoustical model can be expected to give reliable results. The number of iterations used with this model was between 3 (for 630 Hz) and 7 (for 10000 Hz), and since each iteration makes use of the same factorization of $\boldsymbol{A}$ and therefore involves only an order of N^2 flops, the time consumed by the iterations is negligible in comparison with the time used for the factorization of $\boldsymbol{A}$, involving $2/3 \cdot N^3$ flops (for the 160 element model N=321).

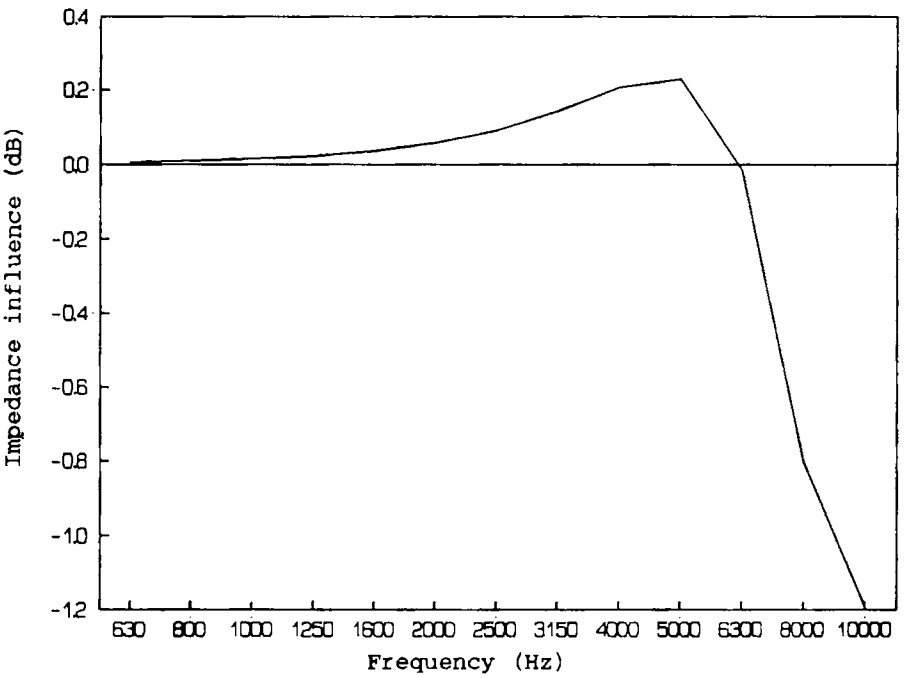

Figure 7-3. Influence of the finite impedance of the diaphragm of the B&K 4160. The curve is the ratio between the free-field corrections in dB obtained with the structural-acoustical model and with the rigid model.

The results of the model with a locally reacting impedance surface as described by equation (7.10) was then compared to the structural-acoustical model. The difference between these two models increases with the frequency as one would expect, because the difference between the pressure at the centre and at the edge of the diaphragm increases. However, the difference between these two models does not exceed 0.01 dB, and hence the 'impedance model' also gives reliable results in this range of frequencies.

The impedance model is therefore used to determine the free-field correction for various angles of incidence and for diffuse incidence. These results are found re-using the factorization of the coefficient matrix obtained by the impedance model, and hence involve the same level of numerical approximation as the results for the axial incidence case. Hence the accuracy of these results is expected to be as good as the accuracy for the standard axial incidence case. Figure 7-4 shows the free-field correction for the B&K 4160 for various angles of incidence and for diffuse incidence.

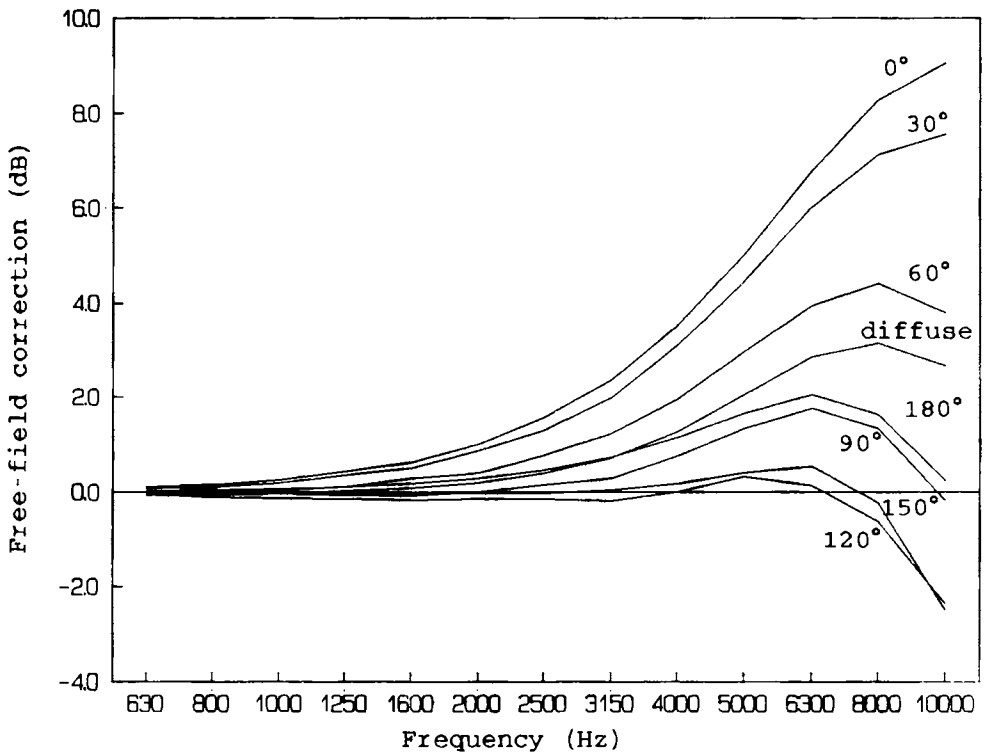

Figure 7-4. Free-field correction curves for the B&K 4160 for various angles of incidence and for diffuse incidence.

For the B&K 4180 similar calculations were carried out using an equivalent volume $V_{eq} = 9 \cdot 10^{-9}$ m^3, a loss factor d=1 and a resonance frequency f_0 = 21500 Hz in the model. Figure 7-5 shows the free-field correction calculated with the impedance model, the corresponding experimental data and the curve provided by Brüel and Kjær [12]. At low frequencies excellent agreement is obtained, but at 8000 Hz and above, the agreement between measurements and calculations is unexpectedly poor considering the experimental and computational accuracy. The reason for this is still unclear, but note that the difference between measurements and calculations is of opposite sign of the corresponding difference for the B&K 4160, see Figure 7-2. However, the calculated curve is between the measured curve and the curve provided by B&K. Figure 7-6 shows the free-field correction for various angles of incidence and for diffuse incidence.

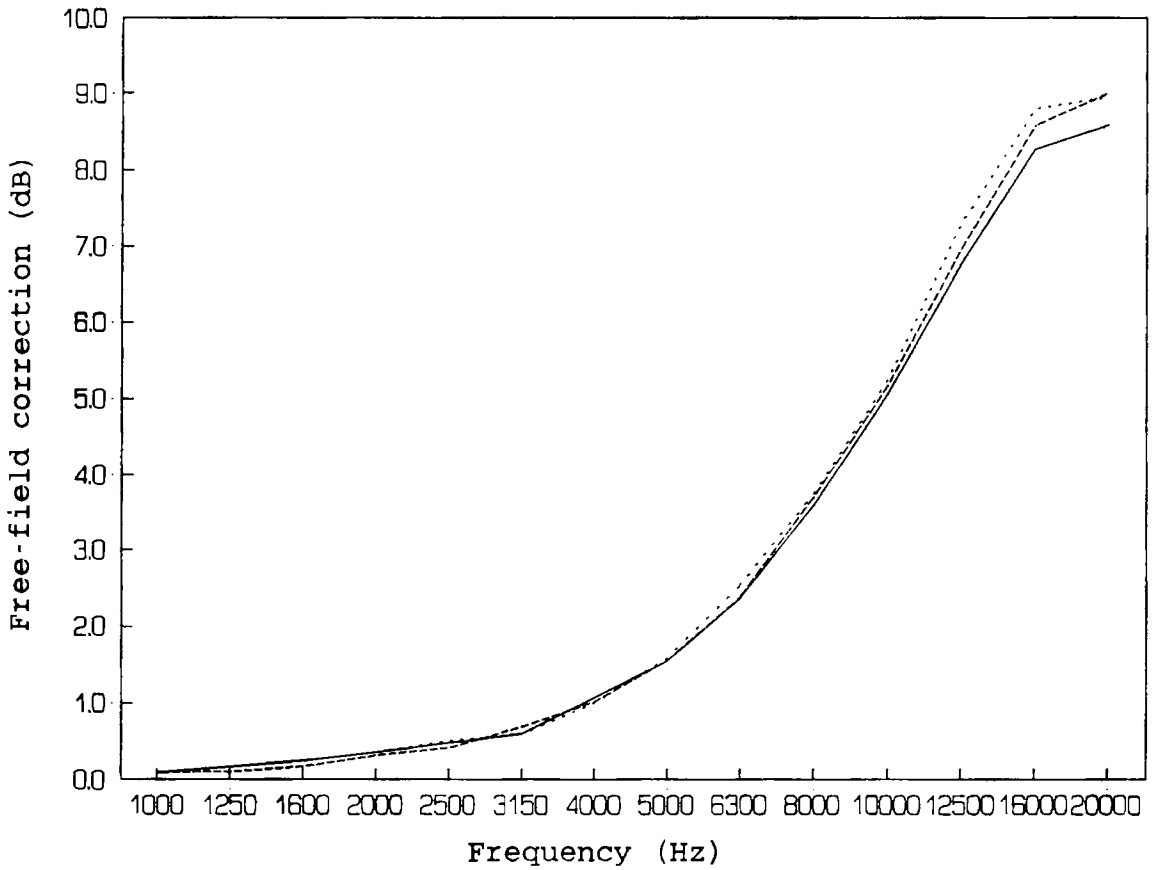

Figure 7-5. Free-field correction for the B&K 4180. ————, measured values; --------, calculated values; ·····, values provided by B&K.

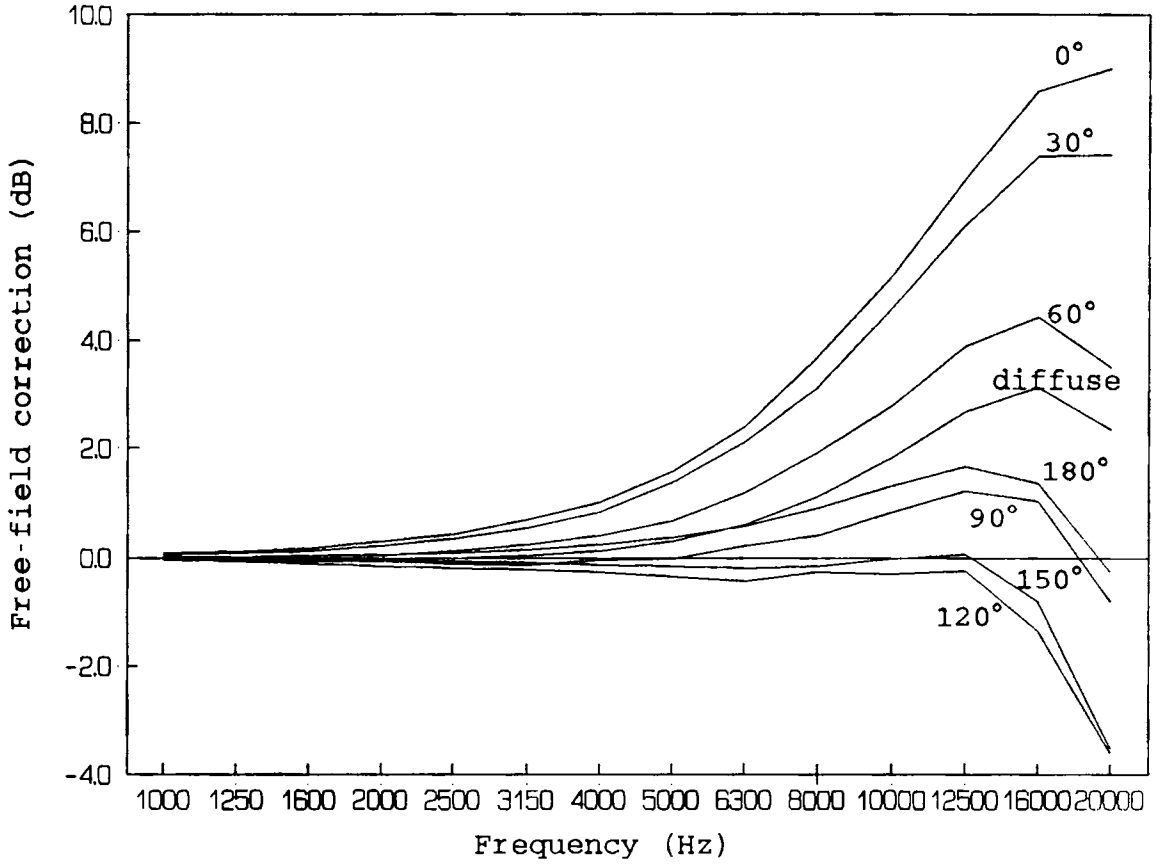

Figure 7-6. Free-field correction curves for the B&K 4180 for various angles of incidence and for diffuse incidence.

7.3.2 ACOUSTIC CENTRES

In the numerical model the acoustic centre was determined by assuming a parabolic movement of the diaphragm. Having calculated the resulting pressure on the surface of the microphone, the calculation point P was moved outside the body in order to calculate the on-axis pressure at various distances from the diaphragm. In the far-field the pressure follows the $1/r$-law, where r is the distance to the diaphragm minus the value of the acoustic centre, $r = d_{dia}-d_{ac}$. Note that the acoustic centre is defined to be positive outside the microphone. Hence the product of the magnitude of the calculated pressure and the effective distance r should remain constant in the far-field, and the estimate of the acoustic centre is adjusted until this condition is met. Figure 7-7 shows the calculated deviations from the 1/r-law on-axis for two fre-

quencies for the B&K 4160 microphone versus the distance to the diaphragm. The effect of altering the estimate of the acoustic centre by 0.5 mm is also shown, and the figure indicates an uncertainty of about 0.2 mm on the value of the acoustic centre.

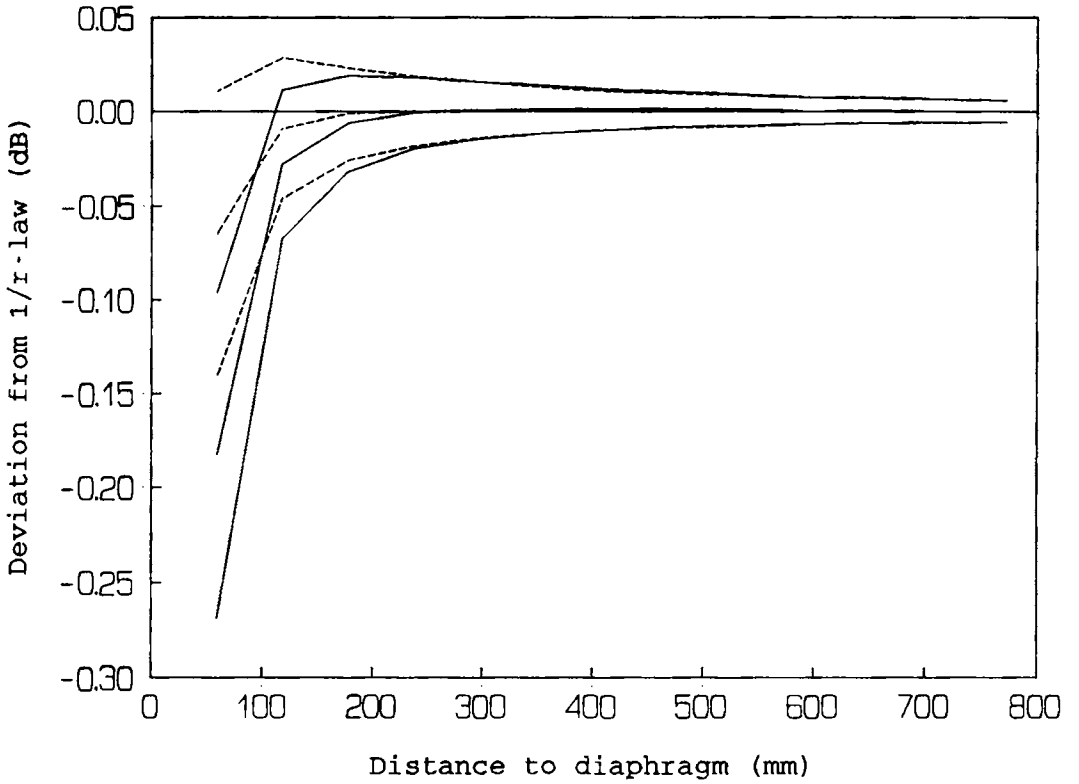

Figure 7-7. Calculated deviations from the 1/r-law for the B&K 4160. ————, 630 Hz; -------- 10000 Hz. The two central curves correspond to the final estimate of the acoustic centre. The two upper and the two lower curves correspond to alterations of ∓0.5 mm of the estimate of the acoustic centre.

Figure 7-7 suggests that at both frequencies the near-field extends to about 200 mm, and this is also the case for the frequencies in between. The extent of the near-field is important for the experimental set-up: The microphones should be placed in the far-field but as close as possible in order to maintain an acceptable signal-to-noise ratio at low frequencies.

Figure 7-8 shows the acoustic centres for the B&K 4160 microphone versus frequency. The calculated values are shown together with the measured value and the values stated in IEC publication 486 [45].

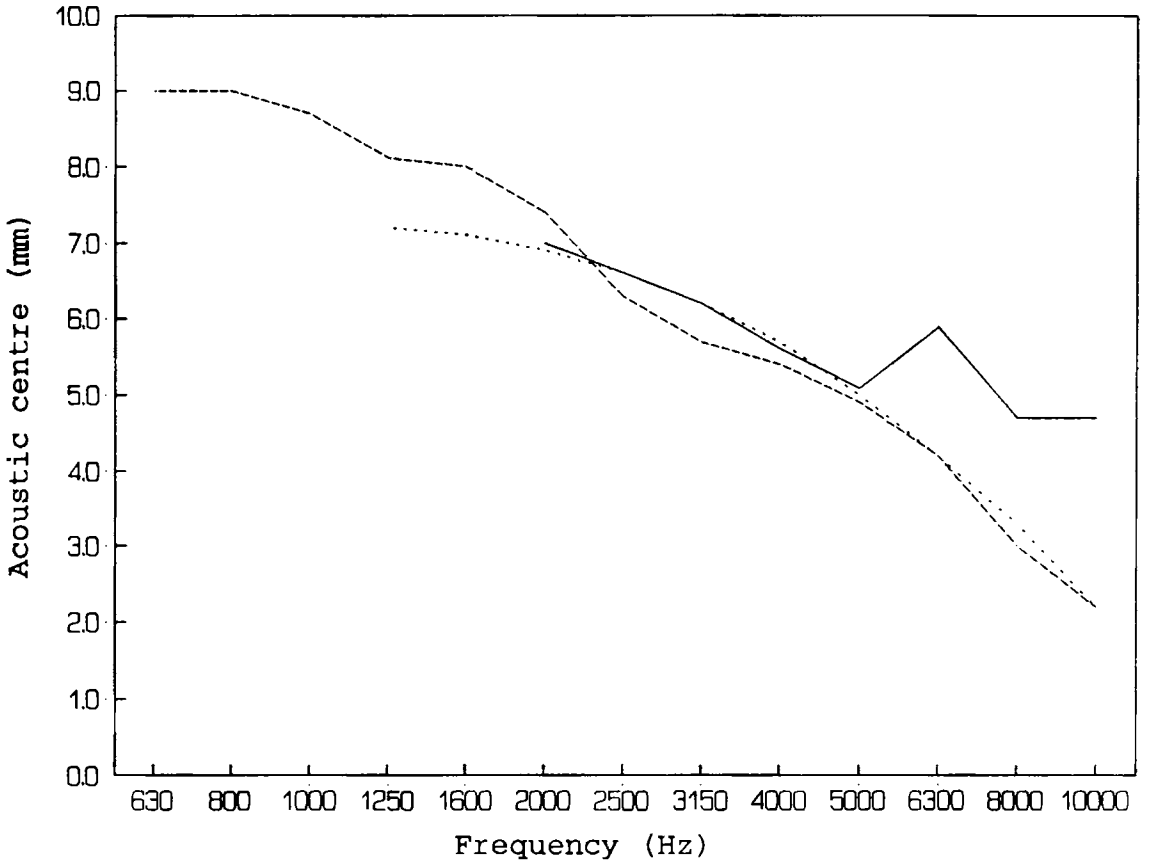

Figure 7-8. Acoustic centre for the B&K 4160. ————, measured; ..... , IEC 486; --------, calculated estimate.

Due to reflections from the end of the microphone model in the code, the calculated values oscillate around a smooth dependence of frequency. The figure shows a good agreement between the calculated and the measured values up to about 6300 Hz. The deviation from 6300 Hz and above is believed to be due to the assumption of parabolic movement of the diaphragm, which is probably not valid at high frequencies. However, the agreement with the values stated in IEC Publication 486 [45] is good.

In Figure 7-9 the calculated acoustic centres for the B&K 4180 are shown together with the measured data. Such values has not yet been published for the B&K 4180. The agreement between the calculated and measured values is acceptable at low frequencies when the experimental uncertainty is taken into account: a change of 1 mm in the position of the acoustic

centre will change the free-field sensitivity about 0.02 dB [71]. At high frequencies the agreement is unexpectedly poor. The reason for this is still unclear.

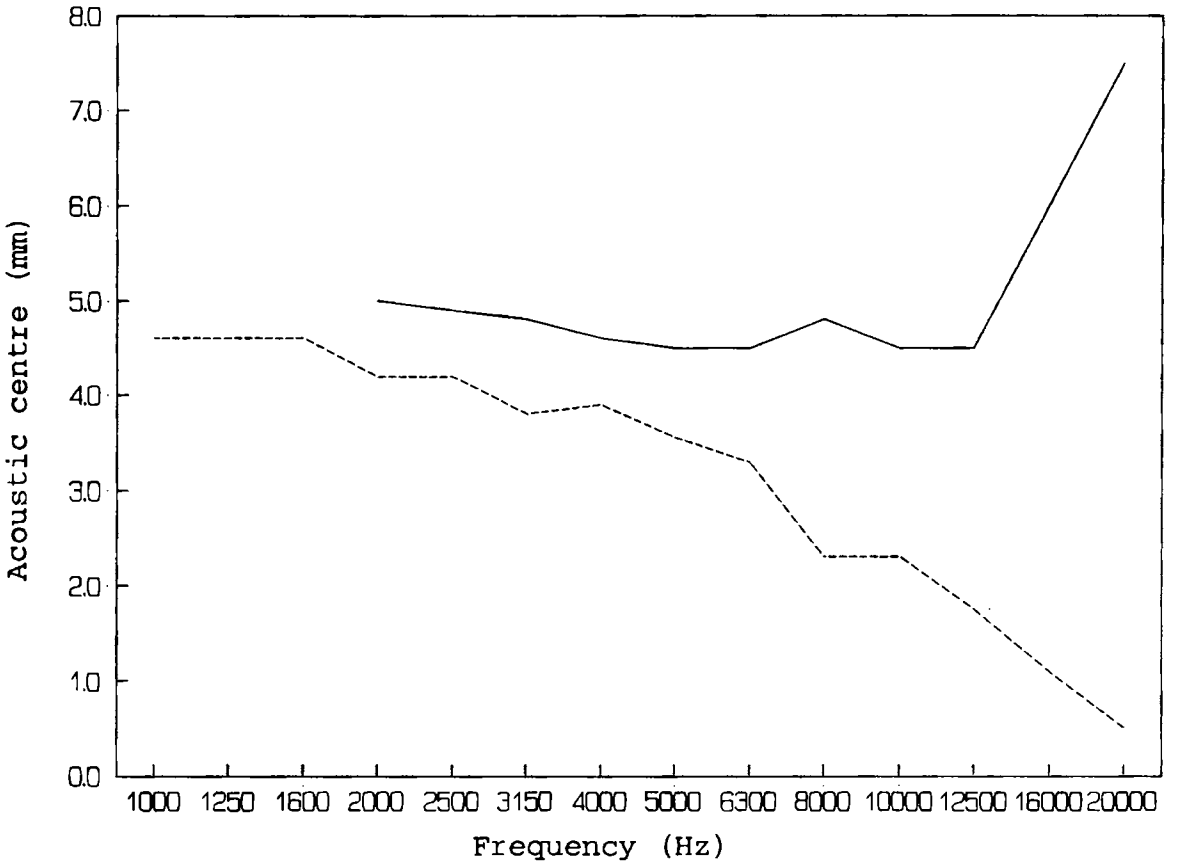

Figure 7-9. Acoustic centre for the B&K 4180.
————, measured; --------, calculated estimate.

7.4 DISCUSSION

The work presented here was motivated in two ways. From the viewpoint of microphone calibration laboratories the free-field correction and in particular the value of the acoustic centre at low frequencies are only known with poor accuracy, and from the viewpoint of boundary element scientists the boundary element formulation has not previously been tested against experimental data with the present degree of accuracy. In this way, it became possible to test a new iterative method of solving coupled structural-acoustical problems.

The approximations made with regard to the geometry and in particular with regard to the shape of diaphragm movement limit

the model to frequencies below the first resonance of the diaphragm. At these frequencies the calculated data are in excellent agreement with the measured data. A better knowledge of the diaphragm movement would be required for improving the results at higher frequencies. All frequencies considered in this study are below the undesirable 'characteristic frequencies' discussed in chapter 5, and hence no special care had to be taken of this phenomenon.

Structural-acoustical coupling is in particular of interest in problems where the coupling is strong, e.g. scattering and radiation by structures submerged in water [6]. Usually such calculations are accomplished by using finite element calculations for the structure and boundary element calculations for the fluid. Normally these calculations are carried out by combining the boundary element equations with the finite element matrix. Hence the elements of the finite element matrix corresponding to the nodes on the interacting surface are changed. However, this approach may give rise to some problems: The very large systems of equations of the finite element method may only be solved effectively if the coefficient matrices are bandlimited and symmetric, but unfortunately the equations from the boundary element method are unsymmetric and may increase the 'bandwidth' of the finite element matrices. Furthermore, it is often desirable to operate with different mesh-sizes for the structural model and for the boundary element model, since the wavelength normally differs in the two domains [67]. The iterative method described in this study may readily be used for different mesh-sizes as well as for different interpolation functions, whereas special care must be taken to handle such cases with the standard approach. Finally, for cases where the number of nodes of the interacting surface is small compared to the number of nodes in both the finite element and the boundary element models, the iterative method might be faster than the standard approach, since the factorization of the two matrices from the respective methods will be 'cheaper' in terms of flops than the factorization of the larger combined matrix, due to the N^3 behaviour of matrix

factorization. Note that when taking the bandlimited structure of the finite element matrix into account a more complex formula for the number of flops required arises, but the general trend of flops versus matrix size remains.

7.5 CONCLUDING REMARKS

In this chapter the free-field correction curve for standard condenser microphones has been calculated by means of the boundary element method. Due to approximations made in the modelling the microphones this investigation is limited to frequencies below the first resonance of the diaphragm. In this range of frequencies the calculated results agree excellently with measured data. The free-field correction curve for various angles of incidence and for diffuse incidence has been calculated as well. For calibration laboratories various secondary characteristics associated with the microphones are important. These quantities are extremely difficult to determine experimentally and the calculation of these may therefore prove to be valuable for calibration laboratories and microphone designers.

In order to achieve the desired high precision, the movement of the diaphragm had to be taken into account. Hence a coupled structural-acoustical problem was considered. In this study a new iterative method of solving coupled structural-acoustic problems has been presented. This method allows the coupled problem to be separated at the surface of interacting, so that the structural and the acoustic problem may be treated separately. The benefits of this method are its simplicity and its flexibility with respect to the handling of problems where different numerical methods, mesh-sizes and interpolation functions are used in the two domains. A paper describing this work has been accepted for publication [53].

8. APPLICATION OF THE BOUNDARY ELEMENT METHOD TO SPECTRAL STEREO THEORY

In a collaborative work with associate professor Karsten Bo Rasmussen the axisymmetric integral equation formulation was used to calculate the diffraction caused by a body with a shape that to some extent resembles the human head. The diffraction caused by the head of a listener is important for determining the relation between the loudspeaker signals in a spectral stereo setup. This work resulted in a paper, which has been published in Journal of the Audio Engineering Society [72]. In this chapter the work will be shortly motivated and the boundary element calculations will be presented. Finally, the conclusions of the joint work will be outlined. The paper in its full length is included as appendix A of this thesis.

8.1 MOTIVATION

Cooper and Bauck have established an elaborate model for the relationship between stereo loudspeaker signals and an equivalent phantom source [23-26]. They have developed mathematical expressions for the determination of loudspeaker signals, which should be able to produce any specified phantom source in the mind of the listener.

The approach is that when superimposed at the ears, loudspeaker signals should closely resemble a plane wave coming from a well defined horizontal direction - the so-called phantom direction. When this assumption is met, the loudspeaker signals will supposedly provide the listener with a clear and unambiguous sense of direction of the sound. Free field conditions are assumed in the sense that the listening room is not taken into account. This may be justified by means of the Haas effect or the law of the first wavefront [7] stating that the first part of the sound field is very important for localization.

Thus a plane wave represent the direction of the phantom source - the direction which should be simulated by the loudspeaker signals. Hence, the loudspeaker signals should be

adjusted so that the total sound field from both speakers at the ear positions of the artificial head is identical to the sound field due to a plane incoming wave from the phantom direction. In order to obtain the relation between the loudspeaker signals, which lead to any particular phantom direction, the diffraction caused by the listener must be taken into account.

Cooper and Bauck have treated the situation as ideal in the sense that room reflections have not been taken into account and that the head was regarded as being spherical. It is the latter assumption regarding the head shape that is investigated further in this study. Obviously the shape of a human head is not spherical, but this simple approximation becomes plausible when combined with ear locations shifted towards the back of the head rather than placed along a diameter. It is of importance to determine the validity of this simple approximation. Ultimately one could wish to make accurate calculations on a dummy head including the effect of the pinna and the torso, but doing this would still with modern computing be quite a time and storage consuming task. In order to be able to solve the problem on a normal PC the improved head shape has been chosen to be axisymmetric so that the axisymmetric integral equation formulation developed in chapter 3 may be used. This is obviously not yet an accurate model of the shape of the human head. However, it becomes possible to take into account the fact that the head is higher than it is wide (frontal view) without any loss of generality as far as the location of the ears is concerned. Since horizontal localisation is to be investigated, the generator of the axisymmetric shape is chosen to be a horizontal section of the Brüel & Kjær 4128 Head-And-Torso-Simulator (HATS) passing through the ear positions as sketched in Figure 8-1. The improved head shape was assumed to be rigid.

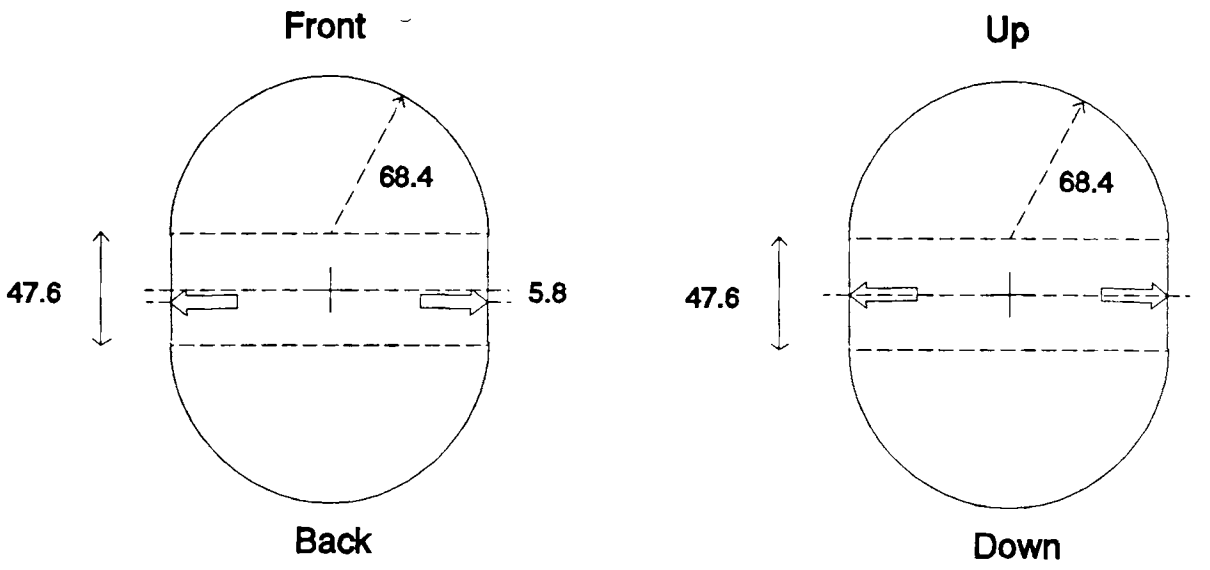

Figure 8-1. Cross sections through the centre of improved head model. The horizontal cross section is that of the Brüel & Kjær 4128 head-and-torso simulator passing through the ear positions. The positions of the ears are indicated by arrows. All measures are in millimetres. The model is symmetrical around horizontal axis through the centre.

8.2 CALCULATION OF THE DIFFRACTION CAUSED BY THE IMPROVED HEAD SHAPE.

Calculations were made using the axisymmetric integral equation formulation described in chapter 3. Isoparametric linear elements were used to discretize the generator of the improved head shape shown in Figure 8-1. Calculations were carried out in the frequency range 100Hz - 6400Hz. In the frequency range 100Hz - 2000Hz 37 elements were used to model the generator, whereas 75 elements were used in the frequency range 2000Hz- 6400Hz. For all frequencies it was found that four terms of the cosine expansion of equation (3.38) sufficed for an accurate calculation. Figure 8-2 shows the pressure at the left ear of the improved head shape relative to the pressure of thje undisturbed plane wave as a function of the frequency and the angle of incidence as defined in the inset in the figure.

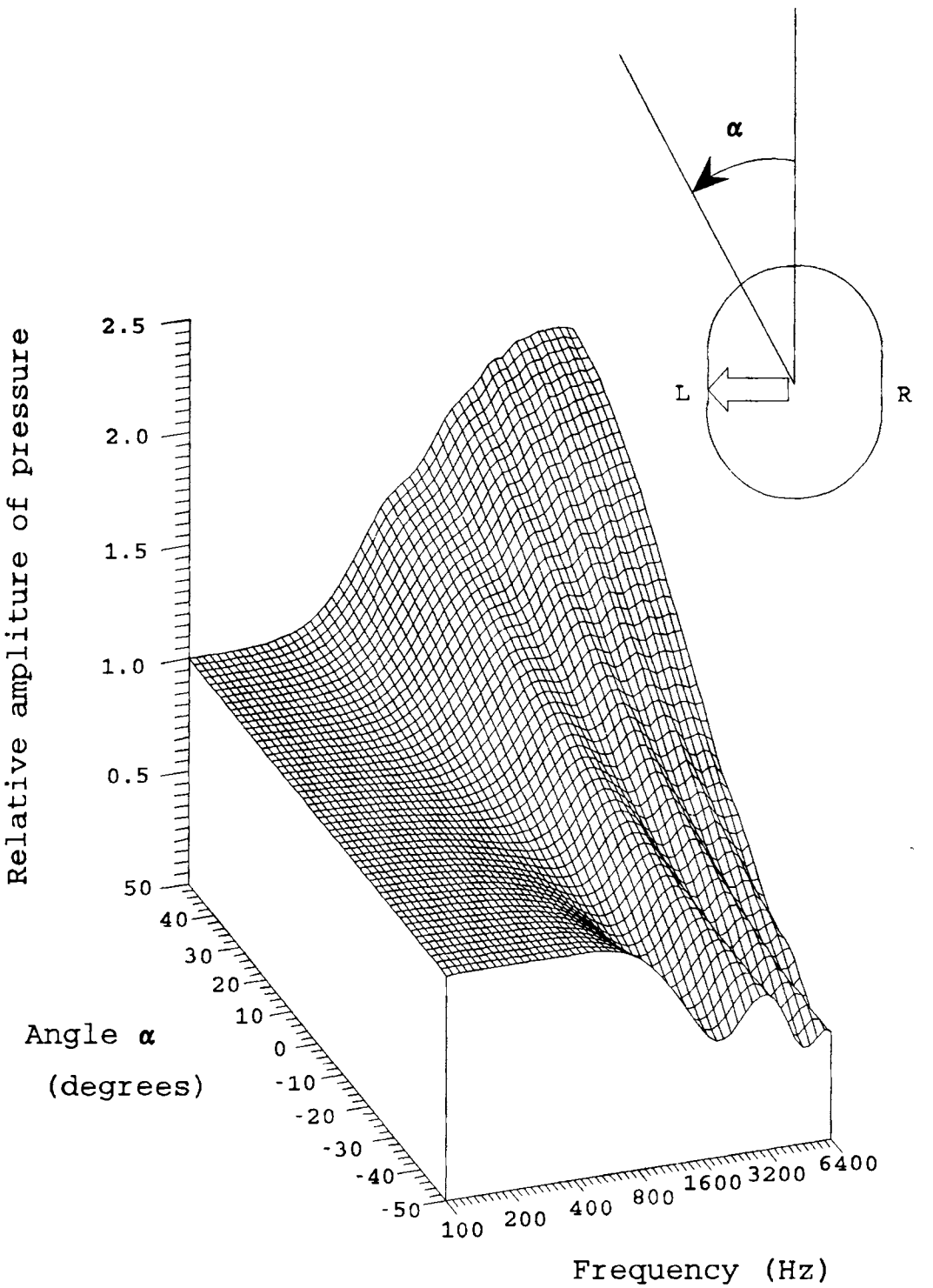

Figure 8-2. Relative magnitude of the pressure at the left ear of the improved head shape when scattering of a plane wave is considered. The relative magnitude of the pressure is shown as a function of the frequency and of the angle of incidence as defined in the small inset in the figure.

8.3 CONCLUDING REMARKS

In the paper included in appendix A the results obtained with the improved head shape were then compared to the results obtained with the original spherical head shape. It was found that since the angles of incidence used for an ideal stereo setup are close to frontal incidence e.g. $-30° < \alpha < 30°$, the spherical head shape assumption produces results of sufficient accuracy. However, it was found that the diameter of 175 mm of the equivalent sphere commonly used was too large, whereas a diameter of 137 mm appeared to be more appropriate.

9. DISCUSSION

The present study has mainly been discussed current with the development of the text in the partial conclusions. However, the author thinks that a few ideas for further work deserves to be emphasized in this chapter. Hence, in this chapter a few suggestions for further work will be given. Section 9.1 deals with the topic of convergence, which was introduced in section 4.6, and section 9.2 outlines some problems for which the QR factorization may advantagously be used.

9.1 DISCUSSION OF CONVERGENCE

The topic of convergence was introduced in section 4.6, and a few test cases were studied. However, the situation turned out to be far more complicated than it was the case with convergence of numerical integration formulas, as discussed in section 4.6. In the following some remarks to a further investigation of convergence of boudary elements formulations are given.

The error made by a boundary element formulation may be divided into two parts. The first part is the initial error, which is the error due to a given discretization, say, two elements per wavelength. If this initial error is altered it corresponds to a vertical displacement of the curves shown in figures 4-17, 4-19, 4-20, 4-21, and 4-24. The second part is associated with the convergence rate of the methods i.e. the rate by which the error decreases when the mesh is refined. This part corresponds to the slope of the curves mentioned above. The desirable behavior of a boundary element implementation is to possess both a small initial error and a high rate of convergence. In the study of numerical integration it was found that a high order formula generally produces both a smaller initial error and a higher rate of convergence than a low order formula. Although the situation is much less clear when studying the error made by boundary element formulations, this conclusion generally holds for the formulations considered in section 4.6 as well. In section 4.6 convergence was investi-

gated at a relatively low frequency, $ka=1$, where a was a typical dimension of the body. At higher frequencies the non-uniqueness problem must be taken into account when examining the convergence, since the error made by the boundary element model increases when there is a characteristic frequency in the neighbourhood of the frequency of interest. Although the accuracy of different methods to overcome the non-uniqueness problem has been adressed in the literature [42,84] no systematic investigation of the convergence of different formulations used to overcome the non-uniqueness problem discussed in chapter 5 has been reported. The author believes that a study of the convergence of the different boundary element formulations would be very valuable at this stage. Such a study should involve higher frequencies, as well as bodies of more complex shapes, such as thin bodies and bodies with sharp edges.

9.2 FURTHER APPLICATIONS OF THE QR FACTORIZATION

The QR factorization is a relatively unknown factorization method for scientists that are working outside the area of numerical linear algebra. Moreover, since the RRQR factorization is a very recent development of the standard QR factorizations, the knownledge of this factorization is even less widespread. However, the QR factorization is almost as efficient as the well-known LU factorization, more stable for solving large systems of equations [39], and more efficient in solving overdetermined systems of equations. Furthermore, the ease with which the QR factorization may be updated when a row or a column of the boundary element coefficient matrix is appended or deleted may be used advantagously in boundary element calculations, as will be described in paragraph 9.2.1. The rank revealing QR factorization may for some applications be used as an alternative to the singular value decomposition, as will be described in paragraph 9.2.2.

9.2.1 UPDATING THE QR FACTORIZATION

In the beginning of section 4.6 it was mentioned that elements of equal size would seldom be the optimal choice with

respect to accuracy *vs.* calculation time for practical boundary element calculations. It was stated that small elements should be used where the geometry or the acoustic variables vary quickly. However, since the variation of the unknown acoustic variable is not known initially, the optimale sizing of the elements is rarely known in advance. In this connexion the ability of the QR factorization to be updated may prove valuable.

Consider for simplicity a constant element implementation of a boundary element formulation. Now, if a given problem has been calculated using a coarse discretization it might be required to refine the mesh locally, where a quick variation of e.g. the pressure is observed. In the boundary element coefficient matrix the refinement of an element corresponds to deleting the row and the column which correspond to that element, and then adding a number of rows and columns corresponding to the new elements. If the number of elements that are refined is small compared to the total number of elements, an updating of the QR factorization may advantagously be carried out instead of calculating a new factorization from scratch. Note that the same technique may be used if the position of a small number of elements is altered, which is the case when making slight changes to the geometry. Slight changes to the geometry is often made in a design process. For higher order elements the general idea is the same - although an element corresponds to several rows and columns in the coefficient matrix in this case.

Updating the QR factorization may also be advantagous when new equations are added to the orginal system of equations by the CHIEF method or a related approach as mentioned in the end of section 6.3.

9.2.2 USING THE RANK REVEALING QR FACTORIZATION AS AN ALTERNATIVE TO THE SINGULAR VALUE DECOMPOSITION

In a recent paper by Bai [3], the singular value decomposition was used to find the eigenfrequencies and eigenmodes of an enclosure. It was demonstrated that an eigenfrequency could be

detected by examining the smallest singular value, which becomes small near an eigenfrequency. For the case of multiple eigenfrequencies a number of singular values corresponding to the multiplicity of the eigenfrequency become small. The corresponding singular vectors contains the eigenmode(s) corresponding to the eigenfrequency [3]. In this case the RRQR factorization could provide the same information as the singular value decomposition much cheaper in terms of computational time. Since the boundary element method operates in the frequency domain the eigenfrequencies was found by generating the boundary element coefficient matrix in a frequency range using a coarse resolution [3]. The estimate of an eigenfrequency was then improved by a so-called golden search algorithm [3]. Recently a frequency interpolation technique has been described [6,90], by which the sound field within an enclosure was obtained approximately in a range of frequencies by means of an interpolation scheme using a small number of key frequenicies, and very recently Wu *et al.* [110] has proposed a so-called 'Green's function interpolation technique' for speeding-up multi-frequency run. These interpolation schemes might advantagously be used instead of the much more time consuming initial frequency sweep used by Bai [3].

10. CONCLUSIONS

In this study a boundary element method based on Helmholtz integral equation has been considered. During the work computer programs have been developed for calculating the sound field exterior to bodies of axisymmetric or general three-dimensional shape, positioned in free space. The study involved the following partial accomplishments.

In chapter 2 some fundamental concepts were presented. Helmholtz integral equation was derived mathematically, and a more intuitive physical explanation was given following that of Baker and Copson [4].

In chapter 3 an axisymmetric integral equation formulation for non-axisymmetric boundary conditions was developed. Non-axisymmetric boundary conditions were handled by expanding the sound field in a circumferential cosine series. In relation to the existing literature [2,82] this work presents a novel way of handling the singularities in the resulting integrals of the expansion by means of elliptic integrals, as suggested for the fully axisymmetric case in reference [82]. However, as this work was submitted for publication [51] it turned out that similar work had been carried out simultaneously by other researchers [55,93].

Chapter 4 concerns the numerical implementation of the boundary element formulations. The benefit of using high order shape functions adopted from the finite element method by Seybert and his co-workers, was intuitively justified by observing the convergence of various numerical integration formulas. A brief investigation of the convergence properties of three implementations of the axisymmetric integral equation formulation, using different shape functions, was then carried out. For the case of scattering by a rigid cylinder it was shown that a new generalized quarter-point technique could improve the accuracy. In this chapter a superparametric implementation of both the axisymmetric and the three-dimensional formulations was proposed. Superparametric elements has not previously been used for acoustic boundary element calculations, as far as the author knows.

Chapter 5 concerns the non-uniqueness problem. The term non-uniqueness problem refers to the fact that the surface Helmholtz integral equation is unable to obtain a unique solution at certain characteristic frequencies. One of the methods - the Combined Helmholtz Integral Equation Formulation (CHIEF) - proposed in the literature for partially circumventing the non-uniqueness problem was studied in detail, and a short survey of other methods proposed in the literature was given. Furthermore, this chapter contains a new explanation of the non-uniqueness problem by means of an analogy to active sound control.

Chapter 6 addresses the problem of solving a set of linear equations. It was demonstrated that the non-uniqueness problem appears as a numerical rank deficiency of the boundary element coefficient matrix. In chapter 6 the use of rank revealing factorizations of the boundary element coefficient matrix, with the CHIEF method or related methods, was then proposed. The combination of the CHIEF method and a rank revealing factorization efficiently ensures a unique solution at characteristic frequencies. The use of rank revealing factorizations in this connexion has not previously been reported, as far as the author knows. For the solution of the system of equations produced by the boundary element method, the author highly recommends the QR factorization, as described in section 6.3. This is due to the rank revealing properties of the RRQR factorization, the efficiency and stability of this factorization when solving overdetermined systems of equations, and the ability of this factorization to be updated efficiently, which is of great importance when adding CHIEF points or making slight changes to the geometry, as discussed in chapter 9.

In chapter 7 the boundary element method was used to calculate the pressure sensitivity correction curves for two standard microphones. The boundary element calculations were tested against very accurate experimental results, allowing the axisymmetric formulation to be verified for more complicated shapes than the sphere extensively used throughout the study.

In this chapter the coupled structural-acoustic problem of the diaphragm of the microphone and the surrounding air was solved by means of an iterative process. Even though this iterative process is straightforward and therefore supposedly has been used by other researchers the author is not aware of any description of this approach in the literature.

Chapter 8 describes a final application of the axisymmetric formulation to spectral stereo theory, where the assumption of spherical head shape was tested against a more realistic head shape. It appeared that the common assumption of spherical head shape is reasonable for angles of incidence close to frontal incidence, but that a smaller diameter of the sphere than usually used, should be preferred.

Finally, chapter 9 contains a discussion of the work with some suggestions for further work.

REFERENCES

The references are listed alphabetically. A recent list of State-of-the-Art references has recently been given in

Boundary Element Methods in Acoustics (R.D. Ciskowski and C.A. Brebbia, editors). Appendix State-of-the-Art References in Boundary Element Applications to Acoustics. Computational Mechanics Publications Co-published with Elsevier Applied Science.

1. ABRAMOWITZ M., and STEGUN I.A. 1965
Handbook of Mathematical Functions. National Bureau of Standards.

2. AKYOL T.P. 1986
Acustica 61, 200-212. Schallabstrahlung von Rotationskörpern. (In German).

3. BAI M.R. 1992
Journal of the Acoustical Society of America 91, 2529-2538. Study of acoustic resonance in enclosures using eigenanalysis based on boundary element methods.

4. BAKER B.B. and COPSON E.T. 1953
The Mathematical Theory of Huygens' Principle. Second Edition Oxford University Press.

5. BANAUGH R.P., and GOLDSMITH W. 1963
Journal of the Acoustical Society of America 35, 1590-1601. Diffraction of Steady Acoustic waves by Surfaces of Arbitrary shape.

6. BENTHIEN G.W. and SCHENCK H.A. 1991
in *Boundary Element Methods in Acoustics* (R.D. Ciskowski and C.A. Brebbia, editors). Chapter 6. Structural-Acoustic Coupling. Computational Mechanics Publications Co-published with Elsevier Applied Science.

7. BLAUERT J. 1983
Spartial Hearing. M.I.T.Press, Cambridge, Mass.

8. BREBBIA C.A., TELLES J.C.F., and WROBEL L.C. 1984
Boundary Element techniques. New York: Springer.

9. BREBBIA C.A., and WALKER S. 1980
Boundary Element techniques in engineering. Newnes - Butterworths London.

10. BROD K. 1984
Journal of the Acoustical Society of America 76, 1238-1243. On the uniqueness of solution for all wavenumbers in acoustic radiation.

11. BRÜEL P.V. and RASMUSSEN G. 1959
Brüel & Kjær, Technical Review no.2. Free-field responce of condenser microphones (Part II).

12. BRÜEL & KJÆR 1986
Instruction Manual. Condenser Microphones One-Inch Type 4160 and Half-Inch Type 4180

13. BURTON A.J., and MILLER G.F. 1971
Proceedings of the Royal Society of London A323, 201-210. The application of integral equation methods to the numerical solutions of some exterior boundary value problems.

14. BUSK T. 1977
Polyteknisk forlag/Special-Trykkeriet a-s Viborg. Numerisk integration (Numerical Integration). (In Danish).

15. BYRD P.F., and FRIEDMAN M.D. 1971
Handbook of Elliptic Integrals for Engineers and Scientists. New York: Springer.

16. CHAN T.F. 1987
Linear Algebra and its Applications 88/89, 67-82. Rank revealing QR factorizations.

17. CHEN L.H., and SCHWEIKERT 1963
Journal of the Acoustical Society of America 35, 1626-1632. Sound radiation from an Arbitrary Body.

18. CHENG C.Y.R., SEYBERT A.F. 1987
SAE 1987 Noise and Vibration Conference. Recent applications of the Boundary Element Method to Problems in Acoustics.

19. CHENG C.Y.R., SEYBERT A.F., and WU T.W. 1991
Journal of Sound and Vibration 151, 119-129. A multi domain boundary element solution for silencer and muffler performance prediction.

20. CHERTOCK G., 1964
Journal of the Acoustical Society of America 36, 1305-1313. Sound Radiation from Vibrating Surfaces.

21. CHERTOCK G., 1969
Journal of the Acoustical Society of America 47, 387-388. Solutions for Sound-Radiation Problems by Integral Equations at the Critical Wavenumbers.

22. CHIEN C.C., RAJIYAH H., and ATLURI S.N. 1990
Journal of the Acoustical Society of America **88**, 918-937. An effective method for solving the hypersingular integral equations in 3-D acoustics.

23. COOPER D.H. 1982
Journal Audio Engineering Society **30**, 34-38. Calculator program for Head-Related Transfer Function.

24. COOPER D.H. 1983
Journal Audio Engineering Society **31**, 760. Phase Reference in HRTF calculation.

25. COOPER D.H. 1987
Journal Audio Engineering Society **35**, 629-642. Problems with Shadowless Stereo Theory.

26. COOPER D.H., and BAUCK J.L. 1987
Journal Audio Engineering Society **37**, 3-19. Prospects for Transaural Recording.

27. COPLEY L.G. 1967
Journal of the Acoustical Society of America **41**, 807-816. Integral Equation Method for Radiation from Vibrating Bodies.

28. COPLEY L.G. 1968
Journal of the Acoustical Society of America **44**, 28-32. Fundamental results concerning integral representations in acoustic radiation.

29. CRISTESCU M., and LOUBIGNAC G. 1978
in *Recent Advances in Boundary Element Methods* (C.A. Brebbia, editor). Gaussian Quadrature Formulas for Functions with Singularities in 1/R over Triangles and Quadrangles. Pentech Press, London.

30. CUNEFARE K.A., KOOPMANN G.,and BROD K. 1989
Journal of the Acoustical Society of America **85**, 39-48. A boundary element method for acoustic radiation valid for all wavenumbers.

31. CUNEFARE K.A., KOOPMANN G.H. 1992
Journal of Vibration and Acoustics - Transactions of the ASME **114**, 178-186. Acoustic Design Sensitivity for Structural Radiators.

32. DANKERT J. 1977
Numerische Methoden der Mechanik 202-206. Springer-Verlag Wien New York. (In German)

33. DONGARRA J.J. *et al.* 1979
LINPACK User's Guide Philadelphia: Society for Industrial and Applied Mathematics.

34. DOKUMACI E. 1990
Journal of Sound and Vibration **139**, 83-97. A study of the failure of numerical solutions in boundary element analysis of acoustic radiation problems.

35. ENGBLOM J.J., and NELSON R.B. 1975
Journal of Applied Mechanics - Transactions of the ASME, ASME paper no. 75-AMPW-54, 295-300. Consistent Formulation of Sound Radiation From Arbitrary Structure.

36. FRANCIS D.T.I. 1991
Journal of Sound and Vibration **145**, 495-498. Partial use of the Helmholtz Gradient Formulation to obtain unique solutions to acoustic radiation problems at characteristic frequencies.

37. FRANCIS D.T.I 1993
Journal of the Acoustical Society of America **93**, 1700-1709. A gradient formulation of the Helmholtz integral equation for acoustic radiation and scattering.

38. FYFE K.R., and ISMAIL F. 1989
Journal of Sound and Vibration **128**, 361-376. An investigation of the acoustic properties of vibrating finite cylinders.

39. GOLUB G.H.,and VAN LOAN C.F. 1989
Matrix Computations, 92-104. The John Hopkins University Press, 2nd Edition.

40. GRADSHTEYN I.S., and RYZHIK I.M. 1965
Table of Integrals, Series, and Products. New York and London: Academic Press.

41. HAHN S.R., FERRI A.A., and GINSBERG J.H. 1991
in *Structural Acoustics* (R.F.KELTIE, A.F.SEYBERT, D.S.KANG, L.OLSON and P.PINSKY, editors), NCA-Vol.12/AMD-Vol.128, ASME, New York, 223-234. A review and evaluation of methods to alleviate non-uniqueness in the surface Helmholtz integral equation.

42. HALL W.S., and ROBERTSON W.H. 1988
Journal of Sound and Vibration **126**, 367-368. Standard Helmholtz integral equation calculations near characteristic frequencies.

43. HWANG J.-Y., and CHANG S.-C. 1991
Journal of the Acoustical Society of America **90**, 1167-1180. A retracted boundary integral equation for exterior acoustic problem with unique solution for all wavenumbers.

44. HENWOOD D.J. 1993
Journal Audio Engineering Society **41**, 485-496. The Boundary-Element Method and Horn Design.

45. IEC PUBLICATION 486 1974
Precision method for free-field of one-inch standard condenser microphones by the reciprocity technique.

46. IEC PUBLICATION 1094-3: WG-draft 1992
Measurement microphones, Part 2: Primary method for free-field calibration of laboratory standard microphones by the reciprocity technique.

47. JEANS R, and MATHEWS I.C. 1992
Journal of the Acoustical Society of America **92**, 1156-1166. The wave superposition method as a robust technique for computing acoustic fields.

48. JONES D.S. 1974
Quarterly Journal of Mechanics and Applied Mathematics 27, 129-142. Integral Equations for the exterior acoustic problem.

49. JUHL P.M. 1991
Report no. 47, The Acoustics Laboratory, Technical University of Denmark. Axisymmetric integral formulation for non-axisymmetric boundary conditions.

50. JUHL P.M. 1992
Proceedings. Second International Congress on Recent Developments in Air. and Structure-Borne Sound and Vibration 965-972. On selecting CHIEF to overcome the nonuniqueness problem in boundary element methods.

51. JUHL P.M. 1993
Journal of Sound and Vibration **163**, 397-406. An axisymmetric integral equation formulation for free space non-axisymmetric radiation and scattering of a known incident wave.

52. JUHL P.M. 1994(?)
To appear in Journal of Sound and Vibration. A numerical study of the coefficient matrix of the boundary element method near characteristic frequencies.

53. JUHL P.M. 1994(?)
To appear in Journal of Sound and Vibration. A numerical investigation of standard condenser microphones.

54. KAWAI Y., and TERAI T. 1990
Applied Acoustics. The Application of Integral Equation Methods to the Calculation of Sound Attenuation by Barriers.

55. KIM H.S., KIM J.S., and KANG H.J. 1993
Journal of Sound and Vibration **163**, 385-396. Acoustic wave scattering from axisymmetric bodies.

56. KLEINMANN R.E., ROACH G.F., SCHUETZ L.S., and SHIRRON J. 1988
Journal of the Acoustical Society of America **84**, 385-391. An iterative solution to acoustic scattering by rigid objects.

57. KOOPMANN G.H., SONG L., and FAHNLINE J.B. 1989
Journal of the Acoustical Society of America **86**, 2433-2438. A method for computing acoustic fields based on the principle of wave superposition.

58. LAMB H. 1932
hydrodynamics Sixth Edition. New York
Dover Publications 1945.

59. MALBÉQUI P., CANDEL S.M., and RIGNOT E. 1987
Journal of the Acoustical Society of America **82**, 1771-1781. Boundary integral calculations of scattered fields: Application to a spacecraft launcher.

60. MARTINEZ R. 1991
Journal of the Acoustical Society of America **90**, 2728-2738. The thin-shape breakdown (TSB) of the Helmholtz integral equation.

61. MATHEWS I.C. 1986
Journal of the Acoustical Society of America **79**, 1317-1325. Numerical techniques for three-dimensional steady-state fluid-structure interaction.

62. MEYER W.L., BELL W.A., ZINN B.T., and STALLYBRASS M.P. 1978
Journal of Sound and Vibration 59, 245-262. Boundary integral solutions of three dimensional acoustic radiation problems.

63. MEYER W.L., BELL W.A., STALLYBRASS M.P., and ZINN B.T. 1979
Journal of the Acoustical Society of America **65**, 631-638. Prediction of the sound field radiated from axisymmetric surfaces.

64. MORSE P.M. 1948
Vibration and Sound. McGraw-Hill; (second edition).

65. MORSE P.M., and INGARD K.U. 1986
Theoretical Acoustics. New York: McGraw-Hill.

66. OCHMANN M. 1990
Acustica 72, 233-246. Die Multipolstrahlersynthese - ein effektives Verfahren zur Berechnung der Schallabstrahlung von schwingenden Strukturen beliebiger Oberflächengestalt. (In German)

67. OCHMANN M., and WELLNER F. 1991
Acustica 73, 177-190. Berechnung der Schallabstrahlung dreidimensionaler schwingender Körper mit Hilfe eines Ranselemente-Mehrgitterverfahrens. (In German)

68. PIASZCZYK C.M., and KLOSNER J.M. 1984
Journal of the Acoustical Society of America 75, 363-375. Acoustic radiation from vibrating surfaces at characteristic frequencies.

69. PIERCE A.D. 1981
Acoustics: An Introduction to its Physical Principles and Applications McGraw-Hill Book Company.

70. PRESS W.H., FLANNERY B.P., TEUKOLSKY S.A., and VETTERLING W.T. 1986
Numerical Recipes. Cambridge University Press.

71. RASMUSSEN K., and OLSEN E.S. 1992
Report PL-07, The Acoustics Laboratory, Technical University of Denmark. Intercomparison on free-field calibration of microphones, Draft.

72. RASMUSSEN K.B., and JUHL P.M. 1993
Journal Audio Engineering Society 41, 135-142. The Effect of Head Shape on Spectral Stereo Theory.

73. REUT Z. 1985
Journal of Sound and Vibration 103, 297-298. On the boundary integral methods for the exterior acoustic problem.

74. REUT Z. 1989
Journal of Sound and Vibration 132, 523-524. Numerical solution of acoustic problems by integral equations.

75. RIZZO F.J., and SHIPPY D.J. 1977
International Journal for Numerical Methods in Engineering 11, 1753-1768. An advanced boundary integral equation method for three-dimensional thermoelasticity.

76. ROGERS P.H. 1973
Journal of the Acoustical Society of America 54, 1662-1666. Formal solution of the Helmholtz integral equation at a nondegenerate characteristic frequency.

77. RUBAK P. 1967
MSc. Thesis, The Acoustics Laboratory, Technical University of Denmark. A theoretical and an experimental determination of the difference between the pressure sensitivity and the free-field sensitivity of 1 in condenser microphones. (In Danish.)

78. SCHENCK H.A. 1968
Journal of the Acoustical Society of America **44**, 41-58. Improved integral formulation for acoustic radiation problems.

79. SEGALMAN D.J., and LOBITZ D.W. 1992
Journal of the Acoustical Society of America **91**, 1855-1861. A method to overcome computational difficulties in the exterior acoustics problem.

80. SEYBERT A.F. 1985
Proceedings. Noise-Con 85. A review of the boundary element method in acoustics.

81. SEYBERT A.F., SOENARKO B., RIZZO F.J., and SHIPPY D.J. 1985
Journal of the Acoustical Society of America **77**, 362-368. An advanced computational method for radiation and scattering of acoustic waves in three dimensions.

82. SEYBERT A.F., SOENARKO B., RIZZO F.J., and SHIPPY D.J. 1986
Journal of the Acoustical Society of America **80**, 1241-1247. A special integral equation formulation for acoustic radiation and scattering for axisymmetric bodies and boundary conditions.

83. SEYBERT A.F., and RENGARAJAN T.K. 1987
Journal of the Acoustical Society of America **81**, 1299-1306. The use of CHIEF to obtain unique solutions for acoustic radiation using boundary integral equations.

84. SEYBERT A.F. 1987
Journal of Sound and Vibration **115**, 171-172. A note on methods for circumventing non-uniqueness when using integral equations.

85. SEYBERT A.F., and CASEY D.K. 1988
Journal of the Acoustical Society of America **84**, 379-384. An integral equation method for coupled fluid/fluid scattering in three dimensions.

86. SEYBERT A.F., WU T.W., and WU X.F. 1988
Journal of the Acoustical Society of America **84**, 1906-1912. Radiation and scattering of acoustic waves from elastic solids and shells using the boundary element method.

87. SEYBERT A.F., and WU T.W. 1989
Journal of the Acoustical Society of America 85, 19-23. Modified Helmholtz integral equation for bodies sitting on an infinite plane.

88. SEYBERT A.F., CHENG C.Y.R, and WU T.W. 1990
Journal of the Acoustical Society of America 88, 1612-1618. The solution of coupled interior / exterior acoustics problems using the boundary element method.

89. SEYBERT A.F., and WU T.W. 1991
in *Boundary Element Methods in Acoustics* (R.D. Ciskowski and C.A. Brebbia, editors). Chapter 3. Acoustic Radiation and Scattering. Computational Mechanics Publications Co-published with Elsevier Applied Science.

90. SEYBERT A.F., and WU T.W. 1991
in *Boundary Element Methods in Acoustics* (R.D. Ciskowski and C.A. Brebbia, editors). Chapter 9. Applications in Industrial Noise Control. Computational Mechanics Publications Co-published with Elsevier Applied Science.

91. SHAW R.P., and HUANG S.-C. 1989
Journal of the Acoustical Society of America 88, 839-842. The fictitious eigenvalue difficulty in the *T*-matrix and the BEM methods for exterior wave scattering.

92. SHAW R.P. 1991
in *Boundary Element Methods in Acoustics* (R.D. Ciskowski and C.A. Brebbia, editors). Chapter 1. A Brief History of "Boundary Integral Equation/Element Methods" in Acoustics. Computational Mechanics Publications Co-published with Elsevier Applied Science.

93. SOENARKO B. 1993
Journal of the Acoustical Society of America 93, 631-639. A boundary element formulation for radiation of acoustic waves from axisymmetric bodies with arbitrary boundary conditions.

94. SONG L., KOOPMANN G.H., and FAHNLINE J.B. 1991
Journal of the Acoustical Society of America 89, 2625-2633. Numerical errors associated with the method of superposition for computing acoustic fields.

95. SPIEGEL M.R. 1968
Mathematical Handbook, 17. New York: McGraw-Hill.

96. STROUD A.H., and SECREST D. 1960
Gaussian Quadrature Formulas Prentice-Hall.

97. TERAI T. 1980
Journal of Sound and Vibration 69, 71-100. On calculation of sound fields around three dimensional objects by integral equation methods.

98. TOBOCMANN W. 1984
Journal of the Acoustical Society of America 76, 599-607. Calculation of acoustic wave scattering by means of the Helmholtz integral equation. I.

99. TOBOCMANN W. 1984
Journal of the Acoustical Society of America 76, 1549-1554. Calculation of acoustic wave scattering by means of the Helmholtz integral equation. II.

100. TOBOCMANN W. 1986
Journal of the Acoustical Society of America 80, 1828-1837. Extension of the Helmholtz integral equation method to shorter wavelengths.

101. TOBOCMANN W. 1987
Journal of the Acoustical Society of America 82, 704-706. Extension of the Helmholtz integral equation method to shorter wavelengths. II.

102. TOYODA I., MATSUHARA M., and KUMAGAI N. 1988
IEEE Transactions on Antennas and Propagation 36, 1580-1586. Extended Integral Equation Formulation for Scattering from a Cylindrical Scatterer.

103. URSELL F. 1973
Proceedings of the Cambridge Philosophical Society 74, 117-125. On the exterior problem of acoustics.

104. WATERMAN P.C. 1969
Journal of the Acoustical Society of America 45, 1417-1429. New formulation of acoustic scattering.

105. WU S.F. 1993
Journal of the Acoustical Society of America 93, 683-695. Nonuniqueness of solutions to extended Kirchhoff integral formulations.

106. WU T.W., SEYBERT A.F., and WAN G.C. 1991
Journal of the Acoustical Society of America 90, 554-560. On the numerical implementation of a Cauchy principal value integral to insure a unique solution for acoustic radiation and scattering.

107. WU T.W., and SEYBERT A.F. 1991
Journal of the Acoustical Society of America 90, 1608-1614. A weighted residual formulation for the CHIEF method in acoustics.

108. WU T.W., and WAN G.C. 1992
Journal of the Acoustical Society of America 92, 2900-2906. Numerical modelling of acoustic radition and scattering from thin bodies using a Cauchy principal integral equation.

109. WU T.W., and WAN G.C. 1992
Proceedings. Second International Congress on Recent Developments in Air. and Structure-Borne Sound and Vibration 993-999. Isoparametric boundary element modeling of acoustical cracks.

110. WU T.W., LI W.L., and SEYBERT A.F. 1993
Journal of the Acoustical Society of America **94**, 447-452. An efficient boundary element algorithm for multi-frequency acoustical analysis.

111. WU X.-F., and PIERCE A.D. 1990
Journal of Vibration and Acoustics - Transactions of the ASME **112**, 263-267. Uniqueness of Solutions to Variationally Formulated Acoustic Radiation Problems.

112. ZIENKIEWICZ O.C. 1979
The finite element Method Third Edition. McGraw-Hill Book Company (UK) Limited.

APPENDIX A

The Effect of Head Shape on Spectral Stereo Theory*

KARSTEN BO RASMUSSEN, *AES Member*, AND PETER MØLLER JUHL

Acoustics Laboratory, Technical University of Denmark, DK-2800 Lyngby, Denmark

The spectral stereo theory, which was developed by Cooper and Bauck in order to determine the theoretical relationship between stereo loudspeaker signals and localization, makes use of a spherical head model. In the present work the theory is combined with calculations for a more realistic head shape. The diffraction effect of the head is determined from boundary-element calculations.

0 INTRODUCTION

Cooper and Bauck have worked out an elaborate model for the relationship between stereo loudspeaker signals and an equivalent phantom source [1]–[4]. They developed mathematical expressions for the determination of loudspeaker signals leading to any particular phantom source. In the present paper the phantom source is represented by a plane wave. The phantom-source direction is determined on the basis of sound-field calculations and is believed to represent the localization sensation occurring in the mind of the listener. Cooper and Bauck treated the situation as ideal in the sense that room reflections were not dealt with and the head was regarded as being spherical. It is the latter assumption, regarding the head shape, that is investigated further in this paper. Obviously the shape of a human head is not spherical, but this simple approximation becomes plausible when combined with ear locations shifted toward the back of the head rather than placed along a diameter. It is of importance to determine the validity of such simple approximations. This is done in the present paper by comparison with calculated results for a more realistic head shape, taking into account the fact that the head is higher than it is wide (frontal view).

Another very important step would be to include the effect of the pinna on the sound field at the ear drum. This has, however, not been taken into account in this paper.

Hence this paper deals with the theory of Cooper and Bauck, reworked for a more realistic head shape. The diffraction problem connected with the improved head shape is treated by means of a boundary-element method, which is described in Section 1. In Section 3 the results are compared with data for the original spherical-head assumption of Cooper and Bauck. Hence the influence of the deviation from sphericity is quantified.

1 THEORY

Boundary-elements methods (BEM) have emerged as successful tools for the solution of radiation and scattering problems in acoustics. In the case of radiation or scattering under free-field conditions BEM has considerable advantages when compared to other numerical methods such as the finite-element method or the finite-difference method. BEM only requires that the boundary of the radiating or scattering body is discretized, whereas the alternative approaches require the entire domain to be discretized. In this section the conversion of the fundamental equations into a complete numerical scheme will merely be outlined. Further details may be found in Juhl [5].

Assuming time-harmonic waves and omitting the time factor $e^{j\omega t}$, the general Helmholtz integral formula [6] can be expressed in terms of the complex pressure p and the complex surface velocity v normal to the surface

* Manuscript received 1992 May 22; revised 1992 December 8.

of the body B (see Fig. 1):

$$C(P)p(P) = \int_S \left[p(Q) \frac{\partial G(R)}{\partial n} + \mathrm{j}kz_0 v(Q) G(R) \right] \mathrm{d}S + 4\pi p^I(P) . \quad (1)$$

This formula is valid in an infinite homogenous medium (such as air) outside a closed body B with a surface S. In the medium, p satisfies $\nabla^2 p + k^2 p = 0$. In Eq. (1) Q is a point on the surface S, and P is a point either inside, on the surface of, or outside the body B. $R = |P - Q|$ is the distance between P and Q; $G(R) = \mathrm{e}^{-\mathrm{j}kR}/R$ is the free-space Green's function; $k = \omega/c$ is the wave number, ω being the angular frequency and c the speed of sound; j is the imaginary unit; z_0 is the characteristic impedance of the medium; and n is the unit normal to the surface S at point Q directed away from the body. The quantity $C(P)$ has the value 0 for P inside the body B and 4π for P outside B. In the case of P on the surface S, $C(P)$ equals the solid angle measured from the medium. ($C(P) = 2\pi$ for a smooth surface.)

Since an analytical solution to Eq. (1) exists only for simple shapes (such as a sphere), numerical methods must be used in order to obtain (approximate) solutions for a more realistic head shape.

As the purpose of the present paper is to rework the theory of Cooper and Bauck for a more realistic head shape and to compare the results presented here with the original ones, the head is still assumed to be rigid. Introducing this assumption in Eq. (1) causes the second term of the integrand to vanish [$v(Q) = 0$]. Eq. (1) then relates the pressure outside a diffracting body to the pressure of the undisturbed incoming wave p^I and the pressure on the surface of the diffracting body. The problem then is to determine the pressure on the surface of the diffracting head. (Although we are interested in the pressure at the ear positions only, the pressure elsewhere on the head surface must be calculated in order to obtain this quantity.) The solution strategy for this scattering problem is to place P on S and solve for the pressure p.

Ultimately one could wish to make accurate calculations on a dummy head, including the effect of the pinna and the torso, but doing this would still be quite a time- and storage-consuming task. In order to be able to solve the problem on a normal PC, the improved head shape has been chosen to be axisymmetric. This obviously imposes restrictions on the accuracy of the head-shape model. Basically it becomes possible to take into account the fact that the head is higher than it is wide (frontal view) without any loss of generality as far as the location of the ears is concerned. From a computational point of view this assumption makes it possible to use a specialized formulation described in the following section, meaning a significant reduction of the required computer time and storage. Since horizontal localization is to be investigated, the generator of the axisymmetric shape is chosen to be a horizontal section of the Brüel & Kjær 4128 head-and-torso simulator (HATS) passing through the ear positions (see Fig. 3).

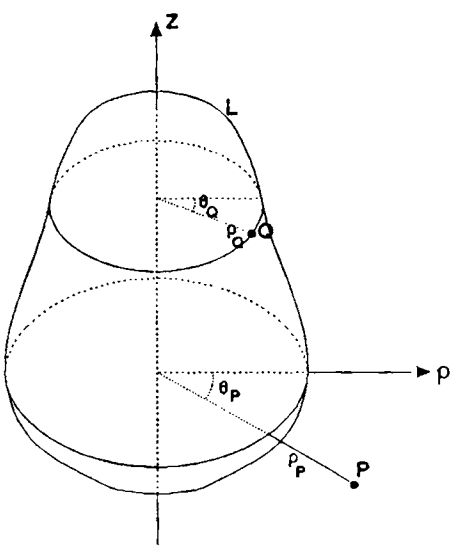

Fig. 1. Axisymmetric body B.

1.1 Axisymmetric Formulation

When the Helmholtz integral equation is applied to a body with axisymmetric shape, the surface integral reduces to an integral along the generator of the body and an integral over the angle of revolution. (For a detailed deduction the reader is referred to Juhl [5].) In this case it is convenient to use a cylindrical coordinate system (ρ, θ, z) as defined in Fig. 1. Eq. (1) with $v(Q) = 0$ then becomes

$$C(P)p(P) = \int_L \int_0^{2\pi} \left[p(Q) \frac{\partial G(R)}{\partial n} \right] \mathrm{d}\theta(Q)\, \rho(Q)\, \mathrm{d}L(Q) + 4\pi p^I(P) \quad (2)$$

where $\rho(Q)$ is the radial coordinate of an arbitrary point Q on the body, $\mathrm{d}\theta$ is the differential angle of revolution, and $\mathrm{d}L$ is the differential length of the generator. The other symbols are as in Eq. (1).

For any body of axisymmetric shape it is possible to expand $p(Q)$ in a circumferential cosine series:

$$p(Q) = \sum_{m=0}^{\infty} p_m \cos m\,\theta(Q) . \quad (3)$$

For scattering problems, where the incident wave is plane or due to a point source, the coordinate system

can always be chosen so that only a cosine expansion is needed. Hence the simplification introduced here is independent of the incident field, but is due to the simple geometry of the scattering body only.

Due to the orthogonality of the cosine terms, Eq. (2) decouples into an integral equation for each term m:

$$C(P)p_m(P) = \int_L p_m(Q) \left[\int_0^{2\pi} \cos m\theta(Q) \frac{\partial}{\partial n} \left[\frac{e^{-jkR}}{R} \right] d\theta(Q) \right] \rho(Q)\, dL(Q) + 4\pi p_m^I(P) \ . \quad (4)$$

The integrand in the integral over the angle of revolution is singular. In order to obtain an accurate result in an efficient manner, the singularity in this latter integral is isolated and evaluated using elliptical integrals. The remaining parts of the integral are nonsingular and may be evaluated by a standard Gaussian quadrature formula. Hence the integral over the angle of revolution may be evaluated without circumferential discretization of the head, and defining its value as $F(P, Q, m)$ reduces Eq. (4) to

$$C(P)p_m(P) = \int_L p_m(Q)F(P, Q, m)\, \rho(Q)\, dL(Q) + 4\pi p_m^I(P) \ . \quad (5)$$

Thus in the case of an axisymmetric body only the generator needs to be discretized, which is a significant advantage in terms of required computer storage and computer time compared with a full three-dimensional implementation of Eq. (1).

In a scattering problem the total pressure on the body B may be found as a sum of cosine expanded pressures obtained by solving Eq. (5):

$$p(P, \theta) = \sum_{m=0}^{\infty} p_m(P) \cos \theta \ . \quad (6)$$

In practice only a finite number of p_m terms is needed to ensure a sufficiently accurate prediction of the pressure p on the body, and for the frequencies considered here (up to 6.4 kHz). It was found that four terms sufficed for an accurate calculation of the sound field.

1.2 Numerical Implementation

Eq. (5) may be solved numerically by assuming that the geometry and the pressure are defined by a finite set of values—the nodal values. In between these nodes the geometry and the pressure are assumed to vary according to certain shape functions; in this work a linear variation has been used. Hence, Eq. (5) is translated into a set of linear equations with the nodal pressures as unknowns:

$$A_m p_m = 4\pi p_m^I \ , \quad m = 0, 1, 2, \cdots \quad (7)$$

where the complex vector p_m contains the nodal pressures, and p_m^I contains the pressure of the incident wave at the nodes in the absence of the body. The matrix A_m depends only on the frequency and on the shape of the body, and may therefore be reused in different problems involving the same frequency and body shape (such as scattering by different angles of incidence). For bodies such as the one considered in this work, which are symmetric with respect to the ρ axis as well, the matrix has symmetric properties: $a_{ij} = a_{M-i+1\,M-j+1}$, where M is the number of nodes. Therefore the time to calculate the elements in the matrices can be halved in this case.

2 PHANTOM SOURCE

Determining the diffraction process around a body with a shape similar to a human head is one thing, but in order to use these results for localization considerations further processing is needed. The approach used here is that when superimposed at the ears, loudspeaker signals must closely resemble a plane wave coming from a well-defined horizontal direction. When this assumption is met, the loudspeaker signals will supposedly provide the listener with a clear and unambiguous sense of direction of the sound. Hence free-field conditions are supposed in the sense that the listening room is not taken into account. This may be justified by means of the Haas effect or the law of the first wave front [7], which states that the first part of the sound field is very important for localization. Practical implementation of a spectral stereo pan pot has been made by MacCabe and Furlong [8] with considerable success.

Hence a plane wave represents the direction of the phantom source—the direction simulated by the loudspeaker signals. The loudspeakers are assumed to be located 60° apart as seen from the listening position (standard listening conditions). Then, per definition, the loudspeaker signals should be adjusted so that the total sound field (that is, from both loudspeakers) at the ear positions of the artificial head is identical to the sound field from a plane wave coming from the phantom direction. The signals from the loudspeakers are denoted by L and R for the left and right loudspeaker, respectively. Two equations are obtained. The sound field at each ear should equal the incoming plane wave S. Since both amplitude and phase are matched, L and R and S are representing complex numbers. Introducing a function $A(ka, \theta)$, which takes the diffraction into account, the equations relating to the sound field at the left and right ear, respectively, read thus [1]–[3]

$$LA(ka, \theta) + RA(ka, -\theta) = SA(ka, \alpha) \quad (8)$$

$$LA(ka, -\theta) + RA(ka, \theta) = SA(ka, -\alpha) \quad (9)$$

where α is the phantom source angle as shown in Fig. 2 and θ is half the opening angle of 60°. In our case θ is therefore 30°. The function $A(ka, \theta)$ denotes the transfer function from plane wave to head diffraction. The plane-wave field is determined at the center of the head. The head-diffracted field is the field obtained at one ear position due to the plane wave and taking the head shape into account. This field is determined by Eq. (6), and the angle is taken to be negative toward the shadow zone.

The loudspeaker signals for a given α are examined and the signal S is set to 1. This leads to

$$L = \frac{A(ka, 30)\,A(ka, \alpha) - A(ka, -30)\,A(ka, -\alpha)}{A^2(ka, 30) - A^2(ka, -30)} \quad (10)$$

$$R = L\,\frac{A(ka, \alpha) - A(ka, 30)}{A(ka, -30)}\,. \quad (11)$$

3 INFLUENCE OF HEAD SHAPE

Traditionally sound-field considerations related to stereo have been using a spherical head model, except for the cases when the head was ignored as a source of diffraction. The spherical approximation is flawed. The pinna is one missing factor, the human torso is another missing factor, and the actual head shape is a first-order approximation only. Furthermore the acoustic impedance of the head is not adequately described by the usual "hard-surface" assumption. In this work one of these factors, the actual head shape, is dealt with. The classical spherical model is compared to what is actually the basic dimensions of the Brüel & Kjær head-and-torso simulator (HATS) (Figs. 3 and 4). This choice permits a comparison with objective measurements at a later stage.

As mentioned earlier, diffraction around a spherical-head model is compared to diffraction around the improved head shape. The comparison is carried out in terms of loudspeaker signals producing a sound field equivalent to a plane wave coming from the direction stated in the figures. The loudspeakers are assumed to be located 30° off axis (common stereo listening setup), and the amplitude of the equivalent plane wave is taken to be 0 dB. For the improved head shape Eqs. (10) and (11) are used and the function A is determined as explained in Section 1. For diffraction around the spherical head model A is calculated as suggested by Cooper and Bauck [1]–[3]. In Figs. 5 and 6 the diameter of the spherical model is 175 mm as was used by Blauert and taken up by Cooper and Bauck. The angle α is positive toward the left. The sound pressure level from the left loudspeaker is dominant since the phantom direction is toward the left. The phase of the left loudspeaker is

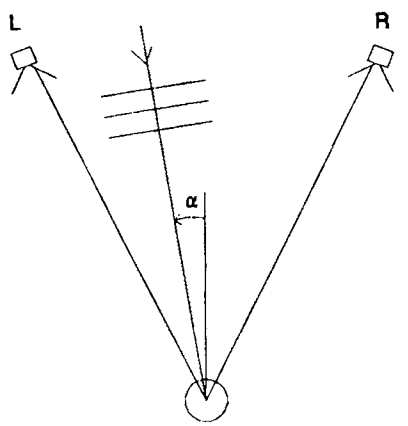

Fig. 2. Idealized listening setup with equivalent plane wave.

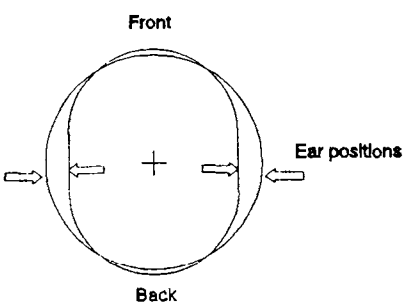

Fig. 4. Horizontal cross section of improved head model and spherical head model having a 175-mm diameter. Note displacement of ear positions relative to diameter.

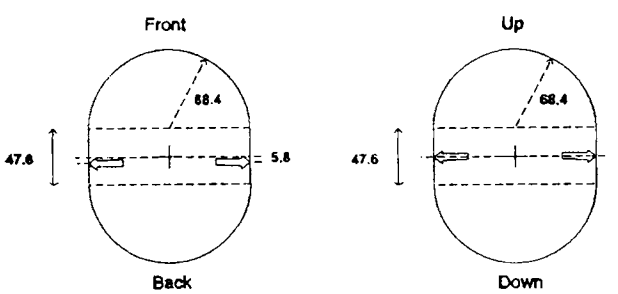

Fig. 3. Cross sections through center of improved head model. Ear positions at arrows; measures in millimeters. Model is symmetrical around horizontal axis through center.

greater than that for the right loudspeaker in these cases. This corresponds to a later arrival of the right loudspeaker signal at the head due to the positive α values.

Comparing the head models, a considerable discrepancy between results is seen for all angles θ. In Figs. 7–10 the comparison is carried out with a spherical head radius equal to the 68.4-mm radius of the half-circles in the improved head-shape model (136.8-mm diameter). These results show a discrepancy which is drastically reduced: only a slight phase change and a slight amplitude change are present when this smaller spherical model is replaced by the improved head-shape model.

The question then arises: why has the head diameter of 175-mm been used extensively by Blauert and others? It turns out that diameters of approximately this magnitude have been used for 100 years [9]–[12]. This is probably due to the fact that 175 mm represents a rough mean diameter in the horizontal plane since according to IEC 959 [13] the head breadth should be 152 mm and the head length should be 191 mm. If the 175-mm head diameter is used in connection with ears located along a diameter (that is, 180° between ears), then the geomtrical path-length difference between the ears at 90° incidence is 225 mm, or close to the 210 mm of Hornbostel and Wertheimer (see [1]). But if the ears are displaced, as they usually are, to an angle of 100° from the front instead of 90°, then the path-length difference becomes as high as 239 mm. The improved head shape used in this work leads to a path-length difference of 205 mm. Turning the problem around and determining the spherical head model with ears displaced toward the back of the head (100° from the front) and leading to 210-mm path-length difference for a sound field coming from 90°, the result becomes a head diameter of 154 mm (153.8 mm). Hence this radius should be appropriate for sounds coming directly from one side where the path-length difference is large, but additional numerical tests (not shown here) reveal that this head size does not lead to improved results for the spherical model in the situations dealt with above (angles below 30°). A diameter of 137 mm is a good approximation for predicting theoretically the localization of sources in the horizontal plane, when the source is not located very far from the median plane. This diameter is not much different from the distance between the ears of a median human.

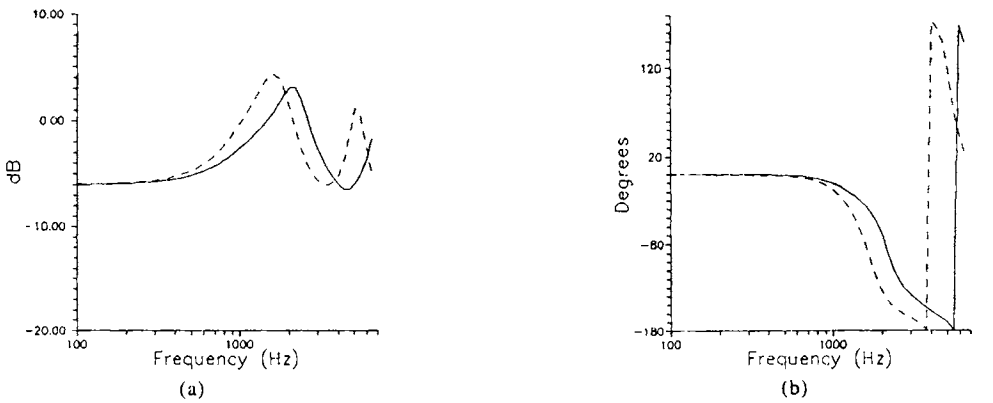

Fig. 5. (a) Amplitude of loudspeaker signals producing same field at ear positions as a plane wave of unit amplitude coming from α = 0°. (b) Phase of loudspeaker signals. Left and right loudspeaker signals are equal in this case. Sphere ---; BEM —.

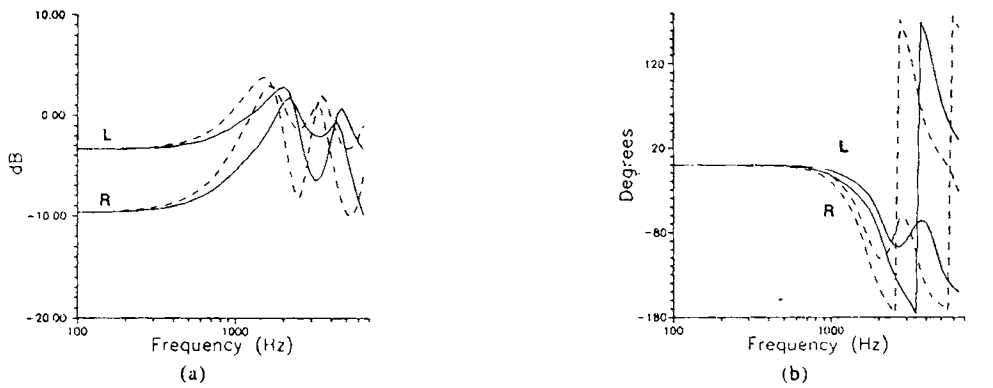

Fig. 6. (a) Amplitude of loudspeaker signals producing same field at ear positions as a plane wave of unit amplitude coming from α = 10°. (b) Phase of loudspeaker signals. Sphere ---; BEM—.

4 CONCLUSIONS

Boundary-element calculations have been made for a realistic, albeit axisymmetric, head shape. The sound field at ear positions has been determined for plane-wave incidence, and these results have been utilized in connection with stereophonic reproduction under free-field conditions. The results indicate that a spherical head model may lead to accurate results for stereophonic reproduction since the sound comes from directions close to frontal incidence. If the ear positions are located at an angle of 100° from the front, the often used head

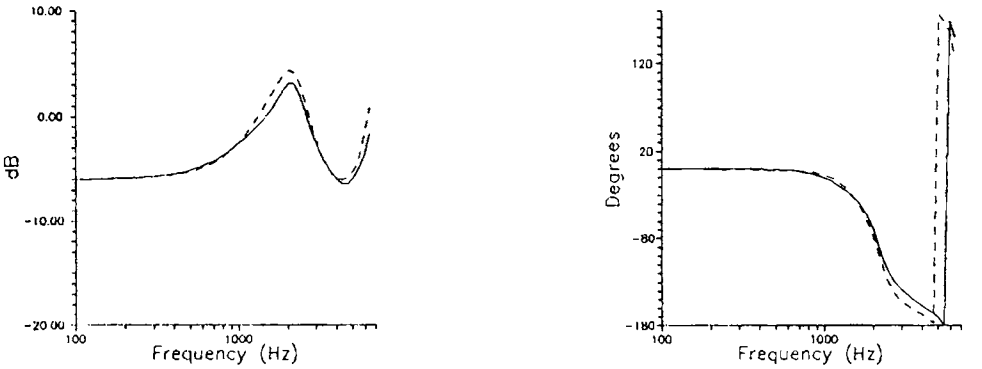

Fig. 7. (a) Amplitude of loudspeaker signals producing same field at ear positions as a plane wave of unit amplitude coming from $\alpha = 0°$. (b) Phase of loudspeaker signals. Left and right loudspeaker signals are equal in this case. Sphere with 68.4-mm radius ---; BEM—.

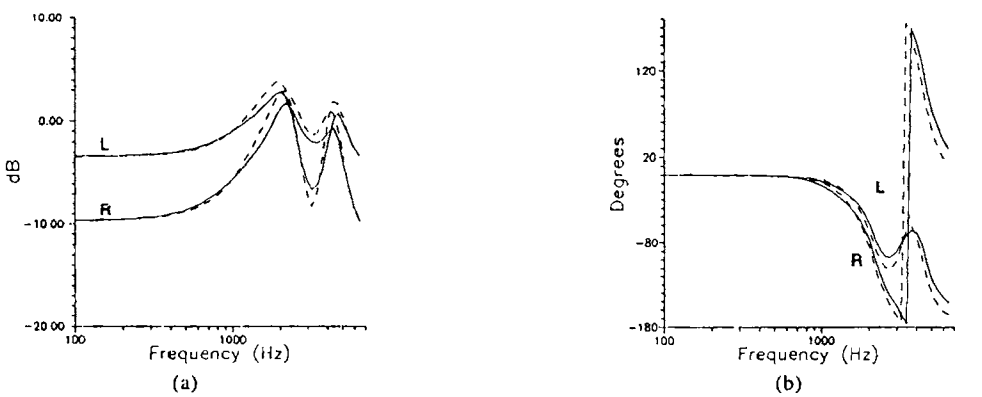

Fig. 8. (a) Amplitude of loudspeaker signals producing same field at ear positions as a plane wave of unit amplitude coming from $\alpha = 10°$. (b) Phase of loudspeaker signals. Sphere with 68.4-mm radius ---; BEM—.

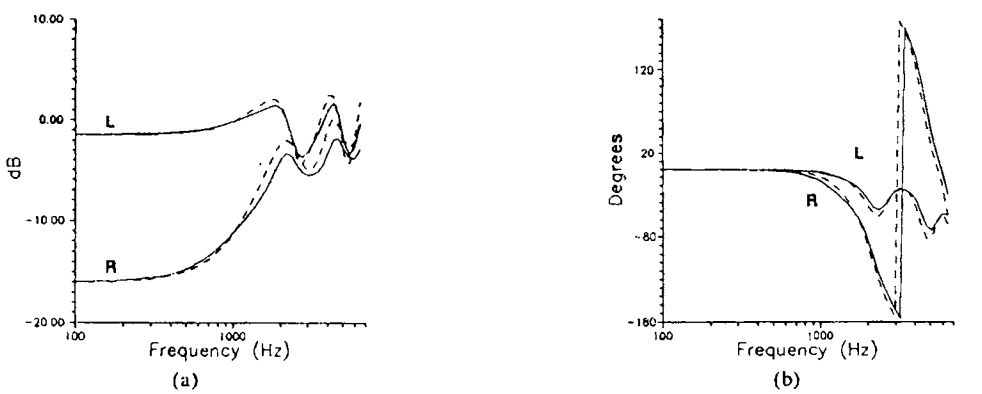

Fig. 9. (a) Amplitude of loudspeaker signals producing same field at ear positions as a plane wave of unit amplitude coming from $\alpha = 20°$. (b) Phase of loudspeaker signals. Sphere with 68.4-mm radius ---; BEM—.

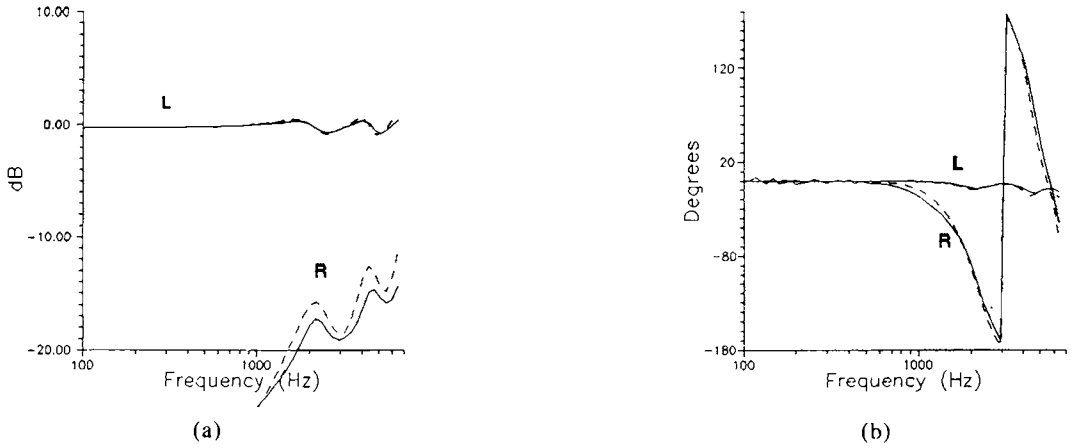

(a) (b)

Fig. 10. (a) Amplitude of loudspeaker signals producing same field at ear positions as a plane wave of unit amplitude coming from $\alpha = 28°$. (b) Phase of loudspeaker signals. Sphere with 68.4-mm radius ---; BEM—.

diameter of 175 mm is too large, whereas a diameter of 137 mm appears to be appropriate. But due to the nonsphericity of the human head, the appropriate "effective" diameter varies with the angle of incidence.

5 ACKNOWLEDGMENT

The authors would like to thank Brüel & Kjær for making the exact head dimensions of the HATS available to them.

6 REFERENCES

[1] D. H. Cooper, "Problems with Shadowless Stereo Theory: Asymptotic Spectral Status," *J. Audio Eng. Soc.*, vol. 35, pp. 629–642 (1987 Sept.).

[2] D. H. Cooper, "Calculator Program for Head-Related Transfer Function," *J. Audio Eng. Soc.*, vol. 30, pp. 34–38 (1982 Jan./Feb.).

[3] D. H. Cooper, "Phase Reference in HRTF Calculation," *J. Audio Eng. Soc. (Letters to the Editor)*, vol. 31, p. 760 (1983 Oct.).

[4] D. H. Cooper and J. L. Bauck, "Prospects for Transaural Recording," *J. Audio Eng. Soc.*, vol. 37, pp. 3–19 (1989 Jan./Feb.).

[5] P. M. Juhl, "Axisymmetric Integral Formulation for Nonaxisymmetric Boundary Conditions," Rep. 47, Acoustics Laboratory, Technical University of Denmark, Lyngby (1991).

[6] B. B. Baker, and E. T. Copson, *The Mathematical Theory of Huygens' Principle*, 2d ed., Oxford University Press, London (1953).

[7] J. Blauert, *Spatial Hearing*, M.I.T. Press. Cambridge, Mass., 1983.

[8] C. J. MacCabe and D. J. Furlong, "Spectral Stereo Surround Pan-Pot," prescribed at the 90th Convention of the Audio Engineering Society, *J. Audio Eng. Soc. (Abstracts)*, vol. 39, p. 388 (1991 May), preprint 3067.

[9] S. G. Weinrich, "Sound Field Calculations around the Human Head," Rep. 37, Acoustics Laboratory, Technical University of Denmark, Lyngby (1984).

[10] Lord Rayleigh, "Our Perception of the Direction of a Source of Sound," *Nature*, vol. 14, pp. 32–33 (1876).

[11] G. W. Stewart, "The Acoustic Shadow of a Rigid Sphere, with Certain Applications in Architectural Acoustics and Audition," *Phys. Rev.*, vol. 33, pp. 467–479 (1911).

[12] G. W. Stewart, "Phase Relations in the Acoustic Shadow of a Rigid Sphere; Phase Difference at the Ears," *Phys. Rev.*, vol. 4, pp. 252–258 (1914).

[13] IEC 959, "Provisional Head and Torso Simulator for Acoustic Measurements on Air Conduction Hearing Aids," International Electrotechnical Commission, Geneva, Switzerland (1990).

THE AUTHORS

K. B. Rasmussen

P. M. Juhl

Karsten Bo Rasmussen was born in Karlebo near Copenhagen, Denmark, on April 18, 1955. He received the M.Sc. degree (electrical engineering) in 1978, the Ph.D. degree in 1983, and the Doctor Technices degree in 1991, all from the Technical University of Denmark, Lyngby, Denmark. Currently he is an Associate Professor at the Acoustics Laboratory, Technical University of Denmark. He has been teaching audio technology for more than five years.

Dr. Rasmussen's research interests include diffraction phenomena, outdoor sound, and stereo theory and he has written many scientific papers. He is a member of the Danish Acoustical Society as well as the AES.

•

Peter Møller Juhl was born in Dragør near Copenhagen, Denmark, in 1966. In 1991 he received the M.Sc. degree from the Technical University of Denmark, Lyngby, Denmark, where he studied electrical engineering. He is now a Ph.D. student on the subject of boundary element methods at the Acoustics Laboratory, Technical University of Denmark. His main areas of research are theoretical acoustics and numerical methods.

LIST OF REPORTS. ISSN 0105-3027

	Report no 1. 1969.	K. Rasmussen:	The Acoustical Behaviour of Cylindrical Couplers. DKK 10.-
	Report no 2. 1969.	S. Boel Pedersen:	On Measuring Transient Distortion in Loudspeakers. (Reprint from IEEE Trans. on Audio. Vol. AU-16, p. 515, 1968) DKK 10.-
	Report no 3. 1970.	O. Juhl Pedersen, J. Ødegaard Jensen:	Sound Power Levels of Small Machines measured in a Room with Frequency Independent Reverberation Time. DKK 10.-
	Report no 4. 1972.	J. Barfod:	Investigations on the Optimum Corrective Frequency Response for High-Tone Hearing Loss. DKK 10.-
	Report no 5. 1973.	K. Rasmussen:	Acoustic Centre of Condenser Microphones. DKK 10.-
	Report no 6. 1974.	P.E. Lyregaard, O. Juhl Pedersen:	Vol. I: Loudness Level of Impulsive Noise. Vol: II: Loudness Level of Impulsive Noise. Appendix D - Data from Subjective Measurements DKK 40.-
*)	Report no 7. 1975.	J. Ødegaard Jensen:	Acoustical Noise from Accomodation Bulkheads in Ships. DKK 15.-
	Report no 8. 1975.	T. Poulsen:	Temporal Loudness Summation of Tone-Pulses. DKK 35.-
	Report no 9. 1975.	J.H. Rindel:	Transmission of Traffic Noise through Windows. Influence of Incident Angle on Sound Insulation in Theory and Experiment. DKK 85.-
*)	Report no 10. 1976.	T. Jacobsen:	Localization in Noise. DKK 10.-
*)	Report no 11. 1976.	J. Barfod:	Multi Channel Compression Hearing Aids. Effects of Recruitment Compensation on Speech Intelligibility. DKK 30.-
*)	Report no 12. 1976.	J. Barfod:	Properties of Intelligibility Test Materials. DKK 15.-
*)	Report no 13. 1976.	J. Barfod:	Automatic Intelligibility Measurements (A Feasibility Study). DKK 15.-
	Report no 14. 1976.	S. Damgaard Kristensen:	A Special Reverberation Test Room for Sound Power Determination. DKK 25.-
	Report no 15. 1976.	Finn Jacobsen:	Free-field calibration of one-inch standard condenser microphones. DKK 20.-
	Report no 16. 1976.	J. Højstrup, S.E. Larsen, K. Rasmussen:	Dynamic Calibration of Temperature Wires. DKK 15.-
	Report no 17. 1976.	Otto Bertelsen:	A Fixed Point Fast Fourier Transform. DKK 10.-
	Report no 18. 1976.	T. Salava:	Measurements of the Acoustic Impedance of Standard Laboratory Microphones. DKK 10.-
	Report no 19. 1977.	Carsten Günthersen:	Perception of Distortion in Electroacoustic Equipment. DKK 20.-
	Report no 20. 1977.	Mary Florentine:	Psychophysical Procedure on Measurements of Critical Bands. DKK 10.-
	Report no 21. 1977.	Nikolai Bisgaard:	A Comparison of three Psychoacoustic Procedures. DKK 20.-
	Report no 22. 1977.	O. Juhl Pedersen, P.E. Lyregaard, T. Poulsen:	The Round Robin Test on Impulsive Noise. DKK 40.-
	Report no 23. 1978.	P. Koefoed Møller:	Digital Evaluation of Fluctuating Noise. DKK 35.-
*)	Report no 24. 1978.	Torben Jacobsen:	Measurement and Assessment of Annoyance of Fluctuating Noise. DKK 85.-
	Report no 25. 1978.	Jesper Wiese:	Correlation Technique in Sound Transmission Measurements. DKK 80.-
	Report no 26. 1979.	Finn Jacobsen:	Sound power determination in reverberation rooms. DKK 35.-

	Report no 28. 1980.	Finn Jacobsen:	Measurement of sound intensity. DKK 35.-
	Report no 29. 1979.	V.V. Bardachenko:	Structural Identification of the Three-Dimensional Random Processes. DKK 10.-
	Report no 30. 1981.	O. Juhl Pedersen, T. Poulsen, C. Günthersen:	Annoyance of impulsive noise. DKK 30.-
*)	Report no 31. 1981.	A. Christian Gade:	Musicians' Ideas about Room Acoustical Qualities. DKK 25.-
	Report no 32. 1982.	A. Christian Gade:	Subjective Room-Acoustic Experiments with musicians. DKK 80.-
	Report no 33. 1982.	Karsten Bo Rasmussen:	Sound propagation over level terrain. DKK 60.-
	Report no 34. 1982.	Carsten Günthersen:	Perception of nonlinear distortion. DKK 80.-
	Report no 35. 1986.	Finn Jacobsen, Mogens Ohlrich:	Vibrational power transmission from multipoint mounted machinery to supporting structure. DKK 50.-
	Report no 36. 1984.	Peter Nøhr Larsen:	Noise generated by air jets from a rectangular slit. DKK 60.- (to be ordered from The Manufacturing Engineering Institute, Building 425)
	Report no 37. 1984.	Søren Gert Weinrich:	Sound field calculations around the human head. DKK 55.-
	Report no 38. 1984.	Søren Gert Weinrich:	A study of directional inversions in the perception of reproduced sound images. DKK 70.-
	Report no 39. 1984.	Finn Jacobsen:	Truncation bias errors in estimating frequency response functions. DKK 20.-
	Report no 40. 1984.	O. Juhl Pedersen, S. Bech:	Effects of impulse noise on human beings. Annoyance in Laboratory. DKK 70.-
	Report no 41. 1986.	Finn Jacobsen:	Measurement of structural loss factors by the power input method. DKK 25.-
	Report no 42. 1987.	Torben Poulsen:	CEC Joint project on impulse noise. Session length study. DKK 30.-
	Report no 43. 1987.	Søren Bech:	Listening Test on Loudspeakers. DKK 100.-
	Report no 44. 1989.	Anders Chr. Gade:	Acoustical survey of eleven European concert halls. DKK 75.-
	Report no 45. 1990.	Karsten Bo Rasmussen:	Outdoor Sound Propagation near Ground Surfaces. DKK 75.-
	Report no 46. 1991.	Mingzhang Ren:	Complex Intensity and Near-Field Description. DKK 35.-
	Report no 47. 1991.	Peter Møller Juhl:	Axisymmetric Integral Formulation for Non-axisymmetric Boundary Conditions. DKK 25.-
	Report no 48. 1991.	Søren Bech:	On the Learning Process in a Standard Profile Analysis Experiment. DKK 25.-
	Report no 49. 1991.	M. Ohlrich and K. Ronge:	Modal analysis of circular cylindrical shell. DKK 45.-
	Report no 50. 1992.	Søren Laugesen:	Active Control of Acoustic Noise Using Adaptive Signal Processing. DKK 100.-
	Report no 51. 1992.	Lars Bramsløw Nielsen:	Subjective Evaluation of Sound Quality for Normal-hearing and Hearing-impaired Listeners. DKK 70.-
	Report no 52. 1993.	Lars Bramsløw Nielsen:	An Auditory Model with Hearing Loss. DKK 50.-
	Report no 53. 1993.	Lars Bramsløw Nielsen:	A Neural Network Model for Prediction of Sound Quality. DKK 50.-
	Report no 54. 1993.	Lars Bramsløw Nielsen:	Objective Scaling of Sound Quality for Normal-Hearing and Hearing-Impaired Listeners. DKK 55.-

***) out of stock**

FORTEGNELSE OVER LABORATORIETS PUBLIKATIONER. ISSN 0105-2853

	Publikation nr. 1.	1975. K. Rasmussen:	Årsberetning 1974. DKK 0,-
	Publikation nr. 2.	1975. J. Ødegaard Jensen:	Støj i apteringen ombord i skibe. DKK 25,-
	Publikation nr. 3.	1975. A. Th. Christensen:	Round Robin Test of Loudspeakers. DKK 10,-
	Publikation nr. 4.	1975. Collected Paper:	Description of Measuring Rooms at The Acoustics Laboratory, Lyngby. DKK 10,-
	Publikation nr. 5.	1976. Otto Bertelsen:	Digital frekvensanalyse af smalbåndssignaler på minidatamat. DKK 40,-
	Publikation nr. 6.	1976. K. Rasmussen:	Årsberetning 1975. DKK 0,-
	Publikation nr. 7.	1977. K. Rasmussen:	Årsberetning 1976. DKK 0,-
*)	Publikation nr. 8.	1977. T. Jacobsen:	Objektive målemetoder til vurdering af genevirkning af støj. (En oversigt).DKK 15,-
	Publikation nr. 9.	1978. K. Rasmussen:	Årsberetning 1977. DKK 0,-
	Publikation nr. 10.	1979. A. Th. Christensen:	Årsberetning 1978. DKK 0,-
	Publikation nr. 11.	1979. Bo B. Vistisen:	Statistisk Energi Analyse. Program til Strukturlydsberegninger. DKK 25,-
	Publikation nr. 12.	1980. J.H. Rindel:	Bygningers lydisolation overfor ekstern støj. DKK 20,-
*)	Publikation nr. 13.	1980. A.Th. Christensen:	Årsberetning 1979. DKK 0,-
	Publikation nr. 14.	1981. Finn Jacobsen:	Lydtransmission i rør med strømning. DKK 20,-
	Publikation nr. 15.	1981. A.Th. Christensen:	Årsberetning 1980. DKK 0,-
	Publikation nr. 16.	1982. A.Th. Christensen:	Årsberetning 1981. DKK 0,-
	Publikation nr. 17.	1982. K. Rasmussen:	Minimumskrav til laboratorier, der udfører akustisk prøvning. DKK 15,-
	Publikation nr. 18.	1983. A.Th. Christensen:	Årsberetning 1982. DKK 0,-
	Publikation nr. 19.	1983. Finn Jacobsen:	Vibrationsovervågning af gear og lejer: Signalanalytisk baggrund. DKK 20,
	Publikation nr. 20.	1983. J.H. Rindel:	Måling af indbygningssystemers lydisolation. DKK 35,-
	Publikation nr. 21.	1983. Søren Bech:	Multidimensional skalering: teori og praksis. DKK 30,-
	Publikation nr. 22.	1984. A.Chr. Gade og J.H. Rindel:	Akustik i danske koncertsale. DKK 90,-
	Publikation nr. 23.	1984 A.Th. Christensen:	Årsberetning 1983. DKK 0,-
	Publikation nr. 25.	1985. A.Th. Christensen:	Årsberetning 1984. DKK 0,-
	Publikation nr. 26.	1985. Lars Bager:	Vibrations- og ruhedsmåling med diodelaser. DKK 50,-
	Publikation nr. 27.	1986. Finn Jacobsen:	Årsberetning 1985. DKK 0,-
*)	Publikation nr. 28.	1987. Finn Jacobsen:	Årsberetning 1986. DKK 0,-
	Publikation nr. 29.	1987. Mogens Ohlrich:	Støj fra mindre vindmøller. Lydudstråling fra maskinhus. DKK 50,-
*)	Publikation nr. 32.	1987. Mogens Ohlrich, LA J. Jakobsen, LI B. Andersen, dk-T:	Støj fra mindre vindmøller, Vejledning i dæmpning af støj fra vindmøller. DKK 0,-
	Publikation nr. 33.	1987. Lars Bager:	Kontinuert måling af rivefinhed. DKK 50,-
	Publikation nr. 34.	1988. Finn Jacobsen:	Årsberetning 1987. DKK 0,-

Publikation nr. 35.	**1989. Finn Jacobsen:**	**Årsberetning 1988. DKK 0,-**
Publikation nr. 36.	**1989. Asger Donovan:**	Rumakustisk beregningsmodel. DKK 100,-
Publikation nr. 37.	**1990. Finn Jacobsen:**	Årsberetning 1989. DKK 0,-
Publikation nr. 38.	**1991. Graham Naylor:**	Odeon Room Acoustics Program. DKK 50,-
Publikation nr. 39.	**1991. Mogens Ohlrich:**	Årsberetning 1990. DKK 0,-
Publikation nr. 40.	**1991. Gitte Keidser:**	Reference-data for Dantale (normalthørende). DKK 50,-
Publikation nr. 41.	**1991. R. Burmand Johannesson:**	Aktiv Dæmpning. DKK 30,-
Publikation nr. 42.	**1991. Karsten Ronge:**	Eksperimentel modalanalyse - teori og anvendelser. DKK 35,-
Publikation nr. 43.	**1992. Mogens Ohlrich:**	Årsberetning 1991. DKK 0,-
Publikation nr. 44.	**1992. Graham Naylor:**	Room Acoustics Program - Version 2.0, User Manual. DKK 50,-
Publikation nr. 45.	**1992. Søren Laugesen:**	Aktiv Dæmpning af Rentonekomponent i Støj fra Kraftværksskorstene. Teoretisk Undersøgelse og Computersimulering. DKK 35,-
Publikation nr. 46.	**1993. Mogens Ohlrich:**	Årsberetning 1992. DKK 0,-

***) Udgået**

Kursus 5101: Grundkursus i Akustik og Støj

Note nr.

	D.A. Bies & C.H. Hansen:	Engineering Noise Control, Theory and Practice, 1988 , Polytek. Bogh.		
0101:	F. Ingerslev:	Hæfte I. Det fysiske og psykofysiologiske grundlag, 1982/89, 170 s.	DKK	80,-*)
0102:	-	Hæfte II. Fysisk Akustik, 1985, 63 s.	-	30,-*)
0104:	-	Opgavesamling, 1990, 148 s.	-	70,-*)
0105:	J.H. Rindel:	Hæfte V. Lydisolation, 1987, 97 s.	-	45,-*)
0106:	S.D. Kristensen:	Hæfte VI. Ekstern støj, 1990, 3. udg., 55 s.	-	30,-
0107:	K.B. Rasmussen:	Grundlæggende diffraktionsteori, 1990, 23 s.	-	10,-*)
0108:	J.H. Rindel:	Acoustic Formulas	-	0,-
0109:	-	Engelsk-Dansk akustisk ordliste	-	0,-
Særtryk:	J. Kristensen & J.H. Rindel:	Bygningsakustik, SBI-anvisning 166, 1989, kap. 1 og 4	-	5,-

Kursus 5121: Elektroakustik

Note nr.

	K. Rasmussen:	Analogier mellem mekaniske, akustiske og elektriske systemer , Polytek. Forlag		
2102:	K. Rasmussen:	Mikrofoner, 1989, 127 s.	DKK	60,-
2103:	A.Th. Christensen:	Den elektrodynamiske højttaler, 1976, 1989, 50 s.	-	25,-
2104:	-	Opgavesamling, 4. udg., inkl. facitliste, 1982, 88 s.	-	45,-
2107:	K. Rasmussen:	Lydfelter, 1992, 148 s.	-	65,-
2108:	T. Poulsen:	Lydopfattelse, 1991, 54 s. foreløbig udgave	-	30,-

Kursus 5122: Videregående Akustik

Note nr.

2201:	K. Rasmussen:	Klassisk lineær akustik, 1973/81/86, 235 s.	DKK	100,-
2202:	F. Jacobsen:	Akustisk intensitet, 1991, 37 s.	-	20,-
2203:	-	Lydfeltet i et efterklangsrum, 1993, 48 s.	-	25,-
2204:	K. Rasmussen:	Svingende membraner, 1989, 19 s.	-	15,-
2205:	F. Jacobsen:	Lydudbredelse i rør og kanaler, 1993, 71 s.	-	35,-
2206:	K.B. Rasmussen:	Teoretisk beregning af lydudbredelse udendørs, 1991, 47 s.	-	25,-
2207:	F. Jacobsen:	Opgavesamling, 1993, 17 s.	-	5,-

Kursus 5126: Audioteknik

Note nr.

2601:	K. Rasmussen:	Magnetisk registrering, 1977/82/87, 140 s.	DKK	60,-*)
2602:	-	Mekanisk registrering, 1974/75/80/89, 79 s. uddrag	-	40,-
2604:	K.B. Rasmussen:	Digital lydregistrering: Compact Disc, 1990, 55 s.	-	30,-
2605:	-	Teoretiske overvejelser vedrørende stereo, 1989, 51 s.	-	25,-
2606:	-	Audiosignaler på magnetisk medium, 1991, 68 s.	-	35,-
2607:	-	Teoretiske modeller for højttalere, 1992, 23 s.	-	10,-

Kursus 5131: Akustisk Kommunikation

Note nr.

3101:	O. Juhl Pedersen:	Ørets indretning og funktion, 1976, 97 s. inkl. appendiks	DKK	40,-
3108:	-	Psykoakustiske målemetoder, 1988, 43 s.	-	25,-
3109:	O. Juhl Pedersen:	Genevirkning af støj, 1982, 54 s.	-	20,-
3110:	O.J.P./T. Poulsen:	Beregning af hørestyrke af stationære lydsignaler, 1983, 24 s.	-	10,-
3111:	T. Poulsen:	Taleforståelighed, 1993, 4. udg., 57 s.	-	30,-
3112:	- :	Høreapparater, 1990, 16 s.	-	5,-
3201:	T. Jacobsen:	Lokalisation af lydsignaler, 1977, 48 s.	-	20,-

Kursus 5142: Bygnings- og Rumakustik

Note nr.

	J. Kristensen & J.H. Rindel:	Bygningsakustik. SBI-anvisning 166, 1989, Polytek. Bogh.		
4201:	J.H. Rindel:	Hæfte IV. Anvendt rumakustik, 1984/90, 97 s.	DKK	45,-
4202:	-	Notat A. Lydudstråling fra plader, 1979, 37 s.	-	15,-
4204:	-	Notat Z. Anvendt geometrisk diffraktionsteori, 1979, 20 s.	-	8,-*)
4206:	-	Notat C. Lydtransmission - statistisk energianalyse, 1980, 27 s.	-	10,-
4208:	-	Notat S. Stationære lydfelter i rum, 1981, 43 s.	-	20,-
4209:	-	Notat P. Lydrefleksion og -absorption, 1981, 41 s.	-	15,-
4210:	-	Notat R. Lydabsorbenter, 1982, 46 s.	-	20,-

Kursus 5170: Lyd og Vibrationer

Note nr.

7001:	F. Jacobsen:	Introduktion til anvendt signalanalyse, 1992, ca. 56 s.	DKK	30,-
7011:	M. Ohlrich:	Struktur-transmitteret lyd. Del 1a, 2. udg. 1991, 196 s.	-	85,-
7012:	-	Struktur-transmitteret lyd. Del 1b, 1993, 80 s.	-	40,-
7013:	-	Opgavesamling, 1991, 26 s.	-	10,-

*) ikke obligatorisk